The cytoskeleton and polarity in the *C. elegans* embryo:

Understanding microtubule dependent signalling in the generation of cellular asymmetries.

By

Jack Martin

A thesis submitted to Newcastle University for the qualification of Doctor of Philosophy.

Faculty of Medical Sciences

Biosciences Institute

Principal investigator: Josana Rodriguez Sanchez

August 2021

Abstract.

Asymmetry within cells relies on the uneven distribution of molecules and organelles required for cell function and viability. For example, epithelial cells form an apical-basolateral polarity which confers different protein and phospholipid compositions at the membrane of each domain. Controlled enrichment of integrins on the basolateral domain ensures that an epithelial cell remains anchored to the basement membrane, required to prevent cell plasticity and epithelial to mesenchymal transition. Migrating cells require the assembly of the cytoskeleton at their leading edge and disassembly at the rear to move with direction, whilst asymmetrically dividing cells rely on different concentrations of proteins and RNAs across the mitotic axis to program the distinct fates of each daughter cell after division. The polarity effector proteins, which control polarity establishment and maintenance in cells are broadly conserved, however respond to different cues and have variable contributions dependent on cell type, organism, and stage, be it inherited or de novo polarity. Failure to generate and maintain correct asymmetry in cells can lead to disease states including cancer.

In our lab, we study the contribution of the cytoskeleton in the establishment of cell polarity. For this, we use the *C. elegans* zygote as a model due to the conserved molecular machinery and its well characterised embryonic development. Asymmetry first initiates in the single cell zygote, post-fertilisation, upon which the globally dynamic actomyosin network underlying the cell membrane undergoes localised relaxation at the site in closest proximity to the matured sperm-derived centrosome pair. The resultant gradient of actomyosin contraction generates a cortical cytoplasmic flow towards the future anterior pole and carries with it, the cortical anterior polarity effector PAR proteins. The newly unoccupied cortex is then inhabited by a cytoplasmic pool of posterior PAR proteins. The cue for this change in cortical dynamics is derived from a signal of sequestered AIR-1 which diffuses from the sperm donated centrosome. A second, lesser studied, pathway to establish polarity in the zygote is believed to occur due to the enhanced stabilisation of posterior PARs at the cortex, aided via centrosomal microtubules which prevent phosphorylation from anterior PARs that initially inhibit posterior PAR membrane recruitment. Through mutual antagonism the anterior and posterior PARs can define their own boundaries and maintain polarity. As both pathways rely on the centrosome, studies to characterise these processes individually have been difficult. Disrupting the centrosome compromises both pathways while interrupting downstream components of either pathway results in masked phenotypes due to effective cell polarisation via the other pathway.

To overcome the functional redundancy that makes studying the microtubule-dependent pathway difficult, I have utilised a functionally null mutant of the gene, *nop-1*, which lacks early actomyosin flows to then screen for regulators of the microtubule-dependent pathway of polarity establishment, now required for embryo viability. Through this, and follow up immunofluorescent stains of polarity markers, I have identified novel proteins required for efficient cellular asymmetry. One such protein was the chromokinesin, KLP-19, previously known to aid chromosomal alignment and segregation during metaphase/ anaphase of

meiosis and mitosis. I have shown that KLP-19 is required to keep the centrosome restricted to the posterior pole during polarity establishment, necessary to facilitate a robust symmetry breaking signal and ensure centrosome separation occurs in a timely manner for the setup of the mitotic spindle. It is likely that KLP-19 performs this role by localising to, and crosslinking, centrosomal and cortical microtubules that meet in an antiparallel manner.

Acknowledgements.

Firstly, I would like to thank Josana for giving me the opportunity to work in her lab through my Masters degree and for believing I had the potential to take this research forward to complete a PhD. Thank you for allowing me the freedom to explore different avenues within this project, giving me advice that sustained the momentum of our work, and lending your spirit that got us through long nights of microscopy.

Thank you to the Rodriguez lab; Camilla, John, Iolo, Aaron, Ra'eesah and Elise for all their support, with a special thanks to Alicia who has been like a PhD sister to me to share the ups and downs with. Thanks to the Higgins and Madgewick labs for all the conversations in the lab and office, the Christmas dinners, the post-work drinks and for putting up with the smell of worm plates.

Thank you to Mike Boxem and his group for taking me in during my time at Utrecht University, and an extra thanks to Ruben Schmidt for his help performing the CRISPR and spindle shooting experiments in this project. It was a fantastic opportunity to share my work with Mike's and Sander van den Heuvel's teams who gave me invaluable feedback towards my research. Thanks to all for giving me a taste of the Dutch life and introducing me to the borrelen, which I will definitely take with me to future jobs.

Thank you to my parents Debbie and Brian for encouraging every decision I've made and for all the experiment kits at Christmas that put me on the path to science. And to my sister Amy, who has also been present in my life.

During my time at Durham and Newcastle I have made friends for life. I can't name everyone but thank you all for keeping me somewhat sane throughout each degree and for plying me with alcohol to achieve this. To my fellow biomeds from Durham, I couldn't be prouder of each of us for what we have all gone on to achieve and can't wait to toast our next steps.

Lastly, I'd like to thank Faizan. I should probably say I couldn't have done this without you, but your unpredictability has certainly kept me on my toes throughout the duration of my PhD. Although it's a trait I'm sure has come in handy in my research. Of course, in the last few weeks of my writeup you had to outdo yourself. Hopefully now that I'm finished, I can look forward to a few less surprises. Thank you for making me laugh and being there for me. I can't wait to see what the future holds.

Table of contents.

List of figures.

Illustrations in this thesis were generated using the online BioRender tool.

List of tables.

Abbreviations

aPARs	Anterior PARs
CAMSAP	Calmodulin-regulated Spectrin-Associated Protein
C. elegans	*Caenorhabditis elegans*
CPC	Chromosomal Passenger Complex
CRISPR	Clustered Regularly Interspaced Short Palindromic Repeats
DNA	Deoxyribonucleic Acid
γ-TuRC	γ-Tubulin Ring Complex
GAP	GTPase Activating Protein
GEF	Guanine Nucleotide Exchange Factor
GFP	Green Fluorescent Protein
GMC	Ganglion Mother Cell
KD	Knockdown
KLP	Kinesin-like Protein
LoF	Loss of Function
MAP	Microtubule Associated Protein
MeiCS	Meiotic Cytoplasmic Streaming
MT	Microtubule
MTOC	Microtubule organising centre
PAR	Partition defective
PCM	Pericentriolar Material
PKC-3	Atypical Protein Kinase C
PN	Pronucleus
pPARs	Posterior PARs
RNA	Ribonucleic Acid
RNAi	RNA interference
SPCC	Sperm Pronucleus-Centrosome Complex
TIRF Microscopy	Total Internal Fluorescence Microscopy
WT	Wild Type

Chapter 1 Introduction and literature review

1.1 Cell polarity.

1.1.1 The role of cell polarity.

Polarity is an essential characteristic and hallmark of almost all cell types and is a pre-requisite for the specialised functions that cells perform. It is the uneven distribution of molecules, organelles and functional processes that allow cells to sense and respond to both their internal and external environments in an asymmetric manner.

The dependence on cell polarity for function and viability is highly conserved and dates far back through evolution. The exact mechanisms to achieve polarity and the roles it serves, however, can vary between cell types and species. In unicellular organisms, polarity is required for motility, growth, shape, sensing the environment, and often asymmetric cell division that generates two cells with differing functions (Bornens, 2018). Multicellular organisms similarly rely on polarity for these processes, although with greater complexity. For example, in higher organisms, embryonic cells which undergo asymmetric divisions will generate branching lineages to produce numerous cell types with distinct fates. Through this, assortments of cells into tissues can be produced, and these cells present a greater spectrum of specialised cell function compared to unicellular organisms (Martin-Belmonte, Bernascone and Galvez-Santisteban, 2016; Veeman and McDonald, 2016).

1.1.2 Conserved features of cell polarity.

Despite differences between the pathways that achieve asymmetry in cells and the molecules involved, there are fundamental steps that must be adhered to in order to establish polarity. 1) A cue, either intrinsic or extrinsic, to dictate the timing and axis of polarity; 2) polarity determinants that respond to the cue and segregate asymmetrically, reinforced by positive/negative feedback mechanisms; and 3) relaying polarity to target downstream components that result in asymmetrical function (Martin-Belmonte, Bernascone and Galvez-Santisteban, 2016; Aw and Devenport, 2017; Lang and Munro, 2017).

A number of conserved protein families explicitly act to regulate polarity across varying cell types and organisms, most notably; the PAR (Kemphues *et al.*, 1988; Kirby, Kusch and

Kemphues, 1990; Nakaya *et al.*, 2000; Tomancak *et al.*, 2000; Leibfried *et al.*, 2008; Denker, Bočina and Jiang, 2013), Crumbs (Tepass, Theres and Knust, 1990) and Scribble (Bilder and Perrimon, 2000) complexes. This project focuses on the role of PAR proteins in the establishment of the anterior-posterior axis of the *C. elegans* embryo. The PARs include the scaffolds PAR-3 and PAR-6, the kinase PKC-3 & the GTPase CDC-42 which localise to the anterior membrane of the embryo hence referred to as the anterior PARs (aPARs) (Kemphues *et al.*, 1988; Watts *et al.*, 1996; Tabuse *et al.*, 1998; Gotta, Abraham and Ahringer, 2001; Suzuki *et al.*, 2001; Motegi *et al.*, 2011). On the posterior membrane are the respective membrane-binding PAR-2 which recruits the kinase PAR-1, and the tumour-suppressor protein LGL-1 (Figure 1.1) (posterior PARs - pPARs) (Guo and Kemphues, 1995; Boyd *et al.*, 1996; Hao, Boyd and Seydoux, 2006; Hoege *et al.*, 2010; Motegi *et al.*, 2011; Beatty, Morton and Kemphues, 2013; Arata *et al.*, 2016; Lang and Munro, 2017).

Most polarising processes rely on a mechanochemical system to generate cellular asymmetries. Polarity effectors, such as the PAR proteins and components of the cytoskeleton, cooperate to drive morphological changes and the redistribution of components within the cell and at the membrane.

Figure 1.1

a.

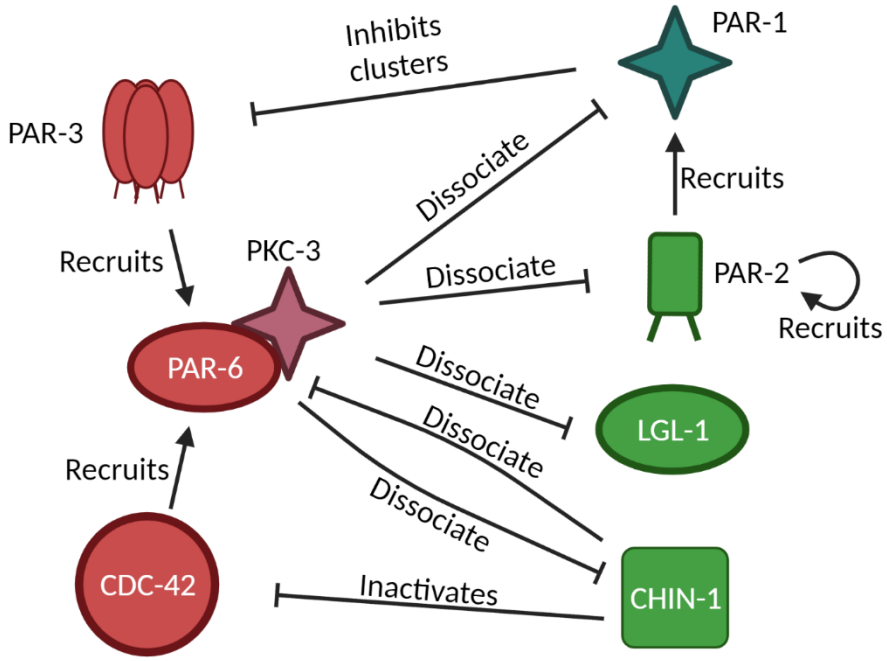

b.

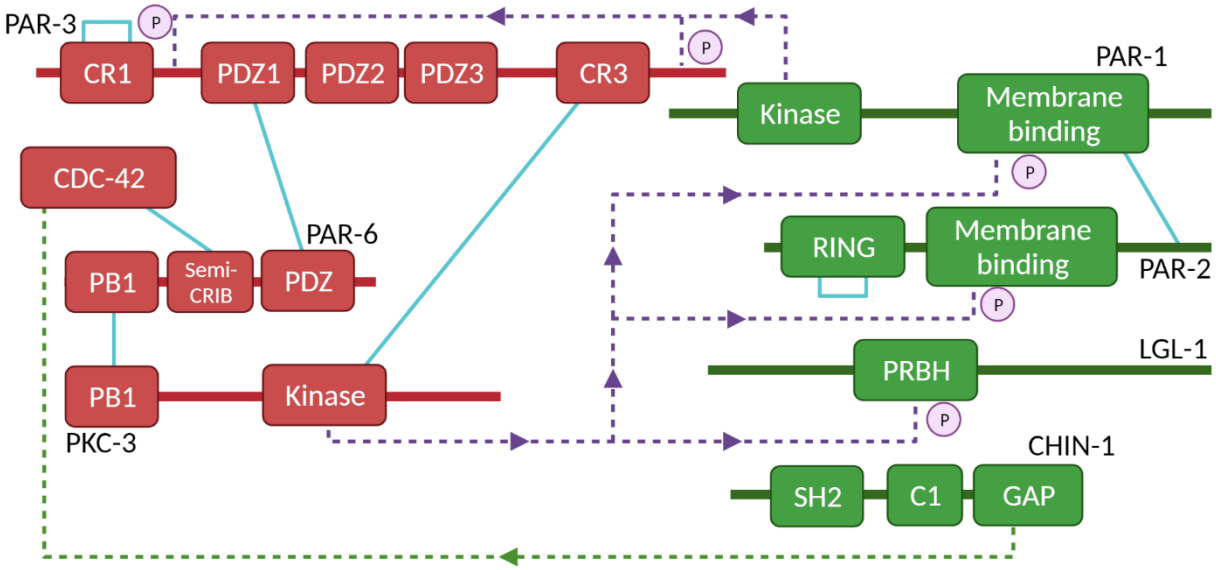

Figure 1.1 **Key PAR protein interactions required for polarity domain stabilisation and maintenance.**
Schematic views of PAR protein interactions and consequences adapted from Lang and Munro (2017) **(a)** Functional interactions between PAR proteins (Anterior PAR-3, PAR-6 & PKC-3 and posterior PAR-1 & PAR-2) and their close associates (Anterior CDC-42 and posterior LGL-1 & CHIN-1). Anterior proteins are coloured red, posterior proteins in green. (b) The same network as (a) showing the protein interaction domains and the type of interaction. Purple broken line: Phosphorylation, Green broken line: GTPase activation, Solid blue line: Direct binding. (Lang and Munro, 2017)

1.2 The cytoskeleton and polarity.

The cytoskeleton, in particular the actin and microtubule (MT) networks, is crucial to guide and maintain the polarity of many cell types. There is an inherent polarity within actin and MT molecules that helps to facilitate cellular asymmetry. Further layers of polarity are then added on top of the molecular builds such as filament orientation, organisation of the networks within the cells, asymmetrical regulation of filament dynamics and the recruitment of interacting proteins such as motor proteins that travel in a specific direction along the filaments (Raman, Pinto and Sonawane, 2018).

1.2.1 Actin.

Actin is the smallest filament type of the cytoskeleton, comprised of globular (G-actin) monomers which bind in a head to tail manner providing the actin filament with an intrinsic asymmetry consisting of a fast-growing "barbed end" and a slow growing "pointed end". Actin has multiple roles in the cell involved in mechanical support, cytokinesis, cell motility, intracellular cargo transport, muscle contraction, cell junction formation, and cell shape (Dominguez and Holmes, 2011).

Actin filaments are formed within cells via nucleator proteins, particularly the formin-family proteins and the Arp2/3 complex, responsible for the formation of linear actin polymers and branching actin networks, respectively (Higgs, Blanchoin and Pollard, 1999; Machesky *et al.*, 1999; Yarar *et al.*, 1999; Sept and McCammon, 2001; Evangelista *et al.*, 2002; Pring *et al.*, 2003). The organisation of actin within a cell is heavily defined by the competitive activity of these nucleators, based on the bias of when and where they act (i.e. there is a limited pool of actin in the cell for both network nucleators to use) (Rotty and Bear, 2014). For example, it was shown in *C. elegans* that the formin CYK-1 is the predominant actin stabiliser in the cytokinetic ring, necessary to produce the linear filaments that contribute to ring constriction and division. Despite not localising to the cytokinetic furrow, reduced levels of ARP2/3 complex subunits resulted in delayed contractile ring formation due to excess formin-dependent actin polymerisation (Chan *et al.*, 2019).

Regulators that promote the assembly of actin (e.g. Arp2/3, Formins) and those that inhibit assembly (e.g. SMIFH2) can be spatially restricted within cells in response to polarity effectors to generate asymmetric actin network growth (Rizvi *et al.*, 2009; Suraneni *et al.*, 2012; Isogai,

Van Der Kammen and Innocenti, 2015; Jordan *et al.*, 2016; Swaney and Li, 2016; Higashi, Stephenson and Miller, 2019). For example, the negative Arp2/3 regulator, Arpin, is recruited by the Rac GTPase to the lamellipodia of migrating cells to disrupt actin assembly and control cell direction (Dang *et al.*, 2013; Gorelik and Gautreau, 2015).

As well as intrinsic molecular polarity along actin filaments, groups of filaments can be organised into different arrays within cells to allow for specialised functions. For example, actin filaments within microvilli are arranged in the same orientation which allows for high crosslink capacity between actin bundles, required for microvilli shape and strength (Chafel, Shen and Matsudaira, 1995; Ferrary *et al.*, 1999; Bartles, 2000; Volkmann *et al.*, 2001). Conversely, actin filaments in stress fibres are aligned in an antiparallel manner and coupled to the motor protein, myosin (together actomyosin), which allows for contraction in non-muscle cells, required for morphogenesis, mechanotransduction, cell adhesion and migration (Naumanen, Lappalainen and Hotulainen, 2008; Tojkander, Gateva and Lappalainen, 2012).

Actomyosin forms contractile networks in cells, the activity of which are regulated by members of the Rho GTPase family. These GTPases are themselves highly susceptible to spatial restriction, dependent on polarity proteins (Cheeks *et al.*, 2004; Motegi and Sugimoto, 2006; Schonegg, 2006; De Matos Simões, Mainieri and Zallen, 2014; Pacquelet *et al.*, 2015; Ly *et al.*, 2017; Tsankova *et al.*, 2017; Zhu *et al.*, 2017). This process will be discussed further in section 1.6.3. Asymmetric dynamics of actomyosin add another degree of polarity to this cytoskeletal component in addition to the intrinsic molecular polarity and organisation of actin.

1.2.2 Microtubules and the centrosome.

In eukaryotes, the primary microtubule organising centre (MTOC) is the centrosome, a structure first described in the 19th century by Theodor Boveri who went on to appreciate the organelle's importance in segregating chromosomes during cell division and their relevance in tumour development. Today we know that the centrosome performs a variety of functions depending on cell type and time in the cell cycle.

The centrosome is composed of two centrioles, each made up of nine short MT triplets, surrounded by a matrix known as the pericentriolar material (PCM). The PCM is composed of densely packed proteins including, but not limited to, the matrix scaffold protein, pericentrin,

and a host of MT stabilising proteins such as γ-tubulin and ninein. Together the PCM hosts the proteins responsible for MT nucleation and anchoring to the MTOC (Pimenta-Marques and Bettencourt-Dias, 2020).

In addition to MT nucleation, the centrosome/PCM unit is involved in processes such as signalling and cell cycle regulation (Berdnik and Knoblich, 2002; Andersen *et al.*, 2003; L *et al.*, 2011; Alves-Cruzeiro, Nogales-Cadenas and Pascual-Montano, 2014). This project focuses on the centrosome's role in polarity induction and MT organisation/ mitotic spindle formation.

MTs are long rigid polymers that span cells as a network of fibres required for cell movement, growth, shape formation, force generation, intracellular transport, and cell division. MTs are highly dynamic and undergo states of polymerisation and depolymerisation that contribute to their growth and shrinkage, respectively (Mitchison and Kirschner, 1984). Structurally, MTs are the largest filament type of the cytoskeleton; they are composed of two globular polypeptides, α & β-tubulin. These heterodimeric subunits polymerise alternately in a head to tail manner forming linear protofilaments with a β-tubulin-tipped end and an α-tubulin-tipped end, deemed the plus and minus-ends, respectively. Thirteen tubulin protofilaments then assemble into the larger hollow rod-shaped MT (Figure 1.2)(Desai and Mitchison, 1997; Nogales, Wolf and Downing, 1998; Nogales *et al.*, 1999; Nogales and Wang, 2006).

Along with plus/minus molecular polarity, MTs have asymmetric dynamics as the polymerisation/depolymerisation rates differ at either end of the MT, with a rapidly-growing β-tubulin-tipped N-terminal plus-end and a slow-growing α-tubulin-tipped C-terminal minus-end (Figure 1.2). MTs assemble through the addition of GTP bound α/β-subunits to the existing fibre. As a self-activating GTPase, tubulin hydrolyses the β-subunit-bound GTP to GDP, once incorporated into the larger molecule (Nogales *et al.*, 1998). As a result, the monomer is believed to deform, preferring an outward curved state which pressures the MT end to splay open and overcome the affinity of neighbouring molecules, hence favouring depolymerisation. Note, monomers within the MT lattice are trapped into the filament's closed configuration, thus only the MT ends are subject to depolymerisation upon hydrolysis (Wang and Nogales, 2005; Burbank and Mitchison, 2006; Nogales and Wang, 2006). In a process known as "dynamic instability" MTs go through cycles of growth and shrinkage dependent on a race between subunit incorporation and GTP hydrolysis. Once hydrolysis exceeds the rate of polymerisation, MTs will lose their stable GTP "cap" necessary for

assembly and the transition from MT growth to shrinkage begins (Mitchison and Kirschner, 1984; Mandelkow, Mandelkow and Milligan, 1991)

Figure 1.2

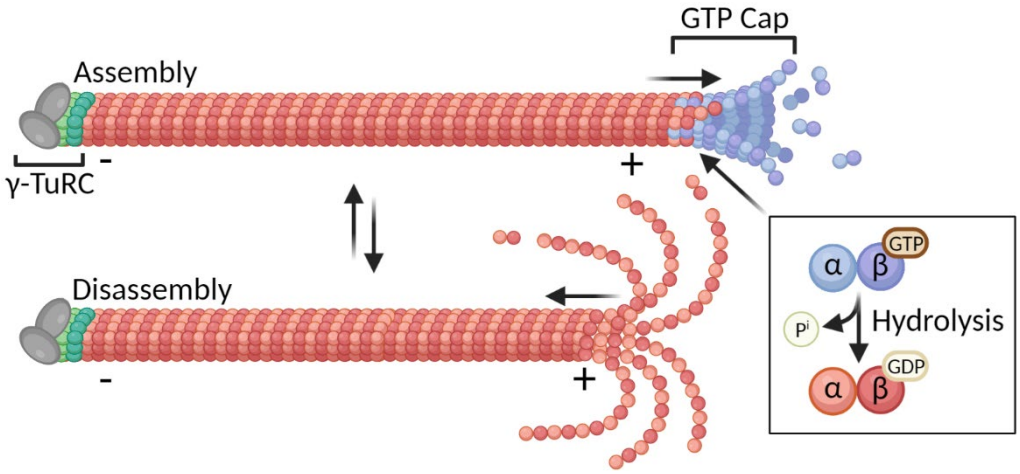

Figure 1.2 **Microtubule dynamic instability.**

MTs are long rigid fibres within cells composed of two alternating globular subunits, α & β-tubulin. MTs undergo phases of assembly (growth) and disassembly (shrinkage), the rates of which depend on multiple factors such as α/β-tubulin subunit availability, temperature, and stabilisation/destabilisation effects of MT associated proteins. Once incorporated into the longer MT filament, GTP bound β-tubulin is hydrolysed to produce GDP bound β-tubulin. In the GTP bound state, β-tubulin is highly stable and can maintain MT integrity/ recruit more tubulin subunits. GDP bound β-tubulin however is unstable and will begin catastrophe events at the MT tip, resulting in MT disassembly. A GTP β-tubulin cap is required to stabilise the hydrolysed subunits within the fibre. As such, it is a race between MT polymerisation and hydrolysation to determine MT assembly and disassembly. Note, the plus-end of the MT is more dynamic than the minus-end which is often stabilised by factors such as the γ-tubulin ring complex which can act to nucleate MTs.

Recent work by Strothman et al. (2019) demonstrated that the rate of hydrolysis is similar at both ends of the MT in a cell-free environment (Strothman *et al.*, 2019). As such, the asymmetric dynamics of MTs are owed to MT associated proteins (MAPs) which have unequal activity on either the plus or minus MT ends.

Numerous components have been shown to promote the stabilisation of the minus-ends of nascent and pre-existing MTs. For example, γ-tubulin forms the γ-tubulin ring complex (γTuRC), along with γ-tubulin ring proteins (GRIPs – e.g. GCP2-6), to form a complex which mimics the plus-end of a MT, required for β-tubulin recruitment. Through this, the complex provides a site which promotes the nucleation of a new MT (Figure 1.2). γTuRC also acts as a cap, preventing minus-end catastrophe, and an anchor when coupled with Nedd1 (Wiese and Zheng, 2000; Anders and Sawin, 2011; Oakley, Paolillo and Zheng, 2015; Muroyama, Seldin

and Lechler, 2016). Other MT minus-end stabilisers include the calmodulin-regulated spectrin-associated proteins (CAMSAPs), the MT anchor ninein, the MT side-branching augmin and the dynein associated NuMA (Merdes *et al.*, 2000; Du *et al.*, 2002; Delgehyr, Sillibourne and Bornens, 2005; Baines *et al.*, 2009; Kamasaki *et al.*, 2013; Petry *et al.*, 2013; Akhmanova and Hoogenraad, 2015; Hueschen *et al.*, 2017; Pavlova *et al.*, 2019).

In addition to direct MT minus-end stabilisation, the plus-ends of MTs are subjected to increased "attacks" that promote depolymerisation. For example, the depolymerising kinesin, MCAK, indiscriminately destabilises the MT ends to induce shrinkage. The minus-end directed kinesin, HSET, however, is able to counteract the depolymerising activity of MCAK, resulting in reduced catastrophe events at the minus-ends compared to the plus-ends (Strothman *et al.*, 2019). The more dynamic plus-ends of MTs utilise their high turnover to undergo roles such as the "search and capture" process in which MTs grow and shrink until finding targets within the cell such as the kinetochore (Wollman *et al.*, 2005; Westermann *et al.*, 2006; Wang *et al.*, 2007; Grishchuk *et al.*, 2008).

Despite their high turnover, MT plus-ends can also interact with MAPs which stabilise MT plus-end interaction with other cellular components. For example, the End Binding (EB) protein family was the first plus-end MAP group to be reconstituted *in vitro*. In these studies, and confirmed *in vivo*, EBs have been shown to localise to the growing tips of MTs and promote the loading of additional MAPs (Bieling *et al.*, 2007; Komarova *et al.*, 2009). It was recently demonstrated in *C. elegans* that EB proteins are involved in the recruitment of cytoplasmic dynein to the cortex which generates the forces required for spindle pulling during mitosis (Schmidt *et al.*, 2017).

The asymmetric assembly of MTs lends itself to downstream polarity. MT motor proteins bind to and recognise the polar composition of MT fibres and "walk" along them with either anterograde (plus-end directed) or retrograde (minus-end directed) direction, typically kinesins and dynein, respectively (Welte, 2004). The fact that MTs permit controlled bidirectional movement is vital for various processes within cells, including vesicle transport, subcellular-specific protein expression via mRNA transport, redistribution of mitochondria for higher local energy production, and repositioning of the MTOC. These processes can act as positive feedback mechanisms to regulate overall cell polarity. (Morris and Hollenbeck, 1993;

Chada and Hollenbeck, 2003; De Vos *et al.*, 2003; De Heredia and Jansen, 2004; Cai and Sheng, 2009).

Due to their dynamicity, MT arrays can undergo major reorganisation within a cell, dependent on cell type, cell cycle stage, and whether their growth is directed by a MT organising centre (MTOC). In a mitotic cell, for example, two centrosomes act as a pair of MTOCs which facilitate the outgrowth of MTs and form a bipolar spindle consisting of three distinct groups of MTs; 1) astral MTs which grow out from the centrosome to the cell cortex; 2) interpolar MTs which grow between the centrosomes; and 3) K-fibres which interact with the kinetochores of the chromosomes (Figure 1.3) (Meunier and Vernos, 2012; Prosser and Pelletier, 2017).

Figure 1.3

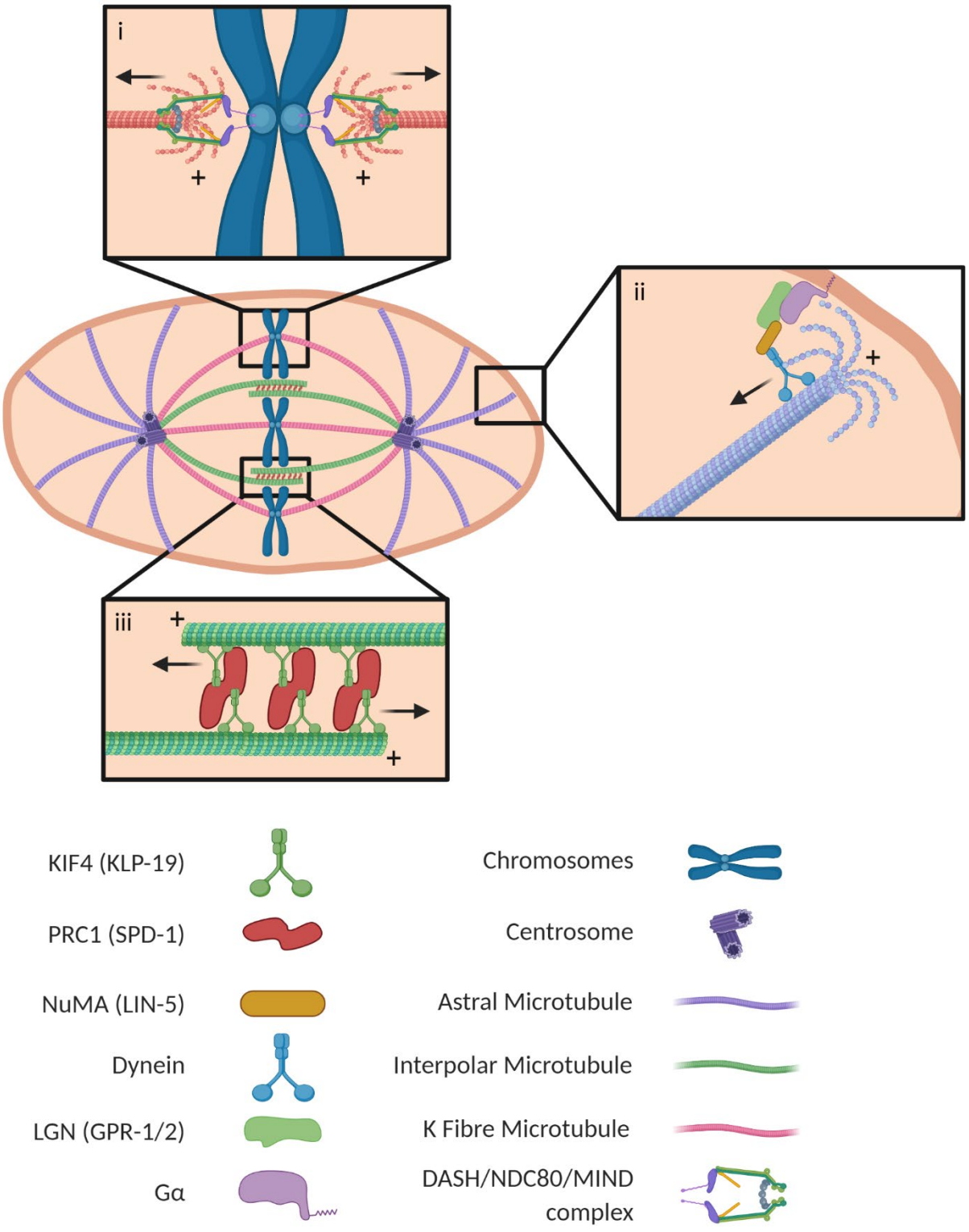

Figure 1.3 **The microtubule groups of mitosis.**

MTs form distinct groups during metaphase/anaphase of mitosis to ensure effective chromosomal segregation occurs prior to cell division. **i**: K-fibre MTs indirectly pull chromosomes as MT depolymerisation forces are transduced via the DASH/NDC80/MIND complex which forms a ring around the plus-end of the MT whilst tethered to the kinetochores. As the MTs depolymerise and recede towards the cell's poles, the chromosomes are pulled

apart. **ii**: Astral MTs bind to cortically anchored dynein motors which walk towards the minus-end, effectively pulling the spindle poles towards each end of the cell and separating the associated chromosomes. **iii**: During metaphase, interpolar MTs grow towards the central region of the spindle where the MT bundling protein, PRC1, crosslinks the overlapping regions of antiparallel MTs. These overlaps go on to form the spindle midzone between segregating chromosomes during anaphase. PRC1 recruits the chromokinesin, KIF4a, which walks towards the plus-end of each MT causing them to slide apart, further contributing to pushing the chromosomes apart. Note: Proteins have been named by the human homologue with the *C. elegans* homologue in brackets.

1.2.3 How microtubule dynamics contribute to centrosome separation, mitotic spindle formation and chromosomal segregating forces.

MTs and their dynamics are critical in the force generation required to separate centrosomes, position the spindle poles and generate the forces required to segregate chromosomes during anaphase.

In dividing cells, the centrioles that were inherited by the parent cell undergo a duplication event. This typically occurs during S-phase of the cell cycle and produces the next pair of centrosomes, necessary to form the mitotic spindle. The centrioles are initially held together by linker proteins, including cohesin and kendrin, which are cleaved by the protease separase in a process known as disengagement. After duplication, the new pair of centrosomes are held together by a proteinaceous complex including C-Nap1, Rootletin, Cep68, Cep135, Ced215, LRRC45 and LGALS3BP (Mayor *et al.*, 2000; Yang *et al.*, 2002; Bahe *et al.*, 2005; Yang, Adamian and Li, 2006; Graser, Stierhof and Nigg, 2007; Kim *et al.*, 2008; Barrera *et al.*, 2010; Fogeron *et al.*, 2013; He *et al.*, 2013; Lin *et al.*, 2013).

The centrosomes are held to the nuclear envelop until the onset of mitosis by BICD2, CENP-F and SUN & KASH family members which anchor the MT minus-end directed motor protein dynein to the nuclear membrane which, in turn, tethers the centrosomal MTs (Splinter *et al.*, 2010; Bolhy *et al.*, 2011; Hu *et al.*, 2013; Turgay *et al.*, 2014; Chang, Worman and Gundersen, 2015; Cain *et al.*, 2018; Nunes *et al.*, 2020). During G2 phase in the cell, the kinase Nek2 phosphorylates components of the centrosome linker complex to facilitate linker dissolution. This phosphorylation aids, but is not necessary for, MT motor protein mediated centrosome separation (Fry, Meraldi and Nigg, 1998; Au, Hau and Qi, 2020). The plus-end directed kinesin, Eg5, acts as the main force generator in pushing centrosomes apart and forms a back-to-back homotetramer. The result is a symmetrical kinesin with motor domains on either side,

allowing it to capture and organise the antiparallel MTs that form between the centrosomes. By walking to the plus-ends of opposing MTs, the kinesin pushes the centrosomes apart (Kapitein *et al.*, 2005; Tanenbaum *et al.*, 2009; Vukušić *et al.*, 2021). In addition, nuclear envelope bound dynein is able to walk towards the minus-ends of centrosomal MTs, in a processive manner, aiding in pulling the centrosomes apart (Figure 1.13.ii)(Raaijmakers *et al.*, 2012; Agircan, Schiebel and Mardin, 2014).

Once the centrosomes have separated, it is generally believed that cortical pulling forces, as opposed to pushing, position the mitotic spindle in large cells. Effective spindle positioning relies on the contributions of dynein motor processivity and MT dynamics. Astral MTs interact with cortical dynein which walks along the MTs to generate the pulling forces on either side of the cell to centre the spindle. Dynein is bound to the inner cell membrane by a conserved ternary complex of NuMA/LGN/$G\alpha_i$ (hence forth called the cortical dynein complex), whose activity responds to upstream asymmetric cues to generate asymmetric dynein pulling forces (discussed further in Section 1.6.1). As such, the bioriented spindle is pulled unevenly, forcing it to rotate and align along the polarity axis of an asymmetrically dividing cell (Burakov *et al.*, 2003; Woodard *et al.*, 2010; Galli *et al.*, 2011; Kotak, Busso and Gönczy, 2012, 2014; Kotak and Gönczy, 2013; Tame *et al.*, 2014; Portegijs *et al.*, 2016; Kotak, 2019; Nunes *et al.*, 2020). In *C. elegans* embryos, the absence of dynein motility has been shown to result in shorter mitotic spindles, indicating that the spindle is not being pulled upon as strongly. Similarly, upon severing of the spindle midzone during anaphase, reduced spindle pole velocities towards their respective side of the cell were observed. These findings suggest a partial dependence of dynein processivity on MTs to generate cortical pulling forces (Nguyen-Ngoc, Afshar and Gönczy, 2007).

To successfully position the mitotic spindle, MTs must undergo depolymerisation (catastrophe) for two supposed reasons. 1) To prevent growing MTs, or MTs being pulled by cortical dynein, from colliding with the cell membrane and pushing away (Figure 1.3.ii) (Adames and Cooper, 2000; Laan *et al.*, 2012; Estrem, Fees and Moore, 2017; Okumura *et al.*, 2018). 2) It is believed that MT depolymerisation can be harnessed to generate additional pulling forces at the cortex which are in fact stronger than dynein motility mediated forces (depolymerisation - ~30-60pN, dynein ~5-7pN per MT (Nicklas, 1983; Desai and Mitchison, 1997; Gennerich *et al.*, 2007; Kozlowski, Srayko and Nedelec, 2007; Grishchuk *et al.*, 2008;

Laan *et al.*, 2012; Estrem, Fees and Moore, 2017)). Indeed localised stabilisation of MTs, via taxol treatment, causes the spindle to displace toward the opposing side of the cell, i.e. loss MT dynamicity results in the loss of cortical MT pulling (Nguyen-Ngoc, Afshar and Gönczy, 2007). The model requires that disassembling microtubules remain associated with the cortex via an anchor such as dynein or NuMA which can also directly interact with MT plus ends (Kozlowski, Srayko and Nedelec, 2007; Seldin, Muroyama and Lechler, 2016). Estrem et al. (2017) explored the relative contribution of dynein motor processivity and MT depolymerisation to force generation in yeast. They suggested that lateral contacts of MTs to the cortex were more subject to motor forces while end-on contacts were subject to depolymerisation generated forces (Estrem, Fees and Moore, 2017). Their findings were similar to those by Gusnowski and Srayko (2011) in *C. elegans* embryos where they propose a model in which lateral MT contacts with the cortex are more prevalent when the centrosomes are positioned towards the periphery of the embryos. This promotes the binding of multiple dynein motors along the MT length and aid in centration of the pronuclei and centrosomes (Figure 1.9.i-v). Once centred, end-on MT-cortical contacts become more prevalent and contribute more to mitotic spindle pulling (Figure 1.3.ii). These mechanisms are unlikely to be exclusive at each stage of the cell but their relative contributions will change (Gusnowski and Srayko, 2011).

MT depolymerisation in force generation has been more comprehensively studied at the kinetochores where K-fibres act to pull chromosomes apart during anaphase (Figure 1.3.i). This has been demonstrated in yeast whereby MTs are tethered to the kinetochores by a ring complex composed of Dam1 heterodecamers. This prevents the uncoupling of MTs to the kinetochore which translates the MTs disassembly into a force capable of pulling chromosomes apart as the MT recedes (Molodtsov *et al.*, 2005; DeLuca *et al.*, 2006; Westermann *et al.*, 2006; Wang *et al.*, 2007; Ciferri *et al.*, 2008; Grishchuk *et al.*, 2008; Wan *et al.*, 2009; Tooley, Miller and Stukenberg, 2011; Suzuki *et al.*, 2016; Volkov *et al.*, 2018; Huis In 'T Veld *et al.*, 2019).

MT stabilisation in the spindle midzone prevents chromosomal hyper-segregation. The chromokinesin Kif4a limits the growth of antiparallel MTs between chromosomes as they separate and then crosslinks the MT overlap to prevent the spindle being excessively pulled apart (Figure 1.3.iii) (Kurasawa *et al.*, 2004; Zhu and Jiang, 2005; Bieling, Telley and Surrey,

2010; Hu *et al.*, 2011; Lee *et al.*, 2015; Wijeratne and Subramanian, 2018; Hannabuss *et al.*, 2019; Pamula *et al.*, 2019; Gaska *et al.*, 2020). This will be discussed further (Sections 1.3.1, 4.3.1, 6.3.1).

1.2.4 Non-centrosomal microtubules.

As mitotic cells differentiate, the centrosome sometimes loses its role as the major MTOC and its components become redistributed, including the MT minus-end stabilisers (e.g. γ-tubulin/γ-TuRC, ninein, CAMSAP) which are sufficient to anchor MTs/ promote MT growth (Mogensen *et al.*, 1997, 2000; Delgehyr, Sillibourne and Bornens, 2005; Akhmanova and Hoogenraad, 2015; Nashchekin, Fernandes and St Johnston, 2016). This is not to say that centrosomes and non-centrosomal MTOCs cannot co-exist. As other components in the cell pick up MTOC responsibility, the overall organisation of MTs within cells drastically changes. How MT arrays become organised depends on cell type (Bobinnec, Fukuda and Nishida, 2000; Muroyama and Lechler, 2017).

For example, as epithelial cells differentiate, they lose their centrosome-based radial array of MTs and develop an apicobasal polarity, along which MTs align with their minus-ends anchored at the apical cortex and their plus-ends extended towards the basal surface (Mogensen *et al.*, 2000; Goldspink *et al.*, 2017). Studies in multiple simple epithelial cell types, such as in the kidney, have demonstrated that the MT anchoring protein ninein becomes associated with apical adherens junctions where it captures the minus-ends of dissociated MTs and stabilises them although does not nucleate them (Mogensen *et al.*, 2000; Moss *et al.*, 2007; Bellett *et al.*, 2009; Goldspink *et al.*, 2017). In *C. elegans* intestinal epithelial cells, the centrosome migrates to the apical membrane where it stops producing MTs. Instead, the MT nucleators γ-tubulin and CeGrip-1 vacate the centrosome and associate with the apical membrane where they grow MTs themselves (Feldman and Priess, 2012).

In the *C. elegans* zygote, non-centrosomal MTs are poorly understood. Research has shown that cytoplasmic MTs are required to position the centrosome prior to polarity establishment (Bienkowska and Cowan, 2012; McNally *et al.*, 2012) and that a population of cortically anchored MTs act to generate bulk cortical cytoplasmic flows during meiosis (Kimura *et al.*, 2017; Kimura and Kimura, 2020). Both processes are discussed in greater detail later (Section 1.7.2). How these MTs originate or localise to the zygote cortex is unclear. It is possible that

they are remnants of cortically grown MTs of the earlier diakinesis oocytes in which γ-tubulin and the *C. elegans* ninein homologue, NOCA-1, localise to the cortex and promote MT growth. Alternatively, the growth of new cortical MTs could continue in the zygote, post-fertilisation, however this has not been investigated (Zhou *et al.*, 2009; Wang *et al.*, 2015).

1.3 Microtubule associated motor proteins.

Motor proteins are force generating molecules which typically act to carry cargo, such as membrane bound organelles and other proteins, along MTs arrays. These molecular motors undergo cyclical conformational changes powered by ATP hydrolysis to generate force and a walk-like movement (Dogan *et al.*, 2015). There are two kinds of MT motor proteins, kinesins which typically walk towards the plus-ends of MTs, and dyneins which walk towards the minus-end. For this project, I focus on the kinesin motors.

Through phylogenetic studies, 14 kinesin super families have been identified, primarily determined by sequence homology and observed function (Lawrence *et al.*, 2004). Kinesins vary in structure, but the typical "walking" kinesin is composed of a kinesin heavy chain, which contains a globular motor domain connected to a long α-helical coiled coil domain, and a kinesin light chain which interacts with cargo. The coiled coil domain of the heavy chain intertwines with that of another kinesin molecule to form a dimer (Hirokawa *et al.*, 1989; Kozielski *et al.*, 1997).

Most kinesins have a role in the transport of various cargoes, although some kinesin families have additional roles (Miki, Okada and Hirokawa, 2005). An example is the previously mentioned Eg5 of the Kinesin-5 family which forms tetramers, binds to antiparallel MTs and aids in centrosome separation and the formation of bipolar spindles (Blangy *et al.*, 1995; Kapitein *et al.*, 2005; Tanenbaum *et al.*, 2009). Members of the Kinesin-13 family highlight the ability of kinesins to alter the stability and dynamics of MTs as they typically act to depolymerise MTs. One of the most studied Kinesin-13 members, MCAK, has been hypothesised to diffuse to the ends of MTs where it catalyses ATP hydrolysis with its central motor domain to induce a bent conformation of the terminal MT protofilament and reduce stability (Moores *et al.*, 2002; Hunter *et al.*, 2003; Ogawa *et al.*, 2004).

1.3.1 Chromokinesins

Over the course of this project, we identified the *C. elegans* motor, KLP-19, as a novel regulator of centrosome positioning during polarity establishment of the zygote. KLP-19 is a chromokinesin, which were first described by Wang & Adler in 1995 as kinesin-like proteins found in the nucleus, capable of direct DNA binding (Wang and Adler, 1995). Typically chromokinesins are required for efficient chromosomal alignment and segregation in metaphase and anaphase during meiosis and mitosis (Kurasawa *et al.*, 2004; Mazumdar, Sundareshan and Misteli, 2004; Powers *et al.*, 2004; Bieling, Telley and Surrey, 2010).

To date, three kinesin families contain chromokinesin members (Figure 1.4.a). The kinesin-4 and kinesin-10 families make up the most of the chromokinesins while the kinesin-12 family contains only one (Figure 1.4.a). The chromokinesins share structural features allowing for their similar roles. Each contain an N-terminal globular motor domain, a C-terminal tail essential for chromatin interaction and an α-helical coiled-coil stalk domain (Figure 1.4.b) (Sekine *et al.*, 1994; Vernos *et al.*, 1995; Wang and Adler, 1995; Tokai *et al.*, 1996; Williams *et al.*, 1997; Lee *et al.*, 2001; Miki *et al.*, 2001; Powers *et al.*, 2004; Wu and Chen, 2008; Vanneste *et al.*, 2009). The ability of chromokinesins to associate with chromosomes depends on sequence motifs and protein interactions that vary for each member. For example, human Kif4a (KLP-19's most likely homologue) contains a cysteine-rich region and zip/basic/leucine zip domain at the C-terminal which allows for direct DNA binding to AT rich sequences (Figure 1.4.b) (Mazumdar, Sundareshan and Misteli, 2004; Mazumdar and Misteli, 2005; Wu and Chen, 2008; Mazumdar, Sung and Misteli, 2011; Vanneste, Ferreira and Vernos, 2011). These domains have not been identified in KLP-19 suggesting it may interact with DNA in a different way to Kif4a.

Figure 1.4

a.

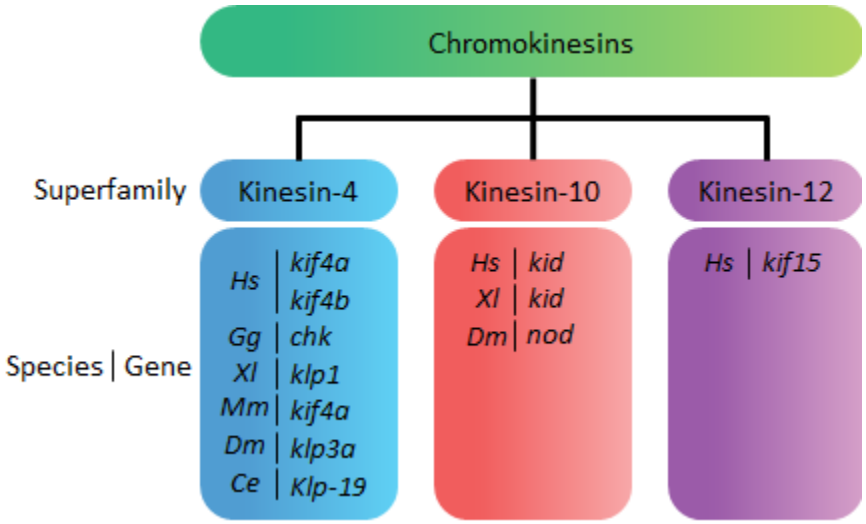

b.

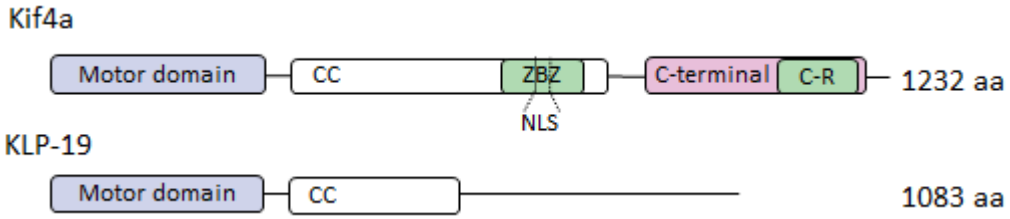

c.

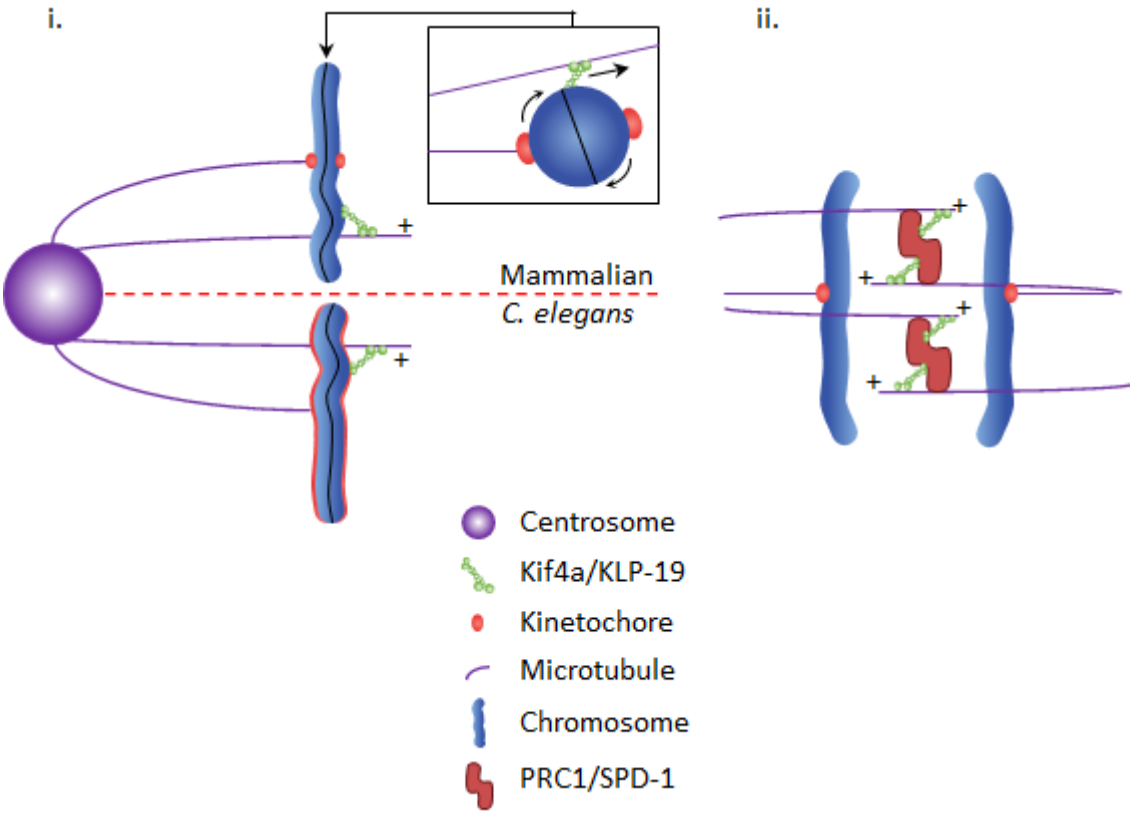

Figure 1.4 **Chromokinesins.**

(a) Chromokinesins can be subdivided in three families according to their protein structure. The majority of the chromokinesins fall within the Kinesin-4 and kinesin-10 families, whereas (to date) there is only one kinesin-12 member identified, the human *kif15*. *Hs – Homo sapiens, Gg – Gallus gallus, Xl – xenopus laevis, Mm – Mus musculus, Dm – Drosophila melanogaster, Ce – Caenorhabditis elegans*. **(b)** Schematics adapted from Almeida & Maiato (2018) of the human and *C. elegans* orthologues of Kif4a and KLP-19. Each has a characteristic motor domain and coiled-coil region (of different lengths). Kif4a also contains a ZBZ (zip/basic/leucine zip – nuclear localisation signal) domain and a cysteine-rich C-terminal which both allow for DNA binding (Almeida and Maiato, 2018). Note: basic sequence alignment tools were unable to identify similar DNA binding domains in KLP-19. **(c) i** - Cartoon of metaphase spindle (monopolar for simplicity) showing the attachment of centrosomal MTs to the kinetochore that faces it. Kif4a (KLP-19) interacts with DNA and provides force towards the centre of the cell (polar ejection forces) allowing for efficient chromosomal alignment. The panel to the top right shows a transverse view of the sister chromatids and their kinetochores at opposite sides, Kif4a provides torque on the chromatids as they travel along the MTs whilst MTs attached to the kinetochores pull back, ensuring that both kinetochores face opposite directions by metaphase, reducing the risk MTs from both centrosomes attach to one kinetochore. Note in *C.elegans*, chromosomes are holocentric with kinetochores spanning the entire length of the chromosome. **ii -** Cartoon of anaphase showing antiparallel MTs of the mitotic spindle. Kif4a homologues have been reported to bind to PRC1 which bundles these MTs allowing it to walk towards the plus-ends and generate forces that aid in sliding the MTs past each other and pushing sister chromatids apart.

KLP-19's homologues have been shown to act on MTs in two ways. First, as a plus-end directed cargo carrying motor protein; second, to stabilise the plus-ends of MTs. Through these roles, the chromokinesin mediates chromosome dynamics (Vernos *et al.*, 1995; Peretti *et al.*, 2000; Kurasawa *et al.*, 2004; Mazumdar, Sundareshan and Misteli, 2004; Bringmann *et al.*, 2004; Brouhard and Hunt, 2005; Midorikawa, Takei and Hirokawa, 2006; Castoldi and Vernos, 2006; Gruneberg *et al.*, 2006; Bieling, Telley and Surrey, 2010; Hu *et al.*, 2011; Bastos *et al.*, 2013; Morris *et al.*, 2014; Heintz *et al.*, 2014; Nguyen, Field and Mitchison, 2018; Wijeratne and Subramanian, 2018; Hannabuss *et al.*, 2019; Heath and Wignall, 2019; Cuijpers *et al.*, 2020). In *C. elegans*, KLP-19's role has so far been characterised in ensuring efficient alignment and segregation of the holocentric chromosomes in meiosis and mitosis (Figure 1.4.c). It does this through its ability to associate with chromatin and carry the chromosomes towards the central spindle as cargo. As the chromosomes are transported, astral MTs capture the kinetochores, effectively holding the kinetochore back, generating torque. As a result, the chromosomes rotate such that the kinetochores adopt a pole-pole orientation. This prevents merotelic MT attachment and ensures each kinetochore is only attached to one spindle pole prior to the onset of anaphase (Powers *et al.*, 2004). Loss of *klp*-19 results in ineffective chromosomal

segregation as the kinetochores do not orient correctly and become exposed to both spindle poles and single chromosomes are inappropriately pulled in both directions (Figure 1.4.c) (Powers *et al.*, 2004; Wignall and Villeneuve, 2009; Dumont and Desai, 2012; Muscat *et al.*, 2015). During meiotic anaphase, in the *C. elegans* zygote, KLP-19 is required for spindle stability to prevent chromosome dispersal as homologous chromosomes segregate (Dumont, Oegema and Desai, 2010). Less is understood of the role of KLP-19 during mitotic anaphase when the chromokinesin shifts localisation from the chromosomes to the central spindle. KLP-19 localisation to the spindle midzone could, however, indicate similar function to the roles described of the better understood homologues (Powers *et al.*, 2004; Dumont, Oegema and Desai, 2010; Muscat *et al.*, 2015).

KLP-19 homologues (e.g. human Kif4a, mouse Kif4a & *X. laevis* Xklp1) are recruited to overlapping MTs organised in an antiparallel manner (Bieling, Telley and Surrey, 2010; Wijeratne and Subramanian, 2018; Heath and Wignall, 2019; Li *et al.*, 2020; Vukušić *et al.*, 2021). This localisation depends on the protein PRC1 (protein regulator of cytokinesis 1) which interacts with the chromokinesin and is responsible and necessary for bundling the spindle MTs into this antiparallel array (Mollinari *et al.*, 2002; Kurasawa *et al.*, 2004; Zhu and Jiang, 2005; Lee *et al.*, 2015; Liu *et al.*, 2018; Wijeratne and Subramanian, 2018; Hannabuss *et al.*, 2019; Jagrić *et al.*, 2021).

Kif4a facilitates the sliding of antiparallel MTs when the MT overlap is large, then acts as a brake once the overlap has shrunk in size (Figure 1.3.iii & Figure 1.4.c). Through this mechanism, Kif4a and PRC1 act on the central spindle to aid chromosomal segregation during anaphase. Sliding antiparallel MTs apart ensures that the sister chromatids are far enough apart from each other by cytokinesis so that they can be efficiently packaged into each of the two-daughter cells. Once the chromosomes are sufficiently separated, the braking force provided in the central spindle counteracts the forces acted upon astral MTs at the cortex. This prevents premature breakup of the central spindle (Nahaboo *et al.*, 2015; Wijeratne and Subramanian, 2018; Gaska *et al.*, 2020; Alfieri, Gaska and Forth, 2021; Jagrić *et al.*, 2021; Vukušić *et al.*, 2021).

Kif4a-PRC1 interaction is inhibited by cyclin-dependent kinase 1 (CDK1) which is itself activated by cyclin B. During prometaphase/metaphase, while cyclin B levels are high, CDK1 prevents Kif4a from associating with PRC1, ensuring the chromokinesin remains associated

with the chromosomes when it is required to help carry them to the centre of the cell. Upon entry to anaphase, cyclin B levels and CDK1 activity in the cell drop and Kif4a makes the transition to spindle midzone localisation (Voets *et al.*, 2015; Dong *et al.*, 2018; Takata *et al.*, 2018).

Previous work has shown loss of Kif4a or its partner PRC1 results in the weakened mechanical resilience and disruption of the spindle midzone, which acts as a platform for both the centralspindlin complex and the chromosomal passenger complex (CPC). (Lee *et al.*, 2015; Wijeratne and Subramanian, 2018; Gaska *et al.*, 2020; Alfieri, Gaska and Forth, 2021). The centralspindlin complex is a heterotetramer composed of a kinesin-6 motor dimer (mammalian KIF23, *C. elegans* ZEN-4) and a RhoGAP dimer (mammalian MgcRacGAP, *C. elegans* CYK-4). This complex bundles the MTs of the spindle midzone and acts to recruit/activate RhoA which is essential to trigger actomyosin driven cytokinesis (Mishima, Kaitna and Glotzer, 2002; Yüce, Piekny and Glotzer, 2005; Zhao and Fang, 2005; Kamijo *et al.*, 2006; Nishimura and Yonemura, 2006; Basant *et al.*, 2015; Basant and Glotzer, 2018). The CPC is composed of the kinase, Aurora B and three additional regulatory subunits, INCENP (Inner Centromere Protein), Survivin and Borealin. Through Aurora B phosphorylation of multiple targets, the CPC performs a range of roles essential for mitosis including promoting chromosome condensation, spindle assembly checkpoint control, regulating correct kinetochore-MT attachments, stabilising the spindle midzone, recruiting/activating the centralspindlin complex and regulating the cytokinetic contractile ring (Kaitna *et al.*, 2000; Ditchfield *et al.*, 2003; Hauf *et al.*, 2003; Minoshima *et al.*, 2003; Lipp *et al.*, 2007; Touré *et al.*, 2008; Xu *et al.*, 2009; Kelly and Funabiki, 2009; Douglas *et al.*, 2010; Lewellyn *et al.*, 2011; Carmena *et al.*, 2012). As such, these two sets of proteins act to determine the cell division cleavage plane and mediate cytokinesis. Therefore premature loss of the central spindle and concomitant loss of central spindlin and the CPC result in cytokinetic defects (Cao and Wang, 1996; Mollinari *et al.*, 2002, 2005; Bringmann and Hyman, 2005; Zhu and Jiang, 2005; Nguyen *et al.*, 2014; Mangal *et al.*, 2018).

Gradual evidence is emerging to suggest that chromokinesins have roles outside of meiosis and mitosis such as DNA damage response during interphase and mediating apoptosis in juvenile neurons. Chromokinesins are also involved in MT transport of cargo; including integrin β1, L1 cell adhesion molecules, ribosomal constituents and the HIV Gag protein (Kim

et al., 1998; Peretti *et al.*, 2000; Midorikawa, Takei and Hirokawa, 2006; Martinez *et al.*, 2008; Wu *et al.*, 2008; Bisbal *et al.*, 2009; Heintz *et al.*, 2014; Yue *et al.*, 2018). Interestingly, Kif4a has been shown to participate in MT stabilisation (reducing dynamic instability) in migrating fibroblast cells. Morris et al. (2014) showed that the motor domain of Kif4a was necessary and sufficient to promote the growth of detyrosinated (stable state) MTs in serum-starved fibroblasts which otherwise have low levels of stable MTs. Through immunofluorescence, this research group detected Kif4a at the plus-ends of detyrosinated MTs where it interacts with, and co-depends on, the MT end-binding protein EB1 to selectively stabilise MTs. Without Kif4a, thus reduced stable MTs, fibroblasts are unable to efficiently migrate, although how Kif4a stabilises these MTs is unknown (Morris *et al.*, 2014). Likewise, EB1 has also been shown to localise to the spindle midzone, dependent upon PRC1, where it may help to stabilise the spindle (Asthana *et al.*, 2020). Whether or not PRC1 and EB1 directly interact is unknown, however both present common binding partners, such as Kif4a and CLASP1 (Kurasawa *et al.*, 2004; Mimori-Kiyosue *et al.*, 2005; Liu *et al.*, 2009; Morris *et al.*, 2014).

Overall, evidence is growing to demonstrate that chromokinesins, such as Kif4a, are less exclusive in their meiotic/mitotic roles than previously thought. We now understand that Kif4a has the capacity to stabilise MTs outside of the spindle midzone, particularly at the membrane of cells.

1.4 Cross-talk between the cytoskeleton and cell polarity effectors in different polarised cells.

Extensive research into different cell types among organisms has demonstrated how the conserved elements of cell polarity (i.e., the polarity effectors) interact and crosstalk with the cytoskeleton. However, the contributions of the components that are involved vary between systems.

1.4.1 Migrating cells

Migrating cells have a dynamic front-rear polarity axis which allows them to change direction whilst mobile. They respond to external stimuli such as chemotactic (Ridley *et al.*, 2003; Van Haastert and Devreotes, 2004) and mechanical gradients (Roca-Cusachs, Sunyer and Trepat, 2013) which reprogram polarity effectors and, in turn, direct reorganisation of the

cytoskeleton, allowing the cells to travel to their destination. The specific polarity proteins that are involved, and their exact roles, vary depending on the migrating cell type.

The actin cytoskeleton is the primary driver of cell migration under the control of Rho GTPase family members. Cdc42 and Rac GTPases are active at the leading edge of migrating cells where they promote actin polymerisation via Arp 2/3 and the formation of lamellipodia and filopodia, required for cell crawling (Figure 1.5.i) (Welch, Iwamatsu and Mitchison, 1997; Miki *et al.*, 1998; Higgs and Pollard, 2000; Kraynov *et al.*, 2000; Rohatgi, Ho and Kirschner, 2000; Small *et al.*, 2002). RhoA GTPase is inactive at the leading edge but active at the rear where it induces actomyosin contraction and retraction of the rear end, allowing the cell to move forward (Figure 1.5.iii) (Arthur and Burridge, 2001; Worthylake *et al.*, 2001). Cau and Hall (2005) demonstrated in migrating fibroblasts that Cdc42 ensures proper polarisation of cell protrusions. Cdc42 activates PAK kinase which triggers the GEF β-PIX to restrict Rac to the leading edge of the cell, thereby promoting actin polymerisation and the formation of lamellipodium. In the absence of this pathway, actin polymerisation and protrusion formation are not stopped; however their spatial control is perturbed (Figure 1.5.iii) (Manser *et al.*, 1998; Cau and Hall, 2005; Nayal *et al.*, 2006; Ten Klooster *et al.*, 2006).

Figure 1.5

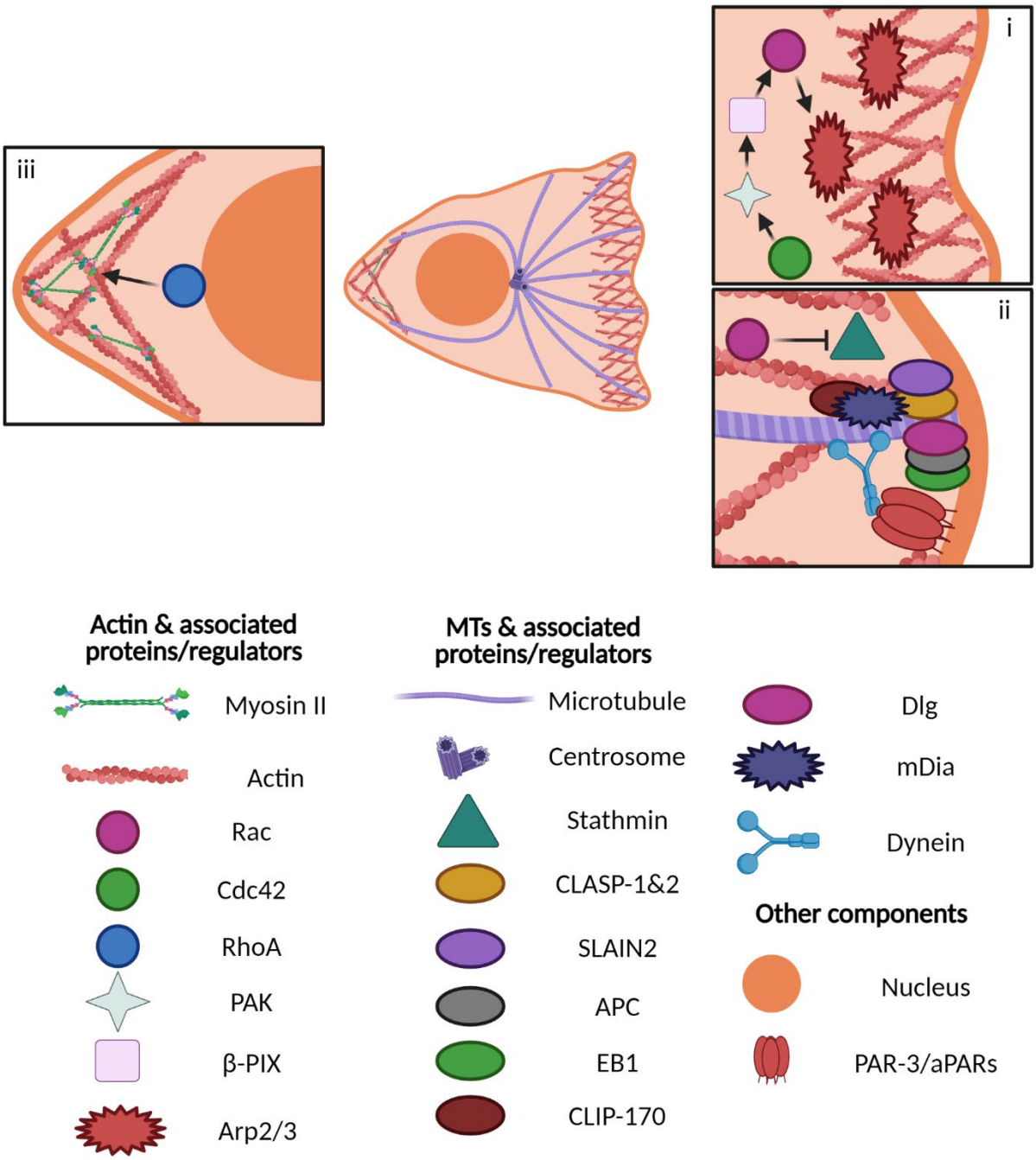

Figure 1.5 **The cytoskeleton and migrating cell polarity.**

i: Under the control of GTPases like Rac, Arp2/3 induces actin polymerisation, required to drive the leading edge of a migrating cell forward. The asymmetry of this event is regulated by Cdc42 which is recruited to the leading edge. **ii**: MTs are stabilised by multiple complexes at the leading edge of migrating cells where they provide support to the protruding cell front. These include MT adaptor complexes (e.g., CLASP-1&2-SLAIN2, APC-EB1, mDia-CLIP-170), the motor protein dynein (guided by the anterior PAR proteins), and inhibition of the MT destabiliser stathmin. Note: mDia is a formin (actin nucleator) but for the purposes of this graphic as a MT stabiliser mDia has been considered a MT associated protein. **iii**: Actomyosin contraction is responsible for the receding of the rear edge of migrating cells under the regulation of RhoA GTPase activity.

The MT network within migrating cells is also highly polarised, allowing it to respond to, and further regulate, asymmetry. MTs have been shown to promote disassembly of focal adhesions, direct vesicular trafficking, aid in cell projection formation and regulate Rho and Rac activity (Waterman-Storer *et al.*, 1999; Etienne-Manneville and Hall, 2001; Krendel, Zenke and Bokoch, 2002; Schmoranzer and Simon, 2003; Prigozhina and Waterman-Storer, 2004; Cau and Hall, 2005; Ezratty, Partridge and Gundersen, 2005; Luxton and Gundersen, 2011).

MTs bind to, and sequester, the Rho GEF, GEF-H1, in order to maintain the GEF in its inactive form. Upon MT depolymerisation, the GEF is released and activated. This triggers RhoA and subsequent non-muscular myosin II activation, thus enhancing actomyosin contractility and promoting focal adhesion stability (Enomoto, 1996; Liu, Chrzanowska-Wodnicka and Burridge, 1998; Ren *et al.*, 1998; Ren, Kiosses and Schwartz, 1999; Krendel, Zenke and Bokoch, 2002). Focal adhesions must be disassembled to allow cell migration. Here, MT polymerisation, in addition to recruiting the Rho GEF, triggers the activation of the Rac GEF, Sif and Tiam1-like exchange factor (STEF). This induces Rac activity and the recruitment of PAK to focal adhesions, instructing focal adhesion disassembly (Nayal *et al.*, 2006; Rooney *et al.*, 2010).

Migrating cells are observed to undergo centrosome-nucleus reorientation so that the nucleus becomes repositioned to face the rear of the cell while centrosome faces the front (Kupfer, Louvard and Singer, 1982; Zhu, Liu and Gundersen, 2018). This has led to a model in which MTs grow in greater number towards the front of the cell where they become enriched and stabilised at the leading edge and generate force, providing support for the cell protrusions, thus the cell's front moves forward (Gundersen and Bulinski, 1988). It has been suggested that MTs act through three mechanisms to position the centrosome prior to migration, 1) being pulled upon by the cortical dynein complex, 2) colliding with other objects in the cell, which pushes back on the centrosome, and 3) being directed inwards in the cell via actomyosin generated cytoplasmic flows. All three effectively maintain the centrosome's position in the centre of the cell. If the centrosome becomes offset, the forces applied counteract the change (Dujardin *et al.*, 2003; Levy and Holzbaur, 2008; Schmoranzer *et al.*, 2009; Laan *et al.*, 2012; Maninová, Iwanicki and Vomastek, 2014; Burakov and Nadezhdina, 2020).

MTs are stabilised at the leading edge of migrating cells via a host of MT associated proteins, small GTPases and polarity effectors. In PtK1 cells MTs are stabilised in a Rac1 (Rho GTPase) dependent manner. MTs underwent fewer catastrophe events near the membrane within

lamellipodium where Rac1 acts to promote actin polymerisation. In a constitutively active Rac1 mutant, highly stable MTs became more prevalent and lamellipodia became uniform around the cell whilst dominant-negative Rac1 PtK1 cells presented with a retracted morphology and less stable MTs (Wittmann, Bokoch and Waterman-Storer, 2003). Through reciprocal regulation, MT turnover appears to be essential for Rac1 activity. Nocodazole and taxol drug treated cells contain depolymerised and stabilised MTs, respectively, and both conditions result in the loss of Rac1 induced lamellipodia protrusion, actin polymerisation and cortical actomyosin flows. It is likely that the growing ends of MTs can act as sites of Rac1 recruitment, thus stable or depolymerised MTs, without growing ends, are incompatible for Rac1 localisation and the actin network cannot assemble (Wittmann, Bokoch and Waterman-Storer, 2003).

Similar phenotypes have been produced in neurons where Rac activation leads to the inactivation of stathmin, a MT destabiliser, necessary for neuronal polarity (Figure 1.5.ii) (Wittmann, Bokoch and Waterman-Storer, 2004; Watabe-Uchida *et al.*, 2006; Tivodar *et al.*, 2015). Interestingly, the posterior PAR-1 homologue, MARK2 kinase, is recruited to the leading edge of migrating cells in a Rac1 dependent manner where it acts to reduce the proportion of long-lived MTs, enhancing MT turnover (Nishimura *et al.*, 2012). The mechanism behind MARK2 dependent MT dynamics regulation is poorly understood, although MARK2 has previously been shown to phosphorylate MT associated proteins, such as the MT stabilising protein Tau. MARK2-dependent phosphorylation reduces Tau's ability to bind to MTs which leads to MT instability, a hallmark of the progression of Alzheimer's disease. Elevated activity of MARK2 has been associated with the disease and has attracted attention as a potential therapeutic target to prevent disease progression (Drewes *et al.*, 1997; Drewes, Ebneth and Mandelkow, 1998; Kosuga *et al.*, 2005; Kojima *et al.*, 2007; Timm *et al.*, 2008; Gu *et al.*, 2013; Schwalbe *et al.*, 2013; Barbier *et al.*, 2019).

In migrating fibroblasts and invading mesenchymal cells it was shown that the cytoplasmic linker associated proteins, CLASP1 and CLASP2, act with SLAIN2 as MT stabilisers specific to the cell leading edge (Akhmanova *et al.*, 2001; Bouchet *et al.*, 2016). These act in parallel with the tumour suppressor protein, adenomatous polyposis coli (APC), recruited by EB1, and the formin mDia, recruited by CLIP-170, again promoting MT plus-end stability (Figure

1.5)(Mimori-Kiyosue, Shiina and Tsukita, 2000; Wen *et al.*, 2004; Kita *et al.*, 2006; Lewkowicz *et al.*, 2008; Ruane *et al.*, 2016).

It was shown in rat astrocytes that integrin signalling mediates the recruitment of Cdc42 to the leading tip where it activates Par6 and aPKCζ. The restricted kinase activity of aPKCζ is essential for proper astrocyte polarisation and helps to position the MTOC via phosphorylation and inhibition of the glycogen synthase kinase-3β (GSK-3β). GSK-3β inactivation induces the two tumour suppressor proteins, APC and Dlg, to localise to, and stabilise, the plus-ends of MTs at the leading membrane (Etienne-Manneville and Hall, 2001, 2003; Etienne-Manneville *et al.*, 2005). Similar findings in migrating epidermal keratinocytes demonstrated the role of anterior PAR proteins in MT stabilisation as Par3 and the Rac GTPase activating protein, Tiam1, are required for proper front-rear cell polarity, chemotactic migration and for the presence of acetylated (stable) MTs (Pegtel *et al.*, 2007).

1.4.2 Neurons

Neuronal cells also heavily rely on cell polarity due to their complex morphology and role in directionally transmitting signals over long distances. Polarity determines which of the immature neuron growth projections (neurites) will become the single axon (signal transmitters) as opposed to the multiple dendrites (signal receivers). In stage 3 cultured hippocampal neurons, the aPARs (Par3, Par6 & aPKC) along with the GTPases, Cdc42 and Rac1, are recruited to, and specify, the future axon tip under the control of phosphotidylinositol 3 kinase (PI3K) activity. The mechanism of polarity specification and axon determination is complex and varies between neurons. Typically, however, positive feedback loops are established in the destined axon whilst negative feedback loops exist in the other neurites to ensure they form dendrites (Etienne-Manneville and Hall, 2002; Burridge and Wennerberg, 2004; Schwamborn and Püschel, 2004; Conde *et al.*, 2010; Shelly *et al.*, 2010; Cheng *et al.*, 2011; Nakamuta *et al.*, 2011; Funahashi *et al.*, 2013; Takano *et al.*, 2017). A number of extracellular molecules have been shown to provide cues for neuronal polarisation depending on their microenvironments such as neurotrophins, insulin-like growth factor, Wnt5a, and cell adhesion molecules such as N-cadherin (Shi, Jan and Jan, 2003; Yi *et al.*, 2010; Cheng *et al.*, 2011; Jossin and Cooper, 2011; Nakamuta *et al.*, 2011; Boitard *et al.*, 2015; Guil *et al.*, 2017; Takano, Funahashi and Kaibuchi, 2019).

Figure 1.6

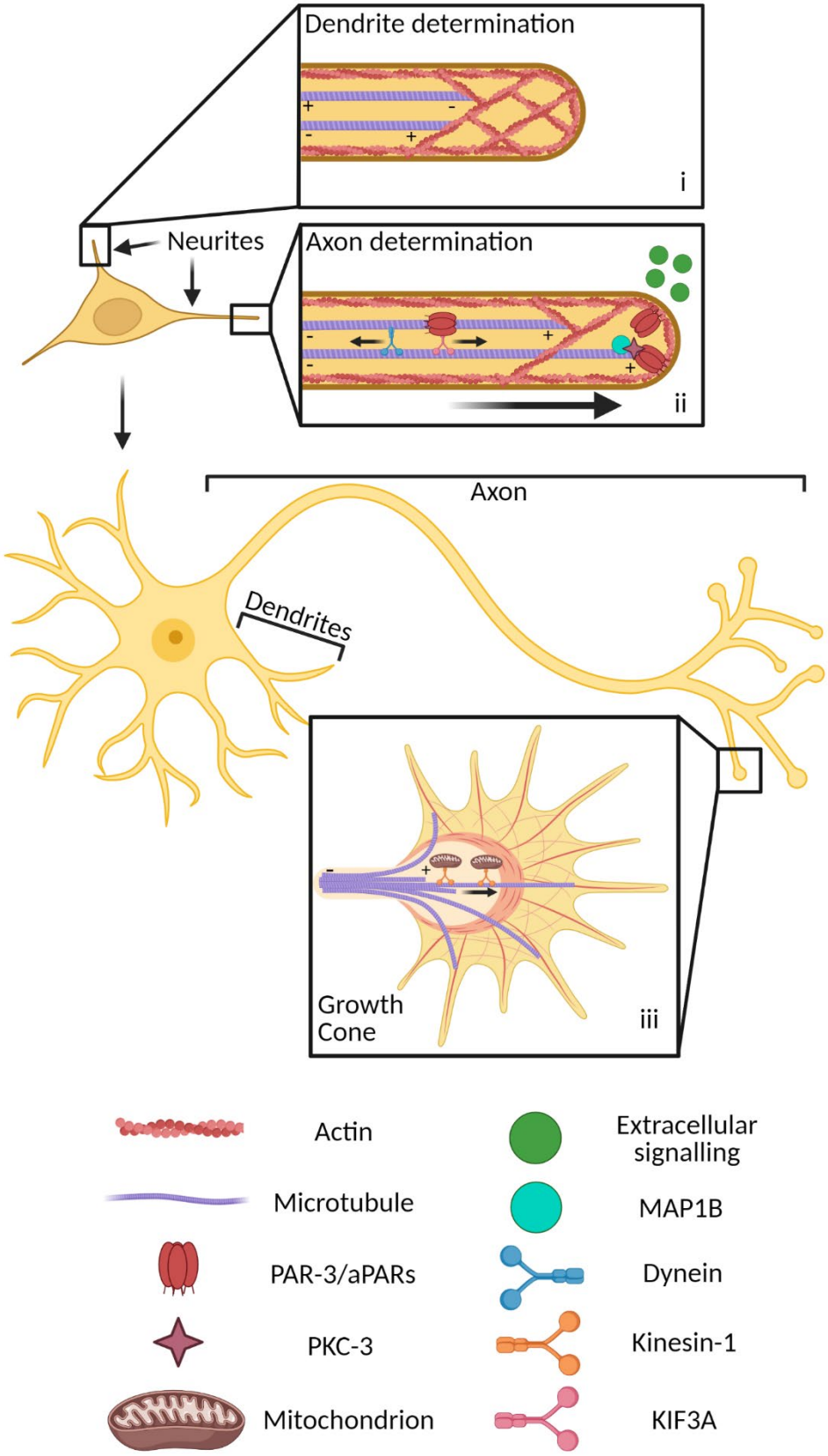

Figure 1.6 **The cytoskeleton and neuronal polarity.**

Top - **i.** The developing dendrites of neurons are restrictive to MT growth which limits projection extension. The dense actin cortex prevents MT invasion, required to generate force for neurite outgrowth. **ii.** In the determinate axon, extracellular cues guide the polarisation

required for axonal specification. Par3 is recruited to the growing tip of axons by APC and the plus-end directed kinesin motor, KIF3A where it stabilises MTs, necessary to provide the force required for neurite projection extension. The actin network within maturing axons undergoes greater turnover under GTPase regulation, making the cortex permissive to MT invasion. The kinase, aPKC, is proposed to activate the MT associated MAP1B, which prevents MT catastrophe and prolongs the MT growth phase at axon tips, further promoting MT length and neurite outgrowth. MTs along the axons are intrinsically polarised with a plus-end and a minus-end and are oriented with their plus-end towards the axon tip. Motor proteins such as dynein and kinesins utilise this polarity for bidirectional transport of components within the neuron over large distances. **Bottom** – The mature neuron has multiple dendrites which receive signals and one long axon which sends signals. **iii.** At the tips of growing axons are growth cones which are guided by growing MTs within them. Energy consumption in the growth cone is high, thus mitochondria are actively transported along the MTs to generate ATP and meet the energy demand.

Polarity effector proteins and MTs act interdependently to regulate asymmetry in neurons. The MT associated protein APC and the kinesin KIF3A are required to recruit Par3 to the tips of growing axons (Figure 1.6.ii). The N-terminal of Par3 has been shown to directly bind to, bundle, and stabilise MTs. This interaction is required for neuronal polarity as mutant Par3, unable to interact with MTs, has been demonstrated as insufficient for correct neurite specification (Figure 1.6.ii) (Witte, Neukirchen and Bradke, 2008; Chen *et al.*, 2013) In the absence of APC/KIF3A, Par3 remains in the neuron cell body and is unable to become enriched at the tips of axons. As a result, neuronal polarity is compromised and multiple neurites grow to a longer length than dendrites yet shorter than axons, showing diminished neurite specification capacity within the cell (Nishimura *et al.*, 2004; Shi *et al.*, 2004).

As in migrating cells, neurons rely on changes in the dynamics and conformation of the cytoskeleton to action polarity cues. The stable actin network in dendrites acts as a barrier to MT protrusion and limits MT growth (Figure 1.6.i) as the actin is highly dense and generates a retrograde cytoplasmic flow that forces advancing MTs back towards the cell centre. Actin in axons, however, shows greater turnover due to increased activation of actin depolymerising factors and cofilin in the neuron growth cone, mediated by Rho GTPase activity. This region becomes permissive to MT extension and neurite outgrowth, allowing for the much greater length of axons compared to dendrites (Bradke and Dotti, 1999; Sumi *et al.*, 1999; Bradke and Dotti, 2000; Edwards *et al.*, 1999; Kuhn *et al.*, 2000; Gallo, Yee and Letourneau, 2002; Gungabissoon and Bamburg, 2003; Bogdan *et al.*, 2004; Schwamborn and Püschel, 2004; Witte, Neukirchen and Bradke, 2008; Flynn *et al.*, 2012; Lu *et al.*, 2013; Craig, 2018). aPKC aids in MT protrusion by increasing the length of time that MTs undergo phases of growth, allowing

more MTs to invade the actin rich regions of the cortex and trigger neurite growth (Kabir *et al.*, 2001). In *D. melanogaster*, it was shown that aPKC is able to form complexes with the MT associated protein Futsch and MTs (Ruiz-Canada *et al.*, 2004). Futsch, and its vertebrate homologue, MAP1B, are able to prevent MT catastrophe events at presynapses, suggesting a likely route in which aPKC is acting in neurons to promote neuron outgrowth (Takemura *et al.*, 1992; Goold, Owen and Gordon-Weeks, 1999; Hummel *et al.*, 2000; Roos *et al.*, 2000; Lepicard *et al.*, 2014; Shi *et al.*, 2019).

As previously mentioned, MT polarity allows motor proteins to walk along the fibre's length carrying cargo to specific sites in cells with anterograde and retrograde direction (Howard, Hudspeth and Vale, 1989; Schnapp and Reese, 1989; Pazour, Wilkerson and Witman, 1998; Yildiz *et al.*, 2004; Beeg *et al.*, 2008). MTs in the axons of neurons are uniformly oriented such that their plus-ends grow outwards from the cell body (Figure 1.6) (Burton and Paige, 1981; Heidemann, Landers and Hamborg, 1981; Stone, Roegiers and Rolls, 2008). This organisation allows the bidirectional transport of cargo along the length of the axon controlled by the net contributions of plus-end and minus-end directed motor proteins (primarily kinesin-1 & dynein respectively) (Glater *et al.*, 2006; Pilling *et al.*, 2006).

During axon extension, there is high demand for ATP production in the growth cone towards the axon tip (Figure 1.6.iii). In response, the balance between directed motor protein transport of mitochondria shifts in favour of walking towards the plus-ends of MTs and the axon tip. Upon termination of axonal growth, plus-end motor activity is downregulated and the relocated mitochondria are returned to the cell body (Morris and Hollenbeck, 1993; Chada and Hollenbeck, 2003; De Vos *et al.*, 2003; Welte, 2004; Cai and Sheng, 2009). Without the intrinsic polar nature of tubulin molecules, this directed transport of mitochondria would not be possible.

1.4.3 Asymmetric cell division – D. melanogaster neuroblasts

All cells in a multicellular higher organism are derived from a single cell which undergoes a series of cell divisions to generate wide branching lineages of cell types that make up the different tissues. Cells high up in these lineages are multipotent and have the capacity to produce different cell types and so are responsible in the decision-making process between cell differentiation and cell renewal. Thus, as a parent cell divides, one daughter cell becomes

specialised in function and loses its multipotency while the other daughter cell retains the identity of the parent cell and can produce more specialised cells. Defects in asymmetrical cell division can result in unbalanced cell fate determination such that excess self-renewing cells develop with disastrous consequences, including the development of tumours (Gateff, 1994; Reya *et al.*, 2001; Caussinus and Gonzalez, 2005; Sastre-Perona, Hoang-Phou and Schober, 2019).

I have discussed the determination of cell polarity within neuronal cells, but the birth of a neuron from a neural stem cell is itself a highly controlled asymmetric event which has been well studied in the fruit fly, *Drosophila melanogaster* (Hartenstein and Wodarz, 2013; Li, Wang and Groth, 2014). In *Drosophila* neural progenitor cells (neuroblasts), the mitotic spindle becomes aligned along an apical-basal axis, defined by the PAR proteins (Izumi *et al.*, 2006). This mitotic spindle is asymmetrical as the distance to midzone is greater from the apical centrosome than the basal (Rebollo *et al.*, 2007). As cell cleavage occurs at the midzone, the daughter cells are unequal in size. The larger apical daughter cell maintains a neuroblast identity and will repeat this cycle while the smaller cell typically becomes a ganglion mother cell (GMC) and commits to cell specification, dividing once more to become two neurons or glial cells (Figure 1.7).

Figure 1.7

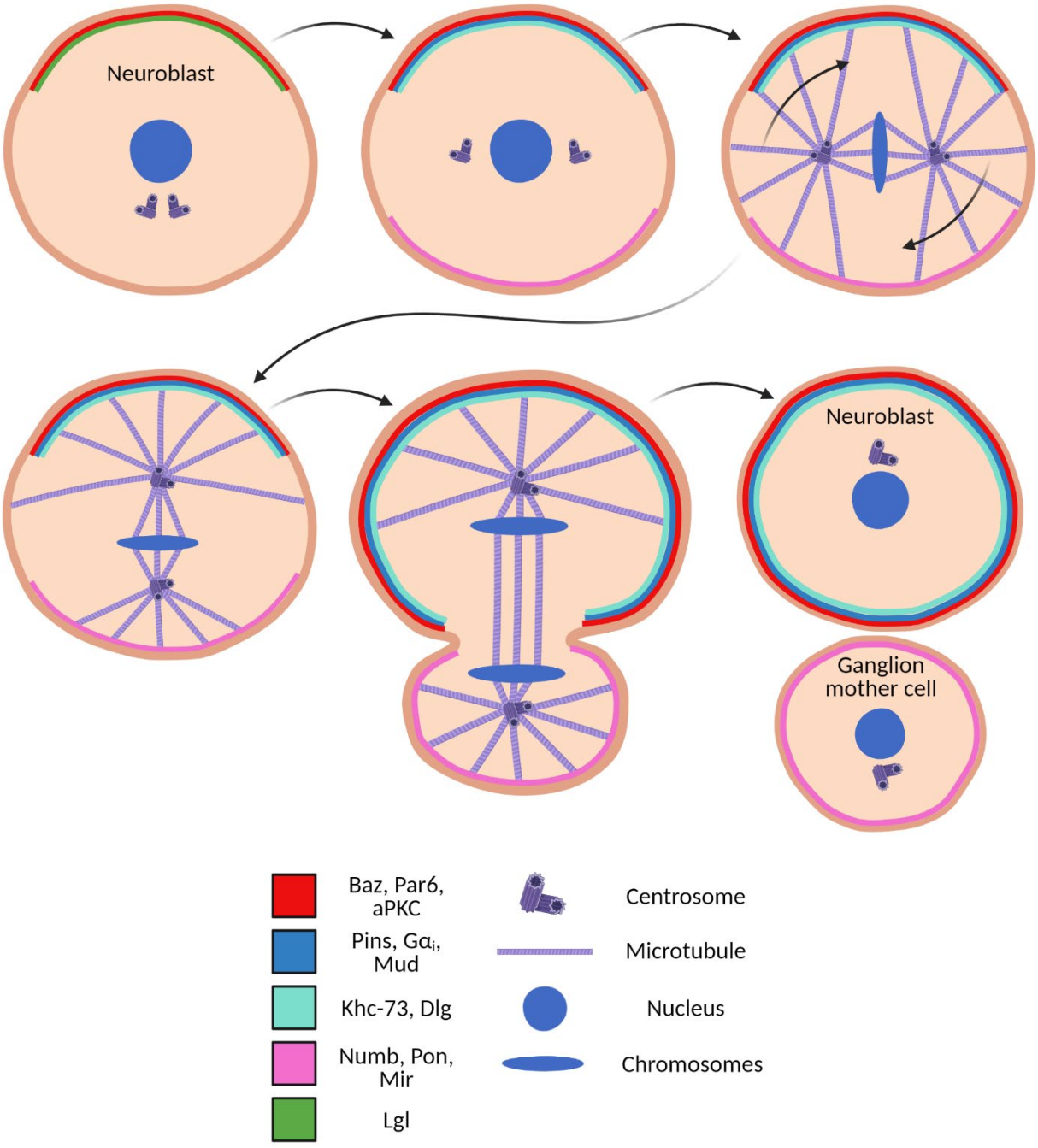

Figure 1.7 **Asymmetrical cell division in the *D. melanogaster* neuroblast.**
Asymmetric localisation of the apical polarity effector PAR proteins (Baz (Par3), Par6 and PKC-3 is predetermined in the neuroblast as site of delamination from the neuroectoderm. At the apical cortex, the PARs remain inhibited by Lgl until the onset of mitosis when Aurora-A kinase phosphorylates Par6 which then releases Lgl. aPKC then phosphorylates Numb, Pon and Miranda, restricting their localisation to the basal membrane. The apical PARs recruit the MT force generating complex Pins, Gαi & Mud which recruit dynein to capture astral MTs and orient the mitotic spindle apico-basally. The kinesin Khc-73 aids in this process via interaction with Pins and MTs. The basal centrosome generates a smaller spindle, resulting in the offset of the spindle towards the basal membrane. As such the cleavage plane is similarly displaced and the resultant ganglion mother cell is smaller than the apical renewed neuroblast which will repeat the process.

Asymmetry of neuroblasts is predetermined in the neuroectoderm, from which they derive, where the Bazooka (Par3), Par6 and aPKC complex localises to the apical membrane (Berger, Urban and Technau, 2001). Initially these PAR proteins are held in an inactive state through interaction with Lgl (Lethal giant larva) which inhibits aPKC kinase activity. During mitosis, a series of phosphorylation events guide downstream polarity. The mitotic kinase, Aurora A, phosphorylates Par6, releasing Lgl and activating aPKC which phosphorylates several cell fate determinants. These include Numb (which recruits Pon – Partner of Numb) and Miranda (which recruits Pros and Brat – Prospero and Brain Tumour) which are excluded from the apical cortex and go on to define the basal daughter cell and promote differentiation (Wirtz-Peitz, Nishimura and Knoblich, 2008; Bell *et al.*, 2015; Carvalho *et al.*, 2015).

As well as excluding basal cortical proteins, the apical PAR proteins guide the orientation of the mitotic spindle by recruiting Inscuteable (Insc) to the apical cortex (Schober, Schaefer and Knoblich, 1999; Wodarz *et al.*, 1999). Insc, in turn, recruits a MT interacting complex of proteins including, Partner of Inscuteable (Pins – Human LGN, *C. elegans* GPR-1/2), G protein Gαi and Mud (Mushroom body defect – Human NuMA, *C. elegans* LIN-5). Mud interacts with astral MTs in a dynein-dependent manner which pulls the daughter centrosome towards the apical membrane and orients the spindle apicobasally (Schaefer *et al.*, 2000, 2001; Yu *et al.*, 2000, 2003; Bowman *et al.*, 2006; Izumi *et al.*, 2006; Siller, Cabernard and Doe, 2006; Johnston *et al.*, 2009; Bosveld, Ainslie and Bellaïche, 2017). Mud/Dynein act partially redundantly with the kinesin, Khc-73, which acts to induce Pins/Gα/Dlg polarity and position the spindle. To achieve this, Khc-73 has been proposed to be recruited to the apical cortex, where it binds statically to astral MTs, via Disc large protein (Dlg) which, in turn, is recruited by Pins (Siegrist and Doe, 2005, 2007; Dewey, Taylor and Johnston, 2015; Bergstralh, Dawney and St Johnston, 2017).

As mentioned, the spindle of the neuroblast is asymmetrical. Upon centrosome duplication, the mother centrosome does not recruit pericentriolar material or organise MTs until the onset of mitosis. This delay results in shorter MTs and a smaller spindle from the mother centrosome compared to the daughter. The daughter and mother centrosomes become oriented towards the apical and basal membrane, respectively, such that the daughter centrosome is inherited by the renewed neuroblast cell while the mother centrosome is inherited by the GMC. The smaller spindle of the mother centrosome results in the offset of

the spindle midzone, which determines the position of cell cleavage, towards the basal membrane. As such, the GMC is smaller than the renewed neuroblast upon cell division (Rebollo *et al.*, 2007; Rusan and Peifer, 2007).

Interplay between polarity and the cytoskeleton has been demonstrated in the neuroblast as the GMC always buds from the same site in subsequent cell divisions in a process that depends on the centrosomes and emanating MTs. This is due to extrinsic signalling from the neighbouring sister GMC (Loyer and Januschke, 2018) and to the intrinsic apical positioning of the daughter centrosome from the last division of the neuroblast. If MTs are disrupted during interphase, the apical domain is established ectopically. Once allowed to regrow, the centrosome/MTs will localise towards the new apical cortex. After the next round of division, the membrane region determined to become apical is once again decided by the position of the centrosome/MTs, although the mechanism is not understood. This demonstrates a reciprocal specification of the polarity and spindle axes (Rebollo *et al.*, 2007; Rusan and Peifer, 2007; Januschke and Gonzalez, 2010).

1.5 *C. elegans* as a model.

Extensive research has been performed in the nematode *C. elegans* for over half of a century (Figure 1.8) since Sydney Brenner proposed that the worm would be the future of research using model organisms. *C. elegans* has become one of the most studied organisms in topics such as aging, metabolism and asymmetric cell division (Tissenbaum, 2015; Watts and Ristow, 2017; Boxem and van den Heuvel, 2019) and has contributed to three Nobel Prizes involving programmed cell death, the use of interfering RNA to knock down genes and the development of green fluorescent protein (Grishok, 2005; Chalfie, 2009; Lord and Gunawardena, 2012).

Multiple genetic approaches have been developed and optimised for use in the worm, offering relatively simple techniques to alter gene expression and sequence such as RNAi knockdown and CRISPR. Approximately 83% of the *C. elegans* proteome have human homologues, providing much transferrable knowledge from the *C. elegans* system to our own.

C. elegans provides a useful model of animal development owed to the highly invariant lineages of all 959 somatic cells which have been defined from the zygote. As a transparent organism, alterations within the worm can also be identified with ease through a microscope (Sulston *et al.*, 1983). Through this, the worm has contributed greatly to our understanding of

cellular polarity as defects in polarity can be traced through *C. elegans* development back to the first asymmetric cell division of the zygote. In addition, *C. elegans* are hermaphroditic with short lifespans, allowing for large datasets in relatively short time frames compared to other animals.

Figure 1.8

a.

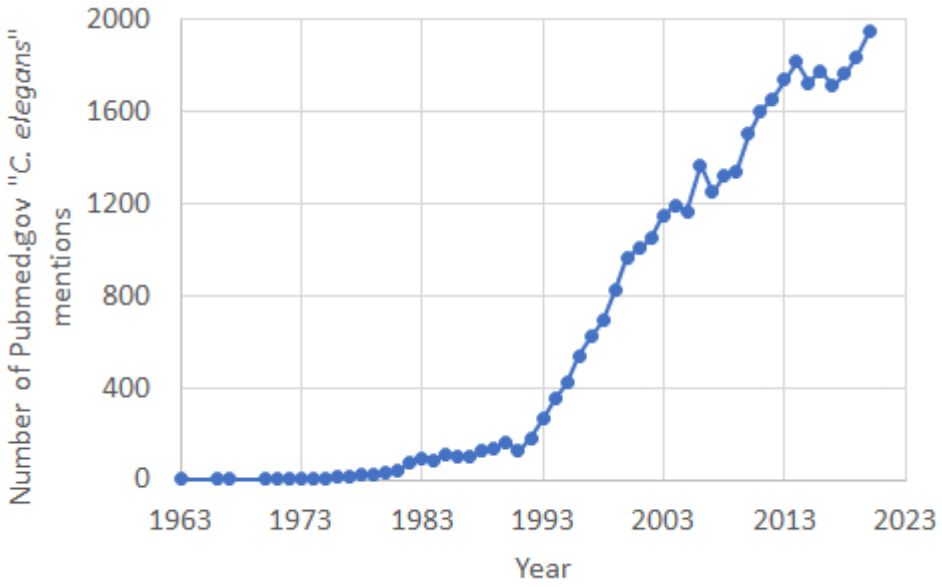

Figure 1.8 **The use of *C. elegans* in research.**

The number of articles published per year mentioning the term "*C. elegans*" according to Pubmed.gov.

1.6 Polarity in the *C. elegans* zygote.

In *C. elegans* development, asymmetry is first observed in the zygote around 30 minutes post-fertilisation. Early experiments showed that this cell develops an anterior-posterior polarity axis dependent on the sperm-derived centrosome (Goldstein and Hird, 1996). As the centrosome develops, the process of symmetry breaking begins, upon which the cytoskeleton undergoes major reorganisation (Strome, 1986; Hird and White, 1993; Guo and Kemphues, 1996; Cheeks *et al.*, 2004; Munro, Nance and Priess, 2004). PAR proteins are the major polarity effector proteins within the zygote. In their absence, the first cell division is symmetric which led to their discovery and naming after their PARtitioning defective phenotype (Kemphues *et al.*, 1988).The initially uniform cortical anterior PAR proteins (PAR-3, PAR-6 & PKC-3) relocate to the cortex that opposes the site of sperm entry and define the anterior domain of the

embryo. In their place, the posterior PARs load onto the vacated cortex and define the posterior domain (Figure 1.9 & Figure 1.11) (Kirby, Kusch and Kemphues, 1990; Guo and Kemphues, 1995; Boyd *et al.*, 1996; Goldstein and Hird, 1996; Cuenca, 2003; Cheeks *et al.*, 2004; Munro, Nance and Priess, 2004; Motegi *et al.*, 2011; Lang and Munro, 2017).

Figure 1.9

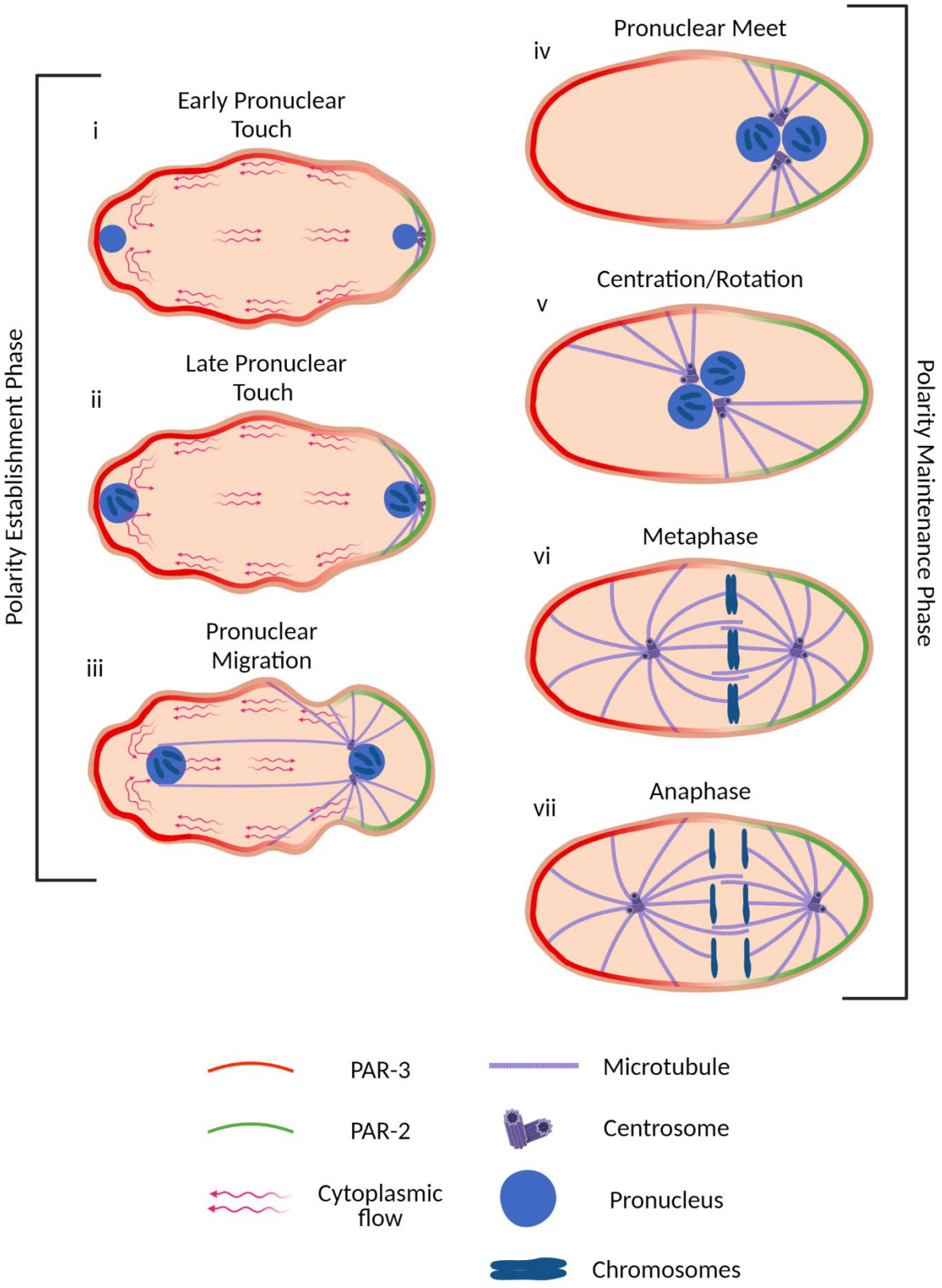

Figure 1.9 **Stages of the *C. elegans* single-cell zygote.**

The setup of the polarity axis within the *C. elegans* zygote is divided into two phases, polarity establishment and polarity maintenance. Within those phases, the zygote's progression from symmetry breaking to pre-cell division have been sub-divided. **(i)** Early pronuclear touch – The time at which the sperm pronucleus and centrosome complex (SPCC) is in contact with the

cortex, chromatin is decondensed, the pronuclei are small, the centrosome may have duplicated but daughter centrosomes are typically unseparated, actomyosin generated flows have initiated, MTs have begun to grow, cortical PAR-3 of the aPARs has begun to retract from the posterior and PAR-2 of the pPARs has begun to load onto the aPAR-cleared posterior membrane. **(ii)** Late pronuclear touch – The sperm pronucleus is still in contact with the cortex, chromatin has begun to condense, the pronuclei have grown in size, the centrosomes will begin to separate around opposite sides of the sperm pronucleus towards the anterior, the anterior domain is further retracted, and the posterior domain grows. **(iii)** Pronuclear migration – The oocyte and sperm pronuclei have begun to move towards each other, pseudocleavage often occurs during this stage where the membrane ingresses similar in appearance to cytokinesis and then relaxes. **(iv)** Pronuclear meet – The pronuclei are in contact with each other, typically meeting in the posterior, actomyosin flows cease. **(v)** Centration/Rotation – The pronuclei and centrosomes move centrally and rotate such that the mitotic spindle aligns along the anterior-posterior axis. Once the spindle is positioned, the nuclear envelopes will break down. **(vi)** Metaphase – The chromosomes become aligned centrally in the zygote attached to MTs of either spindle pole (centrosome), stronger posterior pulling forces offset the mitotic spindle's position to the posterior. **(vii)** Anaphase – Sister chromosomes are pulled apart and segregate to either pole prior to being repackaged into nuclei and cytokinesis occurs.

Prior to symmetry breaking, the posterior PARs (PAR-1 & PAR-2) are prevented from localising to the cortex due to their phosphorylation via the aPAR kinase PKC-3 (human protein kinase C iota) (Hao, Boyd and Seydoux, 2006; Motegi *et al.*, 2011). As such, the system must be shifted in favour of pPAR cortical loading to give them a foothold on their own cortical domain, either through clearance of the aPARs or resistance to phosphorylation (Mechanisms described in sections 1.6.3 & 1.6.4)(Gross *et al.*, 2019). Once pPARs have managed to establish a domain at the posterior cortex they are able to stabilise their own localisation via a positive feedback loop in which PAR-2 oligomerises and recruits the PAR-1 kinase. PAR-1 then phosphorylates the aPARs and excludes them from the posterior domain (Figure 1.11.iii). The biochemical properties of PAR-2 that allow it to overcome PKC-3 phosphorylation are not fully understood, although studies have shown that the RING domain of PAR-2 confers resistance. It is possible that the RING domain increases the affinity of PAR-2 to the cortex or protects the site within PAR-2 that PKC-3 phosphorylates, thus reducing the PAR-2 cortical dissociation rate enough to remain at the posterior cortex. Note, however, that the PKC-3 phosphorylation sites (maximal phosphorylation site – S241) within PAR-2, that prevent PAR-2 membrane localisation (minimal membrane binding region of PAR-2 – amino acids 222-412), are not within the RING domain itself (Ring domain determined by NCBI BLAST tool – amino acids 56-93)(Hao, Boyd and Seydoux, 2006; Arata *et al.*, 2016; Ramanujam *et al.*, 2018).

After polarity has established, mutually antagonistic phosphorylation via PKC-3 and PAR-1 (Figure 1.1) define the anterior-posterior boundary and prevent the invasion of aPARs and pPARs into their opposing domains. Through this, the anterior-posterior axis is able to self-maintain itself after the symmetry breaking cue has ended (Benton and St Johnston, 2003; Hurov, Watkins and Piwnica-Worms, 2004; Hao, Boyd and Seydoux, 2006; Traweger *et al.*, 2008; Hoege *et al.*, 2010; Motegi *et al.*, 2011; Bailey and Prehoda, 2015; Rodriguez *et al.*, 2017). There are other mechanisms by which the pPARs prevent aPAR localisation. The posterior cortical LGL-1, a tumour-suppressor protein, is also an aPAR antagonist believed to interact with PAR-6 and PKC-3 at the anterior-posterior domain boundary. PKC-3 phosphorylates LGL-1 facilitating the cortical removal of PKC-3, PAR-6 and LGL-1, allowing LGL-1 (when over expressed) to restrict the aPARs to the anterior even in the absence of PAR-2 (Beatty, Morton and Kemphues, 2010, 2013; Hoege *et al.*, 2010).

1.6.1 Polarity governs spindle orientation, positioning, and chromosomal segregation.

PAR proteins govern downstream polarity. The formation of the bipolar spindle relies on the asymmetric activity of the dynein microtubule motor protein (and its recruiters LIN-5, GPR-1/2, Gα) at the cortex of zygotes. This cortical dynein complex captures centrosomal MTs in order to generate pulling forces which reorient the mitotic spindle (Figure 1.3.ii) as discussed in section 1.2.3. The cortical dynein complex must align along the anterior-posterior axis prior to cell division to ensure proper spindle organisation and orientation, and hence proper cytokinesis and generation of daughter cells of different size and fates. Studies have shown that the cortical dynein complex responds to signalling cues derived from the PAR proteins. (Tsou *et al.*, 2002; Gotta *et al.*, 2003; Srinivasan *et al.*, 2003; Tsou, Hayashi and Rose, 2003; Wu and Rose, 2007; Panbianco *et al.*, 2008; Park and Rose, 2008; Afshar *et al.*, 2010; Wu, Espiritu and Rose, 2016).

The localisation pattern of the cortical dynein complex during polarity establishment is unclear, however De Simone, Nédélec & Gönczy (2016) show that the G protein regulator GPR-1/2, one of the cortical dynein complex components that tethers dynein to the cortex (Figure 1.3.ii), is carried anteriorly with the polarising actomyosin flow that transport the aPARs away from the posterior (De Simone, Nédélec and Gönczy, 2016). It is possible that the motor complex has a more uniform localisation at the cortex prior to polarity establishment.

After polarity establishment, GPR-1/2 develops a bipolar localisation (anterior dominant) pattern at the cortex. Meanwhile, the DEP domain (Domain found In Dishevelled, Egl-10, and Pleckstrin) containing protein LET-99 is restricted to a band encircling the posterior of the zygote, absent from the posterior pole, via antagonism of the aPARs and pPARs (Figure 1.10). LET-99 downregulates GPR-1/2's activity in its posterior banded domain, resulting in higher net MT pulling forces at the anterior cortex and the posterior pole which act upon the centrosomes. Prior to nuclear envelope breakdown, the centrosomes are tethered to the sperm pronucleus, existing as the sperm pronuclear-centrosome complex (SPCC), by the hook family protein ZYG-12 which is bound to the pronuclear membrane via SUN-1 and to the centrosome via the dynein subunit DLI-1 (Malone *et al.*, 2003; Minn *et al.*, 2009; Zhou *et al.*, 2009). These centrosome-pronuclear membrane attachments are permissive to centrosome reorientation around the nuclear membrane and so, despite initially being attached to each other, the centrosomes can move separately around the PN, post-centrosome duplication. Due to the uneven cortical MT pulling forces, as the SPCC is centred towards the anterior, one centrosome will randomly get ahead of the other, causing stronger pulling forces from each pole of the embryo on each centrosome. This is believed to facilitate SPCC rotation (Figure 1.9.v) along the anterior-posterior axis, a process referred to as pronuclear centration rotation (Figure 1.9.iv)(Tsou *et al.*, 2002; Tsou, Hayashi and Rose, 2003; Wu and Rose, 2007; Park and Rose, 2008).

Loss of LET-99, thus loss of GPR-1/2 asymmetrical activity, results in embryos with hyperactive SPCC movement during PN centration/rotation, with reduced competency of the mitotic spindle to orient correctly along the anterior-posterior axis. Zygotes in which the spindle does correctly orient, only do so due to the embryo's ovoid shape. Loss of asymmetry in spherical embryos (induced by chitinase) results in further dysregulation of spindle orientation (Tsou *et al.*, 2002; Tsou, Hayashi and Rose, 2003).

Asymmetric displacement of the mitotic spindle during metaphase/anaphase is essential to produce differently sized daughter cells (Figure 1.10)(See section 1.3.1 for role of spindle in cell cleavage plane determination). PKC-3 is partially responsible for this due to its ability to phosphorylate LIN-5 at the anterior cortex and disrupt cortical dynein recruitment (Portegijs *et al.*, 2016). This asymmetric regulation of pulling forces was demonstrated in a non-phosphorylatable LIN-5 mutant that developed exaggerated spindle "rocking" (oscillations of

the spindle poles perpendicular to the anterior-posterior axis), particularly in the anterior, during metaphase/anaphase. This increased anterior spindle pole rocking to a similar amplitude as the greater WT rocking of the posterior spindle pole. Conversely, a phosphomimetic LIN-5 mutant resulted in suppressed spindle rocking, akin to the WT anterior spindle pole. Together this data showed that the regulation of spindle dynamics is mediated by the asymmetric phosphorylation of LIN-5, as forcing LIN-5 into a uniform phosphorylated-like or non-phosphorylatable state results in symmetric spindle rocking. Interestingly, PKC-3 regulation of LIN-5 appeared specific to metaphase/anaphase as the absence of PKC-3 had little effect on SPCC rotation which similarly depends on cortical dynein complex pulling forces (Galli *et al.*, 2011).

LET-99 also contributes to anaphase spindle positioning through its previously mentioned attenuation of pulling forces, specifically in the lateral-posterior region which effectively concentrates posterior pulling forces towards the posterior pole, unlike in the anterior where lateral pulling forces apparently dampen anterior pole-ward directed pulling forces (Figure 1.10.ii)(Tsou *et al.*, 2002; Tsou, Hayashi and Rose, 2003; Krueger *et al.*, 2010; Bouvrais *et al.*, 2018). It should be noted that LET-99 is not essential for enhanced posterior pulling forces. During early anaphase, GPR-1/2 becomes enriched at the posterior cortex in a PAR dependent manner, generating stronger posterior pulling forces even in the absence of LET-99, albeit in a more unstable manner as the spindle oscillates excessively (Colombo *et al.*, 2003; Park and Rose, 2008). In the absence of PAR-3, the LET-99 band around the cortex is no longer posteriorly displaced but becomes central, GPR-1/2 becomes uniform and the mitotic spindle is positioned centrally during anaphase, demonstrating that pulling forces are dependent on upstream PAR polarity effector proteins (Grill *et al.*, 2001; Tsou *et al.*, 2002; Colombo *et al.*, 2003). Overall, there is a net pull towards the posterior during mitosis in the *C. elegans* zygote, resulting in spindle displacement, elongation, and asymmetrical cell division.

Figure 1.10

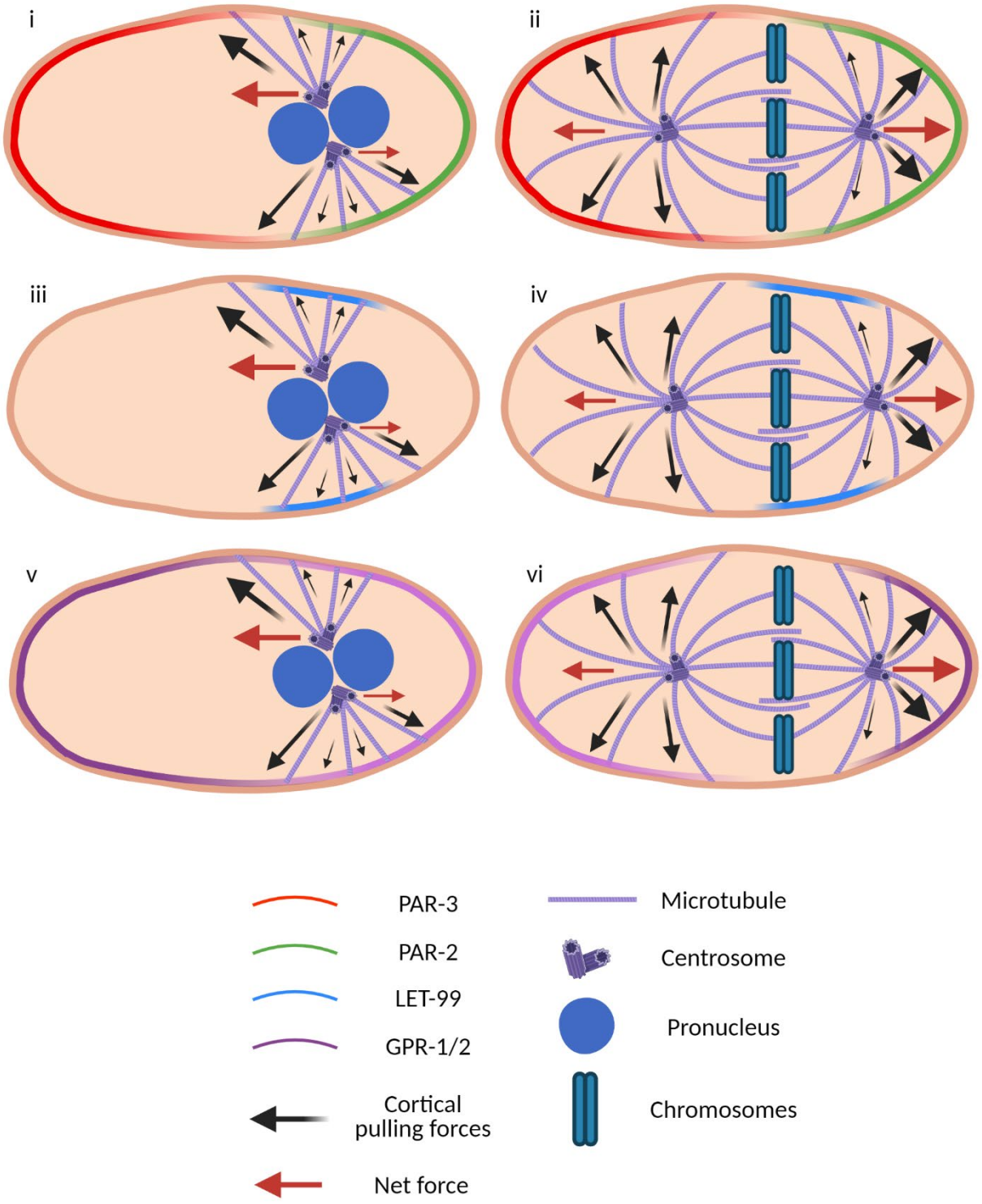

Figure 1.10 **Regulating the cortical forces that bi-orient the mitotic spindle and segregate chromosomes.**

Wild-type localisations of the cortical distribution of polarity proteins and MT force regulators during spindle orientation (i, iii, v) and metaphase/anaphase (ii, iv, vi) are represented here, divided into different figures for clarity (adapted from Tsou et al. (2002) and Krueger et al. (2010)). Under the control of PAR proteins (i), GPR-1/2, of the conserved ternary MT pulling complex, is initially enriched in the anterior (v) where it contributes to greater anterior MT pulling forces and reorientation of the spindle to align along the anterior posterior axis (i). LET-99 contributes to spindle bi-orientation by suppressing pulling forces in the lateral-posterior

region (iii) and increasing the unevenness of pulling forces. Upon the entry of mitosis, GPR-1/2 becomes dominant in the posterior (vi) resulting in stronger net posterior-directed forces, again under the control of PARs (ii). Here, LET-99 (iv) suppresses counterproductive lateral-posterior pulling forces and increases net posterior directed MT dependent pulling forces, displacing the mitotic spindle towards the posterior. Lastly, PKC-3, of the aPAR proteins, phosphorylates LIN-5 and inhibits dynein recruitment, further reducing anterior pulling forces during anaphase. Black arrows represent MT force directions and magnitude. Red arrows represent net force direction and magnitude. (Tsou *et al.*, 2002; Krueger *et al.*, 2010; Galli *et al.*, 2011; Portegijs *et al.*, 2016; Fielmich *et al.*, 2018).

1.6.2 Polarity regulates the cell fate determinants of asymmetric division.

PAR proteins also account for the uneven distribution of proteins and RNAs which determine the fate of each daughter cell during cell division. Examples of PAR dependent cell fate determinants are the RNA-binding protein MEX-5 and the germline RNA granules (RNA & RNA-binding proteins), P granules (Schubert *et al.*, 2000; Tenlen *et al.*, 2008; Daniels *et al.*, 2010; Griffin, Odde and Seydoux, 2011; Strome and Updike, 2015; Seydoux, 2018; Wu *et al.*, 2018). MEX-5 is restricted to the anterior cytoplasm in response to PAR-1 phosphorylation (Griffin, Odde and Seydoux, 2011). In turn, MEX-5 antagonises P granule formation in the anterior resulting in a posterior P granule enrichment (Schubert *et al.*, 2000). P granules are subject to interesting chemistry whereby sequestered molecules by granulation “phase transition” result in reduced concentration of the components in the local cytoplasm around the granule. As a result, molecules from the higher concentrated anterior undergo net diffusion towards the posterior where they are incorporated into more granules. The granules are less diffuse than the free molecules, stabilising their presence in the posterior (Brangwynne *et al.*, 2009; Hoege and Hyman, 2013; Elbaum-Garfinkle *et al.*, 2015; Smith *et al.*, 2016; Putnam *et al.*, 2019). It is believed that P granules are important to prevent premature differentiation of germ cells as absence the of P granules results in the expression of somatic cell markers (Updike *et al.*, 2014). As such, MEX-5 acts to promote the differentiation of the anterior daughter cell (AB cell), of the first cell division, towards somatic cell lines while P granules promote the posterior daughter cell (P1 cell) to generate the germ cell line of the worm (Seydoux, 2018).

As mentioned above, these processes are all the downstream result of a symmetry breaking cue in the single celled zygote derived from the sperm centrosome. In the *C. elegan*s zygote, two pathways have been described in which the centrosome triggers the anterior-posterior

PAR protein axis. One dependent on actomyosin dynamics and a second on MTs (Boxem and van den Heuvel, 2019).

Figure 1.11

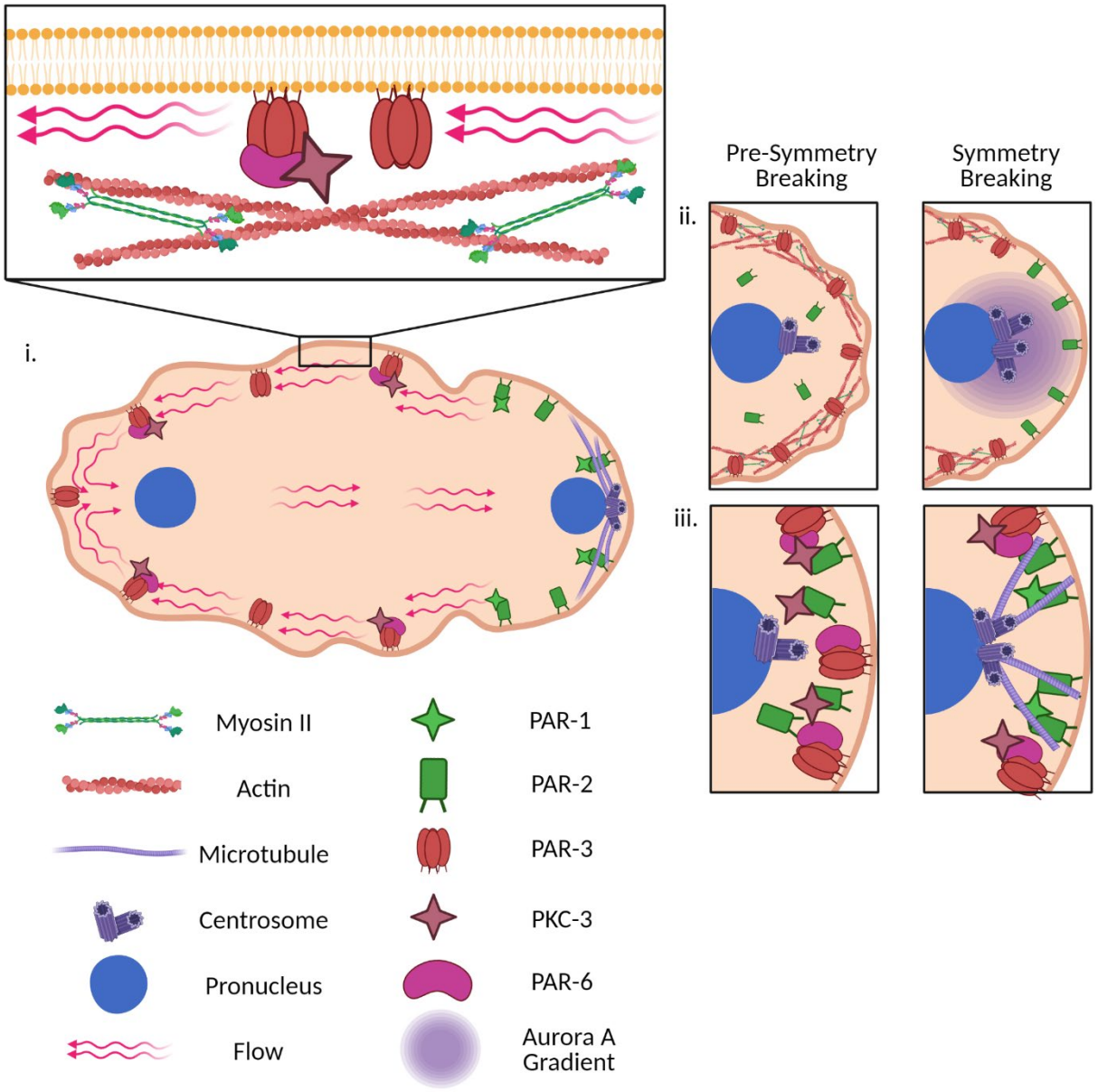

Figure 1.11 **Polarity establishment in the C. elegans Zygote.**
(i) Actomyosin generated flows at the cortex carry the aPAR proteins to the anterior half of the embryo, allowing the pPARs to load onto the vacated posterior membrane. **(ii)** Aurora A diffuses from the centrosome and acts as a cue to instruct actomyosin network relaxation at the posterior pole. This generates a tension gradient required for the anterior directed cortical flows. **(iii)** Pre-symmetry breaking, cortical PKC-3 of the aPARs phosphorylates pPARs to prevent their membrane association. As MTs grow from the centrosome, they interact with PAR-2 and inhibit phosphorylation allowing pPARs to load to the membrane.

1.6.3 Induction of PAR asymmetry via the actomyosin dependent polarisation pathway.

The primary, and better understood, pathway of *C. elegans* zygote polarisation utilises actomyosin force generated cytoplasmic flows, governed by the sperm-derived centrosome, to physically move polarity effector proteins at the cortex and partition the cell (Cheeks *et al.*, 2004; Munro, Nance and Priess, 2004).

Shortly after fertilisation, the actomyosin network exists as a uniform contractile network underlying the membrane (Figure 1.11.ii), controlled by the RhoA GTPase homologue, RHO-1. The activity of RHO-1 is regulated by the guanine nucleotide exchange factor (GEF), ECT-2, and the GTPase activating proteins (GAPs), RGA-3/4 which upregulate and downregulate RHO-1 activity, thus actomyosin contractility, respectively (Jenkins, 2006; Motegi and Sugimoto, 2006; Schonegg, 2006; Schonegg *et al.*, 2007; Fievet *et al.*, 2012; Tse *et al.*, 2012; Masatoshi *et al.*, 2017; Michaux *et al.*, 2018). Upon polarity establishment, the sperm-derived centrosome releases a signal, at the posterior pole of the zygote, which locally shifts the balance of RHO-1 regulation towards its inactive state triggering actomyosin relaxation at this site (Munro, Nance and Priess, 2004; Jenkins, 2006; Zonies *et al.*, 2010; Bienkowska and Cowan, 2012; Kapoor and Kotak, 2019; Klinkert *et al.*, 2019; Zhao *et al.*, 2019). The continued cortical contractions in the distal (future anterior) half of the egg result in a gradient of forces in the cytoplasm close to the membrane. These forces result in the cortical flow of cytoplasm directed towards the contractions – posterior to anterior (Hird and White, 1993; Cheeks *et al.*, 2004; Munro, Nance and Priess, 2004; Mayer *et al.*, 2010; Goehring, Trong, *et al.*, 2011; Wang *et al.*, 2017; Gubieda *et al.*, 2020; Illukkumbura, Bland and Goehring, 2020).

Cortical flows carry cortical components with them including the aPAR proteins (Figure 1.11.i) (Hill and Strome, 1988; Hird and White, 1993; Cuenca, 2003; Cheeks *et al.*, 2004; Munro, Nance and Priess, 2004; Mayer *et al.*, 2010; Goehring, Trong, *et al.*, 2011; Sailer *et al.*, 2015; Dickinson *et al.*, 2017; Padmanabhan, Ong and Zaidel-Bar, 2017). PAR-3's ability to form large clusters is believed to give it the physical properties required to respond to flows. PAR-3 acts as a scaffold to recruit the remaining aPARs, PAR-6 and PKC-3, which are thus also trafficked to the anterior cortex where they define the anterior domain (Robin *et al.*, 2014; Sailer *et al.*, 2015; Dickinson *et al.*, 2017; Rodriguez *et al.*, 2017; Wang *et al.*, 2017). As discussed, PKC-3, acts to prevent the invasion of pPARs onto the same cortical site via phosphorylation and so once the aPARs clear from the posterior, pPARs can then dock to the aPAR-free membrane

(Hurov, Watkins and Piwnica-Worms, 2004; Hao, Boyd and Seydoux, 2006; Hoege *et al.*, 2010; Motegi *et al.*, 2011; Bailey and Prehoda, 2015; Rodriguez *et al.*, 2017). Similarly, pPARs restrict the aPARs to the zygote's anterior which sets up a mutual antagonistic system that allows the anterior and posterior domains to define their own boundaries (Benton and St Johnston, 2003; Cuenca, 2003; Munro, Nance and Priess, 2004; Hao, Boyd and Seydoux, 2006; Traweger *et al.*, 2008; Beatty, Morton and Kemphues, 2010, 2013; Zonies *et al.*, 2010; Hoege *et al.*, 2010; Goehring, Hoege, *et al.*, 2011; Motegi *et al.*, 2011; Sailer *et al.*, 2015; Lang and Munro, 2017).

After polarity establishment, initial strong cytoplasmic flows weaken and the control of actomyosin dynamics is handed over to the now anterior CDC-42 GTPase (Motegi and Sugimoto, 2006; Schonegg, 2006). In the posterior, the CDC-42-GAP, CHIN-1, further helps to maintain the anterior-posterior axis through the inhibition of CDC-42 activity and preventing PAR-6/PKC-3 recruitment (Figure 1.1) (Kumfer *et al.*, 2010; Beatty, Morton and Kemphues, 2013; Sailer *et al.*, 2015).

Just as actomyosin dependent forces are required to polarise the PARs, asymmetric actomyosin activity is dependent on PAR protein domains, generating a co-dependent mechanochemical feedback loop. Indeed, the localisation of the GTPases and their regulators, such as CDC-42 above, that control actomyosin dynamics, are under PAR protein mediated spatial restriction. In the absence of PAR-3 or PAR-2, cortical actomyosin dynamics become uniformly weak or strong in the zygote, respectively. The double loss of PAR-3 and PAR-2 replicates the loss of PAR-3 phenotype suggesting that PAR-3 is capable of stabilising actomyosin at the cortex as opposed to PAR-2 mediated removal (Small and Dawes, 2017). This is backed up by the work of Gross et al. 2019 who used fluorescence recovery after photobleaching (FRAP) to show that the dissociation rate of the *C. elegans* myosin heavy chain orthologue, NMY-2 (non-muscle myosin II), at the anterior cortex is half of that in the posterior. Similarly, co-depletion of *par-2* and *par-6* replicates the NMY-2 dissociation rates of the loss of *par-6* alone suggesting that the posterior domain does not actively antagonise actomyosin dynamics but that the anterior domain promotes them (Gross, Kumar and Grill, 2017; Gross *et al.*, 2019).

Until recently, it was unknown how the centrosome signals for the posterior relaxation of the actomyosin cortex. Three concurrent studies have identified the aurora-A kinase homologue, AIR-1, as a major regulator of the timing of symmetry breaking (Kapoor and Kotak, 2019;

Klinkert *et al.*, 2019; Zhao *et al.*, 2019). Zhao et al. (2019) used FRAP to show that there is a high turnover of GFP::AIR-1 sequestered at the centrosome suggesting high diffusivity, in line with another previous study (Kress *et al.*, 2013). GFP N-terminal tagged AIR-1, however, was incapable of sufficient symmetry breaking, likely through compromised diffusion and/or kinase activity. This was rescued upon drug induced artificial targeting of GFP::AIR-1 to the cell membrane, specifically at the posterior via membrane laser puncture (Zhao *et al.*, 2019). Together this suggests AIR-1 kinase could be the diffuse centrosomal signal which triggers symmetry breaking via local downregulation actomyosin forces (Figure 1.11.ii).

Currently it is unknown how AIR-1 instructs actomyosin relaxation. Targeted inhibition or activation of RHO-1 GEFs or GAPs is an attractive model. Kapoor and Kotak (2019) show that AIR-1 is required for the posterior exclusion of the GEF ECT-2 however there is no current evidence of direct interaction between these molecules (Kapoor and Kotak, 2019).

1.6.4 Induction of PAR asymmetry via the MT dependent polarisation pathway.

In the absence of strong cortical flows, necessary for actomyosin-dependent polarisation, multiple studies were able to show that polarity establishment can still occur in a MT dependent manner (Shelton *et al.*, 1999; O'Connell, Maxwell and White, 2000; Wallenfang and Seydoux, 2000; Hamill *et al.*, 2002; Schonegg, 2006; Tsai and Ahringer, 2007; Zonies *et al.*, 2010; Motegi *et al.*, 2011; Tse *et al.*, 2012; Gross *et al.*, 2019). It has been proposed that MTs are able to protect PAR-2 from PKC-3 phosphorylation which would otherwise prevent pPAR cortical localisation (Motegi *et al.*, 2011).

The relevance of MTs in polarity establishment in *C. elegans* zygotes has been controversial. Tsai and Ahringer (2007) showed that strong depletion of tubulin, with seemingly normal centrosome development, led to delayed polarity establishment (Tsai and Ahringer, 2007). Bienkowska and Cowan (2012), however, later argued that loss of tubulin simply results in the inability to constrain the centrosome to the cortex and reasoned that this results in a weaker symmetry breaking signal required by the actomyosin-dependent pathway. They claimed that embryos matched by centrosome distance to the cortex took the same amount of time from the completion of meiosis II to symmetry breaking regardless of the presence of tubulin. Closer inspection of their graph (Figure 1.12), however, suggests that this is not the case. By comparing their plot of embryos in which centrosomes have been forced away from the cortex

by physical compression (purple) and the embryos in which centrosomal MT growth has been inhibited (*γ-tubulin* RNAi) (green & yellow), there appears to be a larger delay of symmetry breaking of a given distance of the centrosome to the cortex in embryos that do not have MTs. This suggests there is an additional role of MTs in polarity establishment beyond restricting the centrosome to the cortex to aid the actomyosin dependent pathway. A greater N number would have been beneficial to distinguish the datasets, with and without centrosomal MTs (Bienkowska and Cowan, 2012).

Figure 1.12

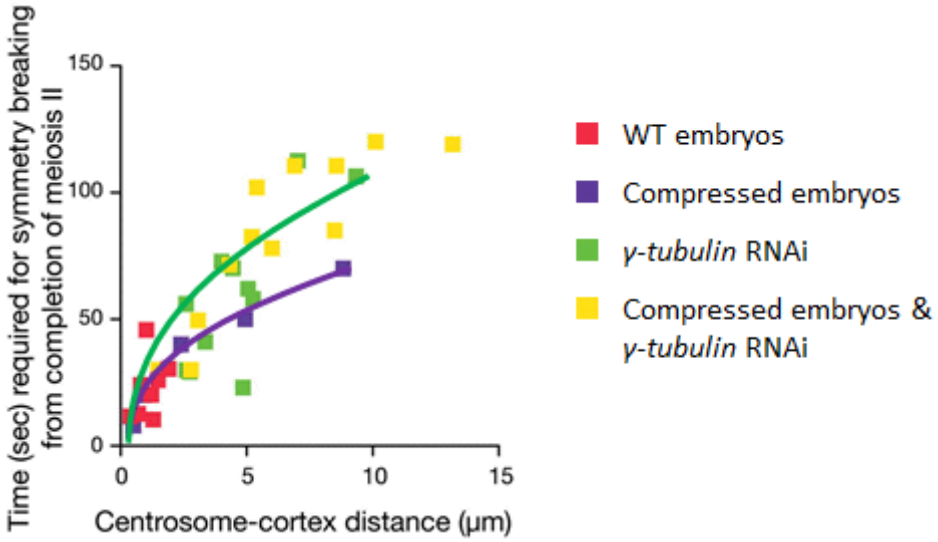

Figure 1.12 **Loss of centrosomal MTs results in delayed symmetry breaking independently of centrosome-cortex distance**.

Graph adapted from Bienkowska & Cowan, 2012 showing the time taken for symmetry breaking post meiosis II. Rough curves of best fit have been overlayed on the compressed embryos (purple) and *γ-tubulin* RNAi (green) data to highlight the difference between these conditions (Bienkowska and Cowan, 2012).

In the absence of flows to physically remove aPARs from the posterior, it has been unclear how pPARs could make the transition from the cytoplasm to the cortex and overcome the initial antagonism of PKC-3 phosphorylation. Through co-immunoprecipitation and immunofluorescent staining, Motegi et al. (2011) were able to show that MTs and PAR-2 interact and colocalise *in vitro.* They also showed that PKC-3 phosphorylates and inhibits PAR-2 binding to phospholipids (required for PAR-2 membrane docking *in vivo*) but that this phosphorylation is blocked upon the addition of MTs. The lab developed two PAR-2 mutants

(R163A & R183-5A) unable to interact with MTs. *In vivo*, they assessed the effect of these PAR-2 mutants and showed that they were incapable of developing a posterior domain in the absence of cortical flows, unlike WT PAR-2 (Motegi *et al.*, 2011; Gross *et al.*, 2019). Motegi et al. presented evidence of a model in which MTs act to protect PAR-2 from PKC-3 phosphorylation and shift the pPAR association/ dissociation rates at the cortex in favour of pPAR membrane recruitment (Figure 1.11.iii). As a result, MTs promote the formation of a posterior domain which is capable of mutual antagonism with the anterior domain to establish and maintain polarity even in the absence of cortical flows.

Klinkert et al. (2019) recently studied the role of MTs further in embryos depleted of AIR-1 (Section 1.6.3) in which they saw PAR-2 establish cortical domains at both poles of a subset of embryos. Under *air-1* RNAi, they assessed the recruitment of PAR-2 to the cortex in the two mutants (R163A & R183-5A) in which PAR-2 is supposedly incapable of interacting with MTs. In this scenario, PAR-2 was completely absent from the cortex, indicating that polarisation in the absence of *air-1* is mediated by PAR-2-MT binding, thus supporting the data of Motegi et al. (2011). Contradicting this finding, however, Klinkert et al. (2019) also show that WT embryos lacking functional NMY-2 and AIR-1 can still form cortical PAR-2 domains upon nocodazole treatment (i.e. PAR-2 domains that form independently of MTs or cytoplasmic flows) (Klinkert *et al.*, 2019). This suggests that these PAR-2 mutants may have secondary defects, such as defective membrane binding that are then insufficient in loading to the cortex with simultaneous compromised MT binding and cortical flows.

Interestingly, Klinkert et al. (2019) showed that the PAR-2 domains that establish at both poles do so due to the high curvature of the membrane in those regions. They forced the shape of embryos to change by placing them in triangular chambers. PAR-2 typically formed a domain at the corners of these triangles upon *air-1* RNAi treatment irrespective of the centrosome's position. This suggests that high membrane curvature shows a propensity for PAR-2 recruitment, possibly through increased sequestration or activation of factors involved in an additional pathway of polarity establishment. What these factors are, however, are unknown (Klinkert *et al.*, 2019).

1.6.5 Centrosomal pleiotropic function between polarity establishment pathways complicates the study of each pathway.

Both the actomyosin and MT dependent pathways rely on the sperm-derived centrosome to initiate. This makes it difficult to assess the true contributions of each pathway to polarity establishment as compromising the centrosome automatically results in both pathways being lost (Cowan and Hyman, 2004; Saturno *et al.*, 2017). Conversely, when trying to identify regulators of one pathway, downstream of the centrosome, it is likely that the alternative pathway will mask measurable phenotypes through redundancy. Thus, regulators of either pathway will not be detected.

1.7 The centrosome and polarity in the *C. elegans* zygote.

1.7.1 The importance of centrosome positioning.

<u>The importance of centrosome positioning in polarity establishment.</u>

As mentioned, around 30 minutes after fertilisation the process of symmetry breaking begins. As the centrosome matures, it releases the AIR-1 signal, previously discussed in section 1.6.3, which instructs the contracting actomyosin network to relax in the vicinity of the centrosome. The AIR-1 signal is believed to be diffuse and, as such, the centrosome can initiate polarity establishment anywhere within the cell at a distance from the cortex. The closer the centrosome is to the cortex, however, the sooner the symmetry breaking process occurs. Bienkowska & Cowan (2012) demonstrated that the distance of the centrosome to the cortex correlates highly with the time taken from the completion of meiosis II to the onset of polarity establishment (Cowan and Hyman, 2004; Bienkowska and Cowan, 2012; McCloskey and Kemphues, 2012).

Centrosome positioning is also important to ensure that aPAR clearing/ pPAR loading does indeed occur at the far posterior so that polarity is established along the correct axis. Multiple studies have confirmed that the axis of polarity highly correlates with the position of the centrosome during symmetry breaking (Goldstein and Hird, 1996; Sadler and Shakes, 2000; Cowan and Hyman, 2004; Kimura and Kimura, 2020). Of note, Kimura & Kimura (2020) demonstrated that although centrosomes typically remain in the posterior half of the zygote, they can drift to the anterior. In zygotes with an anterior centrosome, the polarity axis is

reversed and the anterior-posterior domains are flipped as cortical actomyosin flows are directed away from the anterior centrosome, carrying the aPARs with them (Kimura and Kimura, 2020).

The longer the centrosome remains in contact with the cortex, more robust (i.e. less likely to fail) the symmetry breaking process is (Lyczak *et al.*, 2006; Fortin *et al.*, 2010; Saturno *et al.*, 2017). Saturno et al. (2017) demonstrated that the SPCC becomes aberrantly positioned in mutant embryos of the puromycin sensitive aminopeptidase, *pam-1,* a protein proposed to remove N-terminal peptides and prime proteins for ubiquitylation by ubiquitylase enzymes. In these embryos, centrosome distance to cortex did not correlate with the speed of symmetry breaking as in WT, suggesting PAM-1 may have other unknown effects on polarity (Lyczak *et al.*, 2006; Bienkowska and Cowan, 2012; Saturno *et al.*, 2017). The contact duration of the centrosome to the cortex, however, did contribute to polarity establishment as shorter contact duration to the cortex in *pam-1* embryos resulted in smaller PAR-1 domain sizes. This was rescued upon *dhc-1* depletion which promotes longer centrosome-cortex contact duration. Importantly, this study showed that centrosome-cortex contact is required in both the actomyosin and MT-dependent pathways of polarity establishment. In embryos lacking actomyosin flows (*nmy-2* RNAi), thus relying on MT-dependent pPAR loading, PAR-1 localised more efficiently to the cortex when the centrosome contacted the cortex. Similarly, hallmarks of actomyosin flow-dependent polarity, such as cortical pseudocleavage and posterior NMY-2 clearance, were stronger/ restored in embryos in which the centrosome remained in contact with the cortex for longer (Saturno *et al.*, 2017).

<u>The importance of centrosome positioning in spindle organisation.</u>

The process of organising a bipolar spindle relies on the tight regulation of centrosome positioning in the early zygote. In any dividing mitotic cell, the centrosome must be duplicated, separated, and positioned to flank the genetic material (Processes discussed in section 1.2.3) to produce a bipolar spindle from which the MTs of each centrosome will capture a single chromatid from each chromosome pair to then pull the chromatids apart. Defective centrosome separation can result in embryos in which the spindle poles have not moved far away enough from each other such that the chromosomes do not end up between them. This can lead to improper kinetochore attachment and can result in abnormal chromatid segregation which, if not corrected, can give rise to daughter cells with aberrant chromosome

numbers (aneuploidy) and ultimately lead to cell death or disease states such as cancer (Silkworth and Cimini, 2012).

Centrosome separation relies on multiple active pathways involving both the MTs and actomyosin cytoskeletons, variable by cell type (Agircan, Schiebel and Mardin, 2014). For example, in HeLa cells the centrosomes are held together by MTs which initially resist separation. The linker protein P-cortactin is localised to the centrosomes and interacts with actin to translate actin mediated forces to separate the centrosomes prior to spindle assembly, although the mechanism of force generation is unknown (Wang *et al.*, 2008). In PtK2 cells, astral MTs are tethered to the cell cortex and transmit forces generated by cortical actomyosin dynamics to help pull the centrosomes apart (Rosenblatt *et al.*, 2004) while In *D. melanogaster* embryos, however, actin polymerisation forces drive centrosome separation independently of myosin (Cao *et al.*, 2010). Overall, reducing actin/actomyosin dynamics via drug-induced actin crosslinking or using RNAi to reduce the levels of actomyosin components can reduce the efficiency of centrosome separation in different systems (Rosenblatt *et al.*, 2004; Wang *et al.*, 2008; Cao *et al.*, 2010; De Simone, Nédélec and Gönczy, 2016).

The actomyosin network imbues the zygote with membrane stiffness required to resist being pulled inwards by cortical MT pulling forces. A “soft” membrane results in compromised spindle movement during anaphase and the membrane moves towards the spindle rather than the spindle towards the zygote poles (Redemann *et al.*, 2010). It is unknown whether this membrane rigidity is also required for effective centrosome separation. Although centrosome/spindle dynamics are compromised in the absence of actin/actomyosin activity, centrosomes can still move away from each other due to the dynamics of the MTs that they emanate, and MT-associated proteins (MAPs) (Maddox and Burridge, 2003; Kunda *et al.*, 2008; Ramanathan *et al.*, 2015).

In *C. elegans* zygotes, as MTs grow radially from the centrosomes, they are captured by dynein attached to both the embryo’s cortex and nuclear membrane (Figure 1.13). The motors of nuclear-anchored dynein walk to the minus-ends of the MTs towards the centrosomes, which actively contributes to pulling the centrosomes apart and around the male pronucleus becoming diametrically opposed (Figure 1.13.ii) (Raaijmakers *et al.*, 2012; De Simone and Gönczy, 2017). The contribution of cortical dynein’s motor activity is less clear and appears to act more like a tether to the cortex which responds to actomyosin flows. The force of cortical

flows is transduced via the centrosomal MTs and drives the separation of centrosomes as in PtK2 cells, mentioned above (Rosenblatt *et al.*, 2004; Nguyen-Ngoc, Afshar and Gönczy, 2007; Kotak and Gönczy, 2013; Rose and Gönczy, 2014; De Simone, Nédélec and Gönczy, 2016; De Simone and Gönczy, 2017; Boudreau *et al.*, 2019).

Figure 1.13

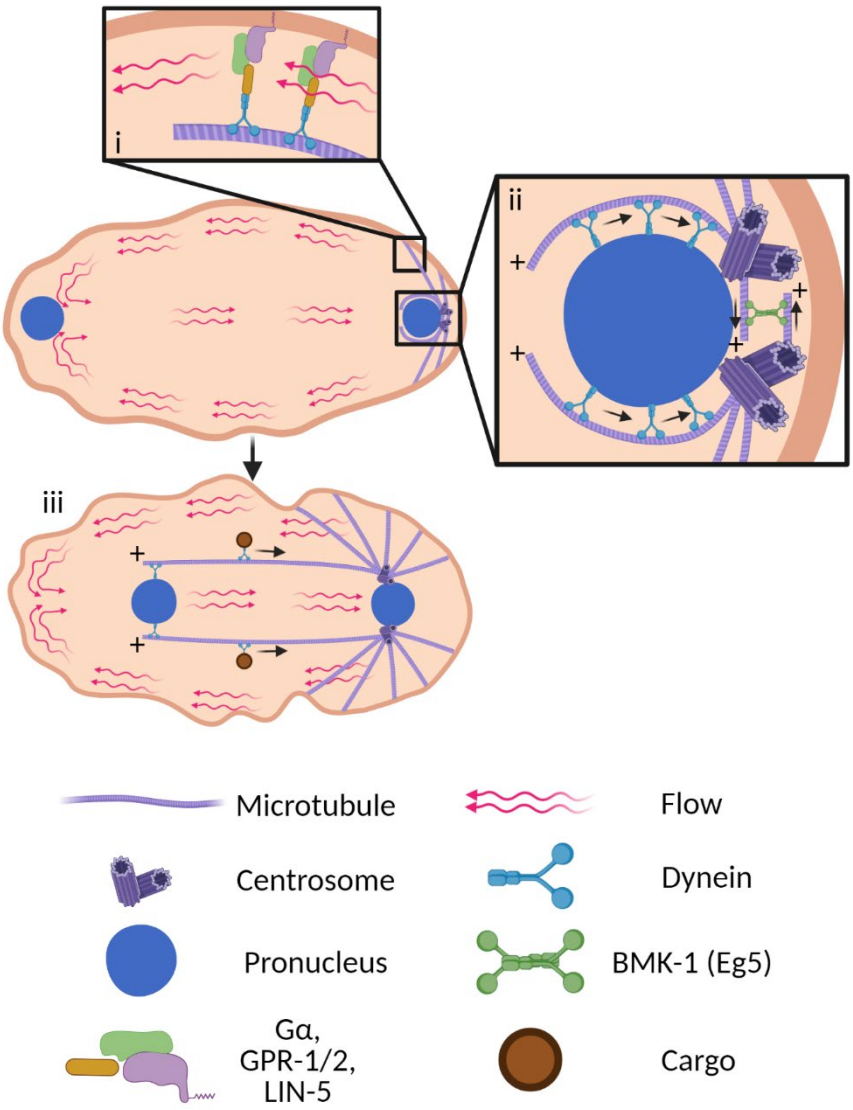

Figure 1.13 **Modes of centrosome separation in the *C. elegans* zygote.**

In *C. elegans* zygotes, centrosomes separate via the dynamics of the MTs that they organise. **i**: Centrosomal MTs are caught by cortically anchored dynein which is carried anteriorly by actomyosin-driven cytoplasmic flows. As a result, the MTs pull on each centrosome at opposite sides of the sperm pronucleus as the centrosomes are typically situated at the far posterior pole. This pulls the centrosomes apart. **ii**: Pronuclear bound dynein binds to MTs growing from the centrosomes and walks towards the minus-ends. The result is the centrosomes being pulled around the pronucleus away from each other. Although not directly demonstrated in *C. elegans*, homotetrameric (back-to-back) Eg5 in mammals has been shown to bind to antiparallel MTs that grow between the centrosomes. As a plus-end directed kinesin, Eg5 walks towards the plus-ends of both MTs and slides them apart, helping to push the

centrosomes apart. The *C. elegans* Eg5 homologue BMK-1 has not been shown as essential for the process suggesting it may act redundantly with another kinesin if this mechanism exists in the worm. Centrosomal MTs also physically push on the opposing centrosome as they grow, further contributing to centrosome separation. **iii**: Once the centrosomes have separated and travelled around the pronucleus to face the anterior, the MTs extend to the anterior and are bound to by dynein tethered to the oocyte pronucleus which then walk towards the centrosomes. This generates force which pulls the centrosome further around the sperm pronucleus and pulls both pronuclei towards each other. Similarly cytoplasmic dynein can bind to the MTs and carry cargo towards the posterior. This generates drag in the cytoplasm which also pulls on the centrosomes and sperm pronucleus towards the anterior.

The position of the centrosome, during early establishment in the *C. elegans* zygote, is critical in the process of actomyosin force-dependent centrosome separation. 1) The centrosomes are initially situated between the sperm pronucleus and the cortex, at the posterior pole of the zygote. 2) MTs growing from the centrosomes are captured by cortically anchored dynein in complex with LIN-5, GPR-1/2 & Gα. 3) Anterior-directed cortical cytoplasmic flows carry the dynein complex anteriorly. 4) Flow forces are transduced to the centrosomes via the cortically tethered MTs. 5) The centrosomes are pulled around the pronucleus, forcing them apart (Figure 1.13) (Rosenblatt *et al.*, 2004; De Simone, 2016; De Simone, Nédélec and Gönczy, 2016; De Simone and Gönczy, 2017; De Simone *et al.*, 2018).

Computer simulations of the zygote have been used to model the potential effects that 1. Increased distance of the SPCC to the cortex, and 2. Altered orientation of the centrosomes around the PN, with respect to the embryo cortex, would have on the distance between the centrosomes over time (centrosome separation efficiency) (De Simone and Gönczy, 2017; Boudreau *et al.*, 2019). The computer modelling data suggested that centrosome separation would indeed be compromised by increased distance to the cortex (De Simone and Gönczy, 2017) and abolished if the centrosomes face the centre of the zygote rather than the cortex (Boudreau *et al.*, 2019). Various techniques have been used to recreate these centrosome position changes *in vivo*. For example, Boudreau et al. (2019) show that loss of protein phosphatase 2A (PP2A) activity results in embryos in which the centrosomes face the centre of the zygote rather than the cortex and so centrosome separation, prior to nuclear envelope breakdown, fails (Boudreau *et al.*, 2019). Labs have also produced embryos in which the SPCC becomes distanced from the cortex through physical compression of the embryo (Bienkowska and Cowan, 2012) or knockdown of *pam-1* (Fortin *et al.*, 2010). These studies, however, focus

on the effect that aberrant SPCC localisation has over polarity specification rather than the effects on centrosome separation.

In addition to cortical forces, forces between the centrosomes can aid in centrosome separation as MTs grown from each centrosome physically push the opposite centrosome away (Figure 1.13.ii) (De Simone and Gönczy, 2017). In certain animals (e.g., humans), the kinesin Eg5 is recruited as a tetramer to these inter-centrosomal antiparallel MTs, bundling them. Eg5, by walking towards the plus-ends of each track, acts to slide the centrosomes apart and form the bipolar spindle (Kapitein *et al.*, 2005; Tanenbaum *et al.*, 2009; Vanneste *et al.*, 2009; van Heesbeen *et al.*, 2017). A homologue of Eg5 has been identified in *C. elegans* (BMK-1). Upon investigating BMK-1's role during spindle formation in the single-cell zygote and centrosome separation in the 2-cell zygote, BMK-1 was found not to be essential to the processes as Eg5 is. This suggests there may be redundancy with another gene in the worm (Bishop, Han and Schumacher, 2005; Saunders *et al.*, 2007; Bondaz *et al.*, 2019). Recent work has demonstrated that Eg5 acts redundantly in human cells with Kif4a/PRC1 during anaphase. Both Eg5 and Kif4a/PRC1 have high affinity to antiparallel MTs of the mitotic spindle where they walk towards the MT plus-ends and slide the MTs apart and aid chromosomal segregation (Vukušić *et al.*, 2021).

As the centrosomes are pulled forwards around either side of the sperm pronucleus, the MTs they emanate are captured by dynein attached to the oocyte-derived pronucleus. Moments before this occurs, the female pronucleus is guided by central posterior directed flows toward the sperm pronucleus in the "slow phase" of pronuclear migration (Figure 1.9.iii). Oocyte attached dynein then walks towards the minus-ends of the centrosomal MTs which pulls the two pronuclei together, the "fast phase" of pronuclear migration. The result is the stage termed pronuclear meet, when the pronuclei are in contact with each other and the centrosomes are positioned at either side (Figure 1.9.iv). The pronuclei and centrosomes then rotate such that the centrosomes align along the anterior-posterior axis with the genetic material between them, ready for the next staged of metaphase/anaphase (Figure 1.13.iii) (De Simone *et al.*, 2018).

1.7.2 Mechanisms of centrosome positioning.

Coordinating the position of the centrosome in the zygote is finely controlled in a timely manner. *C. elegans* eggs are driven through the oviduct and into the spermatheca, proximal side (typical future posterior) first, opposite to the anterior where the oocyte nucleus sits, and meiosis occurs (Figure 1.14.i). As a result, sperm cells typically fuse with eggs at the posterior membrane where polarity establishment is then triggered and anteriorly directed cortical actomyosin flows are initiated (discussed in section 1.6.3) (Goldstein and Hird, 1996; Kimura and Kimura, 2020). Due to the ovoid shape of the embryo, the cortical flows meet at the far anterior and converge inwards to produce a posteriorly directed central cytoplasmic flow. This posterior flow contributes to restricting the SPCC to the far posterior which promotes a stronger signal from the centrosome to the cortex, enhancing polarity establishment (Figure 1.14.iii) (Hird and White, 1993; Bienkowska and Cowan, 2012; Saturno *et al.*, 2017; Mittasch *et al.*, 2018).

Figure 1.14

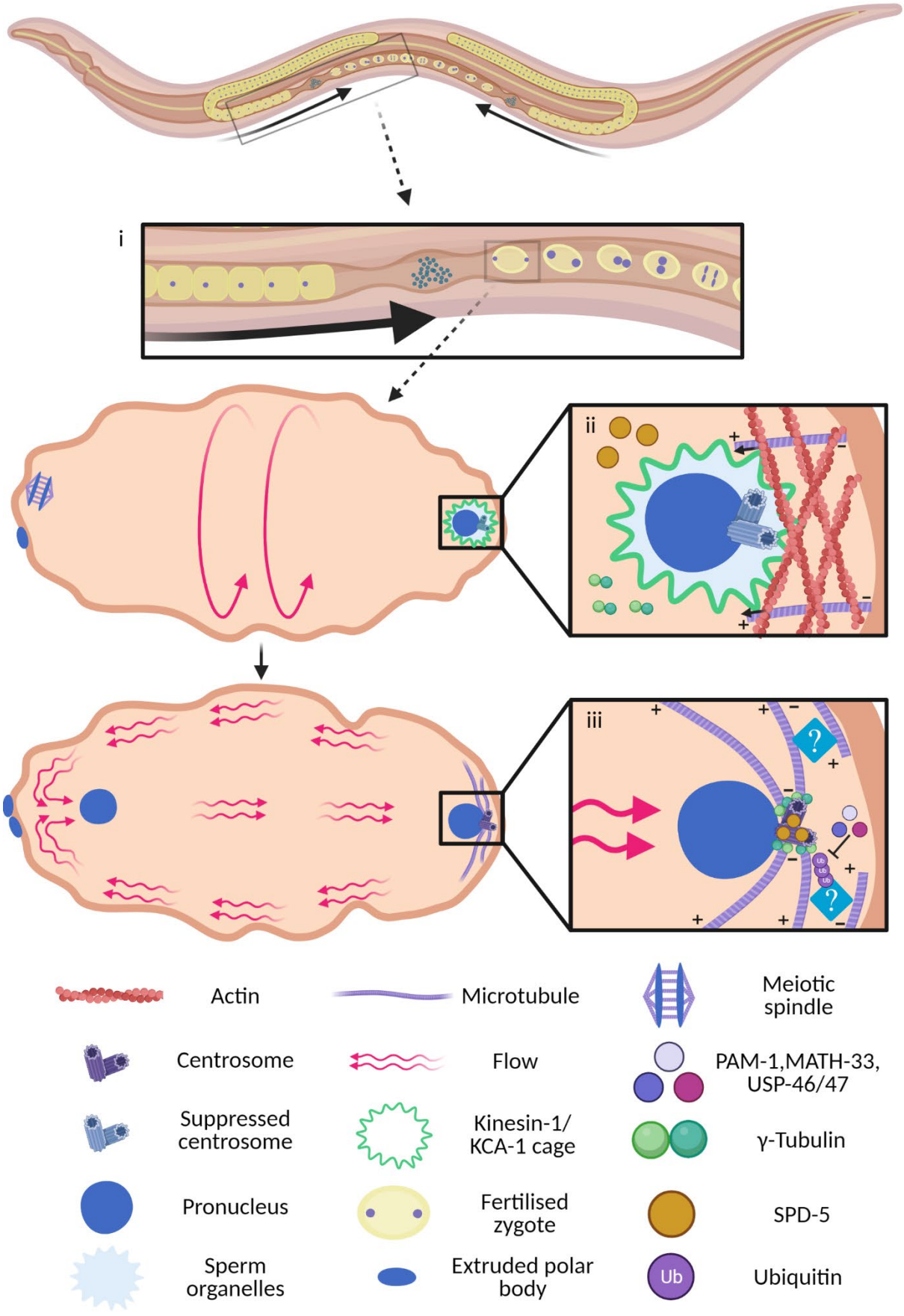
i
ii
iii
Actin
Microtubule
Meiotic spindle
Centrosome
Flow
PAM-1,MATH-33, USP-46/47
Suppressed centrosome
Kinesin-1/ KCA-1 cage
γ-Tubulin
Pronucleus
Fertilised zygote
SPD-5
Sperm organelles
Extruded polar body
Ub
Ubiquitin

Figure 1.14 **Mechanisms of centrosome positioning in the early *C. elegans* embryo.**

Centrosome positioning to the posterior cortex of the *C. elegans* zygote is maintained from the end meiosis to centrosome separation to ensure polarity establishment and centrosome separation occur correctly and in a timely manner. Multiple mechanisms are in place to ensure the centrosome's position is held. **(i)**: Oocytes pass through the oviduct and into the spermatheca such that the site of sperm entry (proximal/future posterior) is invariable at the site opposite to the oocyte meiotic spindle (distal/future anterior). **(ii)**: An unknown component in the cell tethers the sperm-derived unit of organelles (i.e., centrioles, proteasomes, mitochondria, and membranous organelles) to F-actin at the posterior membrane to prevent dissociation of the sperm-pronucleus centrosome complex (SPCC) from the cortex. At the same time, kinesin-1 and its adapter KCA-1 form a "cage" around the unit to prevent the access of SPD-5 and γ-tubulin to the centrosome, hence inhibiting centrosome maturation and MT nucleation. As a result, MTs will not grow and risk interacting with the meiotic spindle should they become near to each other. Kinesin-1 also interacts with MTs tethered to the cortex, oriented plus-end inwards. As a plus-end directed motor, kinesin-1 carries the sperm-derived unit a small distance away from the cell membrane. Finally, the same kinesin generates cytoplasmic streams at the cortex of the zygote during meiosis via carrying the Golgi apparatus along cortical MTs which generates drag within the cytoplasm. These streams are directed around the short axis of the embryos and are prone to directional change, thus making long range travel of the SPCC difficult during meiosis and preventing SPCC translocation to the anterior. **(iii)**: Upon polarity establishment, the actomyosin-dependent cortical flows driven towards the anterior generate a posterior counter current centrally in the cell which forces the centrosome to stay close to the posterior pole. Now that the centrosome has matured, MTs are nucleated radially. We hypothesise that interaction between centrosomal and cortical MTs may contribute to restricting the centrosome to the posterior pole as depletion of MTs via γ-tubulin knockdown results in dissociation of the centrosome from the cortex. How this interaction would be mediated is not yet known. The deubiquitylation enzymes (DUBs) MATH-33, USP46 & USP47 along with PAM-1, suspected to prime proteins for deubiquitylation, are all required to maintain the centrosome's position to the posterior pole. It is likely that they target proteins required for centrosome positioning to prevents its degradation thus ensure the centrosome is positioned normally. For illustrative purposes and theorising, the DUBs are shown here to target the unknown candidate, that mediates centrosomal-cortical MT interaction, after it has been tagged by ubiquitin.

Prior to symmetry breaking, the SPCC has a low chance of moving away from the cortex. In wild-type (WT) conditions the chance of the SPCC settling in the anterior half of the zygote is low but does occur, resulting in reversed polarity (Kimura and Kimura, 2020). This phenomenon must be prevented to stop the premature exposure and interaction of the sperm derived asters and the anterior spindle of the oocyte. Failure to do so can cause erroneous polar body extrusion which results in a triploid zygote or meiotic arrest (McNally *et al.*, 2012). Embryos have multiple mechanisms to ensure the SPCC remains in the posterior half of the zygote, thus ensuring that the centrosome signals for the cessation of actomyosin contractility at the posterior cortex and that the duplicated centrosomes can separate efficiently.

For example, although not well understood, several proteins involved in protein post-translational modification, such as the previously mentioned PAM-1, have been identified as required to regulate the centrosome's position at the posterior pole of the zygote. McCloskey and Kemphues (2012) demonstrated that the absence of the partially redundant deubiquitylating enzymes (DUBs) MATH-33, USP-46 and USP-47 resulted in increased distance of the centrosome to the cortex in fixed embryos and reduced centrosome-cortex contact durations in live experiments, concurrent with compromised loading of pPARs to the cortex (McCloskey and Kemphues, 2012). It is possible that DUBs prevent ubiquitin-mediated degradation of proteins that are required to restrict the centrosomes to the cortex. As such, in the absence of these DUBs, the restrictive proteins would be degraded, and the centrosome cannot be held at the posterior pole as effectively.

During meiosis II, the cytoplasm of the zygote moves in bulk in a process called "meiotic cytoplasmic streaming" (MeiCS). MeiCS depends on the motor protein kinesin-1 (UNC-116) which binds to cortically localised MTs and walks towards their plus-ends (Figure 1.14.ii). The kinesins are able to carry endoplasmic reticulum as cargo along the MTs which generates drag in the cytoplasm and, in turn, produces a localised flow. Through positive feedback, additional MTs caught in the stream align and promote more efficient and stronger flows (Kimura *et al.*, 2017). Immediately after fertilisation, the sperm derived organelles (i.e. centrioles, proteasomes, mitochondria and membranous organelles) act as a cohesive unit (hence referred to as the sperm-derived unit prior to centrosome maturation and becoming the SPCC). This sperm-derived unit moves together in the zygote in response to strong MeiCS (Hajjar, Sampuda and Boyd, 2014; Panzica *et al.*, 2017). Panzica et al. (2017) show that the

components of the sperm-derived unit interact with F-actin, via an unknown intermediate, tethering the sperm-derived unit to the posterior cortex to restrict movement (Panzica *et al.*, 2017). In addition, these MeiCS flow around the long axis of the embryo, prone to frequent directional change, making them inefficient in transporting the sperm-derived unit over long distances, and hence the sperm-derived unit generally remains in the posterior half of the cell (Figure 1.14) (Kimura *et al.*, 2017; Kimura and Kimura, 2020).

Kinesin-1 performs a further role to prevent the sperm aster from being exposed to the meiotic spindle by suppressing centrosome maturation. McNally et al. (2012) showed that, despite being present throughout most of meiosis, the sperm-derived centrioles will not begin to build the PCM from prometaphase I to anaphase II. They showed that kinesin-1 and its cargo adapter protein (KCA-1) encapsulate the sperm-derived unit and propose that this "cage" prevents the premature recruitment of γ-tubulin and SPD-5, markers of centrosomal maturation (Figure 1.14). Upon loss of the kinesin-1 heavy chain (UNC-116) or KCA-1, long astral MTs prematurely grow which interact and interfere with the meiotic spindle, resulting in the failure of polar body extrusion and produce triploid embryos. The absence of either protein also results in a reduced distance of the sperm-derived unit to the cortex prior to MeiCS (McNally *et al.*, 2012). This suggests that kinesin-1 may act to carry the sperm-derived unit a small distance away from the cortex on inward directed cortical MTs using its motor ability. One might expect the centrosomal MTs, prematurely grown in the absence of kinesin-1, to grow and push away from the cortex, thus increase the distance of the sperm-derived unit from the cortex, however this is not the case. In the combined absence of KCA-1 and SPD-5, thus no premature centrosomal MTs, the centrosome regained its distance from the cortex during meiosis. This suggests that centrosomal MTs act to restrict the sperm-derived unit's position, thus reduce the distance of the centrosome to the cortex in the absence of kinesin-1 or KCA-1 (McNally *et al.*, 2012).

Astral MTs have been shown to interact with the cortex of cells in a number of ways, some of which I have described previously (e.g. Sections 1.4.1, 1.4.2 & 1.6.1). We wondered, however, if centrosomal MTs could interact with cortical MTs in such a way that would restrict the sperm-derived unit's position. During *C. elegans* meiosis, MTs are enriched at the cortex; a population of which are anchored there by their minus-ends. Of these MTs, some will grow inwards resulting in a perpendicular orientation to the cortex while others lay parallel

(Kozlowski, Srayko and Nedelec, 2007; McNally *et al.*, 2010; Gusnowski and Srayko, 2011; Bienkowska and Cowan, 2012; Kimura *et al.*, 2017). As centrosomes begin to mature and nucleate astral MTs, those MTs will grow outwards radially either terminating end-on perpendicular to the cortex or bending to run parallel to the cortex. As such, these astral MTs will likely run into the cortical MTs in an anti-parallel manner. Bienkowska & Cowan (2012) demonstrated that a reduction of the cortically enriched MTs via *γ-tubulin* or *ran-1* RNAi, or centrosomal MTs via *spd-5* RNAi resulted in increased distance of the centrosome to the cortex of the *C. elegans* zygote prior to symmetry breaking. This suggests a role for both centrosomal and cortical MTs in the positioning of the early centrosome to the posterior cortex in *C. elegans* zygotes and would support a mechanism whereby antiparallel MTs, cortical and centrosomal derived, interact and restrict the centrosome's position. Note that loss of SPD-5 also prevents cytoplasmic flows, however, which are also required to position the centrosome. Other proteins associated with the centrosome have been shown as required for centrosomal MT growth, ZYG-9, TAC-1 & ZYG-8, without compromising actomyosin flows as loss of SPD-5 causes. Their roles in SPCC positioning during pronuclear touch (Figure 1.9.i&ii), however, have not been studied (Matthews *et al.*, 1998; Bellanger and Gönczy, 2003; Srayko *et al.*, 2005; Bellanger *et al.*, 2007; Werner, Munro and Glotzer, 2007; Tse *et al.*, 2012). How antiparallel MTs at this stage would interact is unknown although kinesins are an attractive possible mediator.

Jolly et al. (2010) demonstrated that the conserved kinesin-1 motor protein is able to bind to two MTs via its head and tail and walk along one of the MTs to facilitate sliding. The lab showed that in actin polymerisation inhibited (cytochalasin D treatment) *D. melanogaster* S2 cells, kinesin-1 mediated MT sliding is required for the formation of peripheral cell projections, likely from the MTs pushing out at the membrane. The lab later repeated this work and found that MT-MT sliding similarly contributes to initial neurite extension in early neurons (Jolly *et al.*, 2010; Lu *et al.*, 2013; Yan *et al.*, 2013). MT-MT sliding also contributes to enhanced cargo transport and the generation of cytoplasmic streaming forces (Kulić *et al.*, 2008; Lu *et al.*, 2016).

As discussed, certain kinesins can capture antiparallel MTs and facilitate sliding if the MT overlap is long enough (Kuan and Betterton, 2016). Eg5, for example, can mediate centrosome separation and bipolar spindle formation (Section 1.2.3) (Kapitein *et al.*, 2005; Tanenbaum *et*

al., 2009; Vukušić *et al.*, 2021). They can also prevent movement once the MTs have slid to their ends, often observed during spindle midzone formation. During anaphase, these opposing roles allow the motor proteins to aid in efficient chromosomal segregation whilst preventing hyper-segregation. In dividing human cells, the conserved chromokinesin Kif4a (*C. elegans* KLP-19) acts during anaphase to perform these roles after it is recruited to antiparallel MTs by the MT bundling protein PRC1 (*C. elegans* SPD-1) (Section 1.3.1, Figure 1.14)(Kurasawa *et al.*, 2004; Zhu and Jiang, 2005; Bieling, Telley and Surrey, 2010; Hu *et al.*, 2011; Subramanian *et al.*, 2013; Wijeratne and Subramanian, 2018; Nguyen, Field and Mitchison, 2018; Hannabuss *et al.*, 2019; Pamula *et al.*, 2019; Asthana *et al.*, 2020; Gaska *et al.*, 2020; Alfieri, Gaska and Forth, 2021; Vukušić *et al.*, 2021; Jagrić *et al.*, 2021).

The shorter overlaps between early astral MTs and cortical MTs would be the ideal conditions for a kinesin to act to limit movement (as Kif4a does in late anaphase) and tether the two MT populations, thereby restricting movement of the SPCC. Further investigation of MT-MT interactions will be important to determine the extent this mechanism plays in the regulation of centrosome-cortex contact and could open the possibility that other organelles and cell types similarly rely on MT-MT interaction.

1.7.3 Motor proteins and cell polarity within C. elegans zygotes.

As previously discussed (section 1.2.2), motor proteins move with specific direction along MT arrays (i.e., minus-end vs plus-end targeting) giving them a large role in targeted intracellular transport. Through this, motor proteins can contribute to establishing & maintaining polarity through polarised cargo transport.

For example, the epithelial cells present with asymmetric enrichment of different proteins at the apical and basolateral membranes. Membrane trafficking has been demonstrated as an important mechanism to regulate the appropriate levels and asymmetrical localisations of proteins at the cell surface. Vesicles containing the proteins, either recently internalised or to be externalised are transported within the cell by motors and the processes of endocytosis and exocytosis remove and replace the protein from the cell membrane, respectively (Jewett and Prekeris, 2018; Xie, Miao and Blankenship, 2018)

Nakayama et al. (2009) demonstrated that endocytosis is enriched in the anterior of *C. elegans* zygotes once the anterior-posterior polarity axis is established. Through depleting the large

GTPase dynamin, required for endosome scission, the lab showed that PAR-6 associated endosomes appear at the membrane because they are unable to pinch off and become internalised. Interestingly, the overall result on polarity is a shrunken anterior domain and an overgrown posterior domain. The lab suggests PAR-6 turnover may be essential to its cortical localisation and that the recycling endosome pathway may contribute to the removal of pPARs that invade the anterior domain (Nakayama *et al.*, 2009). It would be interesting to determine if these phenotypes could be recreated upon depletion of a motor protein.

Motor proteins not only help to establish and maintain polarity, but their activity/localisation is regulated in an asymmetric manner. We previously discussed the cortical MT motor complex containing dynein, tethered to the cortex by LIN-5, and how its asymmetric recruitment positions the mitotic spindle (Section 1.6) (Galli *et al.*, 2011; Portegijs *et al.*, 2016). The mitotic kinase PLK-1 (Polo-like kinase) has also been shown to downregulate LIN-5 localisation and disrupt downstream asynchronous cell division. Prior to cell division, cytoplasmic PLK-1 becomes enriched in the anterior under the influence of PAR proteins, resulting in greater levels of PLK-1 in the anterior AB daughter cell compared to the posterior P1 cell (Budirahardja and Gönczy, 2008; Nishi *et al.*, 2008; Rivers *et al.*, 2008; Bondaz *et al.*, 2019).

It is likely that PLK-1 antagonises LIN-5 via phosphorylation as it does to the human homologue NuMA (S1833/S1834) which downregulates NuMA/dynein/LGN cortical localisation (Sana *et al.*, 2018). This PLK-1-dependent reduction in cortical dynein in the *C. elegans* AB cell has been shown to attenuate the pulling forces required to pull astral MTs and separate centrosomes. Thus, centrosome separation in the AB cell is slower compared to the P1 cell (despite the AB cell undergoing cell division sooner). Interestingly, loss of the kinesin KLP-7 (MCAK) further delays centrosome separation in the AB cell with little effect on separation in the P1 cell. It has been proposed that KLP-7 acts at the cortex to relieve the tension caused by MTs growing and pushing at the membrane through its ability to promote MT depolymerisation. MT depolymerisation can generate pulling forces through persistent interaction with the cortex and by allowing dynein to pull astral MTs more easily and so centrosome separation occurs more efficiently as discussed previously (Section 1.2.3). In the P1 cell, the LIN-5-dynein complex would be sufficient to keep pulling on MTs and induce MT catastrophe in KLP-7's absence whereas the reduced activity of LIN-5-dynein in the AB cell is insufficient to pull on

MTs in the absence of KLP-7. Again, this asymmetric effect of the absence of KLP-7 highlights the interplay between polarity and kinesins (Bondaz *et al.*, 2019).

1.8 Aims/Outline of this work.

This project has aimed to identify potential novel regulators of MT-dependent polarity establishment in the *C. elegans* zygote. Symmetry breaking is a robust process in the worm and, because of this, significant advances in our understanding of the process have been limited to actomyosin force-dependent polarisation which is the dominant driver of polarisation. The role of MTs in polarity establishment are demonstrably important but how is disputed. As such, it is important to investigate other effectors of MT-dependent asymmetry to increase our understanding. To this end, we have screened for genes that result in enhanced lethality in a mutant with diminished actomyosin dynamics during the critical moment of polarity establishment, hence this mutant relies on the MT pathway to induce polarity. We analysed the loss of function (LoF) phenotype from the hits of the screen through immunofluorescent microscopy to characterise the effects of the loss of these genes on polarity and MT organisation.

We further investigated the chromokinesin, KLP-19, from the screen due to its unexpected role during interphase in polarity establishment. Through a combination of fixed and live microscopy techniques, we found that KLP-19 is required for early centrosome positioning and, consequently, efficient cell polarity establishment. We have proposed a model in which KLP-19 mediated interaction between centrosomal MTs and the cortex restricts the centrosome to the posterior pole during polarity establishment, reinforcing robust symmetry breaking.

Chapter 2 Methods and Materials.

2.1 *C. elegans* strains.

Table 2.1 **List of *C. elegans* strains used.**

Code	Genotype	Acquired from/ Reference	Section strain appears in
N2	Wild Type (Bristol)	(Brenner, 1974)	3.2.1, 4.2.1, 4.2.2, 4.2.6, 6.2.2, 7.2.1, 7.2.2, 7.2.3
KK725	nop-1(it142)III	(Rose *et al.*, 1995)	3.2.1, 7.2.3
FGP40	klp-19::GFP(degron);mCherry::His-58	Federico Pelisch (Unpublished)	5.2.1, 5.2.3, 5.2.4, 6.2.1
SV2226	spd-1(he371[egfp::spd-1]) I	Sander van den Heuvel (Unpublished)	6.2.3, 6.2.4
TH66	ebp-2::GFP	(Srayko *et al.*, 2005)	5.2.2, 5.2.3
SV124	lin-5(ev571) II.	(Lorson, Horvitz and Van Den Heuvel, 2000)	4.2.6
TY3558	ruls[pie-1::GFPhis-11] III; ojIs1 [beta-tubulin::GFP]	(Strome *et al.*, 2001)	4.2.2, 4.2.3, 4.2.4
WH12	spd-1(oj5) I.	(O'Connell, Leys and White, 1998)	6.2.2
CZ401	vab-19(e1036) II.	(Ding *et al.*, 2003)	6.2.2

2.1.1 Maintenance of C. elegans.

C. elegans strains were maintained using standard culture conditions on plastic cell culture dishes (60 mm, Jet Biofil, TCD010060) containing 8 ml NGM agar. The plates were seeded with ~300 µl *Escherichia coli* (OP50 - CGC) which was grown overnight at 37 °C in LB (Liquid broth) media before being added to the plate and then left to dry and grow for 2 days before use (Brenner, 1974). Temperature sensitive strains and other mutants were raised at 15 °C and fluorescent reporter strains at 24 °C.

The worms were synchronised for experiments via “bleaching” at the first larval stage (L1) whereby cultured worms and their food supply were destroyed, leaving behind eggs protected by their shell. These eggs hatch into solution with no food and enter a dauer state, suspended as L1 worms until introduced to food, allowing development to resume. Bleaching was performed by collecting worms and eggs from egg-rich plates in M9Tx (M9 with Triton 0.5% (Sigma-Aldrich, T9284)). The solution was centrifuged, the supernatant removed and bleaching solution (~0.7% Sodium Hypochlorite (Honeywell, 239305), 0.7M NaOH (Fisher, 10675692), diluted in ddH_20) added. The supernatant was removed again, and bleach solution re-added. After 4 minutes in bleach solution, the eggs were washed 3x in M9Tx and stored at 15 °C or 20 °C if the worms were grown at 15 °C or 24 °C, respectively. After a minimum of 24 hours, the hatched L1 worms were replated on OP50 seeded agar plates until rich with eggs again for the next round of bleaching or to be plated for experiments.

2.2 RNA mediated interference via feeding.

2.2.1 RNAi plasmids.

The RNase III deficient *E. coli* strain, HT115 (CGC), is transformed with the L4440 vector, which contains a DNA fragment tailored to be specific to genes of interest in *C. elegans* for study. The worms were fed these bacteria as a means of RNAi knockdown in the embryo (*E. coli* provided by the Ahringer RNAi library (Fraser *et al.*, 2000; Kamath *et al.*, 2003)). Controls for RNAi knockdown consist of the HT115 bacteria with no insert in the L4440 vector (Empty vector).

2.2.2 RNAi feeding plate preparation.

NGM plates for RNAi feeding were made as in normal maintenance (Section 2.1.1) with the addition of carbenicillin (50 μg/ml), tetracycline (12 μg/ml), nystatin (50 μg/ml) & IPTG (1 mM) (NGM/C/T/N/I) and stored at 4 °C sheltered from light.

2.2.3 dsRNA bacteria culturing.

RNAi bacteria derived from the Ahringer RNAi library were streaked and grown on LB/C/T/N (Liquid broth with Carbenicillin (50 μg/ml), Tetracycline (12 μg/ml) and Nystatin (50 μg/ml)) agar plates overnight at 37 °C. A few single colonies were used to inoculate 10 ml liquid LB/C/T/N in 50 ml centrifuge tubes inclined at 45° and grown overnight at 37 °C while shaking.

The following day the cultures were induced with 1 mM IPTG for 4 hours and then concentrated 5 times. 300 µl was then seeded onto NGM RNAi plates and allowed to grow for 72 hours before use.

In the cases that we performed simultaneous knockdowns of two genes, we would prepare a 1:1 mixture of concentrated RNAi bacteria of each gene and then seed the NGM RNAi plates with the mix. For each gene knocked down in this way, we would also prepare a mixture of RNAi for that gene and control RNAi to ensure that phenotypes observed by double knockdowns are not a result of each RNAi dilution.

2.2.4 RNAi feeding.

For analyses of knock-down of genes by immunofluorescent assay, synchronised L1 stage worms were plated on OP50 plates and allowed to grow for 72 hours at 15 °C until being transferred to RNAi plates as L4 stage worms for another 72 hours.

For analyses of knock-down of genes by live imaging using fluorescent reporter strains, the strains were plated on OP50 for 24 hours and then transferred to RNAi plates for another 24 hours.

2.3 Genetic enhancer screening.

2.3.1 Screening NGM plate preparation.

6-well plastic cell culture plates (Triplered, TCP011006) were prepared as in section 2.2.2 although filled 5 ml per well with NGM/C/T/N/I agar and seeded with 50 µl RNAi bacteria. The format of the screen was such that the same RNAi was used for all wells on a 6 well plate and those made in triplicate.

Figure 2.1

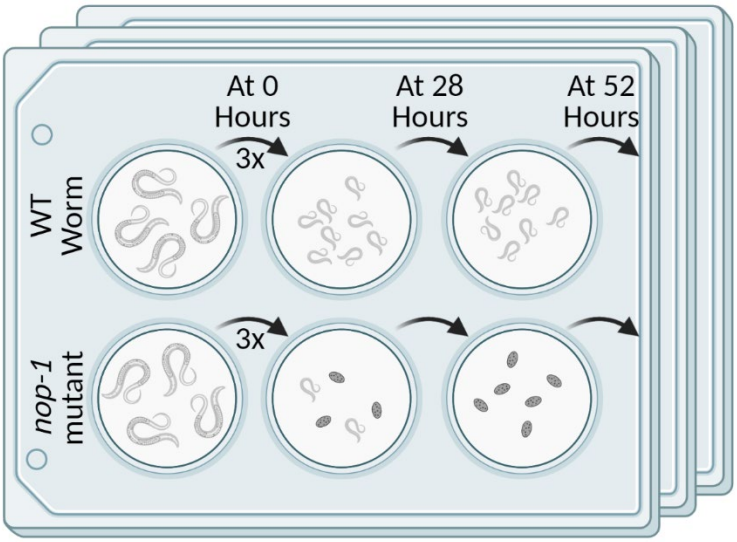

Figure 2.1 **Genetic enhancer screen format.**

6-well format of enhancer screen described below (Section 2.3.2). 4 L4 staged worms represent the ~30 added to the first column.

2.3.2 Worm feeding strategy.

Synchronised N2 (WT) and *nop-1* mutant (KK725) L1 worms were grown on OP50 plates for 72 hours at 15 °C before ~30 were transferred to the first column of the 6 well plates respectively. 3 hermaphrodites were transferred to the next well immediately and grown at 20 °C for 28 hours. The worms were then transferred to the final well of their row and grown for a further 24 hours at 20 °C before being removed from the 6-well plate. If one of the worms died between transfers or a male was mistakenly used, the worm was replaced, and this was noted for analysis.

2.3.3 Scoring fitness.

Each time the worms were removed from the second and third well, the eggs they laid were left overnight and allowed to hatch. The number of eggs and larva were then counted and used to work out the proportion of progeny that hatched (fitness (W)) for each strain and RNAi condition in triplicate.

2.3.4 Screen enhancement analysis.

To determine the degree of enhancement of lethality (ε) that the knockdown of a candidate gene has on the *nop-1* mutant, the fitness (W) of the *nop-1* mutant, fed control RNAi, was multiplied by the fitness of the WT strain fed RNAi of the gene to give an expected fitness

(W_{exp}) if *nop-1* and the candidate gene do not interact. This expected fitness was subtracted from the observed fitness (W_{obs}) when the *nop-1* mutant was fed the RNAi of the candidate gene. This is further explained in 3.2.1 in Figure 3.2.

2.4 Immunostaining.

2.4.1 Glass slide poly-lysine preparation.

Glass slides (30-2066a-brown-ce 24 3 squares 14x14 mm epoxy ERIE SCIENTIFIC COMPANY) were cleaned with detergent, distilled water then 70% ethanol followed by wiping with a Kimberly Clark tissue and incubation at 70 °C for 10 minutes to dry. 0.1% poly-lysine (Sigma P-1524) was then used to cover the central square of the glass slide and left for 30 minutes. Once finished, the poly-lysine was aspirated to leave a small amount remaining and wiped away with a folded Kimberly Clark tissue such that a film of poly-lysine remains (clearly seen to evaporate). The slides were then incubated at 70 °C for 10 minutes and then cooled to room temperature.

2.4.2 Worm collection.

Worms were raised on control and RNAi knockdown bacteria as described in section 2.2.4 (72 hours on OP50 *E. coli* followed by 72 hours on HT115 *E. coli* at 15 °C). For the temperature sensitive *spd-1*ts (WH12) and *lin-5*ts (SV124) strains, the worms were shifted to the restrictive temperature (24 °C) for 2 hours prior to immunostaining (Section 2.4). The cold-sensitive *vab-19*ts was raised at 24 °C (24 hours on OP50 followed by 24 hours on RNAi bacteria) and shifted to 15 °C for 2 hours prior to immunostaining. After the allotted time of feeding, the worms were collected in M9Tx buffer and allowed to pellet by gravity for 2 minutes. The supernatant was removed, and the sample washed in another 1 ml M9Tx. During this step most of the younger larva that might have been on the plate would be removed and bacteria accidentally collected were diluted. After removing the M9Tx again, a final wash with M9 was performed, pelleted by gravity for 2 minutes, the supernatant removed, and the worms were resuspended in 300 µl of M9.

2.4.3 Embryo harvesting.

7 µl of worms in M9 were taken and added to the middle square of a poly-lysine coated slide. The aim was to have around 25-35 worms on the slide for cutting and so this was adjusted

from the collection tube whilst retaining the volume of 7 µl of M9. A medical lancet was used to cut the worms in half, in between the two gonads to release the eggs. Once all worms were cut, a 22x40 mm coverslip (VWR international Thickness no' 1.5; Cat No' 631-0136) was used to squash the worms and embryos with just enough pressure that the embryos can be observed to bulge slightly. The slides were then immediately placed on a dry ice chilled metal rack to sit for 30 minutes.

2.4.4 Fixation.

After chilling, the coverslips were flipped off the slides and the slides submerged in 100% methanol for 30 minutes. After this, the slides were transferred to PBS (phosphate buffered saline) solution for 30 minutes followed by 5 minutes in PBST (PBS & Tween 0.05% (Sigma P-1379)).

2.4.5 Staining.

Slides were removed from the PBST, the edges dried by wiping with a Kimberly Clark Tissue and the central square dried slightly by tilting the slide and dabbing the edge with the tissue. Primary antibodies diluted in PBST were then added to cover the central square (30 µl). The slides were places in a box containing a wet tissue (to maintain humidity and prevent drying) and stored at 4 °C overnight. The next morning the primary antibody was removed, and the slides were washed three times in PBST. The same procedure was then followed for the secondary antibodies. This time however, the slides with secondary antibodies on them were stored at room temperature and away from light due to the fluorophore tags. The slides were then washed twice in PBST and once in PBS for 5 minutes each and briefly in distilled water prior to mounting.

Table 2.2 **Primary antibodies.**

Target	**Animal**	**Source/ References**	**Final concentration**
PAR-3	Mouse	Developmental Studies Hybridoma Bank (p4a1-c) (Nance, Munro and Priess, 2003)	1:25
PAR-2	Rabbit	Eurogentec	1:500
α-Tubulin	Rat	Sigma (MAB1864)	1:5000

Table 2.3 **Secondary antibodies.**

Target	Fluorophore	Source	Final concentration
Rabbit	488 nm	ThermoFisher Scientific (A-11011)	1:500
Mouse	594 nm	ThermoFisher Scientific (A-11032)	1:500
Rat	647 nm	ThermoFisher Scientific (A-21247)	1:500

Note that the stain DAPI (4',6-diamidino-2-phenylindole – ThermoFisher Scientific #62248) and the nanobody GFP-booster (Section 5.2.1, Figure 5.1 – Chromotek #gb2AF488-10) were used at dilutions of 1:50,000 and 1:250, respectively.

2.4.6 Mounting.

The edges of the slides were dried using a Kimberly Clark tissues and then the centre square dabbed whilst tilted to remove water without fully drying. 25 µl of Mowiol (Polyvinyl alcohol Sigma 81386-250G) was added to the centre square and topped with a 22x22 mm coverslip (VWR international Thickness no' 1.5; Cat No' 631-0125) and stored at room temperature away from light to harden for 48 hours and finally stored at 4 °C until day of imaging.

2.5 Genome editing via CRISPR/Cas9.

CRISPR protocol followed from the Craig Mello lab (Dokshin *et al.*, 2018).

2.5.1 gRNA & ssDNA repair templates.

Guide RNA and single stranded DNA repair templates for the KLP-19 CRISPR generated mutant were designed based on previous literature (arginine to alanine at position 205 in the KLP-19 protein sequence (Farrell *et al.*, 2002)) and synthesised by Integrated DNA technologies. The guide RNA was designed over the mutation site ending with a required protospacer adjacent motif (PAM sequence) (Base pair positions within KLP-19's unspliced sequence, including untranslated region: 723-745). The repair template was designed such that the desired

mutation, ^{733}AGG-GCT, was flanked with synonymous mutations (covering 12bp) to prevent re-annealing of the Cas9-gRNA complex and cleavage of successfully transformed sequences. The homology arms of the repair template spanned minus 48bp from the mutated site and plus 54bp.

- Guide RNA (PAM sequence – excluded in Guide RNA design))
    - CATGTCCAGCAGGTCTCATGCGG
- Repair template ssDNA (Mutated sites – **Codon for amino acid R-A change**)
    - GTCGGATGCCACTATCGAACAAAGGCGGAAACTGCGATGAACGCCATGAGTTCT**GC**
      TTCACATGCGGTTTTCACAGTGTTCGTGGAGAAAACTGCCACTGCAGAGTGTGATA
      GC

2.5.2 Injection.

Injection recipe

The CRISPR injection mix was prepared to the concentrations in the table below, diluted in nuclease-free water (IDT, 11-04-02-01). The Cas9 enzyme, TracrRNA and gRNA were combined first and incubated at 37 °C for 15 minutes before adding the remaining ingredients to ensure efficient complex formation without interference of other components. The components of the CRIPSR injection mixture were diluted in nuclease free water. Once combined, the CRISPR mix was centrifuged at 14,000 rpm and the top 17 µl were transferred to a new tube to prevent needle clogging.

Table 2.4 **CRISPR injection recipe.**

Component	**Final concentration**
***S. pyogenes* Cas9 3NLS (IDT, 1081058)**	250 ng/µl
TracrRNA (IDT, 1072532)	100 ng/µl
gRNA (Synthesised by IDT)	56 ng/µl
ssDNA (Synthesised by IDT)	110 ng/µl
pRF4::rol-6 (su1006) plasmid	40 ng/µl

Injection was performed using a Zeiss micromanipulation system. Worms were held in place in halocarbon oil 700 (Sigma H8898) on agar pads and injected with a borosilicate needle (WPI, B100-75-10) into the syncytial gonad. 20 worms were injected and then stored at 20 °C.

2.5.3 Selection of successful CRISPR progeny.

Three days after the injection of F0 worms, F1 progeny were checked for rolling phenotype as a marker of successful injection. 24 F1 worms from the two P0 plates with the highest proportion of rollers were placed onto separate plates and allowed to lay eggs. Usually, multiple F2 progeny would be lysed and genotyped by PCR and sequencing. In our experiment 6 out of 24 F1 worms were infertile. These 6 worms were genotyped individually along with 6 F1 fertile worms.

2.5.4 PCR

Single worms were picked and placed into 3 µl of lysis buffer (recipe below) (without proteinase K) and frozen at -80 °C for 1 hour minimum. Once thawed, the solution was topped up to 7 µl and the proteinase K added. The samples were then processed in a PCR machine at 60 °C – 90 minutes, 95 °C – 15 minutes.

Table 2.5 **Lysis Buffer Recipe.**

Lysis Buffer	
KCl	50 mM
Tris pH 8.3	10 mM
$MgCl_2$	2.5 mM
NP40	0.45%
Tween-20	0.45%
Proteinase K (Ambion)	200 µg/ml

The PCR reaction was then setup with the ingredients in the table below with the following cycles: 1 x 95 °C – 2 minutes, 35 x (95 °C – 30 seconds, 58 °C – 30 seconds, 72 °C – 40 seconds), 1 x 72 °C – 5 minutes.

Table 2.6 **PCR Reaction mix.**

PCR Reaction Mix (per reaction)	
Phusion HF Buffer (5x)	2 µl
Forward primer (10 µM)	0.5 µl
Reverse primer (10 µM)	0.5 µl
dNTPs (2.5 mM)	1 µl
Phusion Hi-Fi DNA Polymerase	0.1 µl
Sample extraction	1 µl
H_20	4.9 µl

- Forward Primer
    - 5’ - GTGAATCTGACGGCAGTTCC
- Reverse Primer
    - 5’ - TGTTACGGACGTCTGTGAGC
- Expected band size
    - 858bp

After PCR, the sample was run on an agarose gel (0.8%). The band was cut out and DNA gel extraction and purification was performed as per the kits (Qiagen – 28704) protocol. The purified DNA was then sent for sequencing (Eurofins).

2.6 Fixed confocal microscopy

Confocal microscopy was performed on an upright Nikon A1 scanning confocal microscope using a 60x/1.4 numerical aperture (NA) lens with oil immersion. Excitation lasers: 405nm,

488nm, 561nm & 647nm. Nikon elements software was used for imaging and microscope settings were maintained across experiments except the Hv (gain) which was adjusted to maximise the dynamic range of the image (i.e., brightness increased until oversaturation of pixels was detected, thus preventing loss of fluorescent intensity information).

2.7 Time-lapse imaging

C. elegans strains were processed as described in section 2.2.4 (72 hours on OP50 *E. coli* followed by 72 hours on HT115 *E. coli* at 15 °C) – unless otherwise stated. Gravid adults were dissected on coverslips in egg buffer (recipe and final concentrations below, ingredients diluted in distilled water) to release their embryos and mounted onto a 2% agarose pad in egg buffer. Temperatures of samples were maintained at 24 °C while imaging (unless otherwise stated) using a custom-built cooling system in which coolant runs directly underneath the agarose pads.

Table 2.7 **Egg buffer recipe.**

Egg Buffer	
$CaCl_2$	2 mM
NaCl	118 mM
KCl	48 mM
$MgCl_2$	2 mM
HEPES (pH 7.4)	25 mM

Table 2.8 **Live microscopy capture settings.**

Relevant results	Microscope	Objective magnification /Numerical aperture	Excitation Laser Wavelength	Software	Camera/ Sensor	Exposure	Frame interval	Z stack planes/ step size	Nikon Perfect Focus System
Figure 4.2, Figure 4.3, Figure 4.4, Figure 4.5	Nikon A1R Eclipse Ti (Scanning confocal)	60x, 1.4 NA	488 nm	Nikon elements	Photomultiplier tube	-	10.7 s	7/1.5 µm	Yes
Figure 5.2, Figure 5.3	Nikon Eclipse Ti (TIRF)	100x, 1.49 NA	488 nm	Nikon elements	Andor Xion X3 EMCCD-camera	0.06 s	0.06 s	-	Yes
Figure 4.6	Nikon Eclipse Ti (Spinning disc)	100x, 1.3 NA	488 nm	Metamorph	Photometrics Evolve 512 EMCCD	0.5 s	0.5 s	-	Yes
Figure 5.1, Figure 5.3	Nikon Eclipse Ti (Spinning disc)	100x, 1.0 NA	488 nm	Metamorph	Photometrics Evolve 512 EMCCD	0.5 s	0.5 s	-	Yes
Figure 6.1	Nikon Eclipse Ti (Spinning disc)	100x, 1.0 NA	488 nm	Metamorph	Photometrics Evolve 512 EMCCD	0.5 s	5 s	-	Yes
Figure 6.3, Figure 6.5	Nikon A1R Eclipse Ti (Scanning confocal)	60x, 1.4 NA	488 nm	Nikon elements	Photomultiplier tube	-	1.0 s	-	Yes

2.7.1 Confocal (Nikon A1R).

Note – To increase N number of GFP::SPD-1 embryos for results section 6.2.3, a temperature control system was not attached to the microscope and so the sample was processed at room temperature around 20 °C during imaging.

2.7.2 TIRF.

Despite using TIRF microscopy, true TIRF videos could not be achieved using *C. elegans* embryos in our experiments. Thus, the resultant videos are more comparable to "highly inclined and laminated optical sheet" (HILO) imaging which captures a thicker optical Z focal plane. This allows for subsurface imaging of the embryo's cortex but introduces a lower signal to noise ratio (Tokunaga, Imamoto and Sakata-Sogawa, 2008).

2.7.3 Spindle shooting (Laser ablation).

Spindle shooting was performed using a UV laser (355 nm) – iLas system (Roper Scientific) as previously described (Grill *et al.*, 2001; Portegijs *et al.*, 2016; Schmidt *et al.*, 2017; Fielmich *et al.*, 2018) (Section 4.2.5). The laser was set to pulse with line thickness 2 pixels and a repetition of 100 pulses (30Hz) and was triggered at the onset of anaphase. Recording was initiated just prior to ablation and the spindles movements were recorded for 25 frames (12.5 seconds) post-ablation to capture the maximum velocity of the spindles as they retract to their respective sides of the embryos. Method used to track of spindle the spindle poles described in Section 2.8.6.

2.7.4 Spinning disc.

The temperature of the spinning disc microscope stage and objective was maintained at 24 °C using a Tokai Hit INUBG2E-ZILCS Stage Top Incubator.

2.8 Image analysis.

All image analyses were performed using the "ImageJ" program loaded with the "Fiji" processing package.

2.8.1 Staging early polarity establishment embryos.

In immunofluorescent based experiments focused on early polarity establishment (stated in relevant results sections) embryos were divided into three sub-stages to distinguish

phenotypes between them. These were early pronuclear touch, late pronuclear touch, and pronuclear migration. Early pronuclear touch (Figure 7.1.a.i) was regarded as when the sperm pronucleus was still in contact with the cortex, chromosomes were decondensed, and the perimeter of the pronucleus was typically <15 µm – measured using the oval selection tool in ImageJ. Late pronuclear touch (Figure 7.1.a.ii) was regarded as when the sperm pronucleus was still in contact with the cortex, gaps could be seen in the nucleoplasm as chromsomes had begun to condense, and the perimeter of the pronucleus was typically >15 µm. Pronuclear migration (Figure 7.1.a.iii) was determined similarly to late pronuclear touch with the exception that the sperm pronucleus was detached from the cortex and migrating towards the oocyte pronucleus.

2.8.2 Quantifying SPCC positioning and centrosome separation defects.

Immunofluorescently labelled embryos (PAR-2, PAR-3, Tubulin, DAPI) were assessed by eye and qualitatively classed as aberrant/defective for SPCC positioning and centrosome separation phenotypes when the SPCC deviated from the WT appearance.

Aberrant SPCC positioning presented with the SPCC situated away from the posterior pole, the SPCC detached from the cortex, or the centrosomes not oriented towards the posterior pole (Figure 4.1.a.ii.iii&iv).

Centrosome separation was considered defective when one or both centrosomes lagged and were still facing the posterior during PN migration/ PN meet, the centrosomes migrate around the same side of the pronucleus, or the centrosomes were still attached to each other by pronuclear meet (Figure 4.3.a.vi.vii.ix&x)

2.8.3 Centrosome-centrosome distance analyses.

To measure the distance between centrosomes over time (Section 4.2.2), the line tool was used to measure the length between centrosomes in the x-y axes. If the centrosome were not in the same focal plane, the distance in the z axis was determined using the number of stacks between the centrosomes multiplied by the z frame interval (1.5 µm). Pythagoras's theorem was used to then calculate the hypotenuse as the real distance between the two centrosomes (hypotenuse length^2 = x-y length^2 + z length^2). This was done for every timeframe between centrosome duplication (the first frame that two centrosomes can be resolved by eye) and

pronuclear meet (first frame that the pronuclei contact each other). Analysis of covariance (ANCOVA) was used to test whether there was a significant difference between the data sets.

2.8.4 Centrosome-cortex distance analysis.

To determine the distance from the centrosome to the cortex over time (Section 4.2.3), the oval selection tool in ImageJ was used. The cursor was place at the centre of the centrosome and grown outwards as a circle until selection reached the cell membrane. The perimeter of the circle was used to calculate the radius (Radius = Perimeter/(2π)) which was the distance of the centrosome to the cortex. This was done for every timeframe between centrosome duplication (the first frame that two centrosomes can be resolved by eye) and pronuclear meet. ANCOVA was used to test whether there was a significant difference between the data sets ($P<0.05$ = significantly different).

2.8.5 Time between centrosome duplication and pronuclear meet.

The time between the frame of centrosome duplication and pronuclear meet (as determined above (Section 2.8.4) was calculated and plotted (Section 4.2.4). Mann-Whitney & Kruskal-Wallis tests of significance were used to assess changes in the data when working two datasets (Figure 4.5.b.i) and more than two datasets (Figure 4.5.b.ii), respectively ($P<0.05$ = significantly different).

2.8.6 Spindle shooting tracking analysis.

The TrackMate plugin on ImageJ was used to track the spindle for 25 frames (12.5 seconds) post-ablation to determine the maximum velocity of the spindle poles within this time (Section 4.2.5)(Settings - Blob diameter: 4 µm, Threshold: 2, Sub-pixel localisation: enabled). The simple LAP tracker function was then used to determine tracks of particle movement (Settings - Linking max distance: 15 µm, Gap-closing max distance: 15 µm, Gap-closing max frame gap: 2). Paired t-tests were used to test for significance between anterior & posterior within the same RNAi treatment and unpaired t-tests used between RNAi conditions ($P<0.05$ = significantly different).

2.8.7 EBP-2, KLP-19 & SPD-1 tracking analysis.

EBP-2::GFP – Track speed, distance, duration. (Sections 5.2.2 & 5.2.3)

250 frames were selected between polarity establishment (posterior membrane relaxation) and pseudocleavage from which a substack of these frames was generated. Using ImageJ, a region of interest was then selected using the freehand selection tool that covered as much of the cortex of the embryo as possible that was in focus. The TrackMate plugin on ImageJ was used to define EBP-2::GFP particles within the region of interest (Settings - Blob diameter: 0.7 µm, Threshold: Not used, Sub-pixel localisation: enabled). The simple LAP tracker function was then used to determine tracks of particle movement (Settings - Linking max distance: 0.8 µm, Gap-closing max distance: 1.3 µm, Gap-closing max frame gap: 10). TrackMate then provided analysis of these tracks, including the speed, distance travelled and duration which we used to compare EBP-2 tracks between control embryos and those depleted of KLP-19. TrackMate provides a measure of mean track quality for each track it identifies (Note – Track quality is an average of the quality of spots within the track. The quality of spots is determined by the brightness of each spot vs the background and the closeness of the diameter of the spot to the user-specified diameter expected). We set an inclusive cut-off of mean track quality 10 and above to eliminate noise and incorrectly identified tracks from the data-set.

The Kolmogorov-Smirnov test of significance used to determine whether there was a difference in the distribution of frequencies of EBP-2::GFP track displacement and speed values in the control and *klp-19* RNAi conditions ($P<0.05$ is significantly different) (Figure 5.2). The Mann-Whitney test used to determine whether EBP-2::GFP average track durations, displacements and speeds were significantly different to KLP-19::GFP ($P<0.05$ = significantly different) (Figure 5.3).

KLP-19::GFP – Track speed, distance, duration. (Section 5.2.3)

Up to 500 frames (~16 seconds) were selected between polarity establishment (posterior membrane relaxation) and pseudocleavage from which a substack of these frames was generated. A region of interest was then selected using the freehand selection tool that covered as much of the cortex of the embryo as possible that was in focus. The TrackMate plugin on ImageJ was used to track KLP-19::GFP (Settings - Blob diameter: 0.5 µm, Threshold: 1, Sub-pixel localisation: enabled). The simple LAP tracker function was then used to

determine tracks of particle movement (Linking max distance: 0.3 µm, Gap-closing max distance: 0.5 µm, Gap-closing max frame gap: 3). TrackMate then provided analysis of these tracks, including the speed, distance travelled and duration which we used to compare EBP-2 tracks between control embryos and those depleted of KLP-19. The Mann-Whitney test used to determine whether EBP-2::GFP average track durations, displacements and speeds were significantly different to KLP-19::GFP ($P<0.05$ = significantly different) (Figure 4.6).

KLP-19::GFP & GFP::SPD-1 – Counting Tracks (Sections 6.2.1 & 6.2.3)

12 frames (60 seconds) were selected between polarity establishment (posterior membrane relaxation) and pseudocleavage from which a substack of these frames was generated (We used the sequential frames of KLP-19::GFP recorded at 5 second intervals and every 5^{th} image taken of GFP::SPD-1 recorded at 1.035 second intervals). A region of interest was then selected using the freehand selection tool that covered as much of the cortex of the embryo as possible that was in focus. The TrackMate plugin on ImageJ was used to track KLP-19::GFP & GFP::SPD-1 (Settings - Blob diameter: 0.5 µm, Threshold: 200, Sub-pixel localisation: enabled). The simple LAP tracker function was then used to determine tracks of particle movement (Settings - Linking max distance: 1 µm, Gap-closing max distance: 1 µm, Gap-closing max frame gap: 2).

Due to a large amount of noise being detected as tracks in these experiments, the mean track quality score assigned by TrackMate was used to determine a cut-off for all tracks identified in each strain. Mean track quality scores are the average of spot quality scores for each particle detected within the track, these individual spot quality scores are determined by brightness and diameter (i.e., brighter spots and spots with diameters closer to the specified diameter result in higher scores). All tracks above the quality score cut-off were then counted (Mean track quality score cut-offs: KLP-19::GFP – 400, GFP::SPD-1 – 550). The Kruskal-Wallis test of significance was used to determine whether there was a significant difference between the number of tracks observed between the control and RNAi conditions within KLP-19::GFP and GFP::SPD-1 embryos ($P<0.05$ = significantly different).

2.8.8 SPD-1 end-tag length.

GFP::SPD-1 embryos under control and *klp-19* RNAi conditions were imaged via confocal microscopy. We selected embryos during telophase when cortical SPD-1 threads were seen at

their greatest quantity. Due to limited numbers of embryos at telophase, only one of each condition was analysed. The embryos were imaged in a Z-Stack (Top to bottom of embryo at 0.5 µm steps) and a maximum intensity projection was made. All SPD-1 threads that appeared to grow at the ends of astral MTs (MTs that grow from the centrosome to the cortex) were measured in length using the segmented line too in ImageJ.

2.8.9 SPD-1 thread shrinkage and duration.

To assess whether SPD-1 threads resolve (shrink) to a central point, GFP::SPD-1 embryos, under control and *klp-19* RNAi conditions, were recorded via spinning disc microscopy (Figure 6.5) between polarity establishment (posterior membrane relaxation) and pseudocleavage. Two threads were selected from three embryos of each condition and followed from the first frame the thread appears until the final frame it disappears. The thread at its maximum length was overlayed with the thread in the final frame, by which point it had shrunk in size to a dot. The relative position of the dot along the thread at its maximum size was measured and recorded with 0.5 set as the centre of the maximal thread and 0 at both ends (i.e., A value of 0.5 indicated that the thread had shrunken to a central point while a value of 0 indicated that the thread had shrunk to one end of the thread). The time difference between the final and first frame the thread could be observed was recorded as the duration of SPD-1 threads.

2.8.10 Posterior PAR domain quantifications.

For analysis of the size of the posterior PAR domain (Sections 7.2.1 & 7.2.2), the segmented line tool (pixel width: 2) in ImageJ was used to trace around the embryo perimeter. The posterior domain was determined by eye using PAR-2 immunofluorescent staining. The length of the PAR-2 domain was divided by the embryos perimeter length and multiplied by 100 to calculate the percentage of the cortex occupied by the domain. The Kruskal-Wallis test of significance was used to determine whether there was a significant difference in PAR-2 domains between the control and RNAi conditions ($P<0.05$ = significantly different).

2.8.11 PAR-3 clearance vs centrosome positioning.

To determine the region of PAR-3 weakening/clearance of a given cell during pronuclear touch (Section 7.2.3), the fluorescent intensity of the PAR-3 cytoplasm was measured. This value was multiplied by 1.75 and used as a cut-off for weak PAR-3 (any value below would be classified as weak). The line tool of ImageJ was used in small sections around the perimeter of the

embryos to find the longest continuous length of cortex that was below the cut-off and could be considered the region of PAR-3 clearance. The centre of this domain was measured clockwise from the anterior pole and considered as a fraction of the whole embryo perimeter. The same was performed for the point of the cortex found closest to the centrosome (determined using the same method as section 2.8.4) such that the position of the centrosome and the clearance of PAR-3 could be compared for their position around the embryo cortex. ANCOVA was used to test whether there was a significant difference between the data sets ($P<0.05$ = significantly different).

Chapter 3 Identifying novel regulators of microtubule dependent embryonic polarity.

3.1 Introduction.

Studies of biological pathways rely on detectable/measurable changes (phenotypes) which arise when the pathway is perturbed. When a phenotype is regulated by only one pathway, that pathway becomes a necessity and, as such, any compromise will result in a phenotype. In biology, however, most processes have evolved to become supported by multiple pathways which ensure their end function can be maintained in the event of a defect in one of the pathways. This is functional redundancy, and it leads to phenotypic masking, where a phenotype is not observed even though a component in one of the involved pathways is disrupted. This complicates the research of biological processes as novel regulators of a pathway become difficult to identify.

Many labs have managed to overcome the challenge of genetic redundancy through synthetic lethality screens. In these screens, relationships between genes can be identified through the loss of function of two genes that do not individually compromise an organism's viability but do so when both genes are concomitantly perturbed. Using organisms with short generation times (e.g. yeast) has allowed high-throughput discovery of networks of genetic interaction (Costanzo *et al.*, 2010). In our case, the self-fertilising hermaphrodite *C. elegans* has generation times of around 3-4 days and produces embryos which have been studied extensively in the field of cell polarity. As such, the worm provides us the ideal conditions to screen for novel regulators of polarity.

As discussed in the main introduction, two pathways have been described in which the newly fertilised *C. elegans* zygote progresses from a symmetrical and uniform oocyte into a polarised embryo (Sections 1.6.3 & 1.6.4, Figure 1.11). Due to limited understanding in the field, we wanted to investigate the microtubule-dependent pathway and how it is regulated. We wondered, for example, does microtubule organisation or dynamicity impact polarity establishment? Do microtubules act to facilitate the delivery of other components required for polarity? Could microtubules regulate properties of the membrane/cortex or modulate polarity through membrane/vesicle trafficking? To date, answering these questions has been difficult as the actomyosin-dependent polarity pathway appears to be more predominant than

the microtubule pathway and so the loss of MT-dependent pathway regulators has only a delaying effect on polarity. In an actomyosin compromised background, however, the absence of microtubules or PAR-2-microtubules binding results in failure to establish polarity (Motegi and Seydoux, 2013; Klinkert *et al.*, 2019). It would be interesting, then, to study the microtubule-dependent pathway of polarity in embryos that lack the actomyosin dynamics during polarity establishment.

Our lab has previously studied the gene, *nop-1*, required for cortical actomyosin dynamics, specifically during polarity establishment. NOP-1 was initially characterised in a functionally null mutant that lacked early embryo contractility (Rose *et al.*, 1995; Fievet *et al.*, 2012; Khaliullin *et al.*, 2018). Our finding agreed with concurrent research by Tse et al. (2012) who further attempted to characterise the molecular pathway that NOP-1 acts through and found that it promotes active state RhoA (*C. elegans* RHO-1) GTPase, triggering actomyosin contraction (Tse *et al.*, 2012). NOP-1 has no recognisable conserved domains, and similar protein sequences have only been detected in other *Caenorhabditis* group members. It remains to be determined if functional homologues of NOP-1 exist in other systems. In the single-cell zygote, NOP-1 localises within the cytoplasm, the nuclei and at the cortex, particularly at the site of membrane ingression during cell pseudocleavage and cytokinetic cleavage. NOP-1 appears to act upstream of the GEF, ECT-2, required for actomyosin dynamics, although how NOP-1 activates ECT-2 is unknown. NOP-1 shares this role in ECT-2 activation with the centralspindlin complex protein, CYK-4, acting in a partially redundant manner (Tse *et al.*, 2012; Zhang and Glotzer, 2015; Kotýnková *et al.*, 2016). Their relative contributions change as the cell develops. NOP-1 acts predominantly to regulate actomyosin dynamics during polarity establishment whereas CYK-4 becomes more important during cytokinesis (Tse *et al.*, 2012).

Despite loss of actomyosin flows in a *nop-1* mutant, PAR-3 becomes enriched in the anterior and the zygote divides asymmetrically as normal (Fievet *et al.*, 2012), likely a result of the MT-dependent pathway followed by mutual antagonism between the aPARs and pPARs which stabilises their respective anterior and posterior domains. As such, one would expect that the loss of any genes required for the MT-dependent pathway would be essential for embryonic viability in the *nop-1* mutant as it relies on this pathway to polarise the zygote. For this reason, the *nop-1* mutant would be an excellent tool to screen for MT-dependent pathway regulators.

Our lab previously performed a large-scale genetic suppressor screen to identify novel genes involved in cell polarity and generated a network of functional interaction between cell polarity genes (Figure 3.1). Approximately 15% of the *C. elegans* genome (essential genes for embryonic development) was screened via RNAi knockdown to assess rescue of lethality in 14 temperature-sensitive (ts) mutants of polarity genes selected for their involvement in actomyosin regulation, PAR protein polarity and microtubule/spindle regulation (Fievet *et al.*, 2012). In theory, when the double loss-of-function of two genes suppress the lethality of each other alone, one can assume that these genes normally act in an antagonist manner. Thus, loss of either cancels out the harmful effects of the other one. Building on this, two genes that suppress the lethality of common third gene have a chance of acting towards the same process in a cell, either in the same pathway or parallel pathways. For example, the screen demonstrated that loss of *par-6* suppressed the lethality of a *par-2* mutant. Indeed, the aPARs and pPARs typically act to exclude each other from their respective domains to maintain asymmetry. When one component of either PAR complex is compromised, the opposing PAR complex out-competes and spreads to take over the zygotes cortex and asymmetry is lost. The competition can be "rebalanced" if the opposing PAR complex is then also compromised, rescuing lethality. Likewise, loss of *par-3* and *pkc-3* also suppressed lethality in the *par-2* mutant and, as we know, PAR-3, PAR-6 and PKC-3 act together to specify the anterior domain in the *C. elegans* zygote, partially through antagonism of posterior PARs.

Our lab identified 184 genes as suppressors of lethality against the 14 mutants screened, accounting to 227 interactions (Figure 3.1). Based on the functional groups of the mutants, many of the genes screened lend themselves to future studies as novel regulators of actomyosin regulation, microtubule/spindle regulation, and PAR polarity. In our case, we wanted to further understand the role of microtubules in the establishment of polarity. To this end, *nop-1* was the most connected suppressor of the microtubule regulation grouped mutants (White arrow in Figure 3.1) (Fievet *et al.*, 2012).

This chapter focuses on the quantitative analyses of *nop-1* enhancer candidates to identify regulators of the MT-dependent pathway of polarity establishment. Positive hits were then further characterised to confirm their implication in this pathway by immunofluorescent staining of markers of polarity and microtubules. Through this we found 7 out of 15 genes screened had enhanced lethality in the *nop-1* mutant. Of those 7 genes, we imaged 5 through

confocal microscopy and found all of them to generate polarity defects, thus showing that we can detect regulators of cell polarity using the *nop-1* mutant as a tool that lacks the actomyosin-dependent pathway.

Figure 3.1

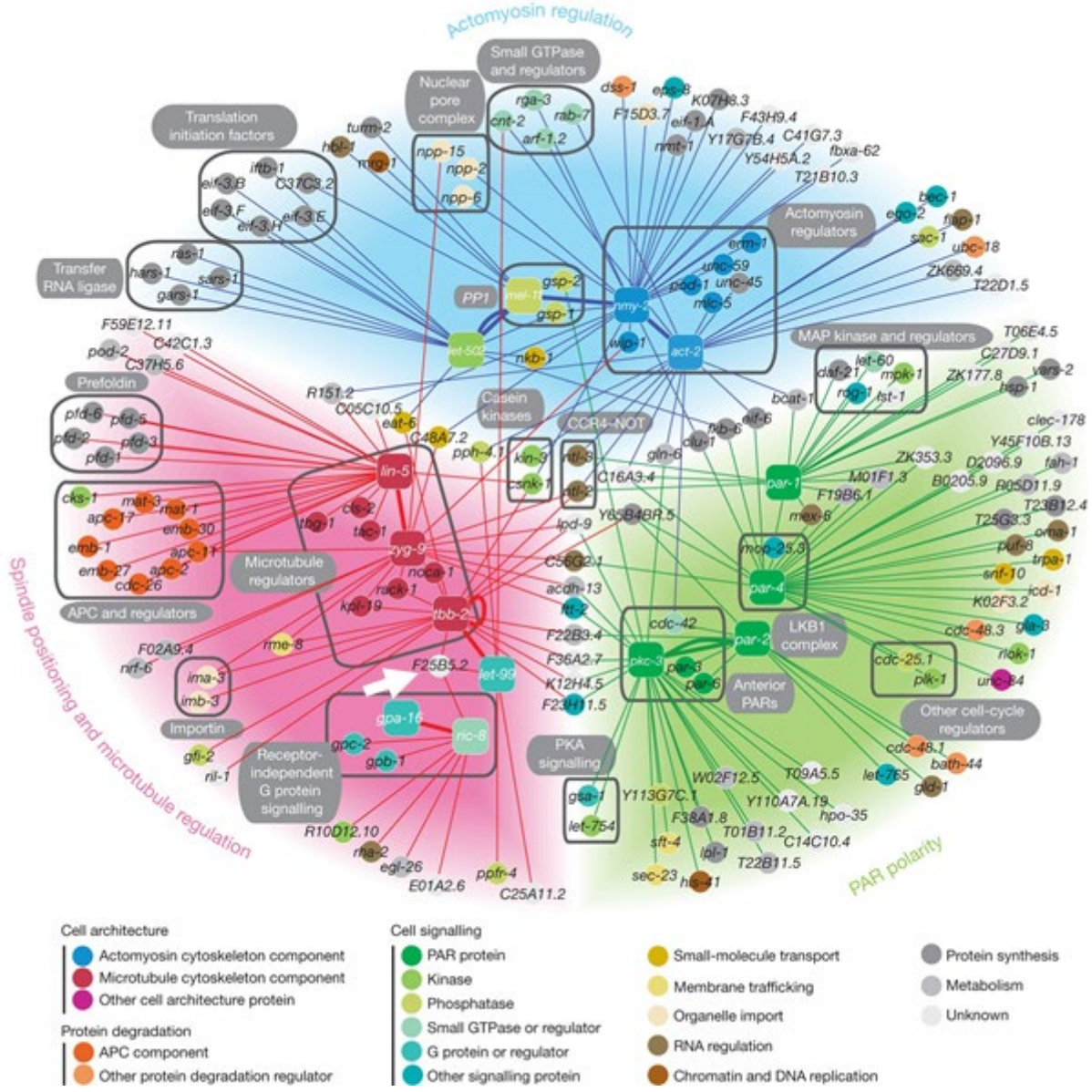

Figure 3.1 **Cell polarity genetic network of large-scale screen**.
Graphical network adapted from Fievet et al. (2012) displaying 227 genetic interactions between 184 genes, divided into the three broad functional groups of actomyosin regulation, PAR polarity and spindle positioning and microtubule regulation. Every circle represents a gene RNAi knockdown with lines (representing suppression of lethality) connecting to the square nodes which represent the 14 temperature sensitive mutants of genes which fit one of each of the three functional groups (Fievet *et al.*, 2012). The white arrow added highlights *nop-1* (F25B5.2).

3.2 Results

3.2.1 A quantitative enhancer screen to identify regulators of the MT dependent pathway in cell polarity establishment.

To shortlist genes from the polarity network (Fievet *et al.*, 2012) for a quantitative enhancer screen, a faster/larger scale semi-quantitative screen was first performed (Unpublished data). In this, visual inspection of worms in liquid culture was used to determine embryonic lethality upon RNAi depletion of the polarity genetic network. The highest scoring enhancers of embryonic lethality in the *nop-1* mutant (KK725), compared to lethality caused in the WT strain, were then taken forward for the more quantitative screening approach of this project (15 genes total) (Table 3.1).

To better assess which genes became essential in the *nop-1* mutant, we raised control and *nop-1* mutant worms on agar plates with control RNAi (empty vector) and RNAi against each of the selected candidates. This allowed us to accurately score the rate of embryonic survival, A.K.A. fitness (proportion of embryos that hatch), and calculate the degree of enhancement of lethality (ε) (Figure 3.2). To calculate ε, the embryonic fitness in the *nop-1* mutant and RNAi knockdown in the control strain conditions were multiplied to give an expected fitness, assuming no genetic interaction. This number was subtracted from the actual fitness (observed fitness) to provide ε. The lower the value of ε, the stronger the enhancement of lethality caused by loss of the gene of interest in the *nop-1* mutant. Thus, we can assume genetic interaction. We set a cut off $\varepsilon \leq -0.15$ to qualify a gene as a strong enhancer of *nop-1.* The results of the screens are shown in Table 3.1. Of 15 genes screened at both 28 and 52 hours of exposure to RNAi, in triplicate, 7 had an average ε score of ≤ -0.15 at one of the time points. Multiple microtubule regulators and known polarity regulators scored as successful enhancers of lethality in the *nop-1* mutant. Note that this data was reanalysed from my Masters project.

Figure 3.2

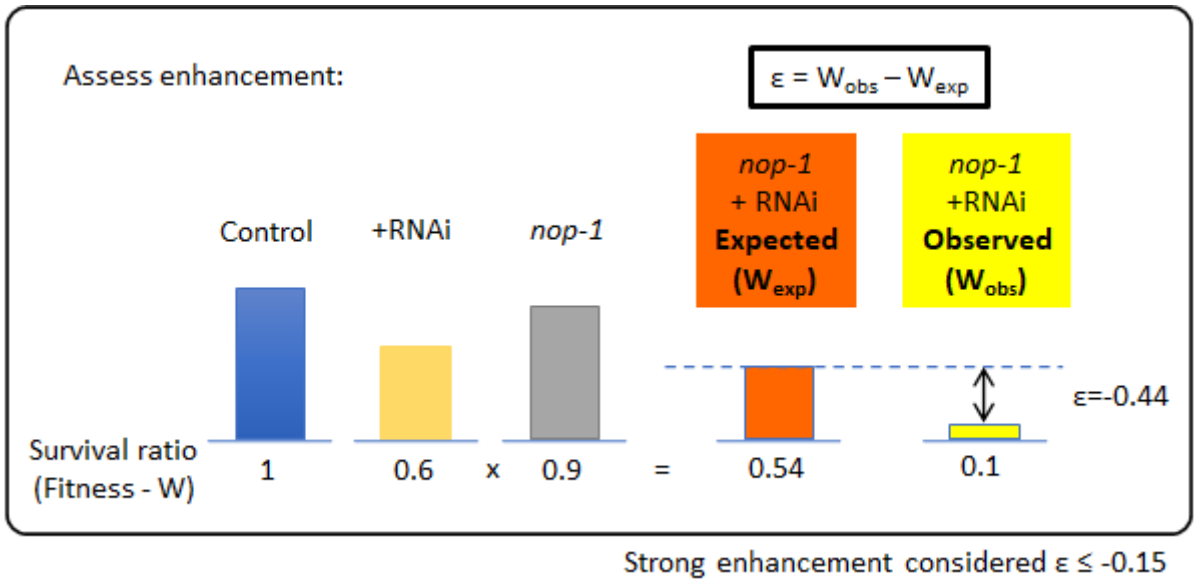

Figure 3.2 **Enhancer screen calculation.**

To determine the degree of genetic interaction between nop-1 and candidate genes suspected to regulate microtubule-dependent polarity establishment, the survival ratio (or fitness (W)) was determined for both the *nop-1* mutant and the RNAi knockdown of each gene. The fitness of nop-1 and a given gene were multiplied to determine an expected fitness of the gene knockdown in the nop-1 mutant, assuming the genes do not interact. The expected fitness was then subtracted from the actual fitness observed in the experiments *nop-1*;gene RNA condition, this gives us ε. Greater lethality in the experimental condition (W_{obs}) compared to the expected (W_{exp}) indicates that the induced lethalities, in the absence of functional *nop-1* and the gene of interest do not simply stack, but that there is greater-than-additive reduction in fitness in the progeny (Negative epistasis). This generates negative ε values and indicates genetic interaction/enhancement of lethality.

Table 3.1

RNAi	Human Homologue	ε (W^{obs} - W^{exp})	Functional Category	Description
rack-1	RACK1	-0.66	Microtubule regulation	Scaffold protein able to regulate the activity of many binding partners. Roles in cell division, cell adhesion, membrane trafficking, protein synthesis and more[1,2,3].
cnt-2	AGAP3	-0.38	Membrane trafficking	ArfGAP involved in membrane trafficking & neuroblast asymmetric cell division[4].
let-754	AK2	-0.35	Metabolism	Adenylate kinase, regulates cell polarity via negative regulation of PKC-3[5].
gpb-1	GNB1	-0.25	Microtubule regulation	G protein β-subunit required for mitotic spindle positioning[6].
klp-19	KIF4a	-0.25	Microtubule regulation	Chromokinesin required for spindle assembly, chromosome congression and segregation during meiosis & mitosis[7,8,9].
arf-1.2	ARF1	-0.17	Membrane trafficking	GTPase involved in membrane trafficking & neuroblast asymmetric cell division[4,10,11,12].
plk-1	PLK1	-0.16	Cell signalling	Kinase required for pericentriolar material assembly, nuclear envelope breakdown and polarity establishment[13,14,15,16,17].
gpc-2	GNG13	-0.14	Microtubule regulation	G protein γ-subunit required for mitotic spindle positioning[6].
Y65B4BR.5 (icd-2)	NACA	-0.14	Metabolism	A regulator of proteostasis, localizes to ribosomes and promotes protein translation and folding. Re-localises to protein aggregates upon cell stress[18].
kin-3	CSNK2A1	-0.11	Microtubule regulation	Casein kinase II catalytic subunit that negatively regulates centrosome duplication and is required for correct cell division[19].
ego-2	PTPN23	-0.06	Membrane trafficking	A positive regulator of the Notch signalling pathway and germline proliferation, possibly via endocytic pathway[20].
ril-1	-	0.00	Unknown	-
B0491.5	-	0.01	Unknown	-
paa-1	PPP2R1A	0.01	Microtubule regulation	Structural subunit of the protein phosphatase, PP2A, required for chromosome alignment and exit from mitosis[21,22].
cdc-25	CDC25A	0.20	Cell cycle regulator	A phosphatase required for cell cycle progression by preventing inhibition of cyclin/cyclin-dependent kinase complexes[23,24,25].

Table 3.1 **Genes screened for lethality against a mutant of the *nop-1* gene.**

All genes knocked down in the *nop-1* mutant and scored for embryonic lethality. Enhancement/suppression score (ε) was calculated by deducting an expected fitness (survival) of *nop-1* and the gene screened from the observed fitness upon knockdown of that gene in the *nop-1* mutant. [1](Marudhupandiyan *et al.*, 2017) [2](Ai, Poole and Skop, 2009) [3](Ai, Poole and Skop, 2011) [4](Singhvi *et al.*, 2011) [5](Fievet *et al.*, 2012) [6](Gotta and Ahringer, 2001) [7](Powers *et al.*, 2004) [8](Wignall and Villeneuve, 2009) [9](Pelisch *et al.*, 2017) [10](Ackema *et al.*, 2013)

[11](Teuliere *et al.*, 2014) [12](Kage-Nakadai *et al.*, 2019) [13](Nishi *et al.*, 2008) [14](Boxem and van den Heuvel, 2019) [15](Mittasch *et al.*, 2020) [16](Velez-Aguilera *et al.*, 2020) [17](Kim and Griffin, 2021) [18](Kirstein-Miles *et al.*, 2013) [19](Medley *et al.*, 2017) [20](Liu and Maine, 2007) [21](Sontag *et al.*, 2012) [22](Lange *et al.*, 2013) [23](Ashcroft *et al.*, 1999) [24](Yoon, Kawasaki and Shim, 2012) [25](Lee *et al.*, 2016)

3.2.2 Positive hits of screening for regulators of the MT-dependent pathway of polarity establishment lead to polarity and MT defects when depleted via RNAi.

Following the screen, we wanted to assess how genes that scored as enhancers of lethality in the *nop-1* mutant affect the MT-dependent pathway, i.e., look for observable changes in polarity and microtubule organisation. RNAi was used to knockdown the genes in the WT and *nop-1* strains and the embryos were processed for immunofluorescent confocal microscopy (Note: due to failed staining, GPB-1 and PLK-1 have not been included in these results). We stained for PAR-2 & PAR-3 (markers of posterior and anterior polarity respectively), tubulin to detect microtubule/centrosome defects and DNA to stage the embryos. Our aim from these experiments was to identify polarity and microtubule phenotypes that can indicate if the positive hits from the screen are indeed required for efficient polarity establishment via the MT-dependent polarity pathway. The WT strain and the *nop-1* mutant, fed control bacteria, were used to set a standard for phenotypes between three sub-stages during polarity establishment (early pronuclear touch, late pronuclear touch, and pronuclear migration – staging described in methods section 2.8.1) so that novel changes in polarity markers and microtubules could be identified upon RNAi depletion of the genes of interest from the screen.

Prior to polarity establishment, at the end of meiosis II, a wild-type zygote has a uniform localisation of aPARs at the cortex and the sperm-pronucleus centrosome complex (SPCC) becomes positioned to the far posterior cortex with the centrosome situated between the male/sperm pronucleus and the membrane (Figure 3.3.a&b)(Section 1.6, Figure 1.9). Shortly after the completion of meiosis, polarity establishment initiates which results in the clearance of aPARs from the posterior pole at the site closest to the SPCC from where the posterior PARs are recruited and expand across the membrane as the aPARs are cleared (Rose and Gönczy, 2014). Therefore, it is typical in fixed early-stage embryos to see a larger anterior domain than posterior domain at the cortex (Figure 3.3.a). As the posterior domain grows and the anterior retracts, they become balanced in domain size upon polarity maintenance (Figure 3.3.a.xiv-xvi).

During early polarity establishment, the centrosome will duplicate while held at the posterior cortex. Microtubules grown from the sister centrosomes bind to cortically anchored dynein which acts to pull the sister centrosomes around opposite sides of the male PN towards the anterior of the zygote. From here the microtubules are captured by dynein on the female PN (normally in the anterior half of the zygote) and the pronuclei are pulled towards each other (Section 1.7.1, Figure 1.9i-iii, Figure 1.13, Figure 3.3.a)(Rose and Gönczy, 2014). We consider the moment that the pronuclei meet as the beginning of polarity maintenance. Deviations in these steps were considered abnormal and reported (Appendices: Table 9.1, Table 9.2 & Table 9.3).

Figure 3.3

a.

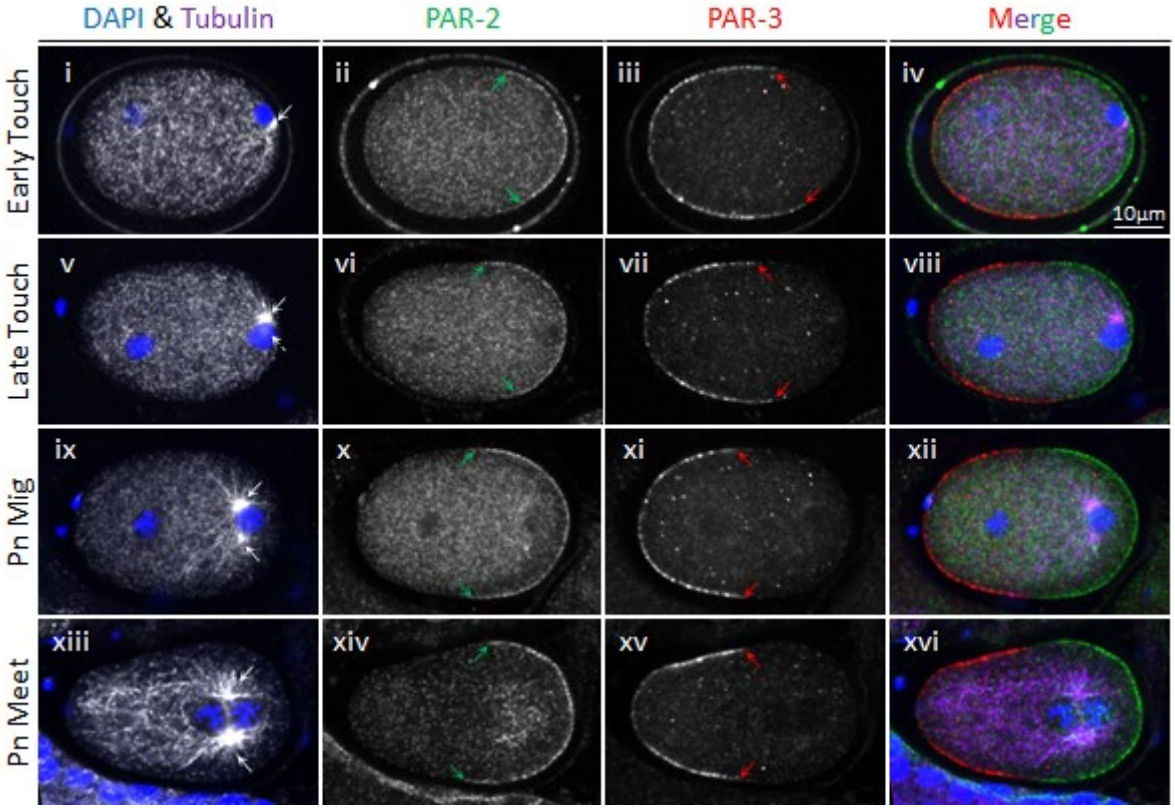

b.

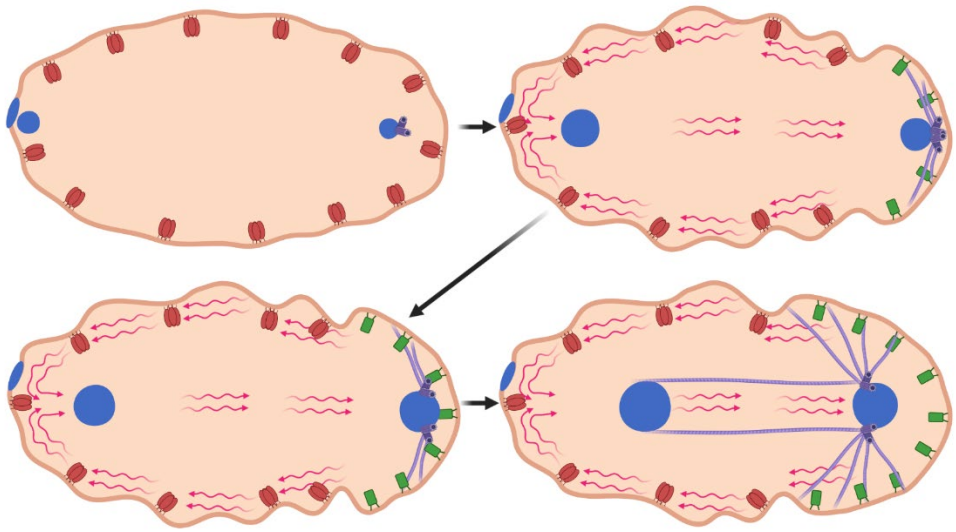

Figure 3.3 **Wild-type PAR proteins & microtubule organisation.**

(a) Fixed immunofluorescent stained single-cell embryos with expected wild-type appearances of anterior and posterior PARs (PAR-3 & PAR-2, respectively) and microtubule organisation, imaged via confocal microscopy. i-iv: Early pronuclear touch, v-viii: Late pronuclear touch, ix-xii: Pronuclear migration, xiii-xvi: Pronuclear meet. White arrows point to centrosomes – Note: in image v, centrosomes have split but second centrosome is out of frame, represented by broken line arrow. Green arrows point to boundaries of PAR-2 domain. Red arrows point to boundaries of PAR-3 domain. Notes – Linear adjustment of brightness and contrast used for representation in figure. **(b) Top left:** A fertilised zygote post-meiosis (pre-polarity establishment) with uniform anterior PARs at the cortex. The sperm pronucleus-centrosome complex is in the posterior. The centrosome has not duplicated yet. **Top right:** Polarity onset, anterior directed cortical flows, initiated nearby the centrosome (now duplicated) flow to the anterior, carrying with them the aPARs. pPARs are recruited to the posterior cortex. Central cytoplasmic flows directed to the posterior pole push the SPCC further to the posterior pole. **Bottom left**: The centrosomes separate diametrically around the sperm pronucleus in response to actomyosin flows pulling on the astral microtubules tethered to the cortex. The posterior domain grows as the anterior continues to retract. **Bottom right:** During pronuclear migration, the pronuclei of the egg and sperm move towards each other. The centrosomes are now oriented to the anterior and will capture the egg pronucleus which will pull the pronuclei towards each other at a faster rate. The posterior domain continues to grow and will eventually become balanced in size with the anterior domain upon polarity maintenance.

Controls

In fixed samples, WT embryos exhibited a low number of phenotypes. The most common phenotype that did occur, however, was the clearance of PAR-3 from the anterior pole as seen by a reduction in fluorescent intensity (5 out of 67 - 7.5% of embryos) (Figure 3.4.a) compared to the WT phenotype (Figure 3.3.a). Interestingly this did not occur in the *nop-1* mutant (0 out

of 43 – 0%) suggesting reversed actomyosin-generated flows, to some extent, may act to drive PAR-3 away from the anterior cortex in a portion of embryos, like normal PAR-3 clearance from the posterior (Appendix: Table 9.1).

In the *nop-1* mutant 11.6% (5 out of 43) of embryos showed a tilted PAR phenotype whereby the boundary that the aPAR & pPAR domains meet was not perpendicular to the anterior-posterior axis (Figure 3.4.b.ii-iv) as in the WT strain (Figure 3.3.a). 30% (3 out of 10) of the *nop-1* embryos lacked PAR-2 at the cortex (Figure 3.4.b.xiv-xvi) during early pronuclear touch and 15.4% (2 out of 13) by late pronuclear touch. In WT embryos, PAR-2 loaded to the posterior cortex in 100% (10 out of 10) of the embryos at both early and late pronuclear touch (Figure 3.3.a.ii&vi). This indicates delayed polarity onset in the *nop-1* mutant. We also observed cases in which the aPAR and pPAR domains show a degree of co-habiting the same cortical space (*nop-1*: 20 out of 43 - 46.5%, control: 1 out of 67 – 1.5%) suggesting a partial loss of mutual PAR antagonism (Figure 3.4.b.vi-viii & x-xii) (Appendix: Table 9.1).

The *nop-1* mutant also presented with centrosome positioning and separation defects. This is likely due to the loss of cytoplasmic flows which help to position the SPCC and facilitate centrosome separation (discussed in detail in Section 4.1) (Cao *et al.*, 2010; Bienkowska and Cowan, 2012; De Simone, 2016; De Simone, Nédélec and Gönczy, 2016). As mentioned above, the SPCC typically becomes positioned to the far posterior cortex during early polarity establishment where it remains until both centrosomes have separated and the orient towards the anterior, after which the SPCC then migrates towards the female pronucleus (Section 1.7.1, Figure 1.9.i-iii, Figure 3.3.a.i,v&ix & b). In the *nop-1* mutant, the SPCC of early embryos was often detached from the cortex with their centrosome improperly oriented (*nop-1*: 9 out of 23 – 39.1%, control: 1 out of 40 – 2.5%) (Figure 3.4.b.v,ix&xiii) or attached to the cortex but not positioned at the far posterior pole (Lateral SPCC) (*nop-1*: 5 out of 23 – 21.7%, control: 1 out of 40 – 2.5%) (Figure 3.4.b.xvii). In later embryos (pronuclear migration) it was common to see embryos in which the centrosomes had not separated yet (*nop-1*: 9 out of 20 – 45%, control: 0 out of 19 – 0%) (Figure 3.4.b.i) when this would be expected (Figure 3.3.a.ix), or the centrosome would have separated but not managed to orient to the anterior (*nop-1*: 6 out of 20 - 30.0%, control: 1 out of 19 – 5.3%), suggesting a delay/slowing of centrosome travel (Figure 3.4.b.xxi) (Appendices: Table 9.2 & Table 9.3).

Figure 3.4

a.

Control

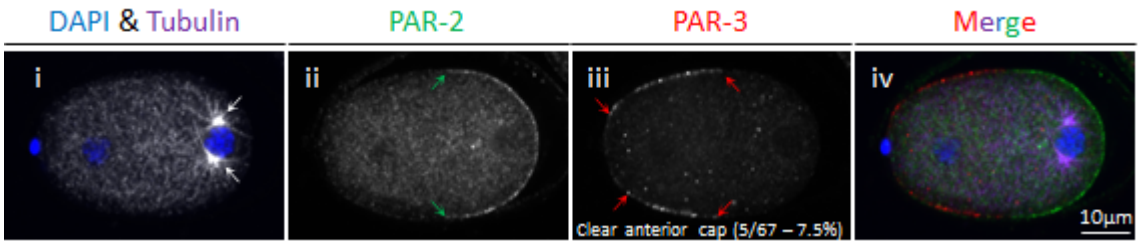

b.

nop-1

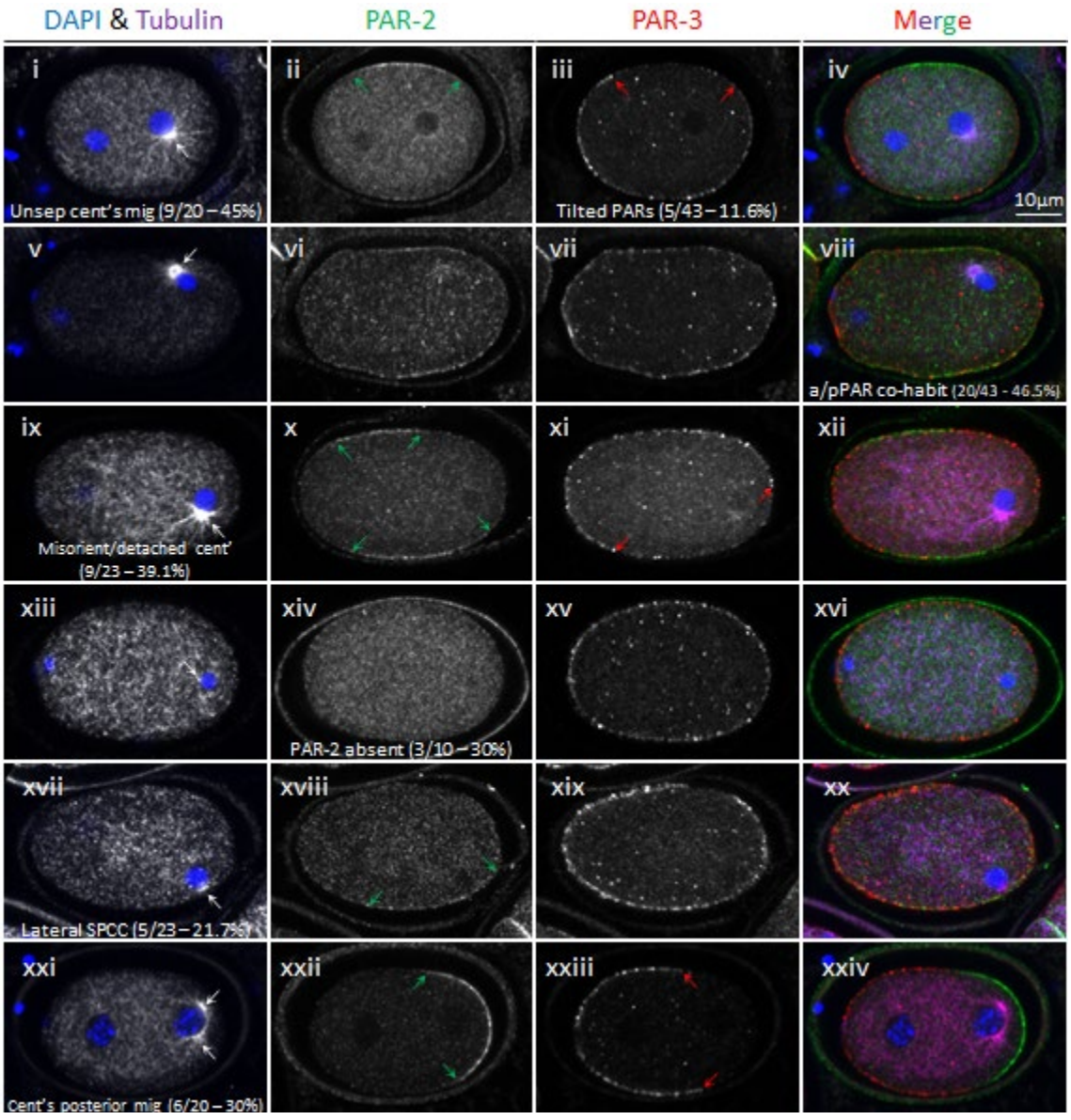

Figure 3.4 **Polarity and microtubule phenotypes observed in controls embryos.**

(a) & **(b)** Fixed immunofluorescent stained single-cell embryos of wild-type and *nop-1* mutant strains with non-wild-type appearances of anterior and posterior PARs (PAR-3 & PAR-2, respectively) and microtubule organisation, imaged via confocal microscopy. White arrows point to centrosomes. Green arrows point to boundaries of PAR-2 domain. Red arrows point to boundaries of PAR-3 domain. Phenotypes are reported in an example frame in which they can be observed including the number & percentage of embryos found with the given phenotype. Notes – Linear adjustment of brightness and contrast used for representation in figure. Number of experiments for control: 11. Number of experiments for *nop-1*: 7. Number of control embryos: 67. Number of *nop-1* embryos: 43.

rack-1

Receptor of activated C Kinase (RACK-1) is a cytoplasmic protein found enriched at the centrosomes and kinetochores of *C. elegans* zygotes. It has multiple roles including; recruiting recycling endosomes to the centrosomes, ensuring effective chromosome separation, cytokinesis and astral microtubule growth (Ai, Poole and Skop, 2009). RACK-1 was the strongest enhancer of lethality in the *nop-1* mutant vs the WT, suggesting it is required for the microtubule-dependent pathway of polarity establishment. It is likely that RACK-1 regulates the MT-dependent pathway via its role in ensuring proper microtubule growth. A previous study had shown that PAR polarity instability during polarity maintenance is correlated with short microtubules induced by RACK-1 depletion (Ai, Poole and Skop, 2011). The study did not observe change during polarity establishment assumedly due to the presence of early actomyosin flows which are still able to drive symmetry breaking at this point.

In this study, loss of *rack-1* produced a tilted PAR phenotype (Figure 3.5.a.ii-iv) in 1 out of 6 (*rack-1*: 16.7%, control: 0 out of 67 – 0%) embryos imaged which was exacerbated in the double LoF with *nop-1 (nop*;*rack-1*: 3 out of 9 – 33.3%, *nop-1*: 5 out of 43 – 11.6%) (Figure 3.5.b.ii-iv). Surprisingly, 5 out of 9 (55.6%) *nop-1*;*rack-1* embryos still polarised as normal, however, despite the absence of flows and compromised MT growth (Appendix: Table 9.1). This suggests that small microtubules are sufficient to drive PAR-2 recruitment to the cortex but prone to compromised orientation of the axis of polarity.

We observed 3 out of 5 (60%) *rack-1* RNAi depleted embryos with SPCC mispositioning. In these scenarios, the SPCC was observed detached from the cortex (*rack-1*: 2 out of 5 – 40%, control: 1 out of 40 – 2.5%) (Figure 3.5.a.i) or positioned laterally (*rack-1*: 1 out of 5 – 20%, control: 1 out of 40 – 2.5%) (Figure 3.5.a.v) rather than at the posterior pole as expected in WT embryos (Figure 3.3.a.v) (Appendix: Table 9.3). In *nop-1;rack-1* embryos, detached and lateral SPCCs (Figure 3.5.b.i) were observed at frequencies - 1 out of 4 (25%) and 2 out of 4 (50%), respectively. We also observed a *nop-1;rack-1* embryo during pronuclear migration in which one centrosome was facing the posterior (*nop;rack-1*: 1 out of 5 – 20%, control: 0 out of 19 – 0%, *rack-1*: 0 out of 1 – 0%) (Figure 3.5.b.v), suggesting a delay/difficulty in centrosome travel to face the anterior as expected in WT embryos.

Figure 3.5

a.

rack-1

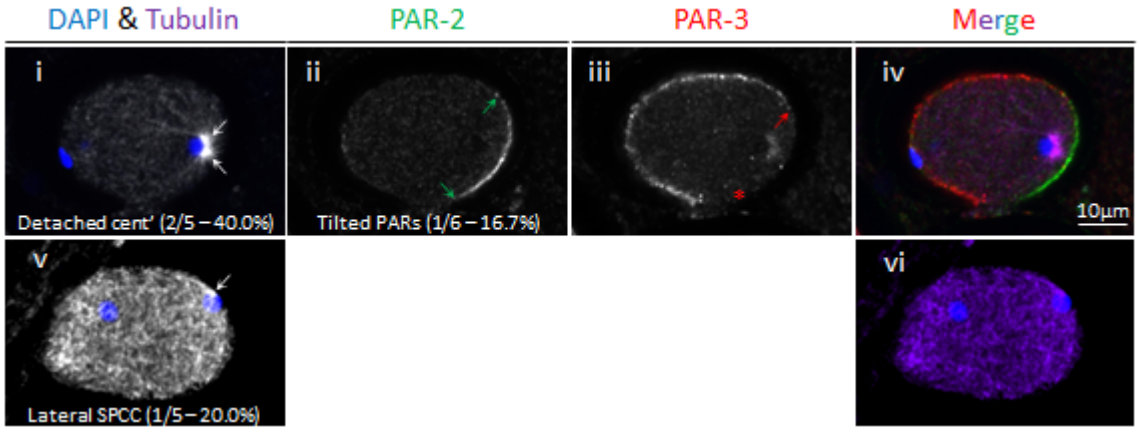

b.

nop-1; *rack-1*

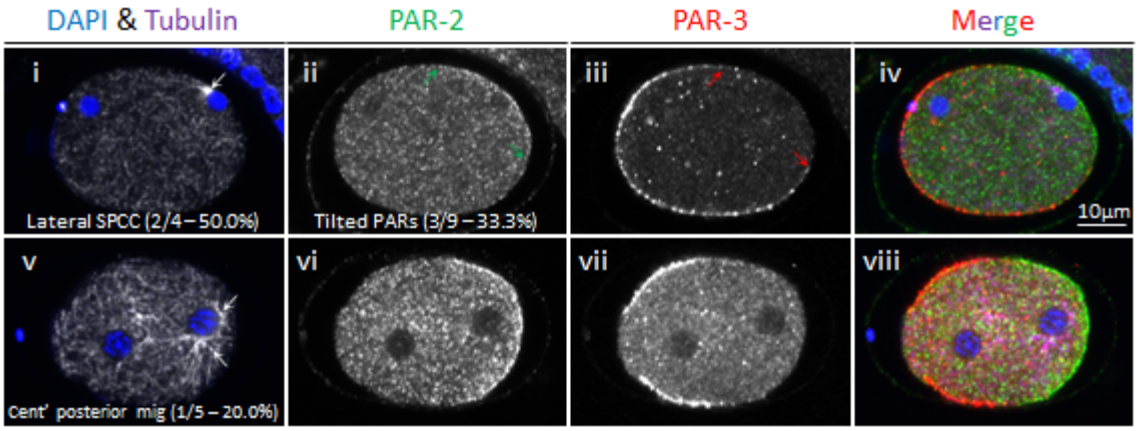

Figure 3.5 **Polarity and microtubule phenotypes observed in *rack-1* depleted embryos.**

(a) & **(b)** Fixed immunofluorescent stained single-cell embryos of wild-type and *nop-1* mutant strains depleted of *rack-1* via RNAi with non-wild-type appearances of anterior and posterior PARs (PAR-3 & PAR-2, respectively) and microtubule organisation, imaged via confocal microscopy. White arrows point to centrosomes. Green arrows point to boundaries of PAR-2 domain. Red arrows point to boundaries of PAR-3 domain. Notes – Linear adjustment of brightness and contrast used for representation in figure. Embryo represented in (a) had burst at aPAR-pPAR boundary so unable to determine where the PAR-3 domain truly ends (*). Embryo (a.v-vi) had poor PAR-2 & PAR-3 staining; thus, these frames were excluded. Number of experiments: 2. Number of *rack-1* embryos: 6. Number of *nop-1;rack-1* embryos: 9. PAR

arf-1.2 & *cnt-2*

The small GTPase, ARF-1.2, localises to the Golgi and endosomes and is required for membrane trafficking and regulating asymmetry in neuroblasts. CNT-2 is an ArfGAP (GTPase activating protein) which regulates ARF-1.2's activity (Singhvi *et al.*, 2011; Teuliere *et al.*, 2014). It was suggested that these proteins' roles in endocytosis are key to regulating asymmetric division in Q.p neuroblast division, making them interesting hits of the screen as the role of recycling endosomes in polarity establishment/maintenance in the zygote is not well understood (Singhvi *et al.*, 2011).

Upon knockdown of *arf-1.2*, we observed tilted PAR domains (*arf-1.2*: 1 out of 5 embryos – 20%, control: 0 out of 67 – 0%) (Figure 3.6.a.ii-iv) and bipolarity in which PAR-2 formed domains at both the anterior and posterior poles (*arf-1.2*: 2 out of 5 embryos – 40%, control: 3 out of 67 – 4.5%) (Figure 3.6.a.vi-viii). LoF of *arf-1.2* in the *nop-1* mutant suppressed bipolarity (*nop-1;arf-1.2*: 0 out of 6 embryos – 0%) (Figure 3.6.b)(Appendix: Table 9.1). Large cytoplasmic vacuoles appeared to form in the absence of ARF-1.2 suggestive of defects in membrane trafficking (*arf-1.2*: 3 out of 5 – 60%, *nop-1;arf-1.2*: 5 out of 6 - 80%, control: 0 out of 67 – 0%, *nop-1*; 0 out of 43 – 0%) (Kage-Nakadai *et al.*, 2019) (Appendix: Table 9.3). We saw defects in centrosome separation as centrosomes travelled together around the pronucleus (Figure 3.6.b.i) rather than opposite sides as in WT embryos in 2 out of 3 (66.7%) of *nop-1;arf-1.2* embryos (control: 3 out of 18 – 16.7%, *nop-1*: 1 out of 13 – 7.7%, *arf-1.2*: 0 out of 2 – 0%).

Knockdown of *cnt-2* similarly produced establishment phase embryos with bipolar PAR-2 domains (*cnt-2*: 6 out of 17 – 35.3%, control: 3 out of 67 – 4.5%) (Figure 3.6.c.ii-iv) as *arf-1.2* which was also rescued in the *nop-1* mutant (Figure 3.6.d). Interestingly, loss of CNT-2 resulted in embryos with an overgrown PAR-2 domain (*cnt-2*: 3 out of 17 – 17.6%, control: 1 out of 67 – 1.5%) suggesting a role in suppressing posterior domain expansion. Combined LoF with the *nop-1* mutant resulted in compromised PAR-2 loading to the cortex (Figure 3.6.d.ii-iv) (*cnt-2*: 1 out of 6 – 16.6%) more similar to the *nop-1* mutant alone (*nop-1*: 2 out of 13 – 15.4%) (Figure 3.4.b.xiv)(Appendix: Table 9.1). Also in the *nop-1;cnt-2* condition, we noticed 4 out of 6 (*nop-1;cnt-2*: 66.7%, cnt-2: 0 out of 4 – 0%, *control*: 1 out of 19 – 5.3%) embryos had their centrosomes oriented towards the posterior during pronuclear migration (Figure 3.6.d.v&viii) when the centrosomes would normally face the anterior in control embryos suggesting

defects in centrosome migration. This only occurred in 6 out of 20 (30%) *nop-1* embryos (Figure 3.4.b.xxi) (Appendix: Table 9.2).

Figure 3.6

a.

arf-1.2

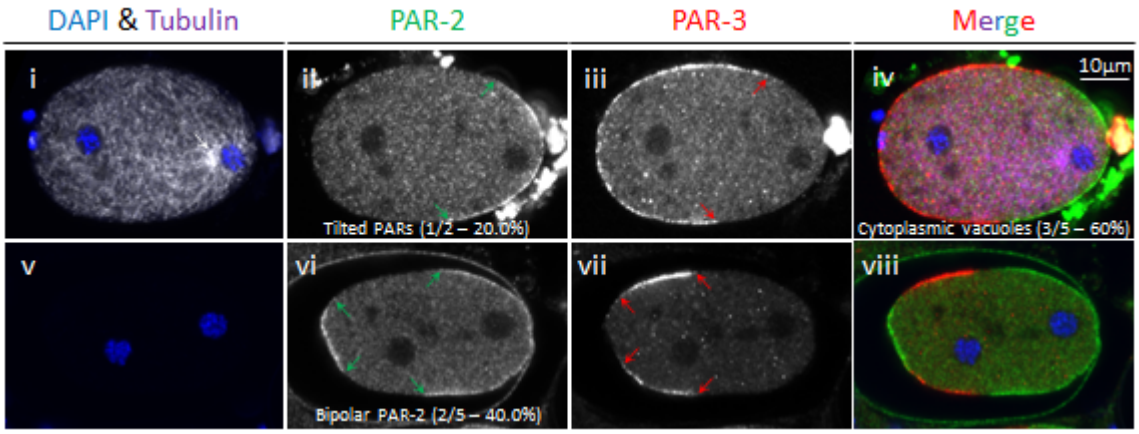

b.

nop-1; *arf-1.2*

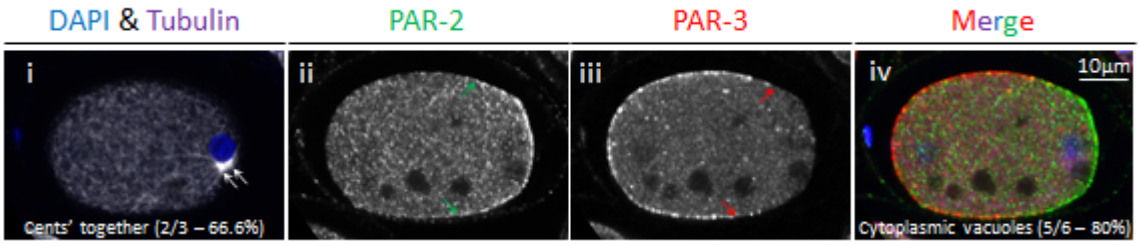

c.

cnt-2

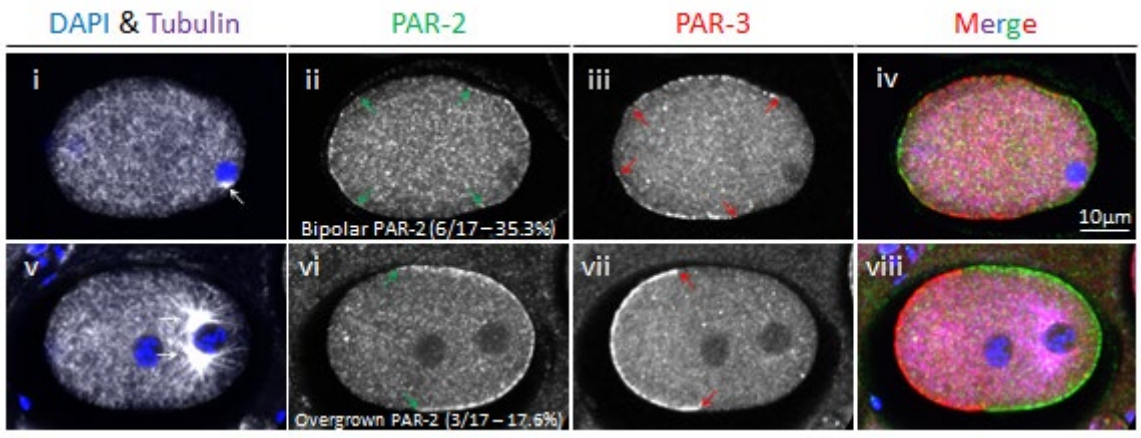

d.

nop-1; *cnt-2*

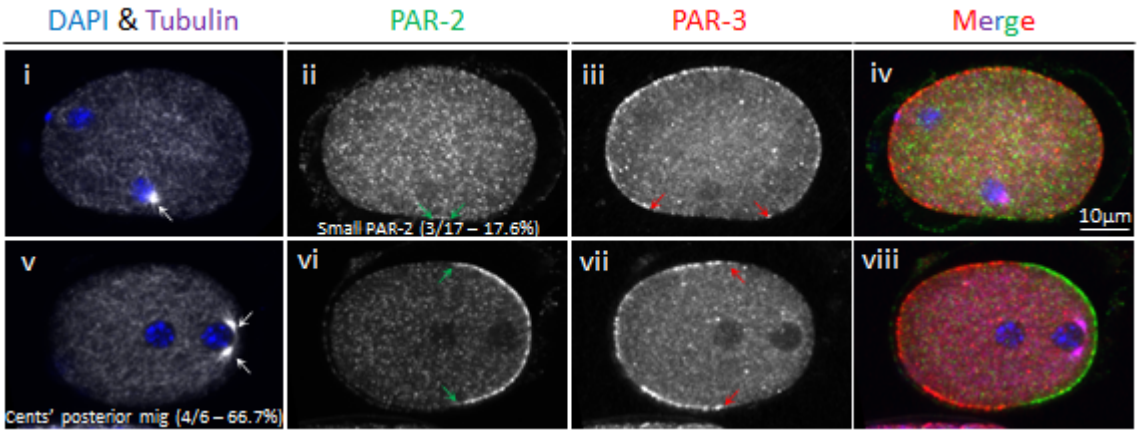

Figure 3.6 **Polarity and microtubule phenotypes observed in *arf-1.2* & *cnt-2* depleted embryos.**

(a) & **(b)** Fixed immunofluorescent stained single-cell embryos of wild-type and *nop-1* mutant strains depleted of *arf-1.2* via RNAi with non-wild-type appearances of anterior and posterior PARs (PAR-3 & PAR-2, respectively) and microtubule organisation, imaged via confocal microscopy. **(c)** & **(d)**, as (a) & (b) upon *cnt-2* RNAi knockdown. White arrows point to centrosomes. Green arrows point to boundaries of PAR-2 domain. Red arrows point to boundaries of PAR-3 domain. Note – tubulin stain missing from a.v. Notes – Linear adjustment of brightness and contrast used for representation in figure. Number of experiments for *arf-1.2*: 2. Number of experiments for *nop-1*;*arf-1.2*: 1. Number of experiments for *cnt-2*: 2. Number of experiments for *nop-1*;*cnt-2*: 1. Number of *arf-1.2* embryos: 5. Number of *nop-1;arf-1.2* embryos: 6. Number of *cnt-2* embryos: 15. Number of *nop-1;cnt-2*: 13.

let-754

LET-754 is a homologue of human AK2 (adenylate kinase) of the protein kinase A signalling pathway. It is predicted to maintain its role in *C. elegans* as a catalyst of ATP ↔ AMP conversion (Shaye and Greenwald, 2011; Kim *et al.*, 2018). Our lab found that LET-754 also likely acts as an antagonist of PKC-3 as knockdown of *let-754* suppresses lethality induced in a temperature sensitive mutant of *pkc-3* suggesting a novel role of LET-754 in regulating polarity (Fievet *et al.*, 2012). This was backed up in recent work by Yang et al. (2017) who set to develop automatic analysis of phenotypes in *C. elegans* embryos and showed that loss of LET-754 results in a reduced difference between the sizes of the two daughter cells after the first cell division. Typically, the anterior and posterior PAR domains guide the cleavage site during cytokinesis with a bias towards the posterior, resulting in a larger AB (anterior) daughter cell

vs the P1 (posterior) daughter cell. This suggests that asymmetry becomes compromised upon depletion of *let-754* (Yang *et al.*, 2017).

In our immunofluorescent stains we observed polarity defects in the WT strain upon *let-754* knockdown including an increased proportion of embryos with bipolar PAR-2 domains (*let-754*: 3 out of 10 – 30%, control: 3 out of 67 – 4.5%) (Figure 3.7.a.ii-iv) and embryos in which PAR-3 became patchy, with regions of the anterior lacking PAR-3 (and not replaced by PAR-2) (*let-754*: 5 out of 10 - 50%, control: 0 out of 67 – 0%) (Figure 3.7.a.vi-vii). Both of these polarity phenotypes were partially suppressed in the *nop-1* mutant (Bipolar PARs - *nop-1;let-754*: 1 out of 6 – 16.7%, Patchy PAR-3 - *nop-1:let-754*: 1 out of 6 – 16.7%). The double loss of *nop-1*; *let-754* function condition resulted in an increased percentage of embryos with tilted PAR domains compared to *nop-1* alone (*nop-1;let-754*: 4 out of 6 – 66.7%, *nop-1* – 5 out of 43 – 11.6%) (Figure 3.7.b.ii-iv) (Appendix: Table 9.1).

In addition to the PAR defects, upon *let-754* knockdown in the wild-type strain and *nop-1* mutant we saw embryos in which the centrosomes were detached from the sperm-derived pronucleus (*let-754*: 1 out of 10 – 10%, *nop-1;let-754*: 2 out of 6 – 33.3%, control: 0 out of 44 – 0%, *nop-1*: 0 out of 43 – 0%) (Figure 3.7.a.v & b.v). A portion of embryos presented with abnormal microtubule accumulation at the cortex (*let-754*: 3 out of 10 – 30%, *nop-1;let-754*: 1 out of 6 – 16.7%, control: 0 out of 44 – 0%, *nop-1*: 0 out of 43 – 0%) (Figure 3.7.a.v & b.ix) suggesting that LET-754 may influence microtubule growth (Appendix: Table 9.2). Embryos were also larger in size after *let-754* RNAi depletion compared to control embryos – note the scale bar in Figure 3.7a&b.

Finally, we saw defects in cell division in *let-754* depleted embryos. We observed embryos that presented with three pronuclei with a two centrosomes or embryos with multiple nuclei and more than two centrosomes suggesting failures in meiosis and mitosis, respectively (note: we did not score the percentage of embryos with division defects as we only took images of these embryos out of interest, however the phenotype appeared highly penetrant and was not observed in the control or *nop-1* mutant) (Figure 3.7.a.ix & b.ix) (Appendix: Table 9.3).

Figure 3.7

a.

let-754

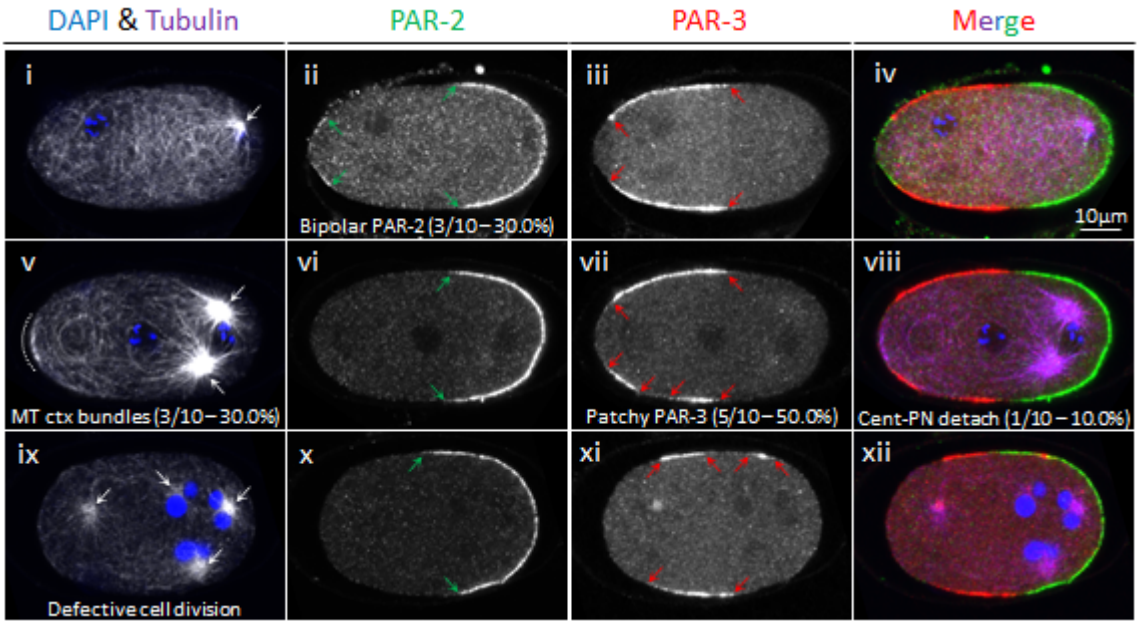

b.

nop-1; *let-754*

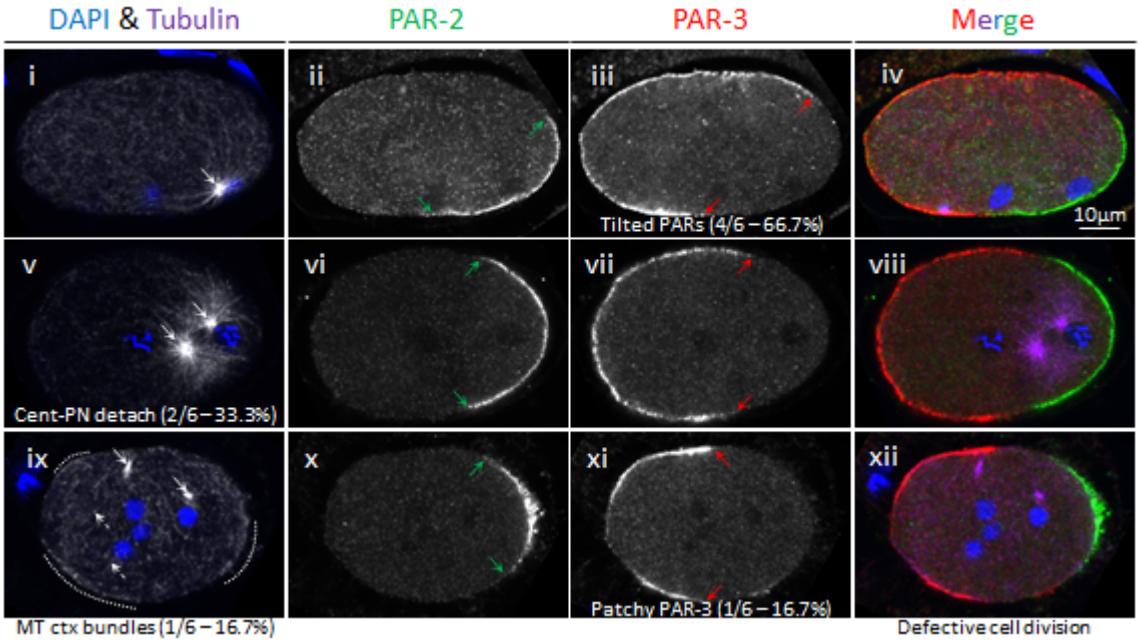

Figure 3.7 **Polarity and microtubule phenotypes observed in *let-754* depleted embryos.** **(a)** & **(b)** Fixed immunofluorescent stained single-cell embryos of wild-type and *nop-1* mutant strains depleted of *let-754* via RNAi with non-wild-type appearances of anterior and posterior PARs (PAR-3 & PAR-2, respectively) and microtubule organisation, imaged via confocal microscopy. White arrows point to centrosomes (note - out of focus centrosomes represented by broken white arrows, b.ix). Green arrows point to boundaries of PAR-2 domain. Red arrows point to boundaries of PAR-3 domain. White broken lines represent cortical microtubule bundles. Note – The tubulin stain for embryo i-iv was taken at a different focus to the PAR protein stains. Linear adjustment of brightness and contrast used for representation in figure. Number of experiments for *let-754* & *nop-1*;*let-754*: 1. Number of *let-754* embryos: 10. Number of *nop-1;let-754* embryos: 6.

klp-19

As previously discussed (Section 1.3.1), KLP-19 is a chromokinesin required for efficient chromosomal congression during metaphase and segregation during anaphase (Powers *et al.*, 2004).

Loss of KLP-19 resulted in an increased proportion of zygotes with bipolar PAR-2 domains (*klp-19*: 12 out of 53 – 22.6%, control: 3 out of 67 – 4.5%) (Figure 3.8.a.ii-iv) and zygotes in which PAR-3 had cleared from the anterior but was not replaced by PAR-2 *(klp-19*: 9 out of 53 – 17.0%, control: 5 out of 67 – 7.5%) (Figure 3.8.a.xiv-xvi). We also saw zygotes with no PAR-2 domain during pronuclear touch (*klp-19*: 4 out of 11 – 36.4%, control: 0 out of 10 – 10%) (Figure 3.8.a.vi), at which point the posterior domain has usually begun to establish in the control. This suggests a role for KLP-19 in ensuring timely polarity establishment (Appendix: Table 9.1).

Upon *klp-19* depletion we also saw strongly tilted polarity axis in 2 out of 53 (klp-19: 3.8%, control: 0 out of 67 – 0%) embryos (Figure 3.8.a.x-xii). This increased to 9 out of 22 (40.9%) in conjunction with the *nop-1* mutant (Figure 3.8.b.ii-iv) compared to 5 out of 43 (11.6%) in the *nop-1* mutant without knockdown. This suggests KLP-19 is important for ensuring proper polarity axis determination although likely acts partially redundantly with actomyosin dynamics (NOP-1) (Appendix: Table 9.1).

We also saw microtubule associated defects in *klp-19* depleted embryos as the positions of the centrosomes became altered. As discussed earlier, during polarity establishment, the centrosome is positioned at the far posterior between the male PN and the cortex where it

duplicates (Figure 3.3). Both centrosomes then move around the PN diametrically to each other until they face the anterior.

Upon *klp-19* depletion, we saw zygotes during pronuclear touch in which the centrosome was misoriented around the sperm pronucleus facing the anterior (*klp-19*: 4 out of 21 – 19.0%, control: 0 out of 25 – 0%) (Figure 3.8.a.xvii) rather than the posterior, between the pronucleus and the membrane. We also observed embryos in which the SPCC was mispositioned (*klp-19*: 9 out of 24 – 37.5%, control: 2 out of 40 – 5%), either detached from the cortex (Figure 3.8.a.v) or attached to the cortex but not at the posterior pole (Figure 3.8.a.ix). This increased in the *nop-1*; *klp-19* double LoF (11 out of 17 – 64.7%) (Figure 3.8.b.v&ix) to a similar frequency as the *nop-1* mutant on control RNAi (14 out of 23 – 60.9%). During pronuclear migration we saw *klp-19* RNAi embryos in which the centrosomes remained attached together (4 out of 21 – 19.0%) rather than separated as in WT (0 out of 19 – 0%), likely a result of the earlier defects (Figure 3.8.a.i)(Appendix: Table 9.2 & Table 9.3). To date, KLP-19 has only been reported to be present on meiotic/mitotic chromosomes, the spindle and the cortex of meiotic embryos or within the nucleus during interphase (Powers *et al.*, 2004; Monen *et al.*, 2005; Wignall and Villeneuve, 2009; Pelisch *et al.*, 2017).

As KLP-19 has predominantly been described during metaphase and anaphase as a chromokinesin, it was interesting to see in this study that it generated the polarity phenotypes (delayed pPAR domain formation & tilted PAR axis) and microtubule defects (mispositioned SPCC) during prophase. This made KLP-19 a good candidate to be involved in microtubule-dependent polarity establishment and called for further investigation.

Figure 3.8

a.

klp-19

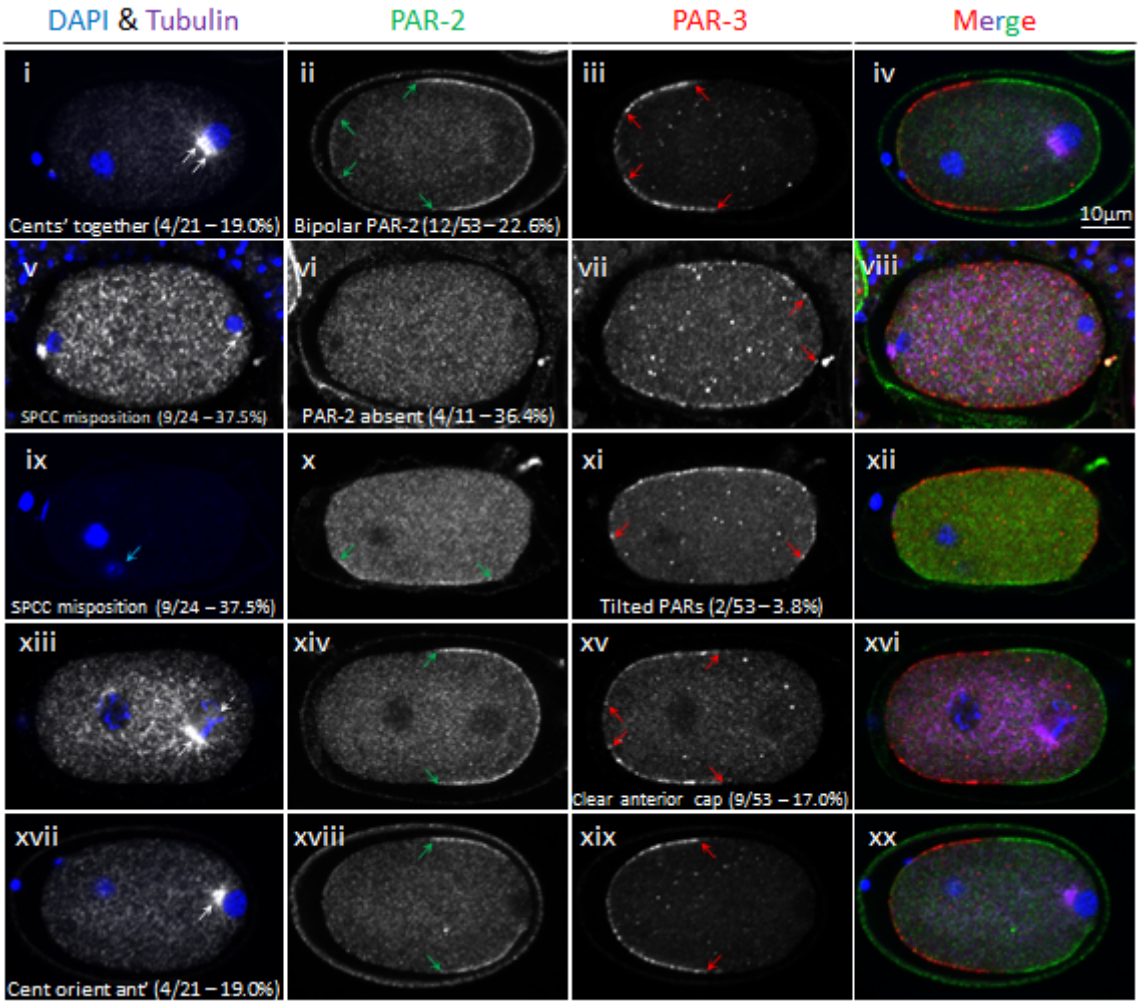

b.

nop-1; *klp-19*

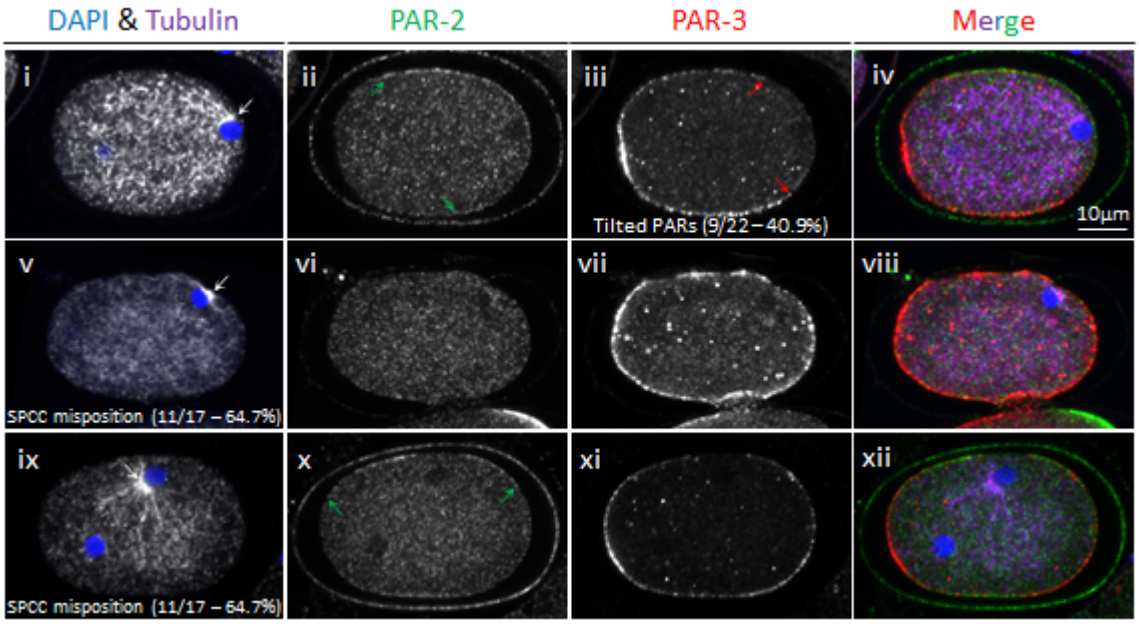

Figure 3.8 **Polarity and microtubule phenotypes observed in *klp-19* depleted embryos.**

(a) & **(b)** Fixed immunofluorescent stained single-cell embryos of wild-type and *nop-1* mutant strains depleted of *klp-19* via RNAi with non-wild-type appearances of anterior and posterior PARs (PAR-3 & PAR-2, respectively) and microtubule organisation, imaged via confocal microscopy. White arrows point to centrosomes (note - out of focus centrosome represented by broken white arrows, a.xiii). Green arrows point to boundaries of PAR-2 domain. Red arrows point to boundaries of PAR-3 domain. Blue arrow points to male pronucleus in a.ix due to being out of focus. Note – tubulin stain missing from a.ix. Notes – Linear adjustment of brightness and contrast used for representation in figure. Figures a.v&ix and b.v&ix all represent embryos with mispositioned centrosomes. a.v and b.ix show an embryo in which the SPCC has detached from the cortex while a.ix and b.v show an embryo in which the SPCC contacts the cortex but not at the posterior. Number of experiments for *klp-19*: 9. Number of experiments for *nop-1*;*klp-19*: 4. Number of *klp-19* embryos: 53. Number of *nop-1;klp-19* embryos: 22.

3.3 Discussion

In this chapter we have shown that a *nop-1* mutant, devoid of early zygote actomyosin-dependent cortical flows, is a great tool that can be used to identify novel genes with a role in polarity establishment, potentially acting via the microtubule-dependent pathway.

Our lab took a 3-tiered approach to identify genes required to regulate the MT-dependent pathway of polarity establishment, starting with a large-scale suppressor screen of cell polarity regulators (Fievet *et al.*, 2012) followed by a smaller semi-quantitative *nop-1* enhancer screen which led us to the quantitative screening approach of this project. This allowed us to home in on candidate genes that regulate polarity establishment. We then assessed this through immunofluorescent staining for polarity and microtubule organisation markers.

Of the fifteen genes screened in this project, we identified seven that enhanced embryonic lethality in the *nop-1* mutant (Table 3.1). Interestingly, four of these seven genes had previously discovered links to the regulation of microtubule dynamics/organisation. RACK-1 is required for efficient microtubule growth (Ai, Poole and Skop, 2011), GPB-1 regulates centrosome migration and orientation around the sperm pronucleus by suppressing cortical forces (Zwaal *et al.*, 1996; Gotta and Ahringer, 2001; Tsou, Hayashi and Rose, 2003; Afshar *et al.*, 2004; Thyagarajan, Afshar and Gonczy, 2011), KLP-19 is a microtubule motor protein (chromokinesin) (Powers *et al.*, 2004; Wignall and Villeneuve, 2009) and PLK-1 is a kinase found to suppress microtubule dynamics (Liu, Davydenko and Lampson, 2012; Rashid *et al.*, 2020).

To follow these results and confirm that the candidates obtained have roles in polarity we depleted embryos of each gene of interest and stained for markers of anterior and posterior polarity along with microtubules. Interestingly, all five knockdowns imaged in this chapter resulted in PAR phenotypes suggesting that the screen had effectively identified regulators of polarity in the *C. elegans* zygote (Appendix: Table 9.1). The phenotypes observed between different genes were variable, however, suggesting that the genes influence polarity through different ways. Note – due to failed staining, GPB-1 & PLK-1 have not been included, however both proteins have previously been implicated in regulating asymmetry in the zygote.

GPB-1 is trafficked asymmetrically within the zygote via the endosomal network and suppresses cortical microtubule pulling forces through the down regulation of GPR-1/2 levels,

with greater efficiency in the anterior during metaphase (Reminder: GPR-1/2 is a member of the cortical microtubule motor complex discussed in Section 1.6.1). How GPB-1 asymmetrically acts to regulate GPR-1/2 is unclear, however, as GPB-1 levels at the cortex appear symmetric. Thyagarajan, Afshar & Gonczy (2011) theorised that asymmetric trafficking of GPB-1 could mediate the availability of Gα, which binds to GPR-1/2. In this scenario, increased posterior internalisation of GPB-1 would increase the availability of Gα at the posterior cortex which subsequently recruits more GPR-1/2 and increases posterior pulling forces (Afshar *et al.*, 2004; Thyagarajan, Afshar and Gonczy, 2011). As previously discussed, the position of the mitotic spindle, as a results of these cortical pulling forces, determines the cleavage plane during cell division and the asymmetric size of the daughter cells (Sections 1.3.1 & 1.6.1).

PLK-1 plays a direct role in the establishment of polarity as it prevents premature symmetry breaking in zygotes (potentially via phosphorylating and preventing PAR-3 oligomerisation) (Dickinson *et al.*, 2017; Reich *et al.*, 2019), and is essential for the asymmetric timing of mitotic entry in the second cell divisions of the AB/P_1 zygote daughter cells (Budirahardja and Gönczy, 2008).

Below I have discussed the common and unique phenotypes, observed via imaging, that arose upon RNAi knockdown of genes that enhanced lethality in the *nop-1* mutant vs the control strain.

Centrosome positioning defects

We commonly saw deviations in centrosome position within the cell and orientation around the pronucleus upon knockdown of the genes of this screen when compared to their respective control (Appendix: Table 9.2 & Table 9.3). This could suggest changes in microtubule dynamics such as altered microtubule growth (i.e., numbers of MTs, length) or it could suggest that the genes knocked down mediate the way microtubules interact with components at the cortex, nuclear envelope or within the cytoplasm. Such changes could affect push and pull forces exerted by or on the microtubules which would compromise centrosome positioning.

For example, *cnt-2* KD in the *nop-1* mutant caused a higher proportion of embryos in which the centrosomes would still face the posterior during pronuclear migration (4 out of 6 - 66.7%) vs the *nop-1* mutant without KD (6 out of 20 - 30.0%) (Figure 3.4.b.xxi). CNT-2 is required for efficient endocytosis in oocytes (Singhvi *et al.*, 2011) and the transport of vesicles is important for centrosome migration via drag generated within the cytoplasm as vesicles are carried towards the centrosomes by dynein (Kimura and Kimura, 2011; Barbosa *et al.*, 2017). It is possible that reduced endosomes in the absence of CNT-2 results in a drop in centring forces of vesicle transport, thus induce centrosome positioning defects.

We also saw centrosome positioning defects in the absence of RACK-1. It is possible that RACK-1's role in microtubule growth is important for microtubule interaction with the cortex to aid in centrosome positioning. Thus, upon *rack-1* RNAi, shorter microtubules would result in reduced contact with the cortex. The spectraplakin protein family are important for inter-cytoskeletal interaction through their ability to bind to both actin and microtubules. It would be interesting to knockdown the sole *C. elegans* spectraplakin, VAB-10 (human MCAF1), and assess whether we observe similar aberrant SPCC positioning defects as loss of RACK-1 (Jørgensen *et al.*, 2014).

Centrosome positioning defects were also seen in the absence of KLP-19. As a kinesin, KLP-19 physically binds to microtubules. It is possible that KLP-19 somehow anchors the centrosome via the microtubules it emanates. To date, however, KLP-19 has not been shown to act outside of meiosis/mitosis (Powers *et al.*, 2004; Wignall and Villeneuve, 2009; Pelisch *et al.*, 2017). We will investigate the role of KLP-19 further in Chapter 4, Chapter 5, Chapter 6 & Chapter 7.

LET-754 deficient embryos presented with defects in centrosome attachment to the sperm pronucleus and abnormal MT growth at the cortex similar to previous work in which the GEF *efa-6* was depleted (O'Rourke, Christensen and Bowerman, 2010). EFA-6 acts to limit MT overgrowth although it is not known if this is through promoted growth or suppressed catastrophe. It is possible that overgrowing MTs, as a result of *let-754*/*efa-6* depletion, push on the cortex/pronucleus which results in abnormal centrosome positioning and detachment from the pronucleus.

Tilted PARs

A common phenotype observed in the *nop-1* mutant was the deviation of the angle that the PAR domains formed along the anterior-posterior axis (i.e. tilted PARs) (Figure 3.4.b.iii-iv, xvii-xx & Figure 3.9). It was clear in these embryos, during pronuclear touch, that the tilted PARs were concomitant with a mispositioned centrosome, and that the establishment of the PAR-2 domain followed the position of the centrosome as seen in Figure 3.4xvii-xx. In wild-type embryos, the cytoplasmic flows, that initiate upon the triggering of polarity establishment, spread outwards at the cortex closest to the centrosome and drive aPARs away from that site allowing pPAR membrane recruitment (Figure 3.9.a) (Bienkowska and Cowan, 2012). Due to the ovoid shape of the zygote, should the centrosome trigger polarity at the lateral cortex, the cortical flows will still converge opposite to the half of the embryo that the centrosome resides and produce a central flow back towards the centrosome. These counter cortical and internal cytoplasmic flows are able to correct the SPCC's position and PAR domain axis, assuming the SPCC is in the posterior half of the zygote – otherwise the centrosome will trigger reversed polarisation (Figure 3.9.b) (Goldstein, Hird and White, 1993; Hird and White, 1993; Goldstein and Hird, 1996; Rappleye *et al.*, 2002; Cuenca, 2003; Reymann *et al.*, 2016; Mittasch *et al.*, 2018). It is unsurprising, then, that tilted PAR domains are captured more often in the *nop-1* mutant when cortical flows are not present to correct the SPCC and PAR localisations. Indeed this is consistent with other work in flow compromised embryos (Hird and White, 1993; Goldstein and Hird, 1996; Rappleye *et al.*, 2002; Schenk *et al.*, 2010; Fievet *et al.*, 2012; Ding *et al.*, 2017).

Figure 3.9

a. Wild Type

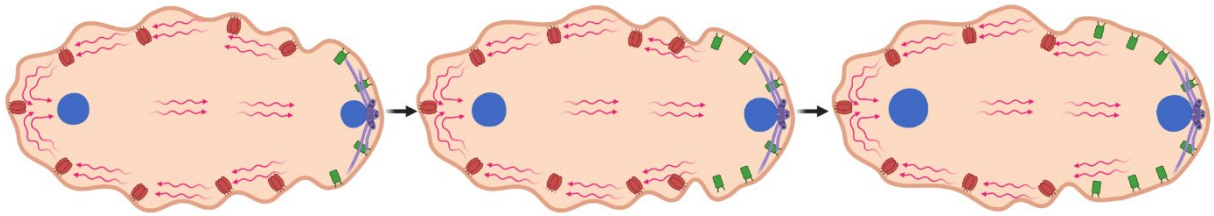

b. Lateral SPCC

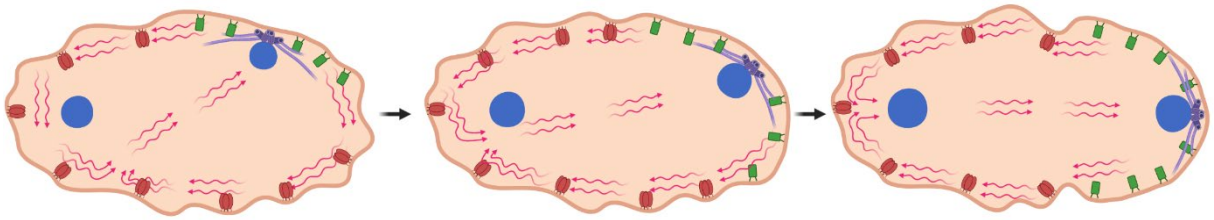

Figure 3.9 **Wild-type and tilted posterior PAR domain formation and resolution.**

(a) In wild-type embryos, the sperm pronucleus is restricted to the posterior pole where the centrosome triggers polarity establishment and recruits pPARs to the nearby membrane. **(b)** Under certain conditions, the sperm pronucleus settles laterally within the embryo which triggers pPAR recruitment at the nearby membrane resulting in a tilted polarity axis. This resolves due to the ovoid shape of the embryo and cytoplasmic flows reposition the sperm pronucleus-centrosome complex back to the posterior pole and corrects the polarity axis.

We observed an increased proportion of embryos with tilted PAR domains upon knockdown of *rack-1*, *let-754* and *klp-19* in the *nop-1* mutant and a small number in the wild-type strain upon *rack-1* and *klp-19 KD*. This was never observed in the WT strain on control RNAi despite having the largest N number, showing that these three genes are important in ensuring proper establishment of the polarity axis. There was a high correlation between aberrant centrosome positioning and the tilted PAR phenotype in these knockdowns. This was particularly obvious for *klp-19* and *rack-1* KD which led to greater SPCC positioning defects than control RNAi. 4 out of 5 (80.0%) pronuclear touch *nop-1*;*klp-19* embryos with tilted PARs had a mispositioned centrosome which correlated with the position of PAR-2 recruitment (Figure 3.8.b). This was the case for 2 out of 2 (100%) *rack-1;nop-1* embryos (Figure 3.5.b).

It is interesting to note that RACK-1 has previously been shown to regulate the angle of the axis of polarity in maintenance phase *C. elegans* embryos via its role in ensuring long astral microtubule growth, although the mechanism remains unclear (Ai, Poole and Skop, 2011). This

previous work had failed to identify polarity defects during establishment, likely as a result of actomyosin flows ensuring correct polarity axis formation, which are absent during maintenance. Of course, this explains why establishment defects in *rack-1* embryos became prevalent in the *nop-1* mutant, which lacks establishment flows, used in this project.

Bipolar PAR-2 domains

We commonly observed the formation of bipolar embryos in which PAR-2 localised to the anterior and posterior cortex upon the knockdowns of *cnt-2*, *klp-19* and *arf-1.2* (Figure 3.10). Anterior PAR-2 domain formation was reminiscent of work by Wallenfang & Seydoux (2000) who presented some of the first evidence of microtubule-dependent polarity. In their work, they induced meiosis I arrest which prevents microtubule growth from the sperm-derived centrosome and prolongs the lifetime of the meiotic spindle. They showed that PAR-2 then formed a domain in the typical anterior which closely matched position of the meiotic spindle. Their work indicated that polarisation is initially inhibited in the zygote as meiotic spindle-induced PAR-2 domain formation does not occur in wild-type embryos when centrosome-induced polarisation takes place in a timely manner. When meiosis is arrested, the instruction to prevent meiotic spindle PAR-2 formation must weaken, allowing reversed polarity to ensue (Wallenfang and Seydoux, 2000). As mentioned, however, it has previously been shown that nocodazole treated embryos, lacking microtubules, still formed bipolar PAR-2 domains in the zygote and suggested that MTs may not be the sole cue for pPAR cortical loading, but that membrane regions of high-curvature act as favourable sites for pPARs (Section 1.6.4) (Klinkert *et al.*, 2019). Interestingly, the position of the centrosome was irrelevant in determining bipolar PAR-2 domain formation in *air-1* RNAi embryos. This was true in KLP-19 depleted embryos, in which the centrosomes position often became aberrant, as only 1 in 4 embryos with bipolarity had a mispositioned centrosome which could suggesting alternative roles of KLP-19 are responsible for this polarity defect (Klinkert *et al.*, 2019).

Klinkert et al. (2019) showed that depletion of the mitotic kinase *air-1* (Aurora A), induced multiple polarity defects, including the bipolar PAR-2 phenotype. In their experiments, they demonstrated that 67% of embryos under meiotic arrest develop anteriorly localised PAR-2 domains. This proportion increased to 79% in arrested embryos upon RNAi knockdown of *air-1* suggesting that AIR-1 acts to suppress anterior PAR-2 domain formation (Klinkert *et al.*, 2019). This was supported by Reich et al. (2019) who demonstrated that the time between

ovulation and symmetry breaking is shortened from 45 minutes to under 30 minutes in the absence of AIR-1. They proposed that AIR-1 acts to prevent the maturation of the polarity network, required to localise the aPARs to the cortex and make them prone to mutual antagonism with the pPARs (Reich *et al.*, 2019).

AIR-1 also appears to initially prevent premature polarisation events through global suppression of actomyosin dynamics. As the centrosome matures, AIR-1 is sequestered to the pericentriolar material and triggers symmetry breaking as it diffuses from the centrosome and inhibits local actomyosin contractility at the presumed posterior pole, generating anteriorly directed cytoplasmic flows (Kapoor and Kotak, 2019; Klinkert *et al.*, 2019; Reich *et al.*, 2019; Zhao *et al.*, 2019). Upon *air-1* depletion, actomyosin activity becomes symmetrical at both anterior and posterior of the embryos. This generates weak flows towards the centre of the zygote and PAR-2 becomes enriched at the poles. It is not fully understood, however, whether these domains are formed due to these weak flows or if they are due to the microtubule-dependent pathway. Downregulating actomyosin activity to reduce flows has had mixed results on the formation of bipolar PAR-2 domains in *air-1* depleted embryos. Klinkert et al. (2019) saw bipolar PAR-2 domains remain in the knockdown of *air-1* in a temperature sensitive mutant of *nmy-2* whereas Kapoor and Kotak (2019), and Zhao et al. (2019) saw the abolition of bipolar PAR-2 domains (resulting in a single posterior PAR-2 domain) through co-depletion of *air-1* with each of *mlc-5*, *ect-2* and *nop-1*, required for flows (Kapoor and Kotak, 2019; Klinkert *et al.*, 2019; Zhao *et al.*, 2019). We also see the return to a single PAR-2 domain when depleting *cnt-2*, *let-754*, *klp-19* or *arf-1.2* in the *nop-1* mutant (i.e., compromised flows). It's possible that the knockdown of these genes could compromise the *air-1* pathway, required to ensure polarity establishment occurs at the correct time and space in the embryo. It would be interesting to monitor NMY-2 dynamics upon knockdown of these genes to determine if they similarly generate bipolar actomyosin-dependent flows and hyper-contractility as with *air-1* depletion.

Our lab previously did this for RNAi depletion of *cnt-2* in an NMY-2::GFP strain and observed that cortical actomyosin contractions became much stronger than in control embryos (Fievet *et al.*, 2012). The bipolarity and overgrown posterior domain size we saw in this project, upon *cnt-2* RNAi depletion, is reminiscent of work in which the GTPase activating proteins (GAPs), RGA-3/4 and CYK-4, were depleted (Schonegg *et al.*, 2007). The absence of these GAPs

similarly resulted in increased actomyosin contractions suggesting that CNT-2 may have scored as an enhancer in this screen due to further perturbed actomyosin dynamics in the *nop-1* mutant rather than disruption of the microtubule dependent pathway of polarity establishment.

We did not measure the timings of meiosis in this study; however KLP-19 has previously been shown to regulate metaphase and anaphase during meiosis and causes arrest upon complete loss of function (Wignall and Villeneuve, 2009; Dumont, Oegema and Desai, 2010; Pelisch *et al.*, 2017). We observed multinucleate embryos in the absence of LET-754 indicative of defects in prolonged meiotic exit which commonly sees failure of polar body extrusion. It is possible then, that these meiotic defects generate the bipolar PAR-2 we have observed upon *klp-19* and *let-754* knockdown. We cannot exclude that absence of either KLP-19 or LET-754 does not have secondary effects on actomyosin dynamics. Later in this project, however, we perform live imaging of *klp-19* deficient embryos and do not observe signs of a hypercontractile cortex as with *cnt-2*.

Figure 3.10

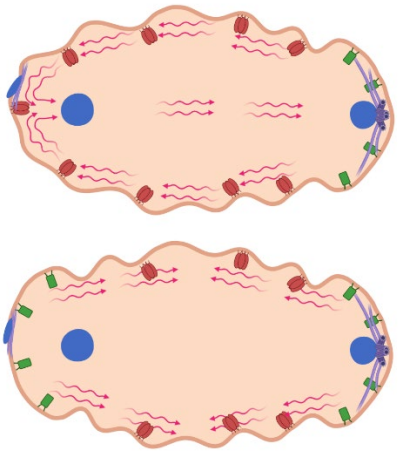

Figure 3.10 **Wild-type and bipolar posterior PAR domain formation.**

Top: In wild-type embryos, the sperm pronucleus is restricted to the posterior pole where the centrosome triggers polarity establishment and recruits pPARs to the nearby membrane. **Bottom**: Under certain conditions, such as meiotic arrest or *air-1* depletion, a temporary second pPAR domain establishes from the anterior pole.

Unique Phenotypes

let-754

PAR-3 in the anterior domain of *let-754* RNAi embryos became absent in patches (Figure 3.7.a.iii,vii&xi). This was striking as LET-754 was suggested to antagonise PKC-3, the kinase of the aPARs which acts to remove the pPARs from the cortex. Without LET-754 we might have assumed that the aPARs would be given a boost at the cortex, enhancing pPAR removal over aPAR. It has been shown in *D. melanogaster* that aPKC (PKC-3) is able to phosphorylate Bazooka (PAR-3) at conserved sites and facilitate its removal from the cortex (Morais-de-Sá, Mirouse and St Johnston, 2010; Walther and Pichaud, 2010). Indeed, Li et al. (2010) demonstrated in *C. elegans* that PAR-3 levels at the cortex increased during early embryogenesis upon inhibition of PKC-3 mediated PAR-3 phosphorylation. Constitutive phosphorylation of PAR-3 at the conserved PKC-3 phosphorylation site resulted in reduced PAR-3 levels at the cortex (Li *et al.*, 2010). It is possible that overactive PKC-3, due to loss of LET-754, is responsible for these patches of PAR-3 that are missing in the zygotes. As PKC-3 prevents pPAR localisation to the cortex, overactive PKC-3 could explain why PAR-2 does not invade the PAR-3 vacant membrane. Depletion of *let-754* also produced embryos with abnormal growth of MTs at the cortex. In Figure 3.7.a.v&vii, a thick bundle of MTs can be observed at the anterior pole, concurrent with the absence of PAR-3 in the same region. It is possible that MTs have a role in facilitating the removal of PAR-3 from the cortex. This hypothesis will be further investigated in Section 7.2.3.

let-754 embryos also presented with strong defects in cell division, as seen by multinucleate zygotes which indicates failure of cytokinesis. Defects in cell division have also been observed in cells depleted of the AK2 target, AMP-activated protein kinase (AMPK), a regulator of energy homeostasis (Thaiparambil, Eggers and Marcus, 2012). AMPK is activated by increased AMP:ATP ratios (Xiao *et al.*, 2007) which occurs in the absence of functional adenylate kinase (Gauthier *et al.*, 2008). Thaiparambil, Eggers and Marcus (2012) showed that, upon AMPK depletion, spindle microtubules were fewer, shorter and unable to contact the cortex of cells which was responsible for spindle orientation and positioning defects (Thaiparambil, Eggers and Marcus, 2012).

arf-1.2

Similar to work by Kage-Nakadai et al. (2019), we saw vacuole formation in zygotes (Figure 3.6.a&b) upon *arf-1.2* RNAi depletion, as they observed in the excretory canals of *arf-1.2* mutants (Kage-Nakadai *et al.*, 2019). These vacuoles are a sign of failure in membrane trafficking. As the recycling endosome pathway has been implicated in polarity maintenance, this opens the possibility of a role for ARF-1.2 and CNT-2 in regulating polarity through this process.

klp-19

The process of centrosome separation, required for spindle formation, appeared strongly perturbed upon *klp-19* RNAi KD. Typically, separation occurs during pronuclear touch while the newly duplicated centrosomes are still sat between the sperm pronucleus and the posterior pole. In the absence of KLP-19 we observed 4 out of 21 (19.0%) embryos in which the centrosomes were still not apart from each other, or lagged, by pronuclear migration suggesting that the separation process had become delayed. This is investigated further in Section 4.2.2.

Conclusions

Overall, this chapter has demonstrated that the *nop-1* mutant can be used as an effective tool to identify regulators of polarity establishment in the *C. elegans* zygote. All genes that scored as enhancers of lethality in the *nop-1* mutant, that were taken forward for immunofluorescent characterisation, presented with phenotypes in PAR asymmetry. Further detailed investigation of the identified genes, determining how they can regulate microtubules/actomyosin structure and dynamics, and PAR protein membrane turnover, will help to unravel the processes at play during polarity establishment.

Of the genes that enhanced lethality in the *nop-1* mutant, we wanted to focus on one that had a high chance to be involved in polarity establishment through the MT-dependent pathway. Two known microtubule regulators, that scored as the enhancers of lethality in the *nop-1* mutant, *rack-1* & *gpb-1*, have previously been the subjects of study with regards to polarity in the *C. elegans* zygote (Zwaal *et al.*, 1996; Gotta and Ahringer, 2001; Ai, Poole and Skop, 2009, 2011; Thyagarajan, Afshar and Gonczy, 2011). As such, we decided to follow-up on the

chromokinesin KLP-19 for further investigation as to how it regulates microtubules and polarity. KLP-19 and its homologues have been predominantly described to act during meiosis/mitosis. This made its role in polarity establishment curious as the stage is more akin to prophase (Mazumdar, Sundareshan and Misteli, 2004; Powers *et al.*, 2004; Bastos *et al.*, 2013; Pelisch *et al.*, 2017; Dong *et al.*, 2018; Heath and Wignall, 2019). Initial characterisation showed that the absence of KLP-19 resulted in delayed polarity establishment and SPCC positioning defects which we have focused on in throughout this project.

Chapter 4 The Chromokinesin, KLP-19, antagonises cortical pulling forces to mediate SPCC and mitotic spindle positioning.

4.1 Introduction.

In Chapter 3 we found that loss of the chromokinesin KLP-19 resulted in delayed polarity establishment and abnormal localisation of the SPCC away from the far posterior cortex in the early *C. elegans* zygote. As discussed in section 1.7.1, sustained centrosome positioning is important for robust polarity establishment as well as centrosome separation and the formation of a bipolar spindle (Bienkowska and Cowan, 2012; De Simone, 2016; De Simone, Nédélec and Gönczy, 2016; Saturno *et al.*, 2017).

In the WT embryo, the centrosomes are pinned between the sperm derived pronucleus and the far posterior cortex at the time of centrosome separation. The microtubules that emanate from the centrosomes are captured by cortical dynein which is carried to the anterior by cortical flows at the onset of polarity establishment. (De Simone, Nédélec and Gönczy, 2016). As a result, the centrosomes, and associated sperm pronucleus (SPCC) are pulled by these cortical forces anteriorly whilst concurrent internal posterior directed cytoplasmic flows push backwards on the sperm pronucleus and so the centrosomes are forced apart and around the pronucleus. In addition, the asters grow in an anisotropic manner from the centrosomes, with short microtubules reaching the nearby posterior cortical pole, where they depolymerise, whilst MTs directed outwards from the sides of the PN cortical contact grow longer in opposite directions from each centrosome. These long MTs permit more dynein motors to bind, thus have greater pulling forces on them, resulting in more efficient movement of the centrosomes away from each other dependent on initial SPCC positioning (Figure 1.13) (De Simone and Gönczy, 2017). As the centrosome are pulled from behind the pronucleus to face the anterior, the SPCC is then pulled anteriorly away from the cortex, thus entering the pronuclear migration stage. Upon aberrant centrosome positioning, it stands to reason that the centrosomes will not be forced apart as they will not be forced to move around opposite sides the pronucleus. The anisotropy of MT growth and pulling forces from each centrosome will also be lost. Thus, centrosome separation would be compromised.

To date, research has shown that microtubules, cytoplasmic flows and deubiquitylating enzymes (DUBs)/proteolytic regulating enzymes (PAM-1, USP-46, USP-67, MATH-33) are key

factors in the regulation of SPCC positioning as the absence of each results in aberrant SPCC localisation (Fortin *et al.*, 2010; Bienkowska and Cowan, 2012; McCloskey and Kemphues, 2012; Saturno *et al.*, 2017). The full mechanisms behind centrosome positioning, however, are poorly understood (Section 1.7.2). For example, the targets of the DUBs that regulate SPCC positioning have not been identified. Similarly, how microtubules facilitate SPCC contact to the cortex in the zygote is unknown. It is attractive to assume that the cortical dynein complex (dynein, LIN-5, GPR-1/2, Gα) that binds to centrosomal MTs could pull the centrosome towards the cortex. The loss of dynein, however, causes the SPCC to remain closer to the cortex for longer rather than result in detachment (Fortin *et al.*, 2010; McCloskey and Kemphues, 2012; De Simone, 2016; Saturno *et al.*, 2017). Therefore, microtubules must have alternative means to restrict the SPCC's initial position/attachment to the posterior cortex (i.e., Prior to symmetry breaking).

In this chapter, we sought to assess the *klp-19* RNAi-induced SPCC positioning defects in greater detail and determine whether the absence of KLP-19 leads to the expected later defects in centrosome separation. Through live imaging, we found that defects in the SPCC's ability to dock to the posterior cortex led to aberrant SPCC migration patterns, with particular regards to the centrosomes (i.e., delayed centrosome separation and delayed PN meet). This is consistent with previous models generated by computer simulations (De Simone and Gönczy, 2017; Boudreau *et al.*, 2019). We also found that KLP-19 seems to regulate SPCC migration and centrosome separation, through another unknown mechanism in addition to its role in initial SPCC positioning. This may be related to our final observation that KLP-19 appears to act antagonistically to forces generated by the cortical dynein complex during anaphase.

This work provides evidence that KLP-19 mediates spindle formation by restricting the centrosome's position to the far posterior cortex prior to centrosome duplication and suggests that KLP-19 has a role in the attenuation of cortical microtubule pulling forces.

4.2 Results

4.2.1 KLP-19 mediates SPCC attachment/positioning to the posterior pole of the zygote.

In Section 3.2.2 we characterised the phenotypes that fixed embryos presented with in the absence of KLP-19, indicating that KLP-19 is involved in SPCC positioning prior to centrosome

separation. As we wanted to further study these phenotypes and their downstream effects on centrosome separation and SPCC migration through live imaging, we compared the positions of the SPCC in control vs *klp-19* RNAi embryos from fixed samples to set the criteria of what WT vs aberrant SPCC positions look like. As previously mentioned, WT embryos appear with the SPCC in contact with the cortex at the far posterior pole with the centrosome positioned between the cortex and the sperm pronucleus (Figure 1.9 & Figure 4.1.a). Embryos were assessed by eye and qualitatively classed as aberrant/defective when the SPCC deviated from the WT appearance. Aberrant SPCCs presented with the SPCC positioned away from the posterior pole, the SPCC detached from the cortex, or the centrosomes not oriented towards the posterior pole (Figure 4.1.a.ii.iii.iv). Using these criteria, 2 out of 25 (8.0%) fixed control embryos had aberrant SPCC positioning during pronuclear touch which rose to 9 out of 21 (42.9%) upon *klp-19* RNAi KD (Figure 4.1.b). These numbers were consistent with the phenotypes scored in the initial characterisation and reaffirm our conclusions that KLP-19 is required for effective SPCC positioning (Section 3.2.2, Appendix: Table 9.2 & Table 9.3). As a protein with MT binding capabilities, it is possible that KLP-19 acts to fix centrosomal microtubules in place at the cortex to restrict the SPCC's localisation prior to symmetry breaking. Fixed images, however, limit our understanding of how phenotypes arise and progress and so the next step was to repeat the *klp-19* RNAi knockdowns in live embryos.

Figure 4.1

a.

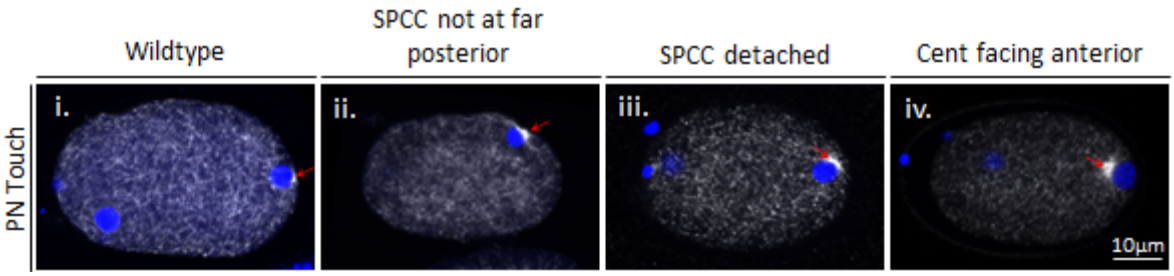

b.

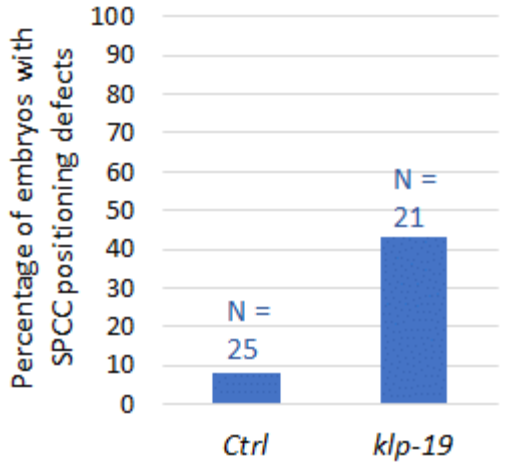

Figure 4.1 **Centrosome positioning defects in the absence of KLP-19.**

(a) Immunofluorescently labelled fixed embryos during pronuclear touch imaged via confocal microscopy (Microtubules-Grey, DNA-Blue) to highlight the phenotypes used to define wild-type vs aberrant initial centrosome positioning. (Red arrows point to centrosomes). Note: Linear adjustment of brightness and contrast used for representation in figure. **(b)** Percentages of embryos with early positioning defects in control (N=25) and KLP-19 RNAi (N=21) embryos. Number of experiments: 8.

4.2.2 KLP-19 is required for efficient centrosomal separation, predominantly through its role in positioning the SPCC at the posterior pole.

We have shown that KLP-19 is required to regulate the initial position/attachment of the SPCC to the posterior cortex. As discussed previously, computer modelling and experimental work have predicted that the centrosome's position and orientation, with respect to the sperm pronucleus and posterior cortex, would be important for effective centrosome separation, essential to form the mitotic spindle (De Simone and Gönczy, 2017; Boudreau *et al.*, 2019). (Section 1.7.1) It makes sense that the initial SPCC position would be important to centrosome separation as the centrosomes must be pinned to the posterior pole by the sperm PN to

ensure that cortical forces enacted by the cortical dynein complex pull the centrosome around opposite sides of the PN (De Simone, Nédélec and Gönczy, 2016). Deviation from this initial position would prevent the centrosomes from being forced apart around the PN.

To test the predictions of the importance of initial SPCC positioning in centrosome separation, we measured the distance between centrosomes over time from centrosome duplication to pronuclear meet in control vs *klp-19* RNAi embryos expressing tubulin::GFP;H2B::GFP (TY3558). As KLP-19 is required for effective SPCC positioning, we expected that loss of KLP-19 would generate a subset of embryos in which the centrosomes take longer than normal to separate (i.e., Those that had aberrant initial SPCC positions). Indeed, upon depletion of *klp-19* by RNAi, there was a significant decrease in the distance between centrosomes over time compared to control embryos when measured from the moment of centrosome duplication up to pronuclear meeting, implicating KLP-19's involvement in centrosome separation (Difference between the slopes significant P=0.0154) (Figure 4.2.a&bi).

Figure 4.2

a.

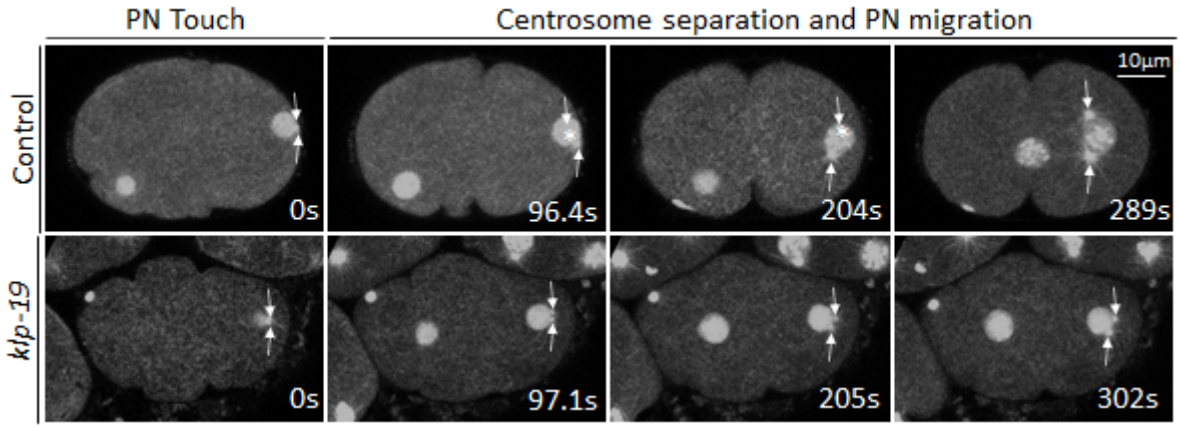

b.i.

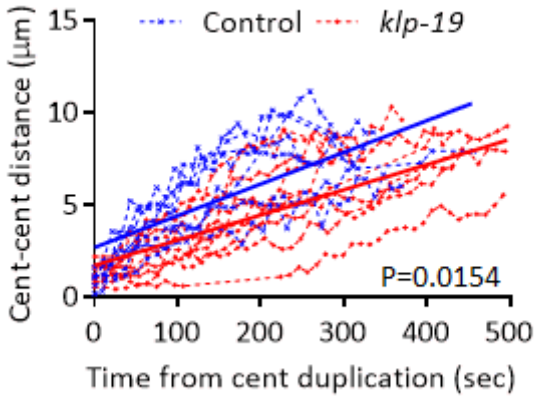

b.ii.

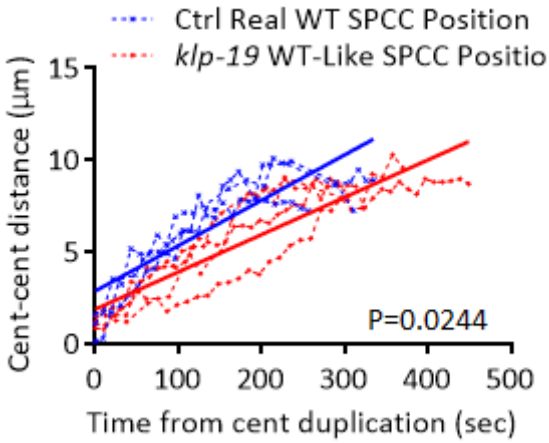

b.iii.

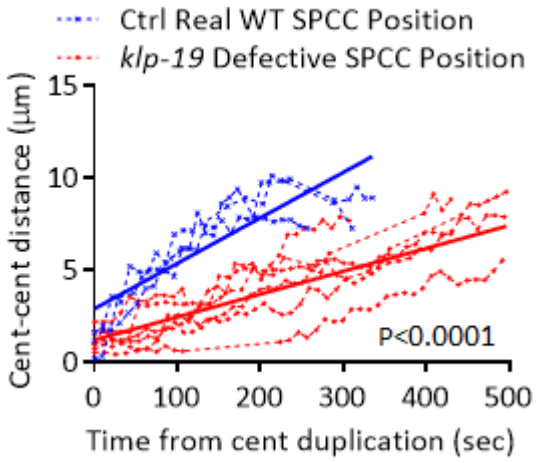

Figure 4.2 **The impact of KLP-19 on centrosome separation over time.**

(a) Maximum intensity projections of embryos expressing Tubulin::GFP;H2B::GFP recorded via live scanning confocal microscopy under control and *klp-19* RNAi conditions (Images acquired with frame interval 10.7 seconds. Frames selected ~100 seconds apart for purpose of figure,

all frames analysed) (0s = centrosome duplication). In the control, at 0s (top left), the SPCC is correctly positioned with centrosomes between the PN and the cortex, while the SPCC is detached in the *klp-19* KD (bottom left). White arrows point to centrosomes, asterisks highlight centrosome position when hidden by pronucleus. For more detailed imaging conditions see methods (Table 2.8). Note - Linear adjustment of brightness and contrast used for representation in figure. **(b)** i - Distance between centrosomes over time in control (N=7) and *klp-19* RNAi (N=10) embryos from centrosome duplication to PN meet. The distance was determined through Pythagoras' theorem which used the length between the centrosomes in the X/Y axes and the Z axis (determined by the number of Z stacks between the centrosomes) to calculate the hypotenuse (See methods). ii & iii – Data divided to plot control embryos with real WT SPCC (N=3) positioning (control embryos with aberrant initial SPCC positions removed) vs *klp-19* RNAi embryos with WT-like (N=4) and defective (N=6) SPCC positioning, respectively. P values indicate the probability that the lines of regression are different (ANCOVA) – $P<0.05$ is significantly different. Note – embryos in which both centrosomes could not be seen at centrosome duplication were removed from this figure as it could not be determined if both had WT initial positioning. Number of experiments: 2.

To take this a step further, we divided the data of *klp-19* depleted embryos depending on whether the SPCC had a WT position (N=4) at the posterior cortex during symmetry breaking (the first frame posterior membrane relaxation could be observed) or a defective position (N=6). Interestingly, *klp-19* RNAi embryos with WT-like positioned SPCCs during symmetry breaking underwent centrosome separation at a rate more similar to real WT embryos (Real WT = Control embryos with WT initial SPCC positioning), albeit still significantly slower (Difference in real WT vs klp-*19* WT-like slopes - P=0.0244) (Figure 4.2.a&b.ii). Embryos with defective SPCC positioning made up the subset of *klp-19* KD data in which centrosomes separate drastically more slowly (Difference in slopes – $P<0.0001$) (Figure 4.2.b.iii). These data suggest that KLP-19's role in coordinating the strict positioning of the SPCC to the posterior pole is important to regulate centrosome separation, however there is likely a separate KLP-19 dependent mechanism which contributes to the process.

To determine the penetrance of centrosome separation defects in the absence of KLP-19, we scored immunofluorescently labelled fixed embryos for centrosome defects between pronuclear migration to pronuclear meet. Centrosomes typically separate while positioned between the pronucleus and the posterior cortex and migrate around opposite sides of the pronucleus, the SPCC then moves towards the female pronucleus which it meets in the posterior half of the embryo (Figure 1.9.i-iv). The centrosomes will settle either side of the two pronuclei as represented in figure (Figure 1.9.iv, Figure 4.3.a.viii & Figure 4.5.a). Centrosome separation was considered defective when one or both centrosomes lagged and

were still facing the posterior during PN migration/ PN meet, the centrosomes migrate around the same side of the pronucleus, or the centrosomes were still attached to each other by pronuclear meet (Figure 4.3.a.vi,vii,ix&x). In control embryos, 3/33 (9.1%) showed defective centrosome separation while *klp-19* RNAi embryos scored 12/37 (32.4%) (Figure 4.3.b) showing that KLP-19 is indeed required to ensure efficient centrosome separation.

Figure 4.3

a.

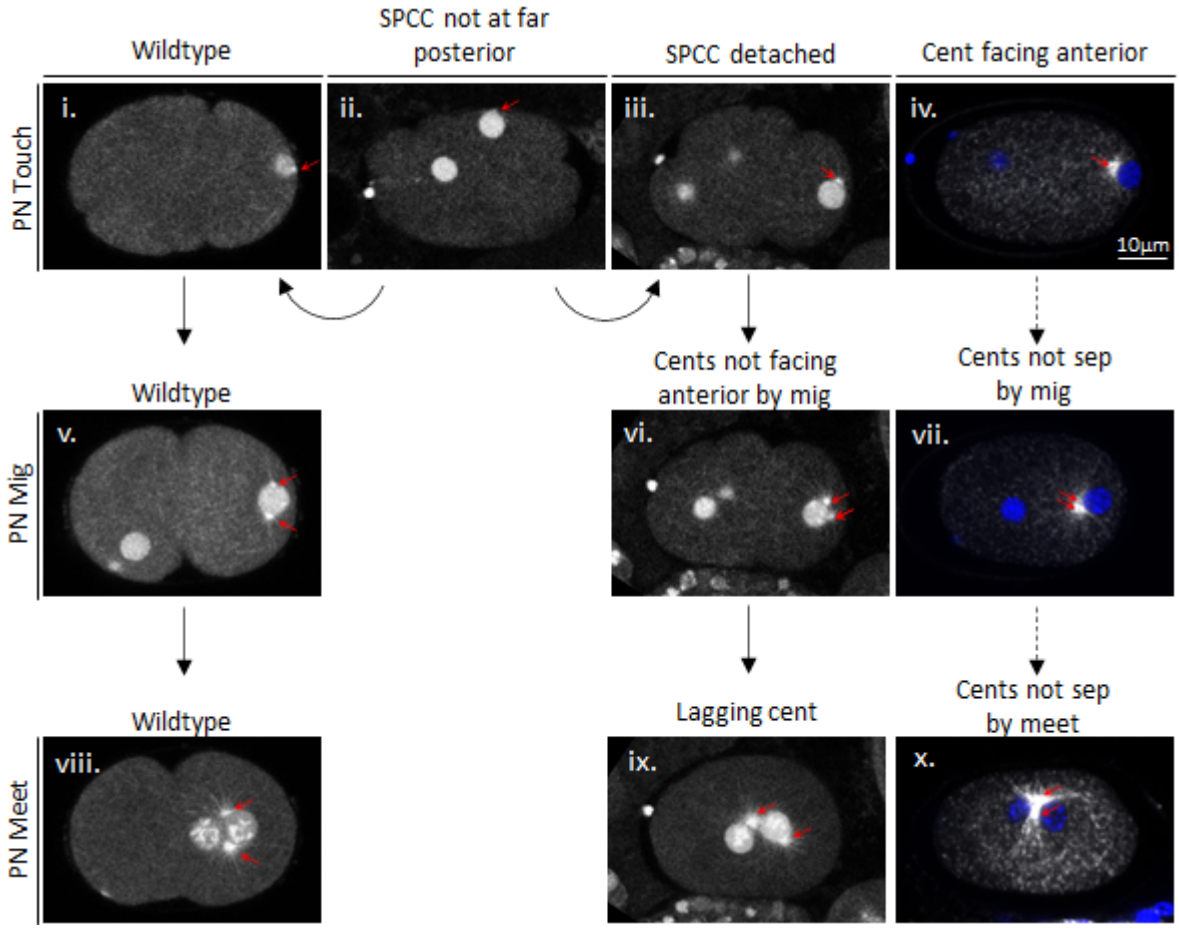

b.

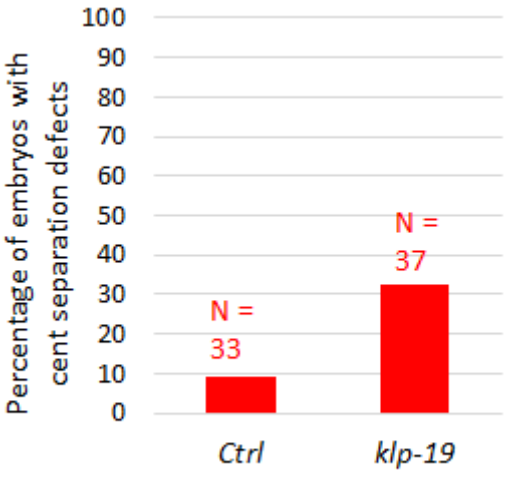

Figure 4.3 ***klp-19*** **RNAi induced centrosome separation defects.**

(a) Still images of embryos expressing Tubulin::GFP;H2B::GFP (TY3558) recorded via live confocal microscopy. For more detailed imaging conditions see methods (Table 2.8). The images represent typical WT and aberrant SPCC initial positions (PN touch) and centrosome separation (PN migration and PN meet) events within embryos and the progressions observed. Images iv, vii & x are confocal microscope images of fixed immunofluorescently labelled

embryos (Microtubules-Grey, DNA-Blue) that display the expected progression of an embryo in which the centrosome was initially misoriented around the PN towards the anterior, prior to centrosome duplication. This phenotype over time was computer simulated and produced by Boudreau et al. (2019) upon the depletion of SUR-6. We did not capture this phenotype in live imaging but saw the expected phenotype in fixed sampled upon *klp-19* RNAi treatment. (Note – that ii, in which the SPCC is lateral at the cortex, was observed to either correct its position prior symmetry breaking or fail, in which case the SPCC would detach from the cortex before it achieves centrosome separation). Black arrows show the typical progression of phenotypes as seen through live imaging. Broken black arrows show the expected progression of phenotypes in fixed samples. Red arrows point to centrosomes. Note - Linear adjustment of brightness and contrast used for representation in figure. **(b)** Percentages of embryos with late/separation defects in the absence of KLP-19 (RNAi) and flows (*nop-1* mutant). Number of experiments 6.

4.2.3 KLP-19 is required for efficient SPCC migration, predominantly through its role in positioning the SPCC at the posterior pole.

Following centrosome separation, the SPCC migrates anteriorly. The process initially depends on cytoplasmic dynein which carries cargo towards the centrosomes from the anterior, the resultant drag generates pulling forces on the SPCC (slow migration phase). This is followed by pulling forces exerted by dynein tethered to the oocyte pronucleus membrane which carries the oocyte pronucleus towards the SPCC posteriorly and brings the pronuclei together at a greater velocity (fast migration phase) (Figure 1.13.iii) (O'Connell, Maxwell and White, 2000; Malone *et al.*, 2003; Schmidt *et al.*, 2005; De Simone *et al.*, 2018). We wondered whether SPCC migratory patterns, like centrosome separation, would be impacted by the loss of KLP-19. To investigate, we performed live microscopy using a GFP-tagged tubulin & histone reporter strain (Figure 4.4.a). As some *klp-19* embryos presented with WT positioned pronuclei but aberrantly oriented centrosomes (classed as aberrant SPCC positioning), we recorded the movement of centrosomes over time, as a proxy for SPCC position, by measuring their distance to the cortex and recording the distance of the closest centrosome to the cortex over time. In real WT embryos (N=3), the centrosome started close to the cortex at an average distance of 0.77 µm at the time of centrosome duplication (Figure 4.4.a.i,b.i&ii). The SPCC remained around this position for approximately 100 seconds before migrating away from the cortex.

Next, we wondered if KLP-19's role in SPCC migration is solely a consequence of its role in initially localising the SPCC to the posterior pole. Or does KLP-19 also act to mediate the forces

that help to guide the centrosomes in the setup of the bipolar spindle. If KLP-19 RNAi-induced aberrant migration is solely a consequence of initial SPCC positioning defects, we would expect embryos lacking KLP-19 with WT-like SPCC positioning to have SPCC migration patterns identical to control embryos. We split the data by those that had an initially WT-like SPCC position (Figure 4.3.a.i) at the time of symmetry breaking (the first frame posterior membrane relaxation could be observed), and those with aberrant SPCC positions (Figure 4.3.a.ii,iii&iv).

In live *klp-19* RNAi embryos which displayed WT-like SPCC positioning (N=4), the centrosomes had an average initial distance of 1.66 µm from the cortex (Control = 0.77 µm) (Figure 4.4.a.v&b.i). As in control embryos, the SPCC remained close to the cortex for approximately the first 100 seconds however moved away from the cortex at a slower rate compared to the control (Significant difference in lines $P<0.0001$).

Embryos with aberrant SPCC positioning, upon *klp-19* RNAi depletion (N=6), started with an average initial SPCC-cortex distance of 3.46 µm, maximum distance - 9.50 µm (Control = 1.22 µm) (Figure 4.4.a.ix&b.ii). In these embryos, the pattern of SPCC migration was drastically altered as some embryos had SPCCs that were already initially at a great distance from the cortex by centrosome duplication. It took much longer for the SPCC to move away from the cortex (when the SPCC started near the cortex), as seen by the more horizontal line of regression in Figure 4.4.b.ii, taking as long as ~500 seconds to move away.

Interestingly, initial positioning of the SPCC in the absence of KLP-19 is stochastic and the position of the SPCC/ orientation of the centrosome appears to directly govern the downstream patterns of centrosome separation/ SPCC migration patterns. In Figure 4.3.a, we have represented the common progressions we observed in embryos that started with WT (i) and aberrant SPCC positions (ii, iii & iv) through live imaging. The panels i, v & viii display the wild-type progression of the SPCC from pronuclear touch to pronuclear meet, which can still occur upon *klp-19* RNAi depletion should the SPCC become initially positioned as the WT control. In the absence of KLP-19, we often saw embryos in which the SPCC remained in contact with the cortex but was more lateral than positioned to the posterior pole (Figure 4.3.a.ii). These embryos appeared to have the chance to correct their localisation prior to symmetry breaking. If they did, they would then follow the WT progression of centrosome separation and PN mig/ PN meet. If they did not correct their initial localisation, however, the SPCC would detach from the cortex before the centrosomes could separate and would

progress as embryos seen in iii, vi and ix in which the centrosomes would often not travel around the pronucleus in the coordinated manner seen in WT and so one centrosome would then lag behind. iv, vii & x demonstrate the expected trajectory of the SPCC when the centrosomes are initially oriented towards the anterior. This phenotype was predicted through computer simulations and recreated *in vivo* by Boudreau et al. (2019) who showed that the centrosomes often become misoriented upon RNAi depletion of the phosphatase PP2A adaptor SUR-6 which contributes to the dephosphorylation of cyclin dependent kinase CDK1 (Castilho *et al.*, 2009; Mochida *et al.*, 2009; Boudreau *et al.*, 2019). In this scenario, the centrosomes are not forced apart by being pulled around the sperm pronucleus. As such, the centrosomes remain together up to PN meet. We did not capture this phenotype in our videos; however we did see the expected phenotype at each stage of the zygote in fixed immunofluorescently labelled embryos depleted of KLP-19. Interestingly, CDK1 has been shown to phosphorylate the KLP-19 homologue, Kif4a and prevent its localisation to antiparallel MTs via PRC1 recruitment (Voets *et al.*, 2015; Dong *et al.*, 2018; Takata *et al.*, 2018) (Discussed further in sections 1.3.1 & 8.3). It is possible that the absence of SUR- 6 leads to active CDK1 which would then suppress KLP-19 activity, thus producing similar centrosome orientation phenotypes.

These data support our hypothesis that KLP-19 plays a major role in timely SPCC migration through its responsibility in ensuring efficient SPCC attachment to the posterior cortex, prior to centrosome duplication. These data also, however, support additional means in which KLP-19 likely regulates SPCC migration as even embryos lacking KLP-19 with more WT-like centrosome positioning/cortical docking appear to move within the cell more slowly than control embryos. Note, however, that the average distance of the SPCC from the cortex in *klp-19* WT-like embryos (1.66 µm) was still further from the cortex than in real WT embryos (0.77 µm) which could account for the changes in centrosome separation and SPCC migration changes.

Figure 4.4

a.

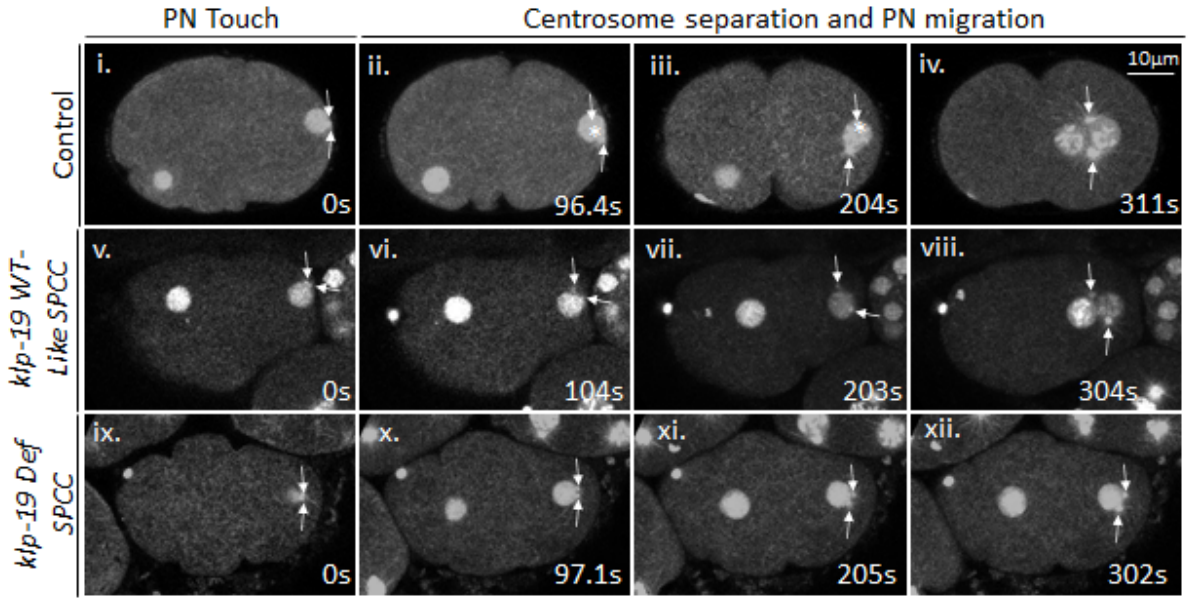

b.i.

b.ii.

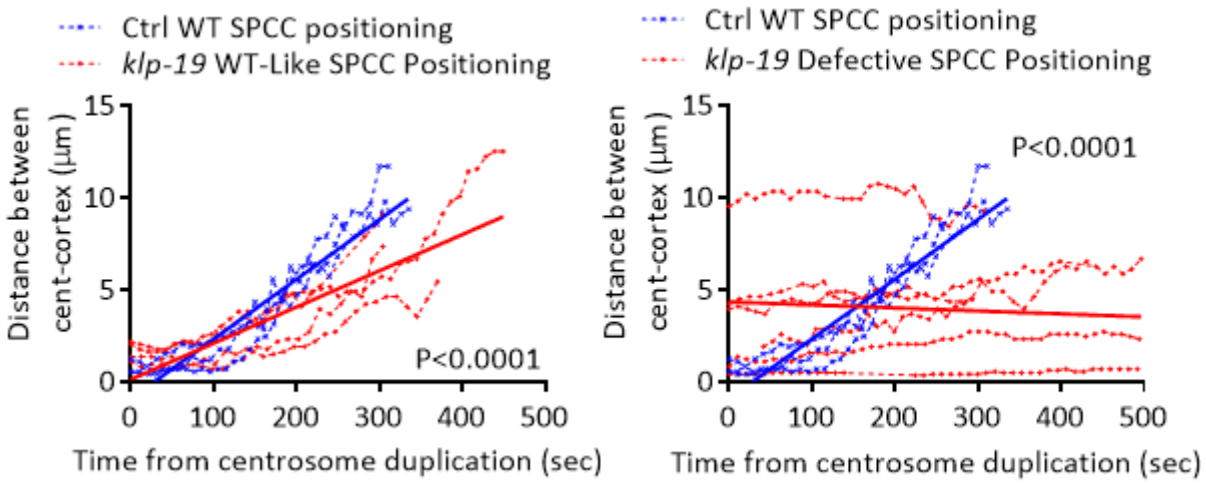

Figure 4.4 ***klp-19* RNAi induced SPCC migration defects.**
(a) Maximum intensity projections of embryos expressing Tubulin::GFP;H2B::GFP recorded via live scanning confocal microscopy under control and *klp-19* RNAi conditions (Images acquired with frame interval 10.7 seconds. Frames selected ~100 seconds apart for purpose of figure, all frames analysed) (0s = centrosome duplication). At 0s in the control (i-iv) and WT-Like *klp-19* RNAi (v-viii) embryos the SPCC is correctly positioned with centrosomes between the PN and the cortex, while the SPCC is detached from the cortex in the *klp-19* RNAi (ix-xii) embryo classed as defective. White arrows point to centrosomes, asterisks highlight centrosome position when hidden by pronucleus. For more detailed imaging conditions see methods (Table 2.8). (Note – v, vi & ix are not maximum intensity projections). Notes – Figures i-iv and ix-xii are the snapshots of the same videos used in Figure 4.2.a top row and bottom row, respectively. Linear adjustment of brightness and contrast used for representation in figure.
(b) Distance between the centrosome and the cortex of the zygote (closest to the cortex, as a proxy of SPCC position) in control and *klp-19* RNAi embryos over time starting from

centrosome duplication (the first frame in which two centrosomes could be seen). Each broken line is of a single embryo, the solid lines are lines of regression. **i** & **ii** – Data divided to plot control embryos (N=3) with initial real WT SPCC positioning (control embryos with aberrant initial SPCC positions removed) vs *klp-19* RNAi embryos with WT-like (N=4) and defective (N=6) SPCC positioning at the time of symmetry breaking, respectively. P values indicate the probability that the lines of regression are different (ANCOVA) – $P<0.05$ is significantly different. Note – embryos in which both centrosomes could not be seen at centrosome duplication were removed from this figure as it could not be determined if both had WT initial positioning. Number of experiments: 2.

4.2.4 KLP-19 is required for timely pronuclear meeting, predominantly through its role in positioning the SPCC at the posterior pole.

Centrosome separation and pronuclear migration are prerequisite to bring the oocyte and sperm genetic material, within the pronuclei, together. The centrosomes become situated on opposing sides of the point of contact of the two pronuclei, ready to rotate and become oriented along the anterior-posterior axis (Figure 1.9.iv & Figure 4.3.a.viii). The timing of pronuclear meeting is important to ensure that the embryo progresses through the cell cycle correctly. It has been demonstrated in mammals that compromised pronuclear meeting does not prevent eventual nuclear envelope breakdown. This results in the formation of two bipolar spindles around each set of oocyte and sperm derived chromosomes which are segregated into four new nuclei with only half of the normal amount of genetic material required (Chaigne *et al.*, 2016; Reichmann *et al.*, 2018; Scheffler *et al.*, 2021). In *C. elegans* zygotes, the depletion of the centrosomal TAC-1 results in shortened microtubules and failure of pronuclear migration. These embryos similarly undergo nuclear envelope breakdown with their oocyte and sperm derived chromosomes far apart. In the *C. elegans* zygote, however, a spindle only forms from the sperm derived centrosome around the paternal chromosomes and segregate them. The result is the same as mammalian cells which become aberrantly multinucleate and incompatible with life (Le Bot *et al.*, 2003).

As the absence of KLP-19 results in slower centrosome separation and pronuclear migration, we reasoned that pronuclear meeting would be delayed in these embryos. We decided to measure the time between centrosome duplication and pronuclear meeting to assess these timings and check whether similar mitotic defects arise as described above.

In control embryos the time between centrosome duplication and pronuclear meet took 5.56 minutes on average in control embryos (Figure 4.5.a.i,ii&b.i). This significantly increased to 8.15 minutes in the absence of KLP-19 (Figure 4.5.b.i).

We divided the data between KLP-19 depleted embryos that had initially WT-like positioned SPCCs, at the moment of centrosome duplication, and those with aberrantly positioned SPCCs. We found that embryos with WT-like positioned SPCCs took an average of 5.95 minutes to go from centrosome duplication to pronuclear meeting. This increased to 9.93 minutes in embryos with aberrantly positioned SPCCs (Figure 4.5.aiii-vi&b.ii), suggesting that KLP-19 is required for timely pronuclear meeting through its ability to position the SPCC. We cannot rule out, however, that KLP-19 has an additional role as there is still an increase in time to pronuclear meeting between control embryos and WT-like *klp-19* RNAi embryos.

In all the embryos recorded, the pronuclei had managed to meet prior to nuclear envelope breakdown. This suggests that KLP-19 is not essential to ensure that the chromosomes are in close proximity prior to metaphase/anaphase, however the kinesin is a part of the process and could exacerbate other defects that arise from other factors required to facilitate sufficient speed of pronuclear meeting.

Figure 4.5

a.

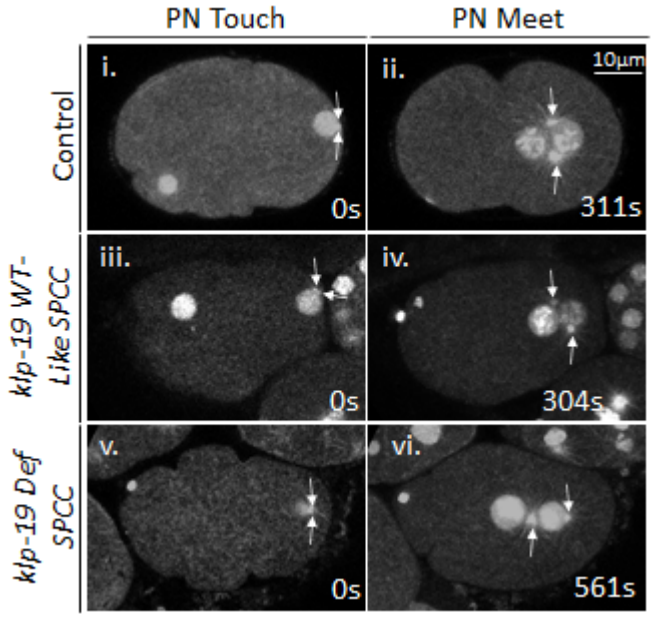

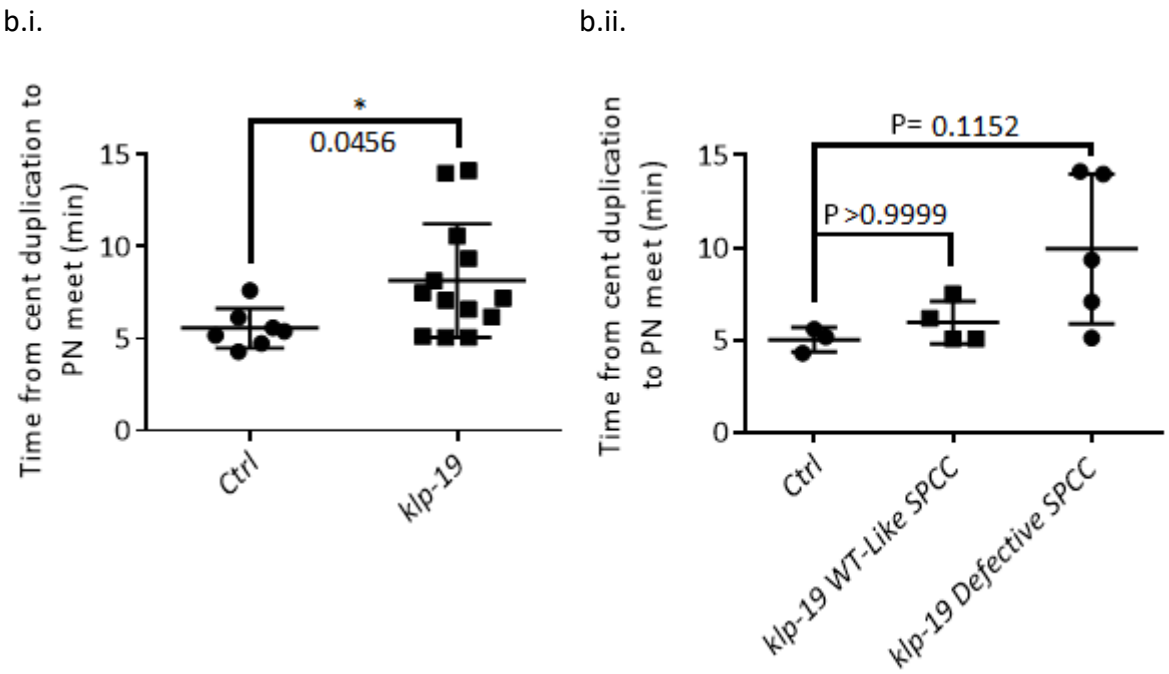

Figure 4.5 ***klp-19* RNAi knockdown delays sperm-oocyte pronuclear meeting.**
(a) Maximum intensity projections of embryos expressing Tubulin::GFP;H2B::GFP recorded via live scanning confocal microscopy under control and *klp-19* RNAi conditions showing the timings of centrosome duplication (0s) and pronuclear meet. *klp-19* RNAi embryos have been divided by one which had a WT-Like initial SPCC position and one in which the position was defective and the SPCCC was detached from the cortex. (Images acquired with frame interval 10.7 seconds). For more detailed imaging conditions see methods (Table 2.8). (Note – iii & v are not maximum intensity projections). Embryos imaged here are snapshots of the same videos used in Figure 4.4.a. Linear adjustment of brightness and contrast used for representation in figure. **(b)** Time between centrosome duplication and pronuclear meet (the frame the centrosomes contact the female pronucleus). **i** – Control embryos (N=7) plotted against all *klp-19* RNAi embryos (N=13). Mann-Whitney test of significance used to determine P values - $P<0.05$ is significantly different. **ii** – same as i but embryos have been divided between control embryos (N=3) and *klp-19* KD embryos that had WT (N=4) and abnormal (N=5) initial centrosome positioning/docking. Note – embryos in which both centrosomes could not be seen at centrosome duplication were removed from this figure as it could not be determined if both had WT initial positioning. Kruskal-Wallis test of significance used to determine P values - $P<0.05$ is significantly different. Number of experiments: 2.

4.2.5 KLP-19 limits microtubule-dependent cortical pulling forces during anaphase.

Thus far, we have shown that KLP-19 acts to promote SPCC posterior pole attachment, SPCC migration and centrosome separation. How KLP-19 could be acting to regulate these processes is unclear.

We made an interesting observation in later staged KLP-19-depleted embryos. During anaphase, as the chromosomes are pulled apart by cortical pulling forces (Section 1.6.1), a phenomenon occurs whereby the spindle begins to oscillate (or "rock") perpendicular to the anterior-posterior axis. This is particularly prominent in the posterior where cortical pulling forces are stronger. We noticed that the posterior mitotic spindle pole rocked with a higher frequency and reduced amplitude in the absence of KLP-19 suggesting that KLP-19 may have a role in regulating cortical spindle forces. As these cortical MT pulling forces are at their strongest during anaphase (Redemann *et al.*, 2010), we focused on embryos at this stage to investigate KLP-19's potential contribution.

Previous work by Schmidt et al. (2017) employed a "spindle shooting" technique whereby a UV laser was used to destroy the spindle midzone at the onset of anaphase. The spindle poles were no longer held together, thus retract to their respective ends of the embryo at velocities proportional to the cortical microtubule pulling forces elicited upon them by the cortical dynein complex (Section 1.6.1) (Grill *et al.*, 2001; Portegijs *et al.*, 2016; Schmidt *et al.*, 2017; Fielmich *et al.*, 2018). With help from the authors of this study, we ablated the spindle midzone of tubulin::GFP embryos (AZ244) under control and *klp-19* RNAi conditions.

Upon midzone severing, we recorded the peak velocity at which both spindle poles retracted in control and *klp-19* RNAi embryos. In control embryos, the peak velocities recorded of the anterior and posterior poles were 0.56 µm/s (±0.11 µm/s) and 0.75 µm/s (±0.16 µm/s) respectively. Upon *klp-19* depletion, these velocities shifted upwards to 0.72 µm/s (±0.21 µm/s) and 0.89 µm/s (±0.21 µm/s) (Figure 4.6.a&b). These data suggest that KLP-19 somehow acts to suppress spindle retraction velocities in anaphase. As cortical dynein is the only force generator described to pull the spindle poles apart, it is possible that KLP-19 is antagonising/attenuating the cortical dynein complex. We cannot rule out, however, that the loss of KLP-19 affects dynein pulling forces, as observed in spindle shooting experiments, indirectly. For example, incomplete centration of the pronuclei prior to mitosis could alter

pulling forces towards the poles and alter spindle retraction velocities. Incomplete spindle severing could also account for the difference in velocities between control and *klp-19* RNAi embryos if spindle midzone localised KLP-19 is able to resist cortical pulling forces.

Figure 4.6

a.

b.

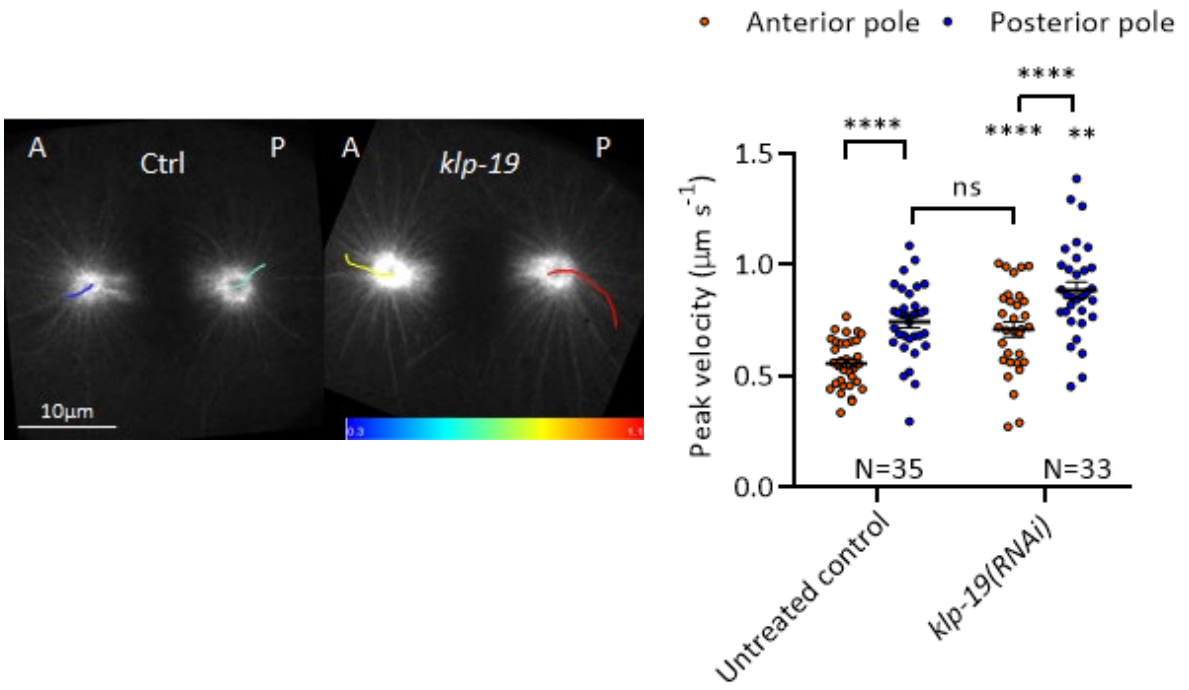

Figure 4.6 **Centrosome peak velocities post-spindle shooting.**
(a) Representative embryos under control and *klp-19* RNAi conditions (oriented anterior to posterior) recorded using spinning disc microscopy, mitotic spindle midzones ablated via UV-laser at the onset of anaphase. Paths of each centrosome were recorded via TrackMate for 12.5 seconds post-spindle midzone laser ablation and shown here as lines colour coded by the maximum peak velocity reached within that time (units – µm/s). (Images acquired with frame interval 0.5 seconds). For more detailed imaging conditions see methods (Table 2.8). **(b)** Peak velocities of anterior and posterior centrosomes within 12.5 seconds timeframe post-laser ablation of the spindle midzone in control and *klp-19* RNAi embryos. Velocities of centrosomes measured via TrackMate (ImageJ). See methods for TrackMate settings used (Section 2.7.3). Paired t-tests used to test for significance between anterior & posterior within the same RNAi treatment and unpaired t-tests used between RNAi conditions ($P<0.05$ = significantly different) (ns = $P>0.05$, * = $P\leq0.05$, ** = $P\leq0.01$, *** = $P\leq0.001$, **** = $P\leq0.0001$). Number of experiments for the control: 3. Number of experiments for the *klp-19*: 2. Experiments were performed with the help of Ruben Schmidt (Utrecht University).

4.2.6 Loss of the dynein cortical anchor, LIN-5, rescues klp-19 RNAi centrosome positioning but not separation defects.

Given that KLP-19 limits cortical MT pulling forces during anaphase, we wondered whether it could also be doing the same during polarity establishment to mediate SPCC positioning/cortical attachment. Previous studies have shown that loss of cortical dynein can rescue defects in which the centrosome is aberrantly positioned and/or prematurely detached from the cortex. This is likely to happen as the cortical dynein complex acts to couple the centrosomal microtubules to cortical cytoplasmic flows. In the absence of factors that otherwise restrict the SPCC's position, the cortical dynein complex would likely respond to cortical flows at the cortex and incidentally move the SPCC inappropriately. As a result, the reduction of dynein rescues SPCC positioning defects by decoupling centrosomes to cortical forces allowing the SPCC to remain close to the cortex at the posterior pole (Fortin *et al.*, 2010; McCloskey and Kemphues, 2012; De Simone, 2016; Saturno *et al.*, 2017). We wondered if SPCC positioning defects upon *klp-19* KD could similarly be rescued. This would suggest that KLP-19 acts to antagonise cortical forces on centrosomal MTs, as in mitosis. As dynein presents two populations, cortical and nuclear, and we wanted to interrogate the cortical population, we studied SPCC positioning in a temperature sensitive mutant of *lin-5* (homologue of vertebrate NuMA) the cortical dynein anchor with and without the knockdown of *klp-19*.

In the *lin-5ts (ev571)* mutant, SV124, 4/25 (16.0%) embryos had SPCC positioning defects and 18/26 (69.2%) had centrosome separation defects, at the restrictive temperature (24 °C), while in the double LoF with *klp-19* RNAi there were 1/12 (8.3%) and 25/32 (78.1%) embryos with positioning and separation defects, respectively (Figure 4.7.a,b&c)(*klp-19* RNAi in control embryos – SPCC positioning defects: 9/21 – 42.9%, Centrosome separation defects: 12/37 – 32.4%). This suggests loss of LIN-5 activity is sufficient to suppress the SPCC positioning defects caused by loss of KLP-19 and would support our theory that KLP-19 and dynein/LIN-5 potentially antagonise each other in order to mediate the correct level of cortical MT pulling forces, critical in SPCC and mitotic spindle positioning. Unsurprisingly, the *lin-5ts* mutant was unable to rescue *klp-19* RNAi-induced centrosome separation defects when the SPCC was returned to the cortex. This is because centrosome separation relies on cortical flows, which the centrosomes would no longer be able respond to due to the lack of functional LIN-5.

Figure 4.7

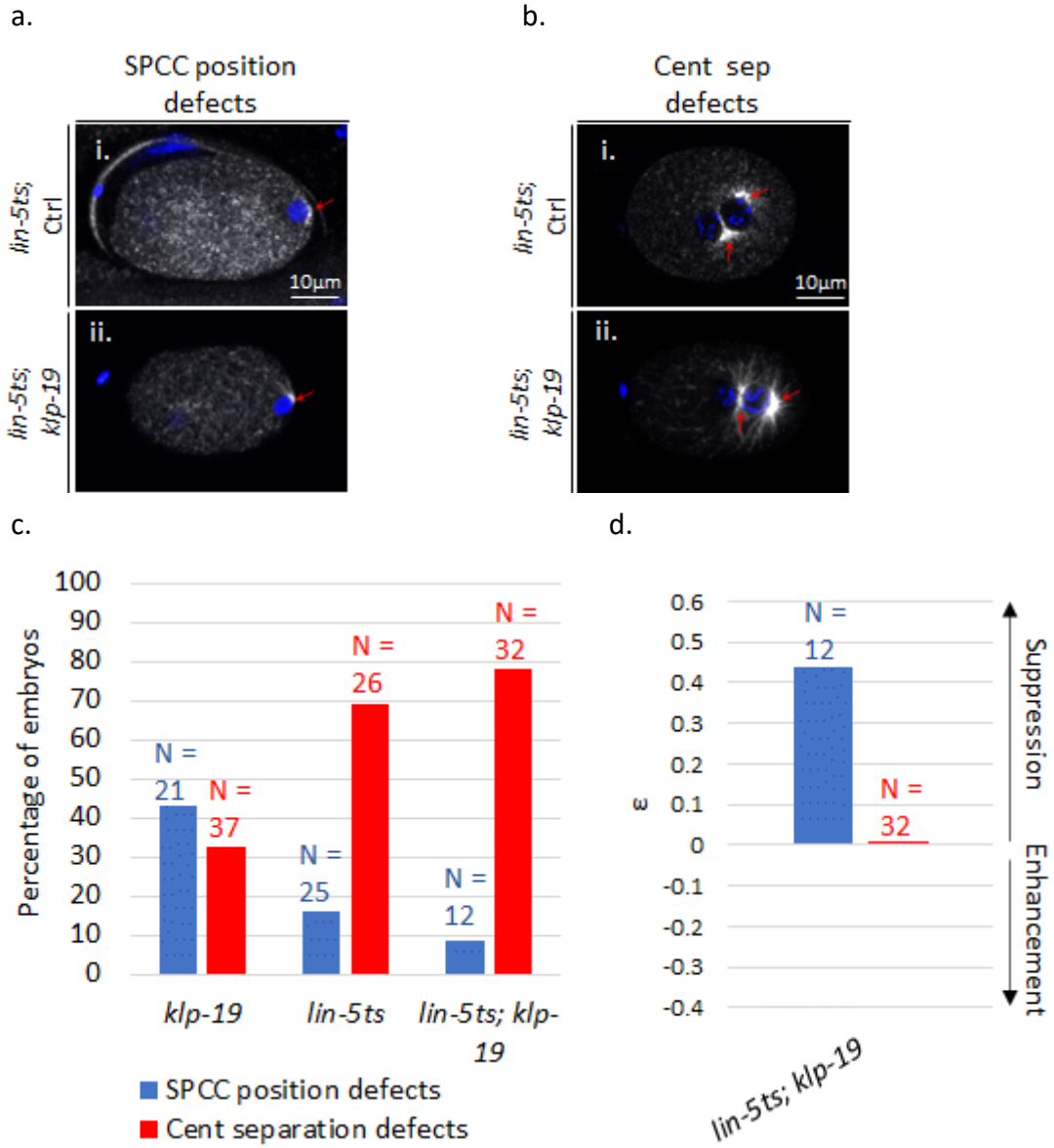

Figure 4.7 ***lin-5* loss of function rescues SPCC positioning and centrosome separation phenotypes.**

(a&b) Immunofluorescently labelled fixed embryos, imaged via confocal microscopy (Microtubules-Grey, DNA-Blue), displaying the SPCC early positioning (a) and late centrosome separation (b) phenotypes observed under different conditions of mutants and RNAi knockdowns (Red arrows point to centrosomes). Note - Linear adjustment of brightness and contrast used for representation in figure. **(c)** Percentages of embryos with SPCC position and centrosome separation defects under different mutant and RNAi knockdown conditions. **(d)** ε values indicate the strength of genetic interaction between the *lin-5* mutants and RNAi of *klp-19* to produce SPCC positioning (0.44) and centrosome separation (0.01) defects. Negative values show enhanced levels of defective phenotypes than expected if there is no genetic interaction whilst positive values suggest suppression of phenotypes (A score of +/- 0.15 is considered a significant suppressor/enhancer, respectively). Number of experiments for *klp-19*: 6, *lin-5ts*: 4, *lin-5;klp-19*: 4.

4.3 Discussion.

Computer modelling had previously predicted that both SPCC cortical contact and centrosome orientation towards the far posterior cortex (prior to centrosome duplication) (Figure 3.3, Figure 4.1, Figure 4.3) are required for timely and efficient centrosome separation, necessary for bipolar spindle formation (De Simone and Gönczy, 2017; Boudreau *et al.*, 2019). Boudreau et al. (2019) previously demonstrated that centrosome separation is compromised in embryos with aberrant centrosome orientation, induced via depletion of the protein phosphatase 2a (PP2A) adapter protein, SUR-6 (previously discussed in Section 4.2.3) (Boudreau *et al.*, 2019). Biological evidence to confirm the importance of SPCC cortical contact to centrosome separation has been missing. We have demonstrated that loss of KLP-19 results in zygotes with aberrant SPCC positioning defects to different degrees. Often, the SPCC would be at a distance from the posterior pole, or the centrosome would be oriented around the sperm pronucleus, facing into the cell rather than the cortex during pronuclear touch. Hence, we have been able to demonstrate a new role of KLP-19 in the tight positioning of the SPCC within the zygote and have been able to study the role of the SPCC's position in the steps that lead to the organisation of the first mitotic spindle of the zygote (i.e., centrosome separation, pronuclear migration, and pronuclear meeting).

We confirmed De Simone & Gönczy (2017) and Boudreau et al.'s (2019) predicted downstream centrosome separation defects after aberrant SPCC positioning. We observed that sister centrosomes within *klp-19* RNAi embryos took longer to move apart after duplication and often remained together throughout pronuclear migration and meet (De Simone and Gönczy, 2017; Boudreau *et al.*, 2019). In addition, the SPCC migrated from the posterior cortex towards the female pronucleus in a slower/delayed manner. These phenotypes became strikingly clearer when the data sets were divided between embryos which had WT-like vs abnormal initial SPCC positioning. Thus, it is clear from this data that SPCC positioning plays a large role in downstream centrosomal dynamics which go on to set up the mitotic spindle.

It is important to note that, although the initial SPCC position played a large role in later SPCC dynamics, the rates of SPCC migration and centrosome separation were also slower in *klp-19* RNAi embryos in which the SPCC was initially positioned more similar to the wild type. One possibility is that, although the SPCC in these embryos was WT-looking, there was still a larger

average SPCC distance from the cortex than in the real WT (i.e WT positioning in control embryos) which could cause the slower centrosome separation and migration phenotypes. Alternatively, these results could suggest that KLP-19 may have an additional, more direct, role in later SPCC dynamics. As previously discussed (Section 1.2.3), the kinesin Eg5 has been previously shown to form tetramers back-to-back which dock to the antiparallel microtubules that grow between unseparated centrosomes. The kinesin then walks to the plus ends of these overlapping microtubules causing the centrosomes to be pushed apart (Kapitein *et al.*, 2005; Tanenbaum *et al.*, 2009; Tanenbaum and Medema, 2010; van Heesbeen *et al.*, 2017). The *C. elegans* Eg5 homologue, BMK-1, is dispensable for centrosome separation, however, suggesting that BMK-1 is not involved in centrosome separation, or it acts redundantly with another kinesin such as KLP-19 (Bishop, Han and Schumacher, 2005; Saunders *et al.*, 2007; De Simone, 2016; Bondaz *et al.*, 2019).

Through an observation in videos of GFP-tagged tubulin anaphase embryos, we noticed that spindle "rocking" oscillations (a product of spindle pulling forces) developed a higher frequency with lower amplitude in the absence of KLP-19. Mitotic spindle segregation forces are derived from the cortical dynein complex leading us to believe KLP-19 may have a cortical role in the zygote which could also influence centrosome separation and SPCC migration.

Given our suspicions, we wanted to assess whether KLP-19 presented a role in cortical MT dynamics. As cortical dynein complex pulling forces are at their strongest during metaphase/anaphase, we chose this stage to investigate any impact that KLP-19 could have. To do this we performed laser ablation of the spindle midzone, allowing the cortical dynein complex to freely pull the spindle poles to their respective half of the embryo. The velocity of the poles is directly dependent on the strength of pulling forces from the dynein complex (Grill *et al.*, 2001; Portegijs *et al.*, 2016; Schmidt *et al.*, 2017; Fielmich *et al.*, 2018). We found that the absence of KLP-19 increases spindle pole retraction velocity, suggesting that KLP-19 acts to suppress the forces of the cortical dynein complex in control embryos. KLP-19 homologues and their recruiter, PRC1 (SPD-1 in *C. elegans*), act together on the spindle midzone to prevent the hyper-segregation of chromosomes during anaphase (Previously discussed in sections 1.2.3 & 1.3.1) (Gaska *et al.*, 2020; Alfieri, Gaska and Forth, 2021). We may have found an additional role of KLP-19 in preventing chromosomal hyper-segregation through dampening dynein pulling forces at the cortex. The asymmetry of pulling forces during anaphase is

maintained in the absence of KLP-19 suggesting the kinesin acts uniformly and does not compromise the asymmetric recruitment of cortical GPR-1/2 & LIN-5 which regulate dynein's mitotic pulling forces (Rodriguez-Garcia *et al.*, 2018).

Seeing that KLP-19 appears to impact forces, derived from the cortical dynein complex on centrosomal MTs, we took our investigations back to the complex proteins' roles in SPCC positioning and centrosome separation to determine whether KLP-19 and the cortical dynein complex could act antagonistically in early-stage zygotes too. The cortical dynein complex is known to facilitate SPCC positioning and centrosome separation as the motor complex responds to actomyosin-generated anterior cortical flows and pulls the centrosomes away from the cortex and around the sperm pronucleus, driving separation. Previous labs have shown that loss of the dynein heavy chain subunit, DHC-1, reduces movement of the centrosome and so the SPCC remains at the posterior pole for longer than WT. In particular, the absence of DHC-1 was capable of retaining the SPCC close to the posterior membrane of *pam-1* embryos which otherwise present with aberrantly positioned SPCCs as in *klp-19* RNAi embryos (Gönczy *et al.*, 1999; Cockell, Baumer and Gönczy, 2004; De Simone, Nédélec and Gönczy, 2016; Saturno *et al.*, 2017). In *C. elegans* zygotes, cortical dynein is anchored to the cortex by the conserved NuMA homologue, LIN-5 (Nguyen-Ngoc, Afshar and Gönczy, 2007; Kotak, Busso and Gönczy, 2012). As such, we expected the SPCC to remain at the posterior cortex in a *lin-5* mutant. Indeed, like in the absence of DHC-1, we observed a reduction in embryos with defective SPCC positioning in the double LoF of *klp-19* and *lin-5.* This suggests that forces at the cortex had been decoupled from the centrosome and are unable to pull the SPCC away from the cortex prematurely as in the absence of KLP-19 alone.

4.3.1 Potential modes by which KLP-19 could oppose cortical forces during polarity establishment and anaphase.

We wondered how KLP-19 could act at the cortex to antagonise cortical dynein complex dependent forces during both polarity establishment (SPCC positioning) and anaphase (mitotic spindle pulling). As a kinesin, we reasoned that KLP-19 is likely acting through its ability to interact with microtubules.

In our experiments, KLP-19 appeared to antagonise the activity of the cortical dynein complex as KLP-19 depletion presented opposite phenotypes to the loss of function of LIN-5. The

cortical dynein complex acts to connect the SPCC to cortical flows via centrosomal MTs. This results in the SPCC being pulled anteriorly and away from the cortex. As such, the absence of cortical dynein complex components results in the SPCC being retained to the posterior pole for longer (Fortin *et al.*, 2010; Saturno *et al.*, 2017). As the absence of KLP-19 resulted in aberrantly positioned SPCC's, we reasoned this could be a result of enhanced coupling of centrosomal MTs to cortical flows. This might occur if the loss of KLP-19 results in an increased numbers of MTs able to respond to flow. KLP-19 homologues have previously been shown to stabilise MTs and prevent growth and shrinkage, *in vitro* and *in vivo*. Typically, the absence of these chromokinesins results in net MT growth within the cell due to favourable conditions (i.e. high availability of tubulin monomers) (Bringmann *et al.*, 2004; Castoldi and Vernos, 2006; Morris *et al.*, 2014). We did not, however, notice an apparent increased size of centrosomal asters upon *klp-19* RNAi treatment.

Alternatively, as a plus-end directed motor protein, KLP-19 could act as a competitive inhibitor of dynein binding to the tips of centrosomal microtubules to reduce cortical pulling forces and prevent premature movement away from the posterior pole. In the absence of KLP-19, more microtubule tips would be exposed to dynein/LIN-5-dependent cortical forces, thus the SPCC becomes aberrantly positioned. This would also account for the increased pulling forces on the spindle poles we observed during anaphase upon KLP-19 depletion. To test this theory, it would be useful to simultaneously image microtubules, LIN-5 and KLP-19 to assess the extent of colocalization between each component. We would expect microtubules to better colocalise with LIN-5 in the absence of KLP-19 if the cortical dynein complex and KLP-19 compete to bind to MT tips.

Our theories above propose that KLP-19 could tamper with the extent at which the cortical dynein complex interacts with, and pulls on, centrosomal MTs. Our final theory proposes that KLP-19 fixes the SPCC in place through tethering centrosomal MTs to the cortex. In this way, KLP-19 would restrict the position of the SPCC and act to resist the initial cortical cytoplasmic flow forces enacted by the cortical dynein complex. We reasoned that there are two possible mechanisms by which KLP-19 could anchor centrosomal MTs to the cortex. 1) As previously mentioned (Section 1.4.3), the *Drosophila* kinesins Khc-73 is recruited to the membrane of neuroblasts where it captures astral MTs and holds them in place (Siegrist and Doe, 2005; Zhu *et al.*, 2016; Bergstralh, Dawney and St Johnston, 2017; Gallaud, Pham and Cabernard, 2017).

It is possible that KLP-19 acts in a similar way in the *C. elegans* zygote to limit SPCC movement. 2) KLP-19 homologues are preferentially recruited to antiparallel MTs (compared to single MTs) on the spindle midzone during anaphase. The chromokinesin acts to crosslink these MTs and prevent chromosomal hyper-segregation and effectively holds the central spindle together (Kurasawa *et al.*, 2004; Bieling, Telley and Surrey, 2010; Nguyen, Field and Mitchison, 2018; Jagrić *et al.*, 2021). It is possible that KLP-19 could facilitate the interaction of antiparallel centrosomal MTs and cortical MTs to restrict the movement of the SPCC during early polarity establishment. In either mechanism, the absence of KLP-19 will reduce the impedance on the SPCC, allowing it to mispositioned by cortical forces.

4.3.2 Concluding remarks

In this chapter we have demonstrated a role for the chromokinesin, KLP-19, in SPCC positioning, centrosome migratory patterns, and in the cortical forces that act upon the mitotic spindle. KLP-19's apparent suppression of forces that are driven by the cortical dynein complex led us to propose that the chromokinesin likely acts at the cortex to counteract dynein's pull on astral MTs. In this way, KLP-19 would prevent inappropriate positioning of the SPCC, ensure timely centrosome separation and migration, and limit mitotic spindle pulling forces. In Chapter 5 we investigate if KLP-19 is present at the cortex of the zygote during the SPCC and mitotic events described so far and assess whether KLP-19 could be regulating these processes by altering the dynamics of MTs at the cortex.

Chapter 5 KLP-19 localises at the cortex where it restricts MT movement.

5.1 Introduction.

As a chromokinesin, KLP-19 is typically known to act in meiosis and mitosis to promote chromosomal congression and segregation during metaphase and anaphase, respectively. It performs both roles through its capacity as a motor where it binds to microtubules and walks along them to generate force. Certain kinesins, including KLP-19 homologues, have the ability to bind to antiparallel MTs and walk to the plus end of each which drives the MTs apart and shortens their overlap (Kapitein *et al.*, 2005; Bieling, Telley and Surrey, 2010; Lüdecke *et al.*, 2018; Hannabuss *et al.*, 2019; Leary *et al.*, 2019). Short MT overlaps become saturated with the kinesin which prevents further sliding whilst reinforcing the integrity of the antiparallel MT bundles. In this way, during anaphase, kinesins acts as a brake and stabilise the spindle midzone, preventing excessive polar segregation of the chromosomes and centrosomes (Saunders *et al.*, 2007; Lee *et al.*, 2015; Wijeratne and Subramanian, 2018; Pamula *et al.*, 2019; Gaska *et al.*, 2020).

KLP-19 homologues have also been shown to inhibit the dynamic instability of microtubules, as their absence leads to increased growth and shrinkage, dependent on substrate availability (Bringmann *et al.*, 2004; Castoldi and Vernos, 2006; Morris *et al.*, 2014) Through *in vitro* work, Bringmann et al. (2004) presented evidence that increasing concentrations of the *Xenopus laevis* KLP-19 homologue, Xklp1, decreases the rate of tubulin polymerisation when tubulin substrates and ATP concentrations are high, favourable for MT growth. Conversely, Xklp1 slows the rate of microtubule depolymerisation upon tubulin and GTP washout (Bringmann *et al.*, 2004). This was later supported *in vivo*. As previously discussed (Section 1.3.1), Morris et al. (2014) showed that human Kif4a induces the formation of, and colocalises with, stable (detyrosinated) centrosomal microtubules with greater accumulation towards the MT plus ends of migrating fibroblasts (Morris *et al.*, 2014). Selectively stabilised MTs are required at the cortex of fibroblast to allow to generate membrane projections that facilitate migration (Wen *et al.*, 2004; Morris *et al.*, 2014).

So far, we have shown that KLP-19 acts to restrict the SPCC to the posterior cortex during polarity establishment (Chapter 3, Chapter 4) and seems to suppress cortical LIN-5-dependent MT pulling forces during anaphase (Section 4.2.5). Both processes rely on microtubule

interactions with the cortex. As previously discussed (Section 1.7.2), centrosomal MTs are captured by the cortical dynein complex, during polarity establishment, which responds to cytoplasmic flows at the cortex to reposition the SPCC. The absence of centrosomal microtubules, via γ-tubulin depletion, or components of the cortical dynein complex (which couple centrosomal MTs to anterior directed cortical flows) results in aberrant SPCC detachment or prolonged attachment to the cortex, respectively (Gönczy *et al.*, 1999; Bienkowska and Cowan, 2012; Saturno *et al.*, 2017). Similarly, microtubule pulling forces during anaphase are governed by the cortical dynein complex which pulls on astral MTs (Colombo *et al.*, 2003; Park and Rose, 2008; Redemann *et al.*, 2010; Galli *et al.*, 2011; Kotak, Busso and Gönczy, 2014; Portegijs *et al.*, 2016; Fielmich *et al.*, 2018).

In the previous chapter, we had observed that KLP-19 is required for efficient localisation of the SPCC to the posterior cortex during polarity establishment. Interestingly, KLP-19 seems to counteract cortical forces exerted on MTs by the cortical dynein complex, as suggested by our spindle shooting experiments in which loss of KLP-19 resulted in higher spindle pulling forces. Together this led us to believe that, like its homologues, KLP-19 has some role in the stabilisation/fixation of microtubules, countering forces that act upon them. In this chapter we used immunofluorescent labelling and a GFP reporter of KLP-19 to assess its cortical presence. We show that KLP-19 does indeed localise to the cortex of zygotes and presents with multiple patterns reminiscent of microtubules to which we suspect it is recruited to.

To test if KLP-19 stabilises/fixes microtubules of polarity establishment and anaphase embryos, as Kif4a does in migrating fibroblasts (Morris *et al.*, 2014), we used high-resolution microscopy to assess whether KLP-19 regulates the dynamics of MTs at the cortex. We found that, in the absence of KLP-19, cortical microtubule tips seem to travel longer distances and at faster rates. This supports our hypothesis that KLP-19 acts at the cortex of embryos to stabilise/fix microtubules and suppress their movement.

5.2 Results

5.2.1 KLP-19 localises to the cortex in zygotes.

To date, there is no evidence of KLP-19 localisation at the cortex during polarity establishment and anaphase where we now suspect it acts to limit microtubule dynamics. KLP-19 has been reported to localise within the nucleus during interphase, on chromatin during mitosis, the

spindle midzone during anaphase, and the cortex of meiotic embryos (Powers *et al.*, 2004; Monen *et al.*, 2005; Dumont, Oegema and Desai, 2010; Pelisch *et al.*, 2017). We confirmed these previous KLP-19 localisation patterns through fixed immunlolabelled embryos of a KLP-19::GFP (FGP40) reporter strain at the relevant embryo stages (Figure 5.1.a). These populations of the kinesin, however, cannot explain the SPCC positioning and spindle pulling force phenotypes we observed upon *klp-19* RNAi knockdown. As SPCC/spindle organisation and dynamics are regulated by microtubule contacts with the cortex, we reasoned that KLP-19 would likely have to localise to the cortex of embryos during the early stages of the zygote while the SPCC is being positioned post-meiosis, and during anaphase. This seemed reasonable to expect as the human homologue of KLP-19, Kif4a has been shown to localise to, and stabilise, the plus-end tips of radially grown MTs that reach the cortex of migrating fibroblasts (Previously discussed in section 1.3.1) (Morris *et al.*, 2014). We sought to characterise the localisation and dynamics of KLP-19 that could explain its novel roles in SPCC positioning and downregulating spindle pulling forces.

We used the KLP-19::GFP reporter strain to record time-lapse sequences of early embryos using a spinning-disc confocal fluorescence microscope. Interestingly, we observed multiple localisation patterns of KLP-19 at the cortex depending on the stage of the zygote. We saw KLP-19 localise to the cortex in punctate-like patterns during polarity establishment (Figure 5.1.b), reminiscent of cortical EBP-2 which decorate the plus-ends of growing microtubules (Figure 5.2.a) (Gusnowski and Srayko, 2011). We observed instances in which the puncta of KLP-19 aggregated to form foci during polarity establishment which looked similar to actomyosin foci (Figure 5.1).

KLP-19 also appeared at the cortex during anaphase. At this stage we observed long microtubule-like threads of KLP-19 appear which laid flat at the membrane. Interestingly, KLP-19 appears to move in both directions along these threads which could suggest KLP-19 movement on antiparallel microtubules (Figure 5.1.b&c).

We were unable to observe the novel cortical localisations of KLP-19, that were imaged via live spinning disc-microscopy, in fixed immunofluorescently labelled samples. This meant that we could not simultaneously stain for KLP-19 and tubulin to assess their colocalization.

Figure 5.1

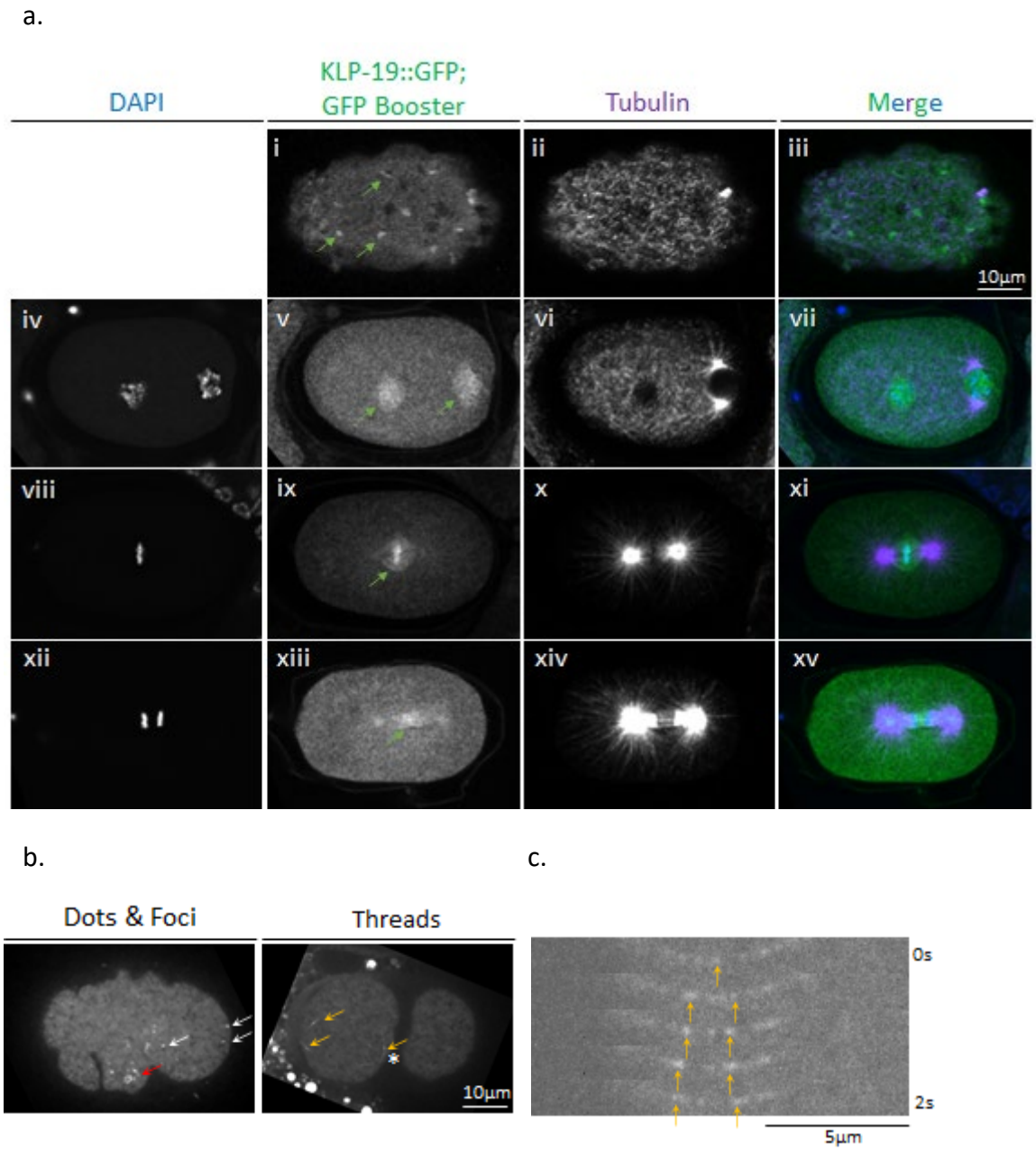

Figure 5.1 **KLP-19 localisation patterns and dynamics.**

(a) Immunofluorescently labelled KLP-19::GFP embryos, imaged via confocal microscopy, (stained with DAPI, Chromotek nanobody GFP Booster, and tubulin antibody) showing the previously known KLP-19 localisation patterns. i-iii: Cortex of meiosis I embryos with "linear elements" of KLP-19, iv-vii: Midplane of pronuclear migration stage embryo with nucleoplasm localised KLP-19, viii-xi: Midplane of metaphase embryo with chromosome and spindle bound KLP-19, xii-xv: Anaphase embryo with spindle midzone localised KLP-19. Green arrows point to KLP-19 localisation. **(b)** A cortical snapshot of polarity establishment phase (left) and maintenance phase (right) embryos expressing KLP-19::GFP, monitored with fluorescent spinning disc confocal microscopy. Localisation patterns of cortical KLP-19 are indicated as puncta (white arrows), foci (red arrow) and lines (yellow arrows). (Images acquired with frame interval 0.5 seconds). For more detailed imaging conditions see methods (Table 2.8). **(c)** Example kymograph of thread of KLP-19 (depicted by asterisk in (b)) showing the bidirectional

movement of two puncta observed to move away from each other over time, indicative of antiparallel MTs. Note - Linear adjustment of brightness and contrast used for representation in figure.

5.2.2 KLP-19 regulates microtubule dynamics at the cortex.

As discussed above, the impact of KLP-19 on SPCC positioning and spindle pulling forces during anaphase led us to wonder whether KLP-19 mediates microtubule interactions at the cortex and/or regulates MT dynamics. To investigate these, we used an EBP-2::GFP (TH66) reporter strain to track the growing tips of microtubules at the cortex of polarity establishment phase embryos in both control and *klp-19* RNAi knockdown embryos.

Due to the high velocity of EBP-2, we opted to use total internal reflection fluorescence (TIRF) microscopy which allows for high frame rate (~17fps – Frame interval = 60ms) and high-resolution imaging at the surface of cells (Figure 5.2.a) (see methods for imaging conditions – Table 2.8). TIRF allowed us to focus on the precise cortical localisation of EBP-2 labelled MT tips. We followed the dynamics of cortical EBP-2 using the particle tracking algorithm of TrackMate (Tinevez *et al.*, 2017)(See methods section 2.8.7) which allows for user-defined object recognition based on particle size and intensity, and track determination over time based on maximum allowed particle distance travelled between frames and maximum allowed number of frames skipped. From the data output of TrackMate, we extracted EBP-2 particle track duration (i.e. the length of time between the first and last frames that TrackMate can detect the particle), displacement (x/y distance between the particle positions in the first and last frame that the particle appears), and average velocity (displacement divided by duration). In the absence of KLP-19 we saw no significant change in the mean track displacement (Control - 0.55 µm, *klp-19* – 0.58 µm), velocity (Control – 0.61 µm/s, *klp-19* – 0.59 µm/s), or duration (Control – 0.97 s, *klp-19* – 1.08 µm/s)

By plotting the frequencies of track dynamics as proportions of each measured outcome (i.e., relative frequencies), we were able to look at the distributions of each parameter to assess the impact of KLP-19 in greater detail than the averages above. After knocking down klp-19, we observed no significant changes in the population of EBP-2::GFP tracks for displacement or velocity (Figure 5.2.b&c). We did however see a significant shift in the duration of tracks as *klp-19* depleted embryos showed a tendency towards longer lived tracks (Figure 5.2.d). EBP-2 track durations of 1.25 seconds and below had higher prevalence in control embryos than klp-

19 RNAi embryos. These data suggest that KLP-19 presence does not impact the distance or velocity travelled of growing MT tips, but that KLP-19 limits the duration that MT plus ends grow.

Figure 5.2

a.

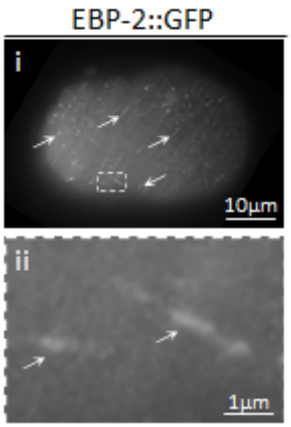

b.

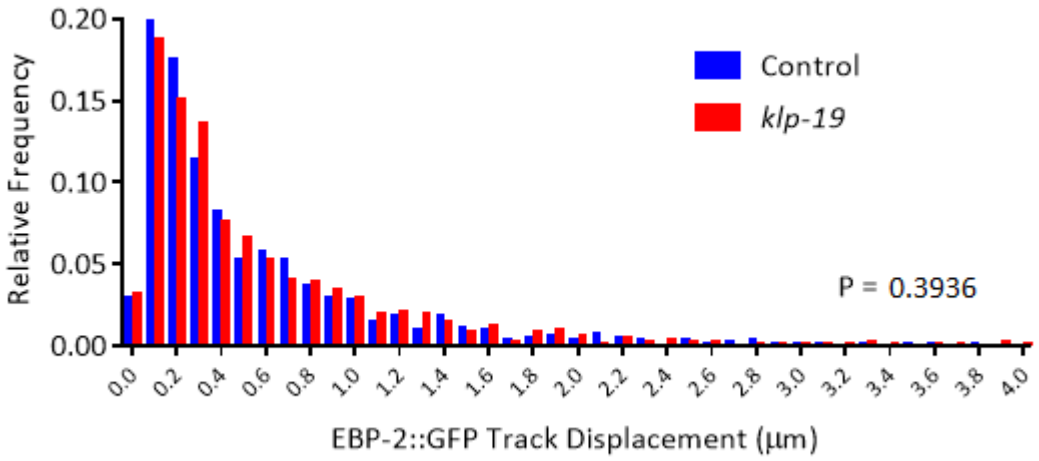

c.

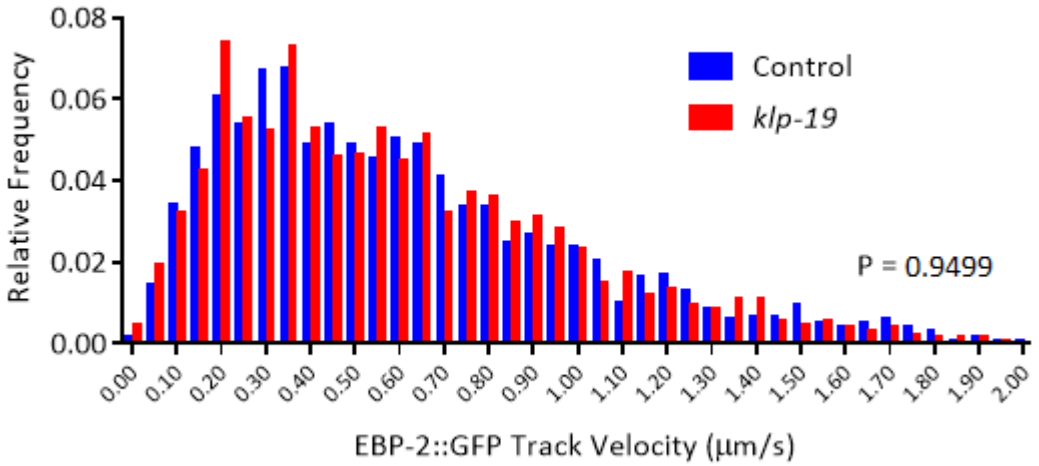

d.

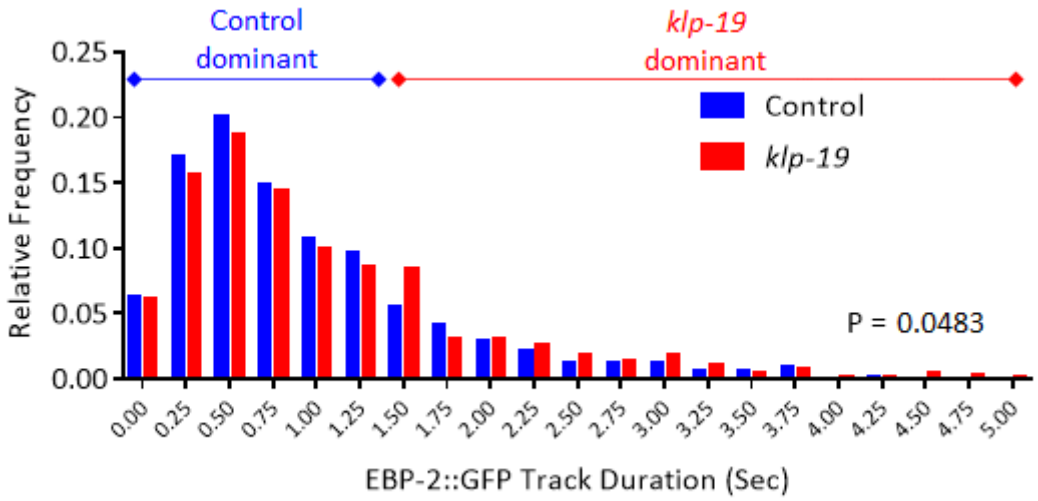

Figure 5.2 **EBP-2::GFP Track dynamics.**
(a) Maximum intensity projection of cortical EBP-2::GFP over 5 seconds, frame rate ~17fps (Frame interval: 60ms). Imaged via TIRF microscopy. i - Whole embryo image. ii - 10x zoom of broken squared region. White arrows point to EBP-2. **(b,c,d)** Histograms of EBP-2 track displacement, velocity, and duration during polarity establishment in both control (Number of embryos = 11, Number of Tracks = 1166) and *klp-19* RNAi (Number of embryos = 12, Number of Tracks = 1246) embryos. Tracks were detected and measured via TrackMate (ImageJ). See methods for TrackMate settings used (Section 2.8.7). Region of the track duration histogram (d) that shows predominant frequency of control embryo or *klp-19* RNAi embryo tracks is indicated at the top. Kolmogorov-Smirnov test of significance used to determine P values - $P<0.05$ is significantly different. Number of experiments: 4. For more detailed imaging conditions see methods (Table 2.8).

5.2.3 Klp-19 localises to stable microtubules.

Given that KLP-19 appears able to regulate microtubule plus-end dynamics, we wondered how KLP-19 itself acts at the cortex. To date KLP-19 localisation has only been presented in fixed samples (Monen *et al.*, 2005; Pelisch *et al.*, 2017).We reasoned that KLP-19 is likely localising to the cortex on microtubules and so decided to compare it with EBP-2 which decorates the tips of all growing MTs. Through this, we aimed to determine what kind of MT population KLP-19 localises to. As KLP-19 seems to fix or stabilise MTs, we predicted that it localises to MTs with lower dynamics, similar to that observed for Kif4a (Morris *et al.*, 2014).

Due to difficulties visualising KLP-19::GFP using TIRF microscopy, we used spinning-disc microscopy for this strain at the compromise of frame rate compared to imaging EBP-2::GFP which required a higher frame rate (Spinning-disc - ~2fps vs TIRF - ~17fps (Frame intervals 500ms vs 60ms, respectively)). We found that KLP-19 puncta had longer track duration at the cortex than EBP-2 (Figure 5.3.c.i). EBP-2::GFP had an average duration at the cortex 0.97 seconds, while KLP-19 puncta were able to last longer at the cortex at an average of 1.39 seconds. A small number of KLP-19 track lasted much longer, reaching up to 56.4 seconds. It is worth noting that the lower frame rate used to image KLP-19 may have resulted in the loss of very short lived KLP-19 puncta. These measurement of KLP-19 cortical residence durations are in line with previous measurements of MT tip duration as other labs have shown that microtubules tend to reside at the cortex for ~1 seconds (Labbé *et al.*, 2003; Kozlowski, Srayko and Nedelec, 2007; O'Rourke, Christensen and Bowerman, 2010; Schmidt *et al.*, 2017; Sugioka *et al.*, 2018; Bouvrais *et al.*, 2021). Specifically, Bouvrais et al. (2021) recently demonstrated that microtubules exist in two populations with distinct MT tip cortical residence times. A shorter-living population of MTs that lasts at the cortex for an average of 0.4 seconds and a longer-living population that lasts 1.8 seconds (Bouvrais *et al.*, 2021). These average durations support a model in which KLP-19 localises to MT tips.

The average displacement and velocity of KLP-19 tracks are 0.13 μm and 0.14 μm/s respectively, both lower than EBP-2 tracks at 0.55 μm and 0.61 μm/s (Figure 5.3.c.ii&iii). As EBP-2 decorates the plus ends of all growing microtubules, our data suggest that KLP-19 localises to a more stable subset of cortical microtubules as it remains at the cortex for longer with more restricted movement.

During polarity establishment, clusters of KLP-19 puncta formed and disassembled in cycles of roughly 30 seconds in duration (Figure 5.1.b & Figure 5.3.d). These foci were reminiscent of actomyosin foci (Vasquez, Tworoger and Martin, 2014; Masatoshi *et al.*, 2017; Michaux *et al.*, 2018) and we wondered if KLP-19 could be reacting to actomyosin dynamics. Preliminary analysis of the two videos which captured these foci showed an anterior directed movement of the clusters at a rate of 4.20 μm/min in one video and 1.81 μm/min in the other (extracted from the slope in the kymographs as represented in Figure 5.3.d). These velocities are in line with previous work which tracked the velocity of GPR-1/2 (Average velocity ~1-2 μm/min, Max ~16 μm/min), a protein required for spindle positioning, which responds to and correlates well with actomyosin flow velocity (De Simone, Nédélec and Gönczy, 2016).

Figure 5.3

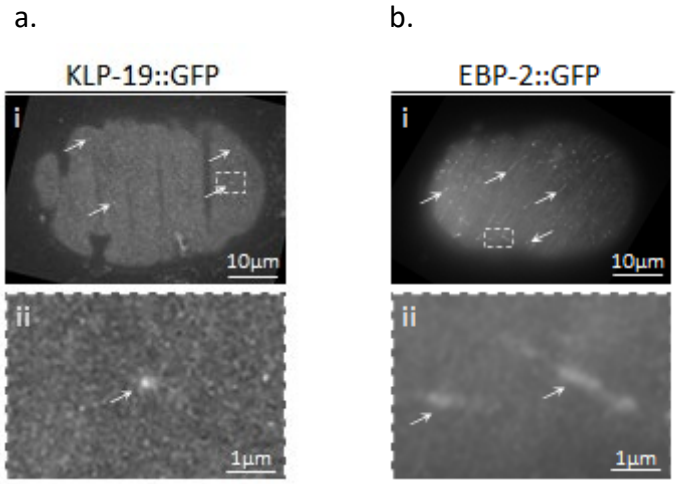

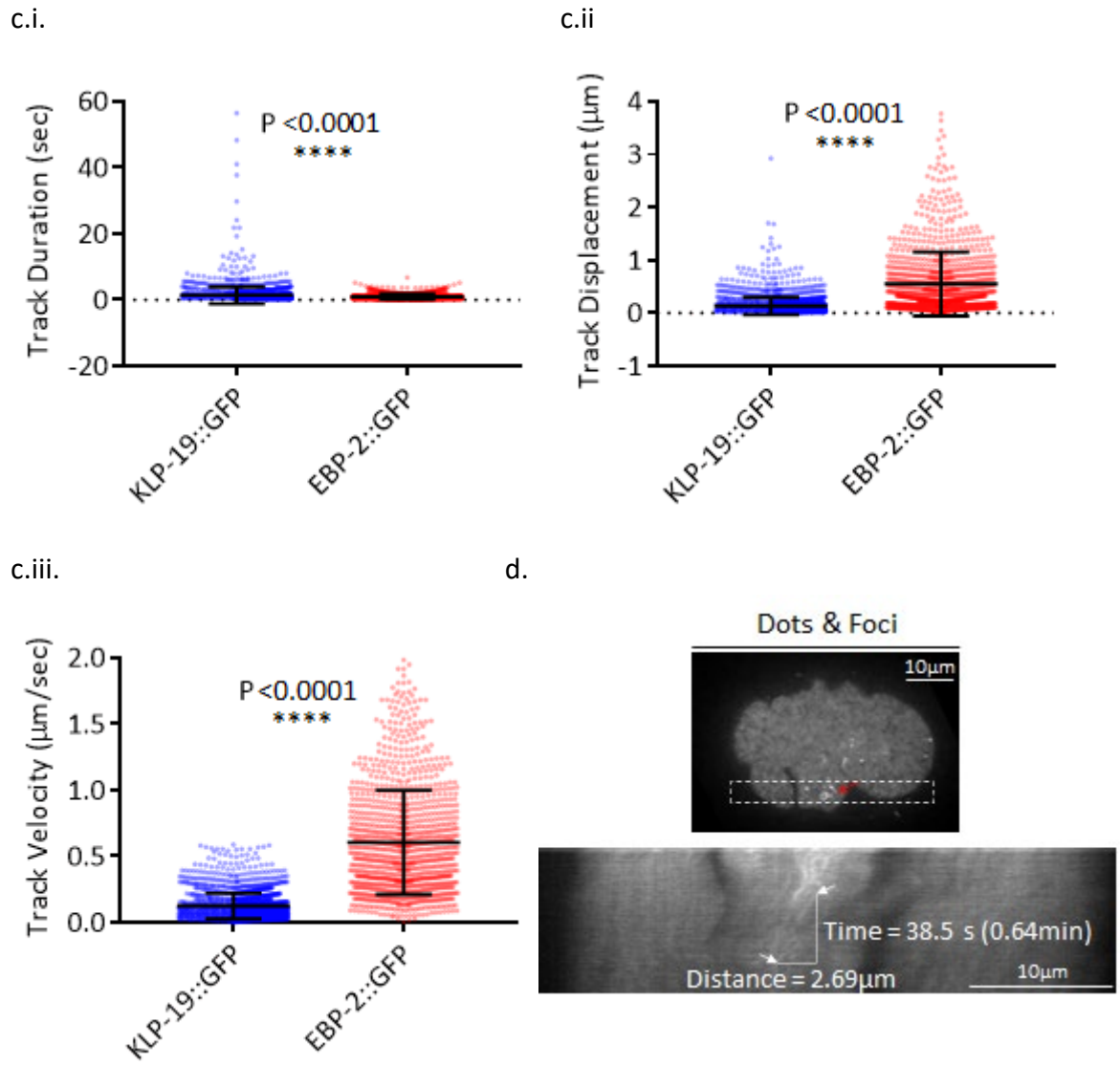

Figure 5.3 **KLP-19 vs EBP-2 cortical dynamics.**
(a&b) Maximum intensity projections of cortical (a) KLP-19::GFP and (b) EBP-2::GFP over 5 seconds, frame rate 2fps (Frame interval: 500ms)(Spinning disc microscopy) and ~17fps (Frame interval: 60ms) (TIRF microscopy), respectively. i. Whole embryo images. ii. 10x zoom of broken squared region. White arrows point to KLP-19 and EBP-2 in their respective images. Note - Figure 5.3.b is the same embryo recorded and used in Figure 5.2.a . **(c)** Duration, displacement and velocity (i,ii,iii) of KLP-19::GFP and EBP-2::GFP puncta as measured by TrackMate (ImageJ). (KLP-19::GFP N= 4 embryos & 2315 tracks, EBP-2::GFP N= 11 embryos & 1166 tracks). See methods for TrackMate settings used (Section 2.8.7). Mann-Whitney test used to calculate P value (P<0.05 = significantly different). Number of experiments for KLP-19::GFP: 2. Number of experiments for EBP-2::GFP: 4. **(d)** Kymograph of KLP-19::GFP foci movement used to measure anterior directed speed (4.20 µm/min) from white broken rectangle (Imaged via spinning disc microscopy). X axis represents distance and Y axis represents time. White arrows highlight start (top) and end (bottom) of the foci track measured. For more detailed imaging conditions see methods (Table 2.8).

5.2.4 An intended rigour mutation in the kinesin switch I of KLP-19 results in a dominant-negative lethal effect in C. elegans.

Given that KLP-19 is a motor protein, we wanted to determine if the kinesin was using its motor activity in its new role at the cortex to restrict the SPCC's position and/or suppress the mitotic spindle's dynamics, or if it acts more like a passive "clamp". We also wondered whether we could trap KLP-19 in its dynamic localisations to gain more insight into where it localises at the cortex. To investigate this, we endeavoured to generate a rigour mutant in which the kinesin can bind to MTs but is then unable to release (i.e. unable to walk). This was successfully achieved *in vitro* using a *D. melanogaster* conventional kinesin (kinesin-1) construct in which arginine at position 210 was converted to alanine. This residue sits in the kinesin switch I required to hydrolyse ATP and facilitate the release of the kinesin bound to the microtubules (Farrell *et al.*, 2002).

The sequence used - NXXSS**R**SH - is well conserved in other kinesins, including KLP-19.

- ^{205}NEHSS**R**SH^{212} – *D. melanogaster*, Kinesin-1 (Human KIF5B)
- ^{200}NAMSS**R**SH^{207} – *C. elegans*, KLP-19

We used CRISPR-Cas9 to introduce the R205A mutation in KLP-19. The CRISPR technique performed had been optimised by Craig Mello's lab (University of Massachusetts Medical School) to expect ~20% efficiency of injection (Dokshin *et al.*, 2018). After injecting the gonads of F0 hermaphrodites, 25% (6/24 isolated worms) of the resultant F1 progeny were infertile, likely those that were successfully transformed. As the method of CRISPR only affects the maternal DNA, leaving the sperm unaffected, successful transformation can only result in heterozygous F1 progeny for the desired mutation. This suggests that our designed mutation is dominant and causes sterility. To confirm this, we sequenced the target site in a sterile worm vs a fertile worm and confirmed that the sterile worm was heterozygous while the fertile worm carried only the WT sequence. Unfortunately, this meant further work using this mutant would not be possible.

5.3 Discussion.

In Chapter 3 and Chapter 4 we identified and quantified the SPCC positioning defects that occur due to *klp-19* depletion (i.e., SPCC cortical detachments & centrosome misorientation).

We also showed that KLP-19 acts to suppress cortical pulling forces that act during in anaphase to pull the mitotic spindle apart. This led us to hypothesise that KLP-19 has a role in microtubule cortical fixation that helps to restrict the SPCC's position prior to centrosome separation and counteract cortical mitotic pulling forces. In support of this hypothesis, we found that KLP-19 localises to the cortex of zygotes during SPCC positioning and anaphase. KLP-19 appeared in puncta and lines that resembled the tips of MTs and MTs running parallel to the membrane, respectively. Below I will discuss what these different localisation patterns could indicate in terms of KLP-19's modes of action.

5.3.1 KLP-19 cortical puncta organisation and dynamics reflect potential interaction with centrosomal MT tips.

During polarity establishment and maintenance, we saw punctate appearances of KLP-19, indicative of either end-on contacts of centrosomal microtubules to the cortex with KLP-19 localising to the MT tip, or of transient localisation to the ends of cortically grown MTs. We saw the KLP-19 puncta form uniformly at the cortex including at the far posterior (Figure 5.1.b) where we would expect centrosomal MT cortical contacts. This could support the role of KLP-19 in SPCC positioning. It is likely, however, that KLP-19 localises to non-centrosomal cortical MTs too which are seen away from the posterior where KLP-19 may have additional roles. It would be useful to use a second fluorescent marker for MTs to simultaneously image MTs and KLP-19 and assess where the MTs originate to confirm the centrosomal MT population of KLP-19. It is worth noting that the cortical imaging we used will only capture centrosomal MTs in this plane and in many cases they will be in the midsection due to the typical positioning of the SPCC to the posterior pole. It would be interesting to align the embryos before imaging such that the posterior pole is oriented towards the microscope objective to see if puncta are more concentrated at the pole where we expect the most centrosomal MTs to be during PN touch.

Our assumption that KLP-19 was localising to microtubules at the cortex was based on their similar appearance to end-on MT cortical contacts and MT-like threads. To gain confidence that KLP-19 puncta are on MT tips, we compared the dynamics of KLP-19::GFP at the cortex with published data on tubulin residency durations and our own data of the end binding protein, EBP-2::GFP, which decorates the plus-end tip of growing microtubules. Previous literature suggests that the amount of time that KLP-19 resides at the cortex was within range

of that of tubulin, supporting a model in which KLP-19 localises to MTs. KLP-19 lasted longer at the cortex, travelled slower, and traversed less distance before disappearing than EBP-2. This suggests that KLP-19 is able to localise to paused-state MTs, unlike EBP-2 which only decorates growing MTs.

Upon the depletion of KLP-19 in EBP-2::GFP embryos, we observed no change in the profile of relative frequencies of track displacements or velocities. We did however see a shift in durations towards longer lived EBP-2 tracks. As a marker of growing MT tips, these EBP-2 data suggest that KLP-19 does not impact the growth rate of polymerising MTs (i.e. no change in EBP-2::GFP displacement or velocity) but does act to limit the duration of growth. This is consistent with previous work that shows that homologues of KLP-19 are able to stabilise the plus ends of MTs and limit MT growth (Bringmann *et al.*, 2004; Castoldi and Vernos, 2006; Bieling, Telley and Surrey, 2010; Hu *et al.*, 2011; Stumpff *et al.*, 2012; Wandke *et al.*, 2012). As such the absence of KLP-19 results in an increased distribution of EBP-2 tracks that last longer at the cortex as they decorate growing MT ends.

As EBP-2::GFP does not mark for stalled or shrinking MTs, we wondered if KLP-19 could impact the stability of MTs (i.e. rate of MT depolymerisation (Stepanova *et al.*, 2003; Harterink *et al.*, 2018)) or if it is able to regulate the movement of stalled MT tips at the cortex (e.g. mediating the attachment of MT tips to the cortex. These potential roles would alter MT displacement, velocity, and duration at the cortex, but changes would not be measurable using the EBP-2::GFP reporter. In future it would be useful to repeat this experiment using a tubulin reporter rather than EBP-2 to see total MTs.

As of yet, it is unknown how KLP-19 would be recruited to the cortex in these punctate patterns. Morris et al. (2014) showed that the N-terminal of EB1 is able to directly interact with the C-terminal of Kif4a which may facilitate Kif4a's recruitment to MT tips (Morris *et al.*, 2014). It is unclear, however, why Kif4a only stabilises a subpopulation of MTs, as KLP-19 appears to, when EB1 seemingly localises to the plus ends of all MTs as they grow. This suggests additional factors likely participate in the recruitment and regulation of these kinesins.

Other proteins have previously been identified to recruit kinesins, which control MT dynamics/organisation, to the cortex of cells. I have previously discussed Khc-73 which is

recruited to the cortex of *Drosophila* neuroblast cells via Dlg where it acts to anchor MTs to the cortex and aids in spindle orientation (Section 1.4.3 & 4.3.1). There is no known/predicted interaction between KLP-19 and the *C. elegans* Dlg homologue, DLG-1. Similarly, the ankyrin domain containing protein, VAB-19 (Human - KANK1) has been shown to recruit another KIF4 family member, KIF21A, to the cortex of neurons where it stabilises MTs to prevent growth (Kakinuma and Kiyama, 2009; van der Vaart *et al.*, 2013; Bianchi *et al.*, 2016; Weng *et al.*, 2018). In the next chapter we will assess whether VAB-19 is involved in KLP-19 cortical recruitment in the zygote and if it is required to regulate the position of the SPCC and the separation of the centrosomes.

5.3.2 Clusters of KLP-19 puncta in foci may follow actomyosin dynamics.

Unexpectedly, we also saw KLP-19 puncta aggregate and form clusters, that disperse and reform, in some early zygotes. This pattern is typical of actomyosin which forms large contractile foci that assemble and disassemble at the cortex during polarity establishment. These actomyosin foci have the ability to act as a sink that concentrates several other membrane proteins, which we suspect could be happening to KLP-19 (Munjal *et al.*, 2015; Coravos, Mason and Martin, 2017; Ko, Tserunyan and Martin, 2019; Gubieda *et al.*, 2020).

Recent work by Ko et al. (2019) demonstrated in *D. melanogaster* that the MT minus-end stabilising protein, Patronin, is sequestered into myosin foci at the apical cortex of mesodermal cells in synchronisation with myosin pulses. Their work suggests that the forces generated by actomyosin contractions can capture Patronin which would likely act as a site of MT nucleation. If something similar holds true in our system, this could suggest that actomyosin foci contraction produces sites which can stabilise the minus ends of MTs which may interact with MTs emanating from the centrosomes. McNally et al. (2010) previously confirmed the presence of plus-end-inward directed MTs which help to restrict the localisation of the SPCC during meiosis (Previously discussed in section 1.7.2) (McNally *et al.*, 2010, 2012). When in contact, clustered cortical and centrosomal MTs would lead to the recruitment of KLP-19 puncta in foci (Ko, Tserunyan and Martin, 2019). In *C. elegans*, Patronin (PTRN1) functions in parallel with the ninein homologue, NOCA-1, to produce non-centrosomal MTs, however only NOCA-1 is active in the zygote (Wang *et al.*, 2015). Preliminary work in our lab using a GFP reporter of NOCA-1 showed that the protein localises at the cortex

and forms foci which appear to form and dissipate as Patronin did in *Drosophila*. Future work would involve determining if these NOCA-1 foci colocalise with KLP-19 and NMY-2.

As discussed earlier, KLP-19 appears to have a second role in centrosome separation beyond restricting the position of the SPCC to the posterior cortex (Sections 4.2.2 & 4.3), potentially a function of the cortical KLP-19 we observed not localised to the posterior. KLP-19 is able to respond to actomyosin directed movement at the cortex (Figure 5.3.d), hence it is possible that the kinesin could help to drive centrosome separation as the cortical dynein complex does by pulling on centrosomal MTs (Cao *et al.*, 2010; De Simone, Nédélec and Gönczy, 2016). How KLP-19 would respond to actomyosin, however, is unknown.

5.3.3 KLP-19 cortical threads indicate the presence of antiparallel MTs.

We also saw KLP-19 at the cortex of the zygote along MT-like threads. This would suggest that KLP-19 is not only recruited to the tips of MTs but also can dock along the length of MTs that either grow along the cortex or reach the cortex from the centrosome and bend. As KLP-19 is a plus-end directed motor protein, we would expect it to only travel in one direction along single MTs. Interestingly, we often observed bidirectional movement of KLP-19 along these MT-like threads (Figure 5.1.c), suggesting that KLP-19 is walking along two oppositely directed MTs.

As previously discussed, KLP-19 homologues are recruited with high affinity to antiparallel MT overlaps by the MT bundling protein PRC1. In the following chapter, we will assess the contribution of the *C. elegans* PRC1 homologue SPD-1's contribution to KLP-19 cortical localisation and SPCC positioning/ centrosome separation to determine the likelihood that this localisation to antiparallel MTs is similarly relied upon to recruit KLP-19 as on antiparallel MTs in the spindle midzone.

5.3.4 The role of KLP-19's motor.

Finally, in this chapter we sought to characterise whether KLP-19's novel role in SPCC positioning and MT dynamic regulation depend on the kinesins motor activity. We attempted to use Crispr-Cas9 to generate a rigour mutant of KLP-19 which would be unable to release from microtubules and walk along them. In this instance, if KLP-19 acts to crosslink antiparallel MTs we would have expected that centrosome positioning would be unperturbed as the

kinesin would still be able to bind to MTs and hold the centrosome in place. Unfortunately, the mutation was dominant and induced infertility in transformed progeny preventing further work. It is possible that a rigour mutant of KLP-19 would lock onto microtubules, becoming crowded along the MT and potentially altering MT dynamics. These outcomes could prevent WT KLP-19 and other MAPs from performing their functions, thus preventing cell viability in the heterozygous mutant (Telley, Bieling and Surrey, 2009). It would be necessary to generate this rigour mutation in an inducible system to determine the contribution of KLP-19's motor activity to SPCC position regulation. Voutev and Hubbard (2008) previously demonstrated the usage of the FLP/FRT site-specific recombination system whereby a gene of interest and its promoter are positioned either side of a reporter gene, in this way interrupting expression of the gene of interest. FRT target sites on either side of the reporter are cut by FLP recombinase which can be placed under the regulation of a heat-shock inducible promoter. The result is the excision of the central reporter gene which brings the gene of interest and its promoter together. In such a system, one can choose when a gene becomes expressed (Voutev and Hubbard, 2008). This could be useful to our need to prevent expression of the KLP-19 rigour mutant protein until experimental setup, at which point the worms can be shifted to a higher temperature.

5.3.5 Concluding remarks

Having shown that KLP-19 can act at the cortex to reduce/restrain MT dynamics, we will further investigate how KLP-19 could be mediating this role in the next chapter through determining possible co-regulators. As previously mentioned, KLP-19 would likely need to be recruited to the cortex, either through anchoring to then capture MTs, recruitment to cortical MTs, or to antiparallel MTs bundled at the cortex. In Chapter 6 we perform a small screen to determine how different candidates can mediate KLP-19 localisation and support its role in SPCC positioning. This additional work has helped us to establish which of the above models KLP-19 likely acts through.

Chapter 6 KLP-19 depends on VAB-19, SPD-1, and NOP-1 to localise to microtubules at the cortex of single cell *C. elegans* zygotes.

6.1 Introduction.

In section 5.2.1, we showed that KLP-19 localises to the cortex of embryos during polarity establishment and late anaphase. As a kinesin, this is likely through binding to microtubules, supported by KLP-19's reminiscent appearance of MT tips as puncta (end-on MTs with cortex) and threads (MTs running parallel to membrane). KLP-19's homologues have been shown to localise to microtubules in two patterns – 1) high affinity docking to antiparallel MTs, and 2) low affinity docking to single microtubules (Kapitein *et al.*, 2008; Bieling, Telley and Surrey, 2010; Subramanian *et al.*, 2010; Hannabuss *et al.*, 2019). Currently, we do not know which MT pattern the KLP-19 we see at the cortex is recruited to.

The MT bundling protein PRC1 recruits KLP-19 homologues to antiparallel microtubules, largely seen in the spindle midzone. Here, they act together to drive microtubule sliding and aid chromosomal segregation while the antiparallel MT overlap is long, and then act as a brake when the overlap becomes short (Section 1.3.1) (Kurasawa *et al.*, 2004; Mazumdar, Sundareshan and Misteli, 2004; Zhu and Jiang, 2005; Gruneberg *et al.*, 2006; Hannabuss *et al.*, 2019; Gaska *et al.*, 2020; Alfieri, Gaska and Forth, 2021). It is possible that microtubule-microtubule (centrosomal-cortical) interactions could limit the movement of microtubules at the cortex facilitated, in this case, through cross-linkage via PRC1 (*C. elegans* SPD-1) mediated MT bundling and KLP-19 recruitment. MT fixation would then restrict the centrosomes position to the posterior cortex. This would explain why the absence of KLP-19 has shown positioning defects of the SPCC prior to centrosome separation as this initial position seems to require centrosomal MTs and cortical MTs (Discussed in section 1.7.2, Figure 1.14, Figure 8.1).

The orientation of centrosomal-cortical MTs would be important in producing antiparallel MT overlaps. During meiosis, the orientations of cortical microtubules are guided by cortical cytoplasmic streaming forces (Kimura *et al.*, 2017). It is likely that the flows of polarity establishment would also move microtubules at the embryo's cortex (Munro, Nance and Priess, 2004). The flows generated during meiosis, however, are more linear and in fact align the microtubules perpendicular to the AP axis. Through this, kinesin-1 carries the endoplasmic

reticulum, generating drag in the cytoplasm which further aligns the microtubules, and flows are enhanced through positive feedback (Kimura *et al.*, 2017). Flows during polarity establishment, however, are a result of pulsatile actomyosin contractions (In Section 5.3.2 we discussed how these pulses may lead to the foci of KLP-19 observed). As such, it is likely that cortical microtubules would be "blown" in different directions including facing into the cell centre, hanging at the cortex from their stabilised minus-end. This constant reorientation of cortical microtubules, during polarity establishment, could be ideal to introduce antiparallel centrosomal-cortical microtubule contacts that KLP-19 would localise to and crosslink, thus restrict the SPCC's position. It is possible, then, that actomyosin induced flows are required for the patterns of KLP-19 we have seen thus far via aligning cortical microtubules such that they face the centrosome and allow antiparallel MTs to form.

KLP-19 homologues also localise to single microtubule, albeit with low affinity. It is possible that, KLP-19 reaches the plus ends of single microtubules and, as the MT grows and reaches the cortex, KLP-19 is somehow anchored and aids in the stabilisation of the MTs. Another KIF4 family member, KIF21A, has previously been shown to localise to the cortex of neurons, dependent on the ankyrin domain-containing protein KANK-1 (*C. elegans* VAB-19) where KIF21A stabilises MTs and inhibits their growth (Kakinuma and Kiyama, 2009; van der Vaart *et al.*, 2013). Interaction between KLP-19 and VAB-19 has not previously been identified but it would be interesting to assess whether KLP-19 relies on other proteins to localise to the cortex.

In this chapter we set to investigate which of the potential mechanisms described above is responsible for KLP-19 cortical function by assessing which factors are involved in the recruitment of KLP-19 to the cortex. To do this we performed RNAi of the KANK1 and PRC1 homologues, *vab-19,* and *spd-1*, respectively, and diminished cortical flows through *nop-1* RNAi. We show that KLP-19 cortical presence is compromised in the absence of all three candidates suggesting that our hypotheses are not exclusive, in fact these data would suggest that the pathways act interdependently. We also show that SPD-1 has similar cortical localisation patterns to KLP-19 supporting the hypothesis that KLP-19 could restrict SPCC movement through a similar mode of action as in the spindle midzone to prevent chromosome hyper-segregation (Section 1.3.1).

6.2 Results

6.2.1 KLP-19 relies on SPD-1, VAB-19, and NOP-1 to localise to the cortex.

Given that our data show that KLP-19 localises to the cortex and that this cortical localisation could be important for KLP-19 function in SPCC and mitotic spindle positioning. We wanted to identify regulators of KLP-19 cortical localisation, such as other proteins that may act as adapters to recruit KLP-19, or factors that may alter cortical dynamics to enable KLP-19 recruitment. As discussed in this chapter's introduction, we have decided to investigate VAB-19 and SPD-1 as potential adapters of KLP-19, and NOP-1 which is required to generate actomyosin contractions which we propose could promote KLP-19 cortical recruitment. Thus, we set to knock down each potential KLP-19-localisation regulator via RNAi and assess the effect on KLP-19 cortical recruitment.

We used the particle tracking software TrackMate (An ImageJ plugin) to identify tracks of KLP-19 at the cortex of KLP-19::GFP embryos during polarity establishment. Due to low signal-to-noise ratios in the samples of this experiment, particularly in the knockdowns, background noise was detected as KLP-19 tracks at the cortex. To account for this, we removed tracks with a mean quality score below 400. In control embryos (KLP-19::GFP treated with control RNAi), we saw an average of 23 (Number of embryos = 4) KLP-19 tracks over 60 seconds during polarity establishment (Figure 6.1.a.i&b).

We investigated whether a known protein that recruits kinesins to the cortex of other cell types is also required for KLP-19 localisation to the cortex of *C. elegans* zygotes. The ankyrin domain-containing protein, KANK1 (VAB-19 in *C. elegans*) recruits another Kinesin-4 family member, KIF21A, to the cortex of neurons where it stabilises microtubules by inhibiting growth (Kakinuma and Kiyama, 2009; van der Vaart *et al.*, 2013). Interestingly, upon *vab-19* RNAi feeding, the average KLP-19 track number dropped to 4 (Number of embryos = 4) (Figure 6.1.a.ii&b) suggesting VAB-19 is also involved in KLP-19 cortical recruitment as KANK1 is to KIF21A. To date, however, there is no known interaction between VAB-19 and KLP-19.

During anaphase, the KLP-19 homologue Kif4a is recruited to antiparallel spindle microtubules via the MT bundling protein PRC1 (Kurasawa *et al.*, 2004; Loïodice *et al.*, 2005; Zhu and Jiang, 2005; Bieling, Telley and Surrey, 2010; Mullen and Wignall, 2017; Pamula *et al.*, 2019). If KLP-19 localisation at the cortex similarly relies on recruitment via *C. elegans* PRC1 (SPD-1), we

would expect KLP-19 to be absent upon *spd-1* RNAi depletion. Upon knockdown of *spd-1*, the average number of KLP-19 tracks detected during polarity establishment fell to 2.5 (Number of embryos = 4) (Figure 6.1.a.iii&b), compared to 23 observed in the WT, over the course of 60 seconds. This suggests SPD-1 is similarly recruiting KLP-19 to the cortex of early embryos as it does on the spindle midzone during anaphase and supports our theory that KLP-19 may be mediating antiparallel MT contacts at the cortex.

Finally, we wondered how cortical dynamics could affect the recruitment of KLP-19 to the cortex. Cortical flows have been shown to align the orientation of microtubules parallel to the cortex during meiosis (Kimura *et al.*, 2017). Our earlier KLP-19 localisation experiments provided preliminary data of the formation of clusters reminiscent of actomyosin foci which appear to respond to cortical flows as they travel anteriorly (Figure 5.1.b & Figure 5.3.d). Strikingly, after suppressing cortical dynamics via *nop-1* RNAi knockdown, we saw the average number of KLP-19 tracks during establishment drop to 0.25 (Number of embryos = 4) (Figure 6.1.a.iv&b) over a 60 second period. This indicates that cortical contractility may be important in the recruitment of KLP-19 at the cortex, possibly by induced favourable cortical microtubule organisation required for KLP-19 docking.

Together these data suggest that KLP-19 relies on multiple factors to localise to the cortex including the suspected direct recruiters, VAB-19, the homologue of which (KANK1) has previously been shown to recruit another KIF4 family member KIF21A to the cortex of neurons (Kakinuma and Kiyama, 2009; van der Vaart *et al.*, 2013), and SPD-1, which recruits KLP-19 homologues to antiparallel MTs of the mitotic spindle midzone (Mollinari *et al.*, 2002; Kurasawa *et al.*, 2004; Zhu and Jiang, 2005; Lee *et al.*, 2015; Liu *et al.*, 2018; Wijeratne and Subramanian, 2018; Hannabuss *et al.*, 2019; Jagrić *et al.*, 2021). KLP-19 also relied on the actomyosin contraction activator NOP-1, indicating a role for cortical actomyosin dynamics in KLP-19 recruitment. The loss of cortical KLP-19 in all three knockdowns suggests that KLP-19 relies on the simultaneous activity of these three proteins to localise to the cortex.

Figure 6.1

a.

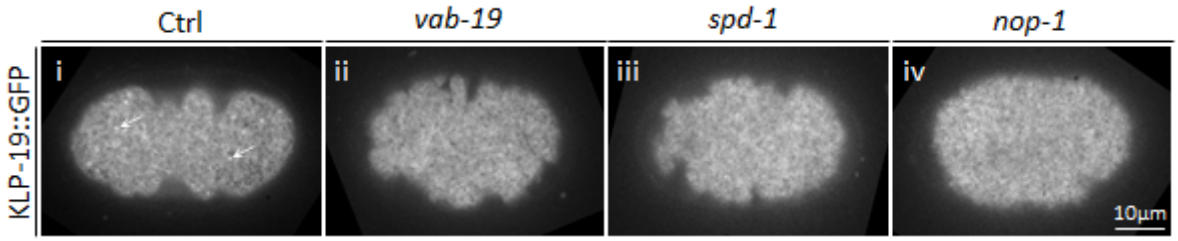

b.

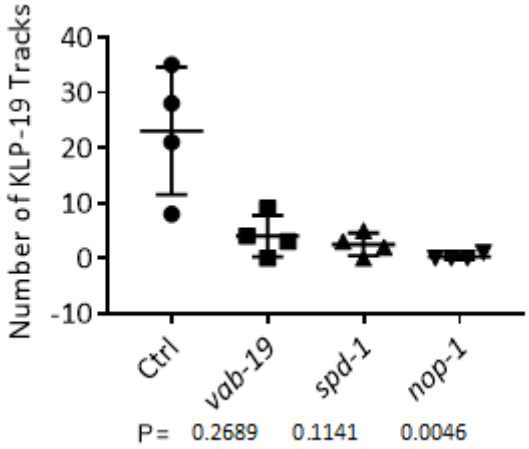

Figure 6.1 **KLP-19 cortical localisation dependency**.

(a) Cortical snapshots of polarity establishment phase (symmetry breaking-pseudocleavage) live embryos expressing KLP-19::GFP with indicated RNAi conditions, imaged via spinning disc microscopy. (Images acquired with frame interval 5.0 seconds). For more detailed imaging conditions see methods (Table 2.8). Note - Linear adjustment of brightness and contrast used for representation in figure. **(b)** The number of KLP-19 tracks detected by TrackMate (ImageJ) over 60 seconds during polarity establishment in KLP-19::GFP embryos represented in (a) under control and named RNAi KD conditions. See methods for TrackMate settings used (Section 2.8.7). 4 embryos per RNAi analysed. Kruskal-Wallis used to calculate P value ($P<0.05$ = significantly different). Number of experiments: 1. Experiment was performed with the help of Ruben Schmidt (Utrecht University).

6.2.2 Loss of the KLP-19 recruiting proteins, SPD-1, and VAB-19, result in centrosomal defects similar to the loss of KLP-19.

KLP-19 homologues show limited microtubule binding in the absence of an adapter protein (Bieling, Telley and Surrey, 2010). Given that the absence of VAB-19 and SPD-1 result in the loss of KLP-19 from the cortex, we wondered if KLP-19's proposed functional role in SPCC positioning and centrosome separation, similarly relies on these proteins. In addition to VAB-19 and SPD-1 dependent KLP-19 recruitment, we also postulated that actomyosin contractility was important to orient microtubules at the cortex to enable KLP-19 localisation. As

demonstrated in section 3.2.2 (*nop-1* mutant) and previous studies (Bienkowska and Cowan, 2012; Kimura and Kimura, 2020), cytoplasmic flows are required to position the SPCC and separate the centrosomes around the male PN. As a result, it will not be possible to assess whether actomyosin contraction dependent MT orientation impacts SPCC positioning and centrosome separation independently from the cortical and central cytoplasmic movement (flows).

We returned to VAB-19, the homologue of KANK1 which recruits another KIF4 kinesin family member, KIF21A, to the cortex of neurons. Loss of VAB-19 via RNAi did result in centrosome positioning (2/6 – 33.3%) and separation (3/14 – 21.4%) defects (Figure 6.2.a,b,c&d). This would support a potential pathway in which VAB-19 could recruit KLP-19 to the cortex of zygotes. Alternatively, VAB-19 could be involved in SPCC positioning in a KLP-19 independent pathway. We tried to test for same/parallel pathways by depleting KLP-19 via RNAi in a *vab-19* cold-sensitive mutant (CZ401), at the restrictive temperature (15 °C), expecting enhanced defects if VAB-19 and KLP-19 act in parallel pathways. In this condition, however, the *vab-19* mutant resembled the WT strain suggesting that this *vab-19* mutant may not impact VAB-19's ability to regulate centrosome position and separation, as demonstrated by *vab-19* RNAi (Figure 6.2.a,b,c&d). As such, we can conclude that VAB-19 has a comparable role to KLP-19 in SPCC defects and recruiting KLP-19 to the cortex but have been unable to test the genetic relationship between the two.

As mentioned, the KLP-19 homologue Kif4a is recruited to antiparallel microtubules during anaphase by PRC1 and we have shown that KLP-19 localises to the cortex of zygotes in a SPD-1 dependent manner (Section 6.2.1) (Kurasawa *et al.*, 2004; Loïodice *et al.*, 2005; Zhu and Jiang, 2005; Bieling, Telley and Surrey, 2010; Mullen and Wignall, 2017; Pamula *et al.*, 2019). We wanted to know if SPCC positioning and centrosome separation defects caused by loss of KLP-19 could be reproduced upon knockdown of the *C. elegans* PRC1 homologue, SPD-1. We found that loss of SPD-1 does indeed result in similar defects in SPCC positioning and centrosome separation as seen upon the loss of KLP-19. 3/10 (30.0%) *spd-1* RNAi embryos, in fixed samples, showed a centrosome initial positioning defect and 5/15 (33.3%) had a centrosome separation defect, compared to *klp-19* RNAi which presented 9/21 (42.9%) position and 12/37 (32.4%) separation defects (Control: 2/25 (8.0%) position defects, 3/33 (9.1%) separation defects)(Figure 6.2.a,b,c&e).

The similar phenotypes between *klp-19* and *spd-1* knockdown are supportive of a common pathway in which they regulate SPCC positioning and centrosome separation. To test this further, we knocked-down *klp-19* in a *spd-1* temperature sensitive mutant (WH12) at the restrictive temperature (24 °C). Interestingly SPCC positioning and centrosome separation defects were similar in proportion between both *spd-1* & *klp-19* RNAi knockdowns and the double LoF (Figure 6.2.a,b,c&e). This supports the hypothesis that SPD-1 and KLP-19 are acting in a common pathway to regulate centrosome dynamics. Note that the spd-1 temperature-sensitive mutant had a greater proportion of SPCC positioning defects than RNAi depletion, possibly indicating that *spd-1* RNAi is not as efficient in producing LoF zygotes.

Figure 6.2

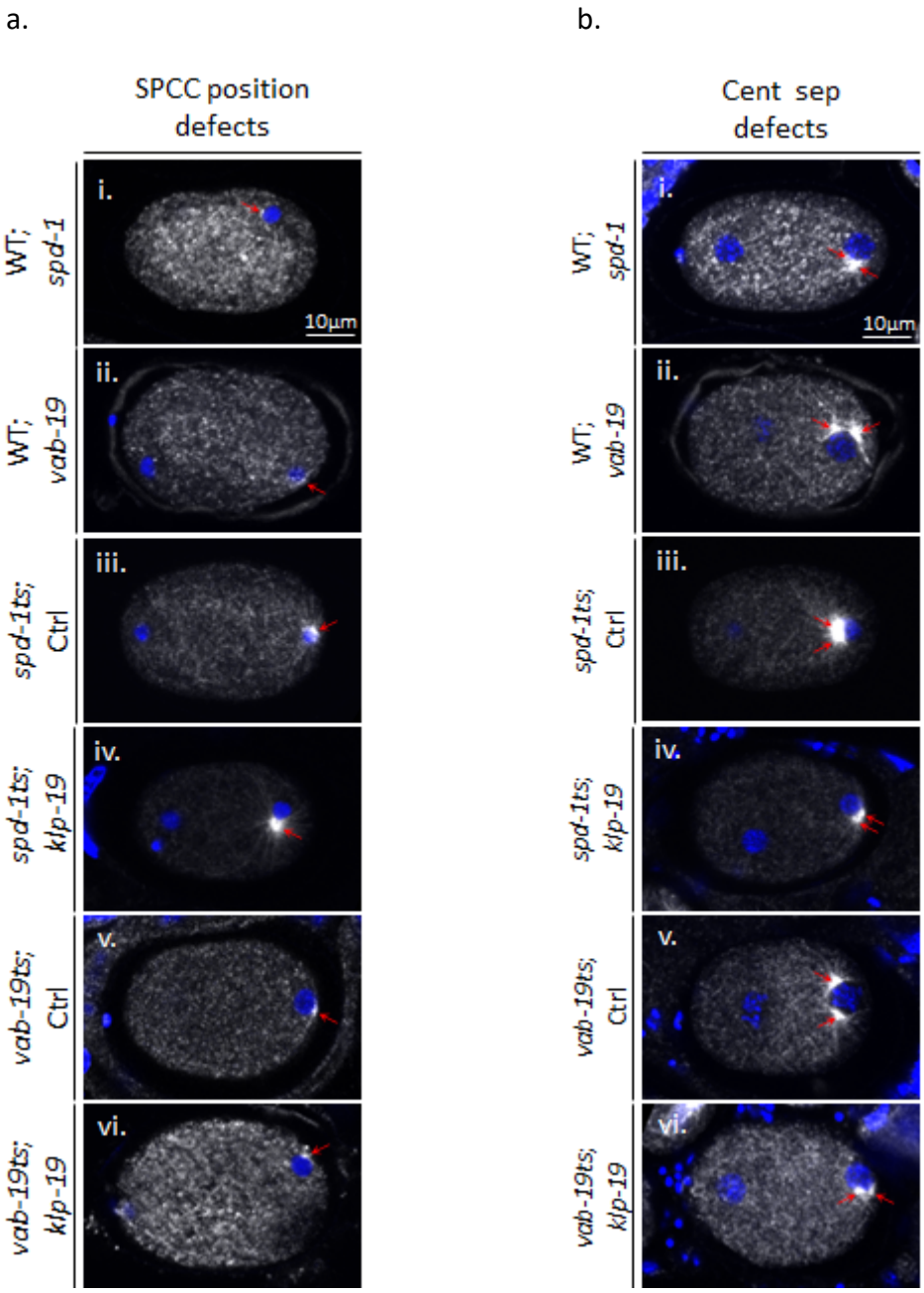
a.
b.
SPCC position defects
Cent sep defects
WT; spd-1
WT; vab-19
spd-1ts; Ctrl
spd-1ts; klp-19
vab-19ts; Ctrl
vab-19ts; klp-19
i.
ii.
iii.
iv.
v.
vi.
10µm

c.

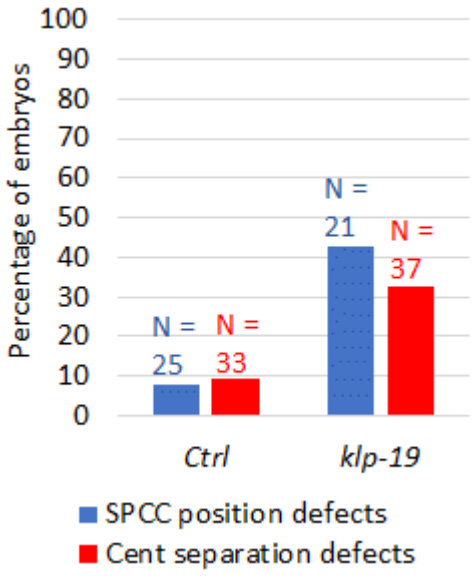
100
90
80
70
60
50
40
30
20
10
0
Percentage of embryos
N = 25
N = 33
N = 21
N = 37
Ctrl
klp-19
SPCC position defects
Cent separation defects

d.

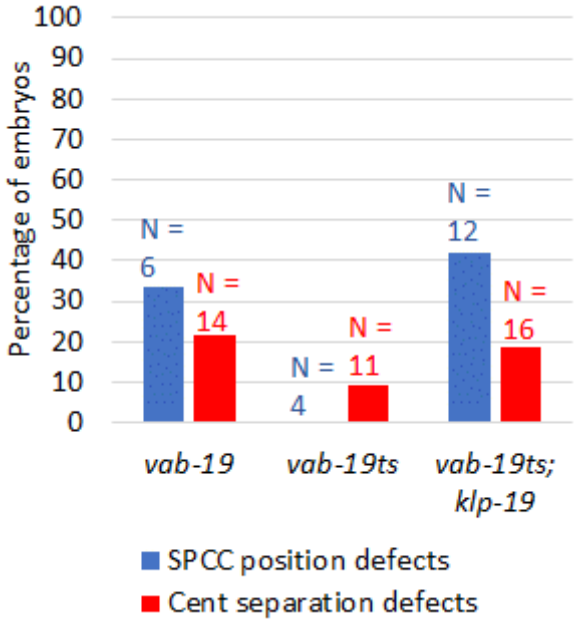
100
90
80
70
60
50
40
30
20
10
0
Percentage of embryos
N = 6
N = 14
N = 4
N = 11
N = 12
N = 16
vab-19
vab-19ts
vab-19ts; klp-19
SPCC position defects
Cent separation defects

e.

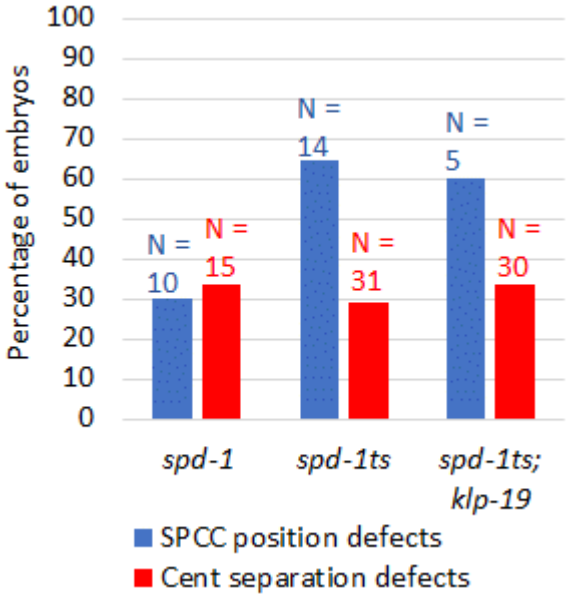
100
90
80
70
60
50
40
30
20
10
0
Percentage of embryos
N = 10
N = 15
N = 14
N = 31
N = 5
N = 30
spd-1
spd-1ts
spd-1ts; klp-19
SPCC position defects
Cent separation defects

Figure 6.2 ***spd-1* & *vab-19* loss of function induced SPCC positioning and centrosome separation phenotypes.**
(a&b) Immunofluorescently labeled fixed embryos, imaged via confocal microscopy (Microtubules-Grey, DNA-Blue), displaying the centrosome early positioning (a) and late separation (b) phenotypes observed under different conditions of mutants and RNAi knockdowns (Red arrows point to centrosomes). Note - Linear adjustment of brightness and contrast used for representation in figure. **(c,d&e)** Percentages of embryos with SPCC positioning and centrosome separation defects under different mutant and RNAi knockdown conditions. Note - Number of experiments for the control: 6, *klp-19*: 6, *spd-1*: 2, *spd-1ts*: 3, *spd-1ts*;*klp-19*: 3, *vab-19*: 2, *vab-19ts*: 2, *vab-19ts*;*klp-19*: 2.

6.2.3 The PRC1 homologue SPD-1 localises to the cortex in a similar pattern to KLP-19.

Homologues of SPD-1 are known to be able to directly interact with the respective KLP-19 homologues and promote the chromokinesins recruitment to anti-parallel MTs (Mollinari *et al.*, 2002; Kurasawa *et al.*, 2004; Zhu and Jiang, 2005; Lee *et al.*, 2015; Liu *et al.*, 2018; Wijeratne and Subramanian, 2018; Hannabuss *et al.*, 2019; Jagrić *et al.*, 2021). Jagrić et al. (2021) recently utilised a light-inducible system in which the dimerising proteins SsrA and SspB were tagged to the cell membrane bound peptide CAAX and PRC1, respectively. Through this, the team were able to trigger the acute removal of PRC1 from the mitotic spindle by using light to promote rapid SsrA-SspB dimerization to pull PRC1 to the membrane. This resulted in the near total loss of midzone microtubule bound Kif4A. They show that Kif4a localisation on the chromosomes is unperturbed and does not appear to follow PRC1 to the membrane upon light induction translocation. Assuming that the PRC1-Kif4a interacting domains are not compromised in this mutant, their results show that PRC1 is not always necessary or sufficient to recruit Kif4A within the cell. I.e., Kif4a can localise to chromatin independently of PRC1 and PRC1 does not bring Kif4a to the membrane upon light induction. The loss of Kif4a from the spindle midzone shows that antiparallel MTs are not sufficient to recruit Kif4 to high levels without PRC1 (Jagrić *et al.*, 2021). It is possible that both PRC1 and antiparallel MTs must be present when Kif4a is recruited to either of them.

Given SPD-1's role in KLP-19 cortical recruitment and SPCC positioning, we decided to investigate SPD-1 localisation in the zygote further and assess whether it has similar localisation patterns as KLP-19.

Upon imaging GFP::SPD-1 (SV2226) at the cortex, we saw that SPD-1 does indeed have similar puncta / threads localisation patterns at the cortex to KLP-19. Interestingly, however, SPD-1 tended to form threads at the cortex in early embryos (meiosis, polarity establishment) unlike in KLP-19::GFP which formed puncta. This could be due to the stronger fluorescent signal in the GFP::SPD-1 strain or imaging conditions as KLP-19::GFP was recorded on a spinning disc microscope while GFP::SPD-1 was recorded via a scanning confocal microscope. Spinning disc microscopes typically have a larger pinhole size which results in thicker specimen optical sectioning (i.e. greater amount of out of focus light recorded) which would contribute to a worse signal-to-noise ratio. We should note that to improve speed of capturing early embryos at greater numbers for this experiment, we did not use the same temperature regulating

system as KLP-19::GFP which maintained the strains at ~24 °C. It is possible that imaging GFP::SPD-1 at room temperature (~20 °C) could alter foci formation.

Using TrackMate (ImageJ) on control embryos, we observed an average of 185.5 SPD-1 tracks per embryo (N=6) over a course of 60 seconds during polarity establishment (Figure 6.3.a.i&b), much greater than the average 23 KLP-19 tracks observed in the same time-frame (Figure 6.1). Note that, although a greater amount of SPD-1 protein may localise to the cortex, differences between KLP-19 & SPD-1 imaging conditions (i.e. microscope, frame rate, temperature) may be responsible for the large difference in numbers of SPD-1 and KLP-19 tracks (Section 6.2.1) detected by each system. We did not see foci of GFP::SPD-1 form as KLP-19:GFP did. This could indicate that foci-clustered puncta of KLP-19 are not recruited by SPD-1, or again be a result of different imaging conditions.

We next wanted to investigate if SPD-1 cortical localisation dependent on KLP-19 and/or the other factors that seem to regulate KLP-19 localisation. As KLP-19 cortical localisation also depended on the ankyrin domain VAB-19, we tested whether SPD-1 similarly required VAB-19. Upon VAB-19 RNAi depletion, we did not see a significant change in SPD-1 localisation (Average number of SPD-1 tracks: 219.4, N=5) (Figure 6.3.a.iii&b) suggesting that VAB-19 and SPD-1 might recruit KLP-19 to the cortex through different mechanisms. Note that, although through different mechanism, both VAB-19 and SPD-1 seem to alter KLP-19 cortical organisation similarly (loss of thread, weak puncta, and foci).

We performed *klp-19* RNAi to assess whether KLP-19 and SPD-1 are co-dependent on each other to localise to the cortex. Unsurprisingly, loss of KLP-19 did not impact SPD-1 localisation (Average number of SPD-1 tracks: 137.5, N=5) (Figure 6.3.a.ii&b) as was previously shown to be the case on the spindle midzone (Kurasawa *et al.*, 2004; Jagrić *et al.*, 2021). Supporting our model that, at the cortex, SPD-1 is recruited to the cortex on antiparallel microtubules, then likely acting to recruit KLP-19 but not vice versa.

Next, we depleted embryos of NOP-1 expecting that SPD-1 should similarly rely on NOP-1 to localise to the cortex if KLP-19 is recruited to microtubules oriented by actomyosin flows. Interestingly, however, we saw no significant changes in SPD-1 cortical localisation upon *nop-1* RNAi (Average number of SPD-1 tracks: 138.4, N=5) (Figure 6.3.a.iv&b).

Together, these data suggest that SPD-1 is recruited to the cortex independently of actomyosin flows (NOP-1), VAB-19 and KLP-19.

Figure 6.3

a.

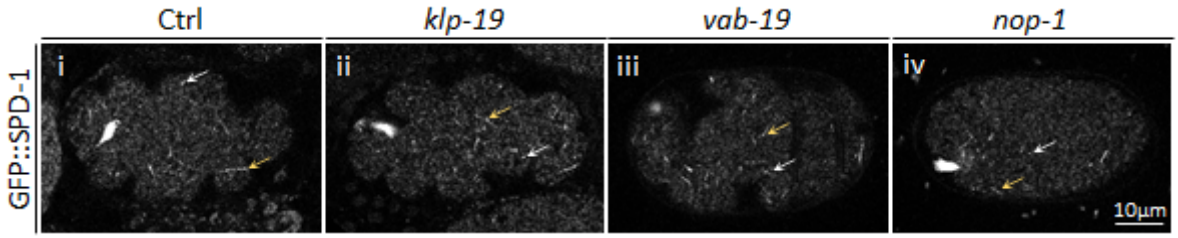

b.

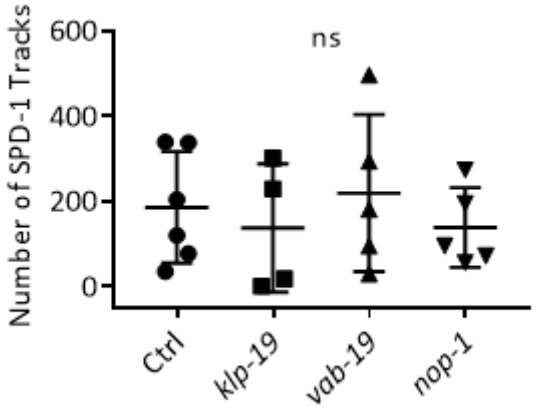

Figure 6.3 **SPD-1 cortical localisation dependency.**

(a) Cortical snapshots of polarity establishment phase (symmetry breaking-pseudocleavage) live embryos expressing GFP::SPD-1 with indicated RNAi conditions, imaged via scanning confocal microscopy. (Images acquired with frame interval 1.0 seconds). For more detailed imaging conditions see methods (Table 2.8). Note - Linear adjustment of brightness and contrast used for representation in figure. **(b)** The number of objects detected by TrackMate (ImageJ) over 60 seconds during polarity establishment in GFP::SPD-1 embryos represented in (a) under control and named RNAi KD conditions. See methods for TrackMate settings used (Section 2.8.7). Each point represents the number of tracks detected in an embryo – Control: N=6, *klp-19*: N=5, *vab-19:* N=5, *nop-1*: N=5. Kruskal-Wallis used to calculate P value ($P<0.05$ = significantly different). Number of experiments: 1.

6.2.4 SPD-1 is likely recruited to cortical antiparallel microtubules during early polarity establishment and to end-tags on single microtubules during late anaphase.

The KLP-19/SPD-1 complex is known to localise with higher affinity to antiparallel microtubule overlaps than to single microtubules (PRC1 is estimated to localise to antiparallel MTs 28x more strongly than to single MTs) (Kapitein *et al.*, 2008; Bieling, Telley and Surrey, 2010; Subramanian *et al.*, 2010; Hannabuss *et al.*, 2019). KLP-19 and SPD-1 homologues have, however, been shown to localise to single microtubules, on which the kinesin transports both proteins to the plus-end tips where they become enriched and form end-tags. As a result, both end-tags and antiparallel microtubule overlaps of the KLP-19 and SPD-1 homologues appear in fluorescent imaging as much brighter regions compared to the remaining length of single microtubules (Hu *et al.*, 2011; Subramanian *et al.*, 2013; Nguyen, Field and Mitchison, 2018).

We fixed GFP::SPD-1 embryos and immunofluorescently labelled for tubulin and found SPD-1 was enriched on the spindle midzone (as expected), and a subset of centrosomal and cortical microtubules. In Figure 6.4.a&b, threads of SPD-1 can be observed in the cytoplasm and at the cortex of early polarity establishment and late anaphase embryos. SPD-1 threads present with distinct populations of high and low fluorescent intensities that both colocalise with microtubules. This suggests SPD-1 indeed localises to MT but it becomes enriched at certain locations, likely end-tags or antiparallel MTs, through directed transport and/or enhanced recruitment.

Subramanian et al. (2013) propose that, during anaphase, PRC1 crosslinks antiparallel spindle MTs in the midzone whilst forming end-tags on MTs that extend outwards from each centrosome (Subramanian *et al.*, 2013). Consistent with this statement, we observed GFP::SPD-1 become enriched within the midzone and at the ends of single astral MTs of anaphase embryos (Figure 6.4.c). Interestingly, upon knockdown of *klp-19*, the length of SPD-1 end-tags increased to cover more of the astral microtubules, supporting the hypothesis that KLP-19 carries the SPD-1-KLP-19 complex to the plus tips of MTs (Figure 6.4.c&d).

Figure 6.4

a.

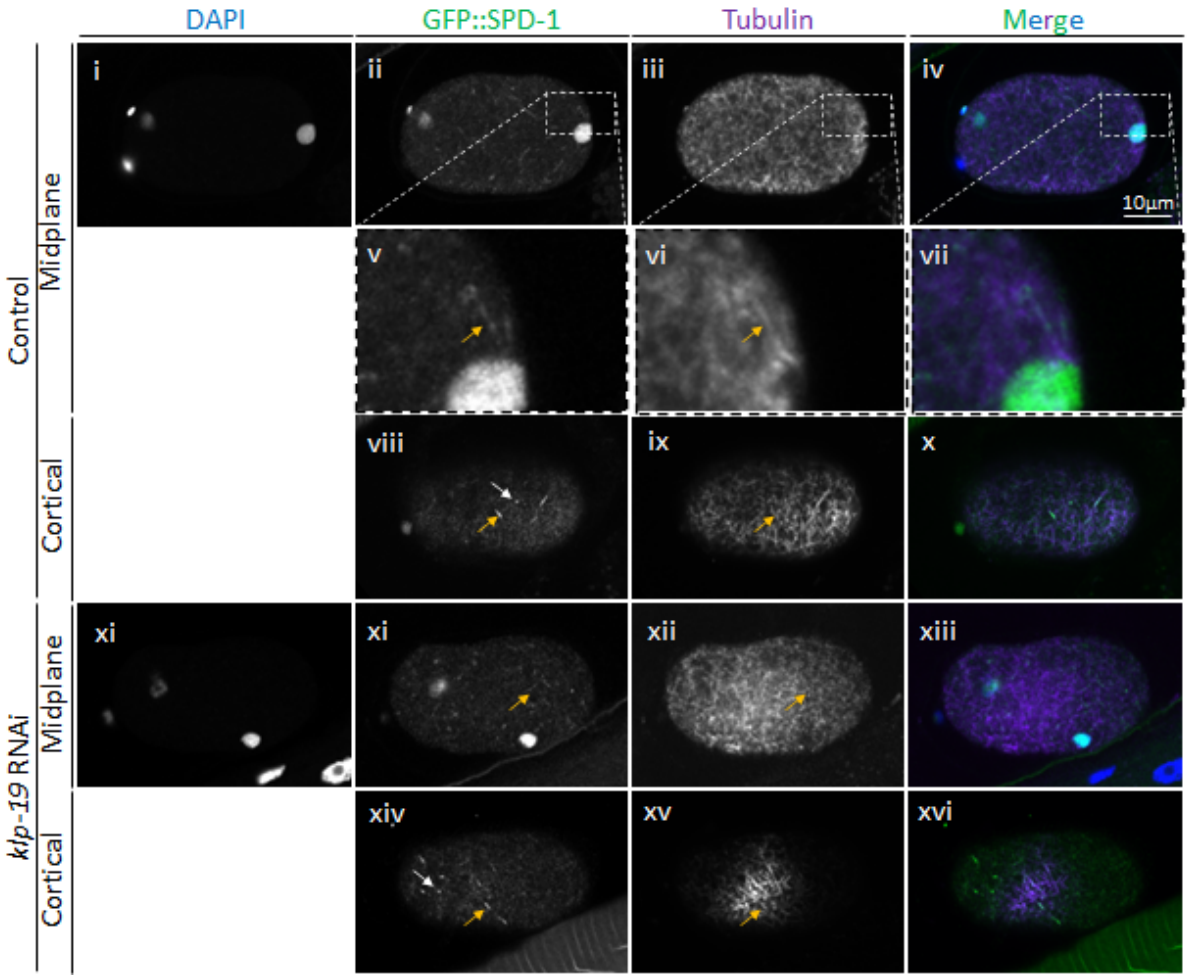
DAPI
GFP::SPD-1
Tubulin
Merge
Control
Midplane
Cortical
klp-19 RNAi
Midplane
Cortical
i
ii
iii
iv
10µm
v
vi
vii
viii
ix
x
xi
xi
xii
xiii
xiv
xv
xvi

b.

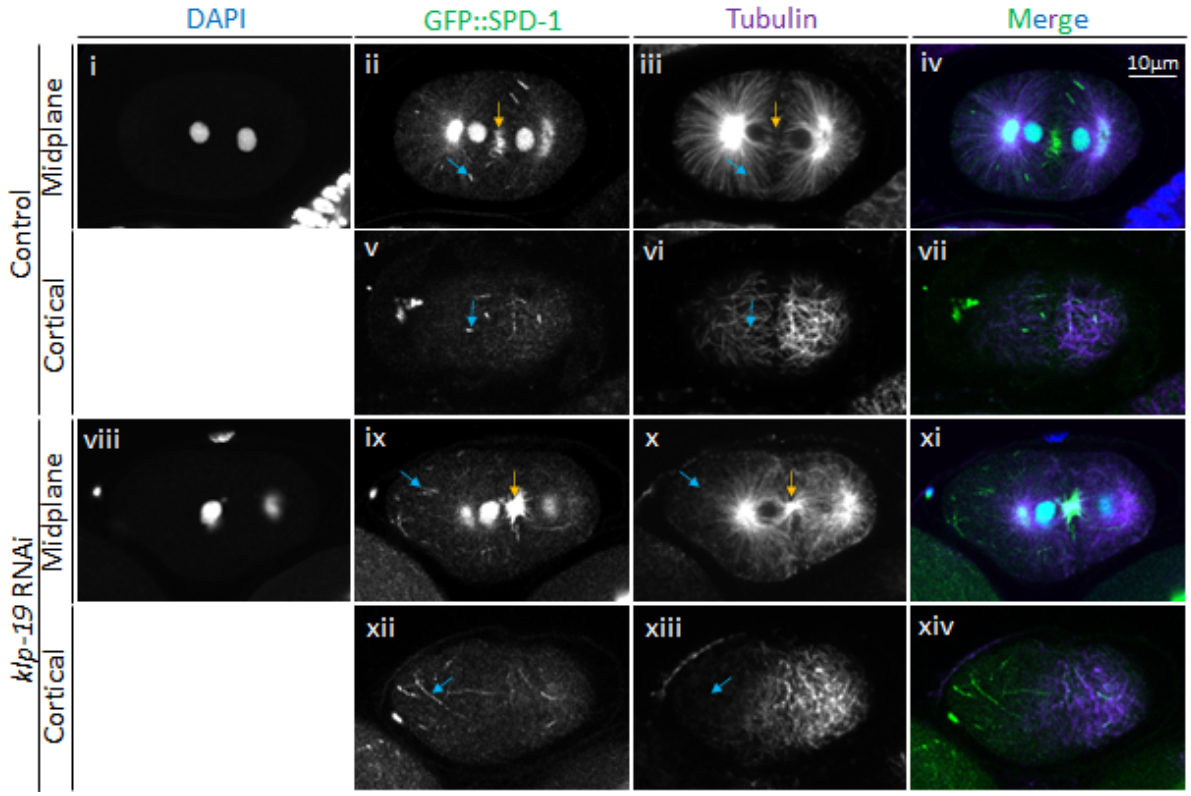

c.

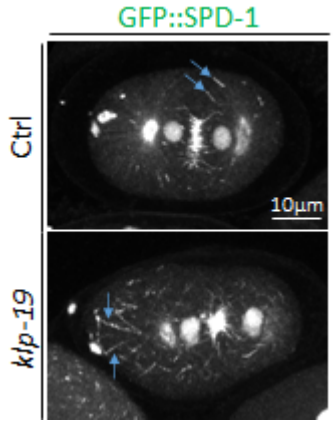

d.

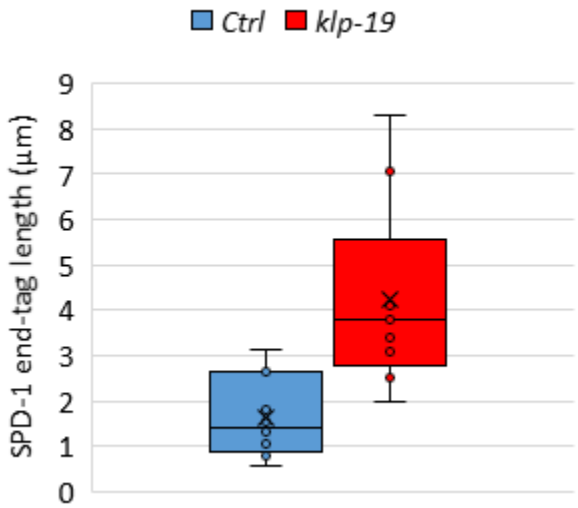

Figure 6.4 **SPD-1 antiparallel microtubule and end-tag localisation.**
(a) Midplane and cortical images of immunofluorescently labelled fixed early establishment phase GFP::SPD-1 embryos, imaged via confocal microscopy (fluorescently stained with DAPI and tubulin antibody), showing that SPD-1 colocalises with microtubules under control and *klp-19* RNAi conditions with enrichment to a subset of microtubules. (Yellow arrows = enriched threads of SPD-1, White arrows = enriched puncta of SPD-1). The row of boxes surrounded by broken lines magnifies colocalization of SPD-1 and microtubules emanating from the

centrosome. **(b)** As (a) but cytokinesis stage embryos. At this stage SPD-1 is enriched at the plus-ends of individual astral MTs as “end-tags” (blue arrows). In the absence of KLP-19, SPD-1 end-tag localisation becomes more spread out along the microtubule. Antiparallel MT-dependent enriched SPD-1 remains restricted to the spindle midzone after KLP-19 KD (Yellow arrows). Notes – Linear adjustment of brightness and contrast used for representation in figure. Tubulin difficult to detect on left side of embryo cortex xiii, likely due to uneven antibody staining during sample fixation. **(c)** Maximum intensity projections of Z-stacks of GFP::SPD-1 embryos undergoing cytokinesis pictured in b.ii&ix under control and *klp-19* RNAi conditions (Blue arrows = “end-tags”). **(d)** Lengths of end tags observed in maximum intensity projection images of (c). The lengths of the higher fluorescent intensity enriched regions of SPD-1 at the end of astral MTs were measured via ImageJ. N number = 1 embryo of each condition as preliminary data.

We wanted to determine if the high fluorescent intensity regions we see of SPD-1 (and by proxy, KLP-19) at the cortex of polarity establishment phase embryos were due to enrichment at end-tags or antiparallel microtubules. In the spindle midzone, MT overlaps resolve over time as the KIF4a/KLP-19 kinesin slides the MTs apart (Kurasawa *et al.*, 2004; Zhu and Jiang, 2005; Hu *et al.*, 2011; Pamula *et al.*, 2019). As such, the MT overlap contracts which is reflected by a shrinking PRC1/SPD-1 midzone localisation. This would contrast the appearance of end-tag formation overtime where SPD-1 would become concentrated to the plus end of a microtubule over time while SPD-1 recruited to antiparallel MTs would shrink in size to a central point. We reasoned that, by monitoring SPD-1 threads over time, we would be able to distinguish end-tags and antiparallel MTs. Interestingly, once GFP::SPD-1 threads were formed at the cortex of polarity establishment phase embryos, they often resolved to a central point before disappearing, indicating they are localising to antiparallel MT overlaps at the cortex.

In Figure 6.5.b we determined the position of GFP::SPD-1 in the final frame of the time-lapse it could be detected and measured where it aligned relative to the thread at its maximum length. Through this we could quantify when the thread shrinks to a central point, as suspected, or to either end of the thread which would suggest that KLP-19 is transporting SPD-1 to the MT end, suggestive of single MTs (0 = either end of the thread, 0.5 = the centre of the thread). We observed a mixture of threads that resolved either closer to the ends of threads and to the centre suggesting that there is possibly a mixture of SPD-1 localisation patterns to single and antiparallel MTs. It should be noted, however, that the threads often drifted at the cortex (likely in response to movement in the cytoplasm) which altered the position of the threads over time and would have impacted the relative position of the threads to each other between frames.

The overlaps become shorter in length as the MTs are slid apart. Upon knockdown of *klp-19*, these overlaps tended to take longer to resolve, implying that the kinesin indeed slides the MTs apart (Figure 6.5.a&c). As the microtubule overlap does still shrink, it is possible that KLP-19 knockdown was incomplete, or the microtubules slide apart via other means such as another kinesin.

Figure 6.5

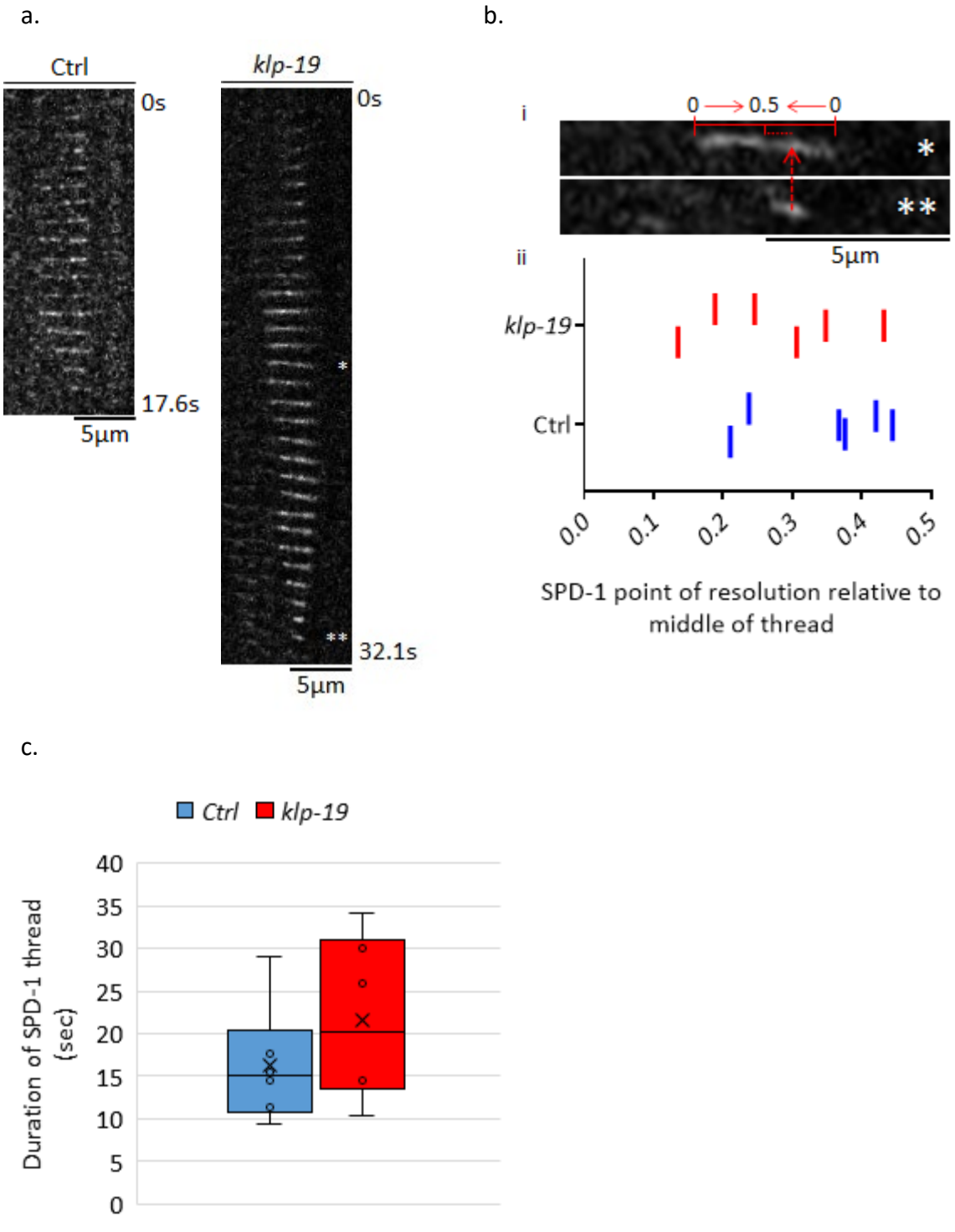

Figure 6.5 **SPD-1 thread dynamics.**
(a) Kymograph of representative GFP::SPD-1 threads over time localised at the cortex of establishment phase control and *klp-19* RNAi embryos imaged via confocal microscopy. Note – GFP::SPD-1 shrinks to a central point (suggestive of localising along antiparallel MTs) and takes longer to shrink upon *klp-19* RNAi. (Images acquired with frame interval 1.0 seconds). For more detailed imaging conditions see methods (Table 2.8). **(b)** The position of GFP::SPD-1 threads in the final frame detected (depicted in (a) **) were recorded relative to the middle

of the thread in the frame at the threads largest size (*). This was to determine whether the threads shrink to a central point, indicative of SPD-1 localising to antiparallel MT overlaps which shrink as the MTs slide apart, or to either end of the thread, indicative of single MTs **(i)**. This analysis was performed in control and *klp-19* RNAi embryos. 0.5 = the centre of the thread, 0 = either end of the thread. Threads that ended closer to position 0.5 (>0.25) resolved more centrally which likely suggest the MTs were slid apart while those that ended closer to 0 (<0.25) resolved closer to one end of the MT likely suggesting that SPD-1 was carried to one end of a single MT **(ii)**. Note that other movement at the cortex, such as cytoplasmic drift, could account for movement of the threads which would alter the relative position of the threads between frames. The Mann-Whitney test used to calculate P value ($P=0.3095$, $P<0.05$ would be considered significantly different). **(c)** The duration of the threads measured in (b) were recorded to determine how long it took SPD-1 threads to resolve for both control and *klp-19* RNAi conditions. The Mann-Whitney test used to calculate P value ($P=0.4848$, $P<0.05$ would be considered significantly different). For each condition in (b) & (c), N=6, Number of embryos = 3

6.3 Discussion

6.3.1 KLP-19 candidate interactors.

To elucidate the mechanisms by which KLP-19 performs its novel roles in centrosome positioning at the cortex, we went back to the literature to identify candidate genes that could either interact with the chromokinesin or facilitate its cortical recruitment. We then screened these genes (VAB-19, SPD-1, NOP-1) to determine if they are involved in KLP-19 localisation.

As it was previously unknown that KLP-19 can localise to the cortex of polarity establishment phase *C. elegans* zygotes, we investigated the KANK1 homologue, VAB-19. VAB-19 has previously been shown to recruit another kinesin-4 family member, KIF21A, to the cortex of neurons where the complex mediates MT contact with the cortex (Kakinuma and Kiyama, 2009; van der Vaart *et al.*, 2013; Weng *et al.*, 2018). It was striking to see that loss of VAB-19 did indeed result in a strong loss of KLP-19 localisation to the cortex, concurrent with SPCC posterior pole positioning and centrosome separation defects that were similar to *klp-19* depletion. To further test this, we attempted to knockdown *klp-19* in a *vab-19* temperature sensitive mutant. We did not observe a difference between the *vab-19* mutant and the WT strain which may indicate that this mutant acts differently to LoF RNAi of *vab-19*. Hence *vab-19*ts; *klp-19* RNAi might not be testing the double LoF, but rather just *klp-19* KD.

KANK1 contains an ankyrin domain (aa 1081-1360), semi-conserved in VAB-19, which in turn recruits KIF21A via a KANK1-binding domain spanning 19 amino acids (1138-1156) (Weng *et al.*, 2018). Sequence alignment via BLAST did not detect a similar sequence in KLP-19, nor did we observe localisation of VAB-19 in the single cell zygote of a GFP reporter strain. Future work including protein-protein interaction assays such as co-immunoprecipitation could clarify whether VAB-19 and KLP-19 do in fact interact with each other. Immunofluorescent staining using a VAB-19 specific antibody as opposed to a GFP reporter strain could identify if VAB-19 has cortical localisation in the early zygote.

Next, we investigated the homologue of the human MT-bundling protein, PRC1 (SPD-1 in *C. elegans*) as this protein recruits the KLP-19 homologue, Kif4a, during anaphase. Here PRC1 acts to bundle antiparallel MTs and then binds to Kif4a, bringing the motor protein to the spindle midzone where it acts to aid in chromosome segregation by sliding inter-spindle microtubules apart by walking towards their bi-oriented plus-ends (Discussed further in 1.3.1,

Figure 1.3.i, Figure 1.4.c) (Kurasawa *et al.*, 2004; Mazumdar, Sundareshan and Misteli, 2004; Zhu and Jiang, 2005; Gruneberg *et al.*, 2006; Hannabuss *et al.*, 2019). Bieling, Telley & Surrey (2010) showed, in *Xenopus laevis* extracts, that PRC1 binds with high specificity to antiparallel MTs and that the KLP-19 homologue, Xklp1, had no detectable MT localisation in the absence of PRC1. This was recently replicated using human Kif4a and PRC1 (Bieling, Telley and Surrey, 2010; Hannabuss *et al.*, 2019). We reasoned that KLP-19 could crosslink astral and cortical MTs that run antiparallel to anchor the centrosome during polarity establishment. As KLP-19 homologues have low affinity to antiparallel MTs in the absence of PRC1, we reasoned that SPD-1 should be present on these centrosomal and cortically grown MTs in order to stabilise KLP-19 to them. This would allow for the KLP-19 localisation patterns that we have observed (Figure 5.1), and facilitate KLP-19's role in SPCC positioning and centrosome separation (Figure 4.1 & Figure 4.2).

Upon *spd-1* RNAi knockdown, we saw a large reduction in the number of KLP-19 particles at the cortex, suggesting that this novel cortical localisation of KLP-19 similarly relies on SPD-1 as the localisation of KLP-19 homologues do during anaphase on the spindle midzone. As previously mentioned, it is likely that these early populations of KLP-19 and SPD-1 are specific to antiparallel microtubules, supporting our model in which KLP-19 crosslinks centrosomal-cortical MT overlaps which restricts the SPCC position to the posterior cortex during polarity establishment. Indeed, we saw very similar SPCC positioning and centrosome separation defects in *spd-1* depleted/ temperature-sensitive mutant embryos.

If SPD-1 acts in a different pathway to KLP-19, we would have expected an enhancement of positioning and separation defects as both pathways would be compromised if both proteins were simultaneously disturbed. Knockdown of *klp-19* in the *spd-1* temperature sensitive mutant did not enhance SPCC defects, however. Thus, we conclude that SPD-1 and KLP-19 act in the same pathway. This supports a model in which SPD-1 recruits KLP-19 to the cortex to position the centrosome during symmetry breaking.

We found that GFP::SPD-1 took on similar cortical localisation patterns as KLP-19::GFP as puncta and threads. It has previously been shown that PRC1 is required for Kif4A localisation to the spindle midzone, but not vice-versa (Mollinari *et al.*, 2002; Kurasawa *et al.*, 2004; Zhu and Jiang, 2005; Bieling, Telley and Surrey, 2010; Lee *et al.*, 2015; Liu *et al.*, 2018; Wijeratne and Subramanian, 2018; Hannabuss *et al.*, 2019; Jagrić *et al.*, 2021). Here, we saw the same

one-sided dependency at the *C. elegans* cortex as the depletion of KLP-19 did not impact SPD-1 cortical localisation. This suggests that SPD-1 localises to cortical MTs first and then recruits KLP-19.

Although SPD-1 can apparently localise to cortical antiparallel MTs in the absence of KLP-19, SPD-1 does not appear to be sufficient to crosslink and maintain the centrosome's position on its own as we observed SPCC positioning defects upon *klp-19* RNAi. A similar occurrence takes place during anaphase. The spindle midzone is believed to be strengthened via Kif4a and PRC1 which initially act to slide antiparallel MTs apart while the MT overlap is large. As the overlap shrinks, Kif4a and PRC1 become overcrowded, and the motor protein cannot walk further. The complex maintains MT-MT crosslinks and prevents further MT sliding, effectively turning the Kif4a and PRC1 complex into a brake. Although PRC1 homologues can localise to the midzone in the absence of Kif4a, the spindle poles become excessively pulled apart due to cortical pulling forces, demonstrating PRC1's insufficiency as a brake (Zhu and Jiang, 2005; Bieling, Telley and Surrey, 2010; Hu *et al.*, 2011; Lee *et al.*, 2015; Gaska *et al.*, 2020; Alfieri, Gaska and Forth, 2021). Kif4a's microtubule binding must be critical to apply this braking force to prevent spindle hyper-segregation. We reasoned that KLP-19 must similarly be required to overcome early cortical forces which cause the centrosome to become mispositioned in its absence. As in the spindle midzone during anaphase, SPD-1 is clearly unable to restrict the SPCC's position on its own, while KLP-19 cannot localise to MTs to perform its role without SPD-1.

As we saw multiple localisation patterns of KLP-19/SPD-1 at the cortex, that we believe are recruited to microtubules, we wondered if altering the organisation of microtubules could alter patterns of KLP-19 and SPD-1. Cytoplasmic flows at the cortex have been shown to alter the orientation of microtubules previously (Kimura *et al.*, 2017), thus we used *nop-1* RNAi to compare early zygotes with and without flows. We reasoned that puncta-like appearances of SPD-1 would represent the overlap of outward growing centrosomal microtubules with inward growing cortical microtubules (hanging from the cortex into the cytoplasm) (Figure 6.3 & Figure 8.1). Threads of SPD-1 would then indicate microtubules running against each other flat at the cortex (either cortical-cortical microtubules or centrosomal-cortical microtubules). Kimura et al. (2017) showed that cytoplasmic streaming promoted microtubules to favour running parallel to the cortex during meiosis along the same orientation (Kimura *et al.*, 2017). Microtubules running in the same direction would not be as hospitable to SPD-1 and KLP-19

which prefer antiparallel MT overlaps. Prior to polarity, establishment actomyosin contractions across the cortex begin which cause turbulent flows within the cytoplasm. It is possible that these pulsatile contractions allow more random orientations of cortical microtubules that allow MTs to meet in opposing orientations more suitable to SPD-1/KLP-19 recruitment, including MTs that hang perpendicular to the cortex stabilised by their minus end. If true, we would expect to see a reduction in SPD-1 and KLP-19 cortical localisation at the cortex of zygotes in the absence of actomyosin contraction (i.e., *nop-1* RNAi). In our experiments, we saw a drastic decrease in the number of cortical KLP-19::GFP objects recorded but not of GFP::SPD-1 suggesting that KLP-19 is more dependent on antiparallel MTs than SPD-1 to localise to the cortex during polarity establishment.

It is worth noting that only one experiment was performed for each of the KLP-19::GFP (Figure 6.1) and SPD-1::GFP (Figure 6.3) strains with RNAi knockdowns of *klp-19*, *spd-1*, *vab-19* and *nop-1*. As such, the findings and assumptions should be regarded as preliminary and further experiments will be required to provide strength to the conclusions drawn above.

6.3.2 SPD-1 on antiparallel MTs and End-tags.

As mentioned, KLP-19/Kif4a homologues colocalise with SPD-1/PRC1 which is itself enriched on antiparallel MTs (Bieling, Telley and Surrey, 2010; Nguyen, Field and Mitchison, 2018; Hannabuss *et al.*, 2019). However, both have been shown to localise weakly to single microtubules where the kinesin translocates PRC1 towards the plus-ends causing both proteins to become enriched as end-tags (Hu *et al.*, 2011; Subramanian *et al.*, 2013; Nguyen, Field and Mitchison, 2018). The biological relevance of this localisation is not fully understood although a study by Nguyen, Field & Mitchison (2018) propose that Kif4A is required to "prune" microtubules via promoting catastrophe of accidental anti-parallel overlaps to prevent disarray of radial asters in large cells. Note: They show that these overlaps resolve in the order of minutes and so would not exclude a time window in which we propose Kif4a/KLP-19 acts to crosslink antiparallel MT (Nguyen, Field and Mitchison, 2018).

We wanted to determine whether the cortical SPD-1/KLP-19 we observe in early embryos, while centrosomes separate, was due to antiparallel microtubules or enrichment at the plus-ends of single microtubules. GFP::SPD-1 in fixed embryos presented with distinct populations of weak and strong fluorescent intensities that colocalised with microtubules, likely reflecting

SPD-1's different affinity to single and antiparallel MTs, respectively. We reasoned that in the absence of KLP-19 transport, end-tags of SPD-1 would be unable to form, and the protein would remain more uniform along single microtubules whereas SPD-1 recruited to antiparallel microtubules, enriched due to higher binding affinity, would be unaffected by loss of KLP-19 as in the spindle midzone. By knocking down *klp-19* through RNAi feeding, we confirmed that the enriched regions of SPD-1 at the cortex of early embryos remained, supporting the hypothesis that antiparallel microtubules do exist at this time point. Additionally, the cortical GFP::SPD-1 threads through live imaging shrunk over time to a central point which we would expect if SPD-1 is localising to MT overlaps and KLP-19 is sliding the overlap apart, as it does to the spindle midzone during anaphase. Interestingly, however, the shrinkage of SPD-1 threads still occurred in the absence KLP-19 quite efficiently, albeit a bit slower indicating that KLP-19 is not the only kinesin here that slides MTs apart.

Although antiparallel MTs seem apparent through SPD-1 localisation and dynamics, antiparallel MT existence between astral and cortical microtubules requires further investigation. By specifically preventing centrosomal microtubule growth (e.g. *tac-1*, *zyg-9* RNAi (Bellanger and Gönczy, 2003; Bellanger *et al.*, 2007), we would expect a reduction in KLP-19 and SPD-1 at the cortex if the antiparallel MTs they localise to are between centrosomal and cortical microtubules.

6.3.3 Concluding remarks

In this chapter we have shown that KLP-19 is recruited to the cortex of establishment stage zygotes, dependent on the kinesin recruiting proteins VAB-19 (KANK1) & SPD-1 (PRC1), and contractility of the cortex (NOP-1). We observed a lack of redundancy between VAB-19, SPD-1, and NOP-1, suggesting that they act in the same pathway, or multiple pathways that are insufficient on their own to recruit KLP-19. We favour the latter as these proteins have no previously identified relationships and SPD-1 localisation was not impacted by the absence of VAB-19 or NOP-1. Between our work on visualising KLP-19 and SPD-1 we have reasoned that these proteins are recruited to both antiparallel MTs and the plus ends of single MTs to the cortex, although the relative contributions of each localisation type to the contribution of SPCC positioning in unclear thus far and requires future study.

Chapter 7 KLP-19 regulates polarity establishment by restricting the centrosome's position.

7.1 Introduction

In this project, we set out to identify regulators of microtubule-dependent polarity establishment and homed in on the chromokinesin KLP-19 due to its known interactions with microtubules and apparent novel role outside of meiosis and mitosis. In section 3.2.2 we immunofluorescently stained embryos, depleted of KLP-19, and briefly characterised the phenotypes that they developed. Upon *klp-19* RNAi, these embryos often presented with absent cortical PAR-2 during pronuclear touch, when the posterior domain would be expected to have begun forming in WT (Section 3.2.2 & Appendix: Table 9.1). As discussed earlier, delayed polarity establishment can arise in embryos with defects in which the centrosome is aberrantly situated at a distance from the cortex prior to symmetry breaking (Section 1.7.1). This was demonstrated in embryos depleted of PAM-1, in which increased centrosome-cortex distance was correlated with increased time between the end of meiosis II and polarity onset (Section 1.7.1) (Lyczak *et al.*, 2006; Fortin *et al.*, 2010; Saturno *et al.*, 2017). Indeed, we also noticed aberrant SPCC positioning in embryos lacking KLP-19 and recorded that the distance of the centrosomes was often further from the cortex than in control embryos (Sections 3.2.2 & 4.2.3). This leads us to believe that KLP-19 regulates polarity establishment through its role in regulating the position of the SPCC.

Loss of KLP-19 also presented embryos in which bipolar PAR-2 domains formed, reminiscent of embryos in which centrosome maturation is impaired, e.g., SPD-5 or AIR-1 depletion. As previously discussed (Section 1.6.4), how bipolar PAR-2 domains form is not well understood but recent experiments in *air-1* embryos demonstrated that bipolarity can occur as a result of premature activation of the PAR network (Hamill *et al.*, 2002; Tsai and Ahringer, 2007; Klinkert *et al.*, 2019; Reich *et al.*, 2019). Bipolar PAR-2 domains, in *klp-19* RNAi embryos, did not correlate with aberrant SPCC positioning as multiple bipolar embryos had WT positioned SPCCs. This suggests that KLP-19 likely has another role in the regulation of polarity in the zygote, in addition to its role in preventing delayed polarity establishment through SPCC positioning. As we discussed bipolar PAR-2 domain formation in section 3.3, this chapter will focus on how the position of the SPCC impacts PAR-2 cortical domain formation.

To understand the extent at which KLP-19 effects polarity, we have tried to answer the following questions:

- Does loss of KLP-19 alter asymmetry in the *C. elegans* zygote?
- Is disruption of asymmetry, in the absence of KLP-19, a result of aberrant centrosome positioning?

Through RNAi depletion of KLP-19 and fixed immunofluorescent imaging of the microtubules and pPARs, we found that delayed PAR-2 loading to the cortex of embryos is in indeed a result of aberrant centrosome positioning in KLP-19's absence. We also made an interesting observation as a result of the *klp-19* RNAi-induced phenotypes in that PAR-3, of the aPARs, appeared to clear from the cortex local to the centrosome's position, even in the absence pPARs and cortical actomyosin-dependent flows. This finding implies that additional mechanisms must be in place to ensure that aPARs clear the posterior cortex beyond the previously known, and discussed (Sections 1.6.3 & 1.6.4), actomyosin and MT-dependent pathways of polarity establishment.

7.2 Results

7.2.1 Loss of KLP-19 leads to a delay in posterior PAR cortical recruitment.

To quantify the effect of loss of KLP-19 on PAR asymmetry, we fixed and stained for markers of the anterior and posterior polarity domains, PAR-3 and PAR-2, respectively. We focused on early zygotes during polarity establishment and divided those into three stages based on chromosome condensation and sperm-pronucleus size (Figure 7.1.a) and measured the percentage of the cortex occupied by PAR-2 to determine the efficacy of posterior domain formation. As seen in Figure 7.1.b&c, the posterior domain of WT zygotes is already formed by early pronuclear touch (28.8% average cortex occupied by PAR-2) at which point meiosis is completed but the sperm-derived chromosomes have not begun to condense and the pronucleus is typically less than 15 µm in perimeter. As the embryo develops through late pronuclear touch, when the chromosomes condense & the pronucleus grows (>15 µm perimeter), and pronuclear migration, when the male PN detaches from the cortex, the posterior domain grows (37.8% and 44.8% average cortex occupied by PAR-2, respectively) and the anterior-posterior polarity domains become more balanced.

Upon *klp-19* knockdown, we observed a reduction in the average percentage of the cortex occupied by PAR-2 during early pronuclear touch (15.5%), with portion of embryos (3 out of 9) in which PAR-2 has not yet loaded to the cortex. This is rescued, however by late pronuclear touch (36.5%) and migration (45.9%), suggesting that polarity establishment is delayed upon loss of KLP-19 but that the polarity establishment pathways are eventually able to establish the pPAR domain to a similar degree as in WT.

Figure 7.1

a.

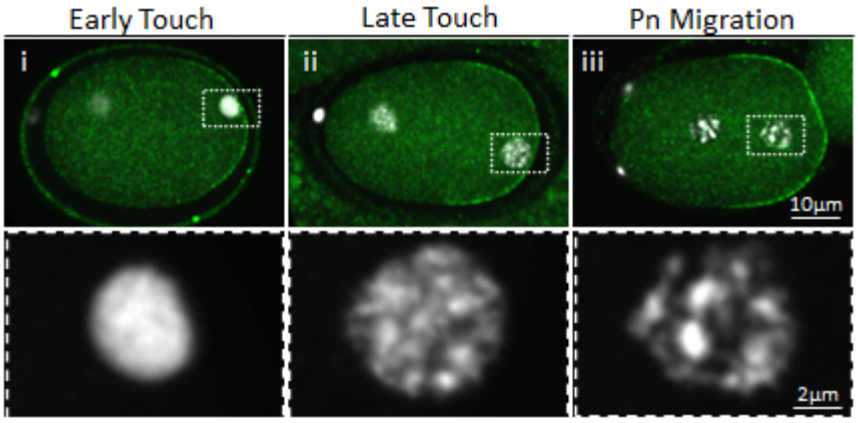

b.

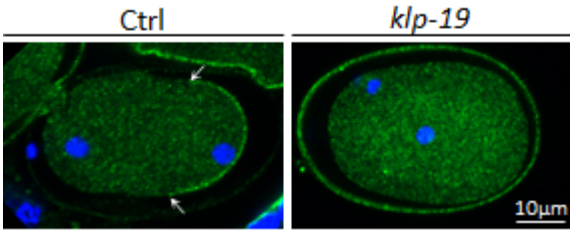

c.

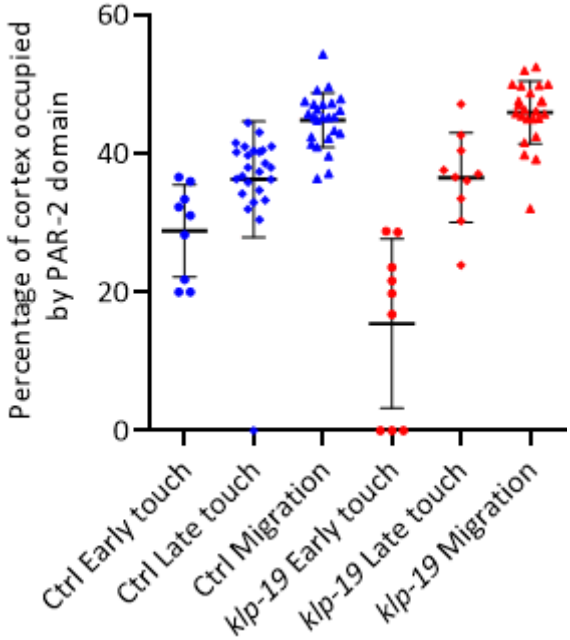

Figure 7.1 **The impact of loss of KLP-19 on PAR-2 cortical recruitment.**

(a) Fixed immunofluorescently stained control embryos, imaged via confocal microscopy (DNA-White, PAR-2-Green), highlighting how the pronucleus was used to divide the stages of early embryos. Broken rectangle in top the row shows the zoom in of the pronucleus of each

embryo in the bottom row. i – Early pronuclear touch: Decondensed DNA, pronucleus perimeter typically <15 µm ii- Late pronuclear touch: Condensed DNA, pronucleus >15 µm, iii- Pronuclear migration: Male and female pronuclei have begun to move towards each other. Note - Figure 7.1.a.i is the same embryo represented in Figure 3.3.a.i-iv. **(b)** Fixed immunofluorescently stained control embryos (DNA-Blue, PAR-2-Green) with and without the knockdown of *klp-19* via RNAi. Note – In the control embryos the PAR-2 domain has established (boundaries marked by white arrows) but not in the *klp-19* RNAi embryo in which the sperm-pronucleus centrosome complex has become distanced far from the cortex at the same stage. Linear adjustment of brightness and contrast used for representation in figure. **(c)** The PAR-2 domain sizes of early control and *klp-19* RNAi embryos as a percentage of the overall embryos perimeter during polarity establishment subdivided into the three stages as shown in (a). Note: the difference between each condition for a given stage were non-significant as determined by the Kruskal-Wallis test. Number of experiments for control: 10. Number of experiments for *klp-19*: 7. Number of control embryos: 59. Number of *klp-19* embryos: 43.

7.2.2 Delayed polarity establishment in klp-19 embryos is most likely due to aberrant centrosome positioning.

We wanted to determine if the polarity establishment defects in *klp-19* depleted embryos are associated with the centrosome positioning defects observed in sections 3.2.2 & 4.2.1. To answer this, we divided the analysis of posterior domain size in *klp-19* KD embryos at early PN touch according to whether the centrosome is normally or abnormally positioned (Figure 7.2).

Interestingly, there was a significant decrease in the average percentage of cortex occupied by PAR-2 between control embryos (28.8%) and embryos with mispositioned centrosomes as a result of *klp-19* KD (10.1%). The percentage of the cortex of occupied by PAR-2 in *klp-19* KD embryos with normal centrosome positioning was not significantly different to that of control embryos.

This result suggests that changes in polarity due to loss of KLP-19 are due to KLP-19's role in the correct positioning of the centrosome in early zygotes.

Figure 7.2

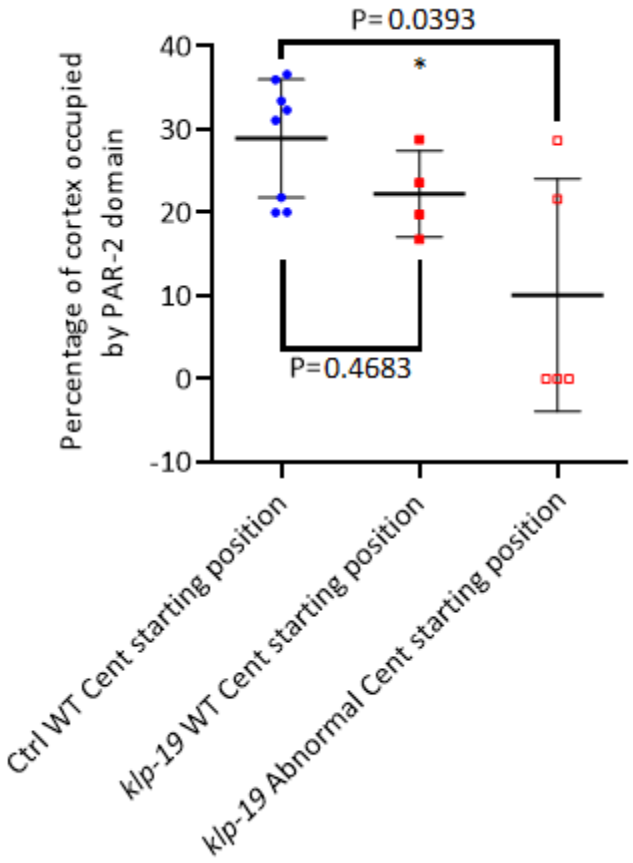

Figure 7.2 **The impact of centrosome positioning upon *klp-19* RNAi on PAR-2 cortical recruitment.**

The same data as Figure 7.1.c early polarity establishment embryos although *klp-19* RNAi embryos have been divided between those with wild-type centrosome positioning at the posterior pole (between the sperm pronucleus and the cortex) and those with aberrant centrosome positions. P values determined using Kruskal-Wallis test of significance. Number of experiments for control: 4. Number of experiments for *klp-19*: 3. Number of control embryos: 8. Number of *klp-19* embryos: 9.

7.2.3 Anterior PARs clear in the absence of cortical flows and posterior PARs.

A consequence of studying KLP-19 depletion was the observation that the centrosome frequently became mispositioned. In these events, we could see that the initially uniform PAR-3 cleared from the cortical region closest to the position of the centrosome, as expected (Goldstein and Hird, 1996; Sadler and Shakes, 2000; Cowan and Hyman, 2004; Bienkowska and Cowan, 2012; McCloskey and Kemphues, 2012; Kimura and Kimura, 2020). In section 1.6, I described the actomyosin and microtubule-dependent pathways that, to date, are the only known routes to break symmetry in the *C. elegans* zygote. If true, one would expect polarisation to fail in the absence of both pathways, resulting in embryos with aPARs uniformly

distributed at the cortex and the absence of cortical pPARs. In section 3.2.2, we showed that 4 out of 11 (36.4%) early pronuclear touch embryos lacked cortical PAR-2 upon *klp-19* depletion, yet still showed a reduction of intensity of cortical PAR-3 local to the centrosomes position (Figure 7.1.b). This occurred in 3 out of 10 (30.0%) embryos in the *nop-1* mutant and increased to 6 out of 11 embryos (54.5%) when *klp-19* was knocked down in the *nop-1* mutant (Section 3.2.2 & Appendix: Table 9.1). Cortical PAR-2 or functional NOP-1 are required to clear aPARs from the posterior cortex via the microtubule and actomyosin dependent pathways, respectively. It was interesting, then, to see that cortical PAR-3 still showed clearance/reduction in intensity local to the centrosome despite the absence of cortical flows or apparent cortical PAR-2 in *nop-1;klp-19* embryos (Section 3.2.2 & Appendix: Table 9.1). This prompted us to further investigate how aPARs are being displaced.

To quantify the coincidence of the centrosome and PAR-3 clearance, we determined the position of the cortex at which the centrosome was closest, and the midpoint of PAR-3 clearance in embryos prior to pronuclear migration (Figure 7.3.a). From this, we developed the graphs of Figure 7.3.c. The X axis represents the position of the cortex closest to the centrosome (closest CTX to cent) as a proportion of the embryo's perimeter. Cortical positions relate to the anterior pole (0) around the cortex clockwise to the posterior (0.5) and back to the anterior (1). The Y axis represents the same for the midpoint of the region of PAR-3 clearance (mid clear PAR-3). In control embryos, we observed that PAR-3 removal is tightly regulated, invariably cleared from the posterior pole by the combined action of flows, MTs and mutual antagonism with the pPARs, hence showing little variability in the Y axis from the posterior pole (Average position (Y-axis): 0.50, Standard deviation: 0.02) in spite of slight variations of the position of the centrosome (Average position (X-axis): 0.49, Standard deviation: 0.06) Note that the gradient of the line of regression is low at 0.15 showing that alteration in the x axis (centrosome position change) results in little alteration in the y axis (position of mid PAR-3 clearance)(Figure 7.3.b.i-iv&c.i). This changed in the *nop-1* mutant in which the centrosome's position became more variable (Average position (X-axis): 0.51, Standard deviation: 0.08). In *nop-1* embryos, the position of the centrosome correlated well with the region of the cortex that became cleared of PAR-3 (Average position (Y-axis): 0.50, Standard deviation: 0.09). Note that the gradient of the line of regression increased to 0.88, showing that change in the x axis (centrosome position) results in a similar change in the y axis (position of mid PAR-3 clearance)(Difference between the slopes was significant – P=0.0362)

(P values indicate the probability that the lines of regression are different (ANCOVA) – $P<0.05$ is significantly different)(Figure 7.3.b.v-viii&c.ii). These results suggest that centrosome positioning can influence the clearance of aPARs, although flows will ensure that PAR-3 clears from the posterior pole in WT embryos.

Figure 7.3

a.

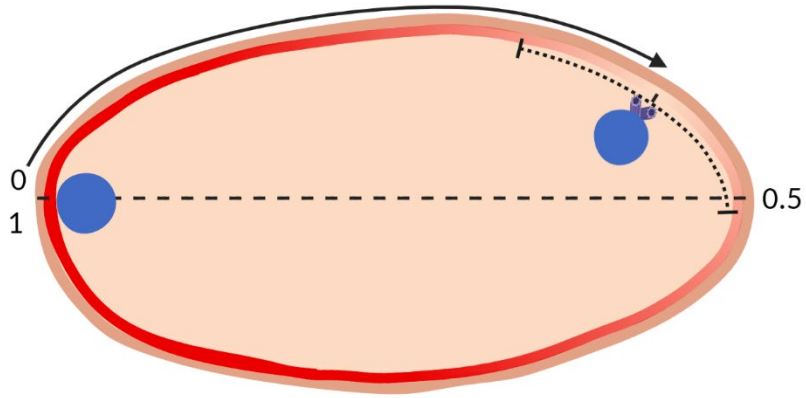

b.

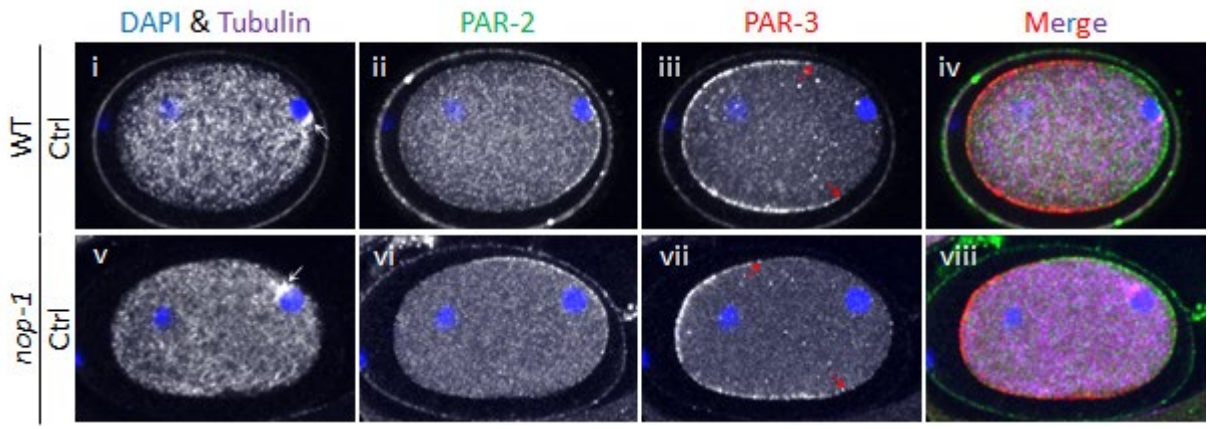

c. i. ii.

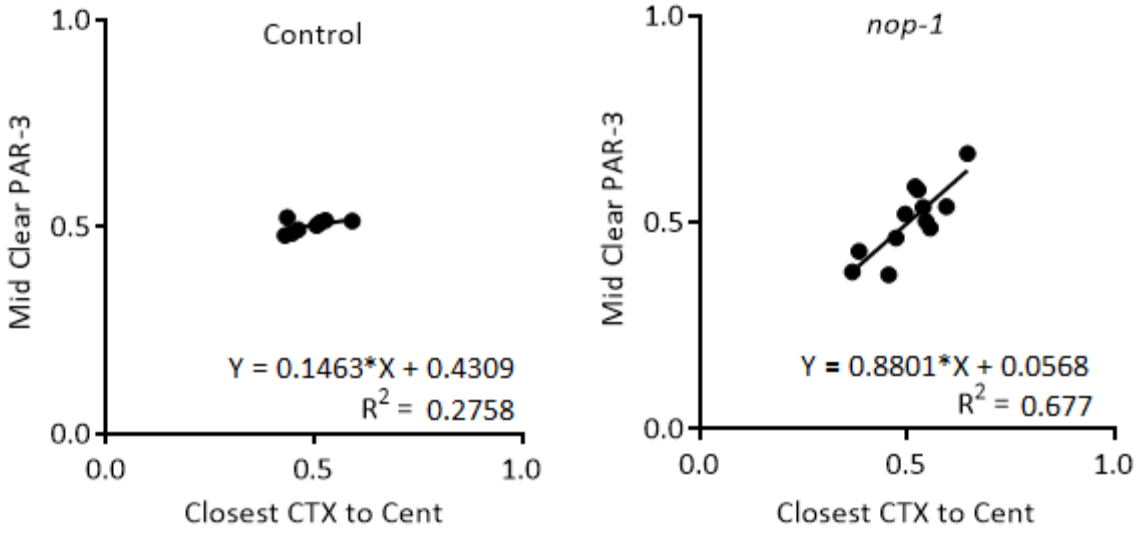

Figure 7.3 **The correlation between the position of the centrosome in the zygote and the clearance of PAR-3 in wlidtype and embryos lacking flows.**

(a) To measure the correlation between the centrosome position and PAR-3 clearance, the cortex length was measured and converted to a proportion. The far anterior was regarded as point 0, following clockwise the posterior was 0.5 and returning to the anterior was 1. The position of the middle of the cortically cleared PAR-3 region was then plotted against the position along the cortex closest to the centrosome. Note: Position of the cortex closest to the centrosome determined using the circle tool in ImageJ, grown out from the centrosome until contacting the cortex. PAR-3 clearance was determined by using the line tool in ImageJ to measure the fluorescent intensity of small sections of PAR-3 around the cortex until the boundaries of a region of intensity less than 1.75x the PAR-3 background cytoplasmic intensity (allowing for standardisation across embryos) was found; the middle of this region was determined as the midpoint of PAR-3 clearance. Figure 7.3.b.i-iv is the same embryo represented in Figure 3.3.a.i-iv. **(b)** Representative midsection images of fixed immunofluorescently stained wild-type & *nop-1* mutant embryos during early pronuclear touch, imaged via confocal microscopy. PAR-3 and PAR-2 stains are markers of the anterior and posterior domains, respectively. In the wild-type embryo, slight offset of the centrosome (white arrow) does not significantly cause the cleared PAR-3 region (red arrows point to PAR-3 boundaries) to shift from the posterior. In the *nop-1* mutant, the cleared region of PAR-3 directly reflects the position of the centrosome and recruited PAR-2. Notes – Linear adjustment of brightness and contrast used for representation in figure. **(c)** Positions of the cortex closest to the centrosome plotted against the position of the midpoint of the PAR-3 cleared region of WT and *nop-1* mutant embryos during pronuclear touch. Lines of regression fitted by GraphPad Prism. Number of experiments for control: 4. Number of experiments for *nop-1*: 2. Number of control embryos: 8. Number of *nop-1* embryos: 12.

As mentioned, the observation that led us to these experiments was that PAR-3 had cleared in *nop-1* mutant embryos in which PAR-2 had not yet localised to the cortex. In theory, these embryos have no cortical flows or pPAR antagonism of aPARs (Section 3.2.2 & Appendix: Table 9.1). As we did not deplete the embryos described in this chapter thus far of PAR-2, it is possible that undetectable cortical PAR-2 is responsible for clearing PAR-3 from the cortex. To be confident that PAR-2 is indeed redundant for PAR-3 clearance in the absence of flows, we performed PAR-2 RNAi knockdown in the *nop-1* mutant and still observed PAR-3 clearance (7 out of 7 embryos that strongly matched the position of the centrosome)(Figure 7.4).

Figure 7.4

a.

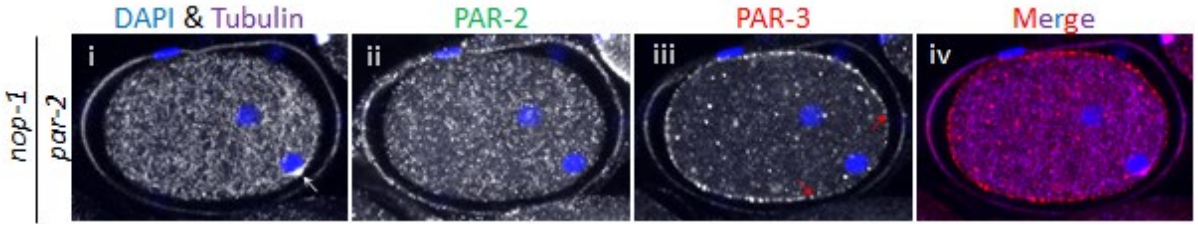

b.

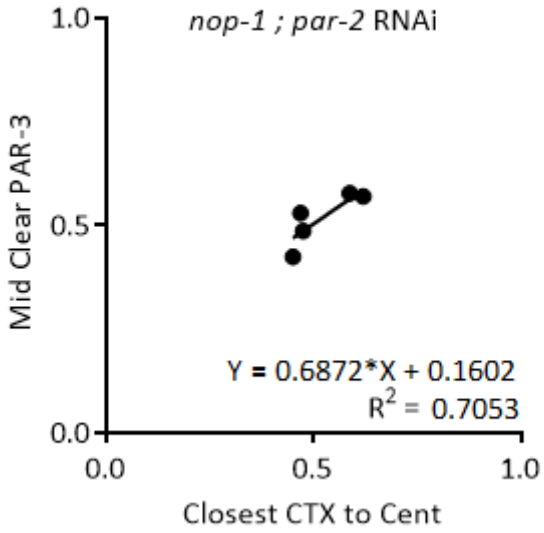

Figure 7.4 **The correlation between the position of the centrosome in the zygote and the clearance of PAR-3 in the *nop-1* mutant depleted of *par-2*.**

(a) Representative midsection images of fixed immunofluorescently stained *nop-1* mutant embryos (early pronuclear touch stage) depleted of *par-2* via RNAi feeding, imaged via confocal microscopy. Note – PAR-2 staining has not been included in the merged colour image. (White arrow points to centrosome, Red arrows point to boundaries of PAR-3 domain) Linear adjustment of brightness and contrast used for representation in figure. **(b)** Positions of the cortex closest to the centrosome plotted against the position of the centre of the PAR-3 cleared region of *nop-1* mutant; *par-2* RNAi embryos during pronuclear touch. Line of

regression fitted by GraphPad Prism. Number of experiments: 1. Number of *nop-1;par-2* embryos: 5.

In WT embryos, cortical PAR-2 acts to recruit the kinase PAR-1 which removes PAR-3 from the cortex via phosphorylation. The posterior LGL-1 also removes aPARs from the cortex through binding to PAR-6 & PKC-3 to mediate their dissociation (Section 1.1.2 & Figure 1.1). We wondered if either could be acting as the active component in clearing PAR-3 from the cortex in the absence of flows. In the *nop-1* mutant we observed that PAR-3 still cleared from the cortex in the absence of PAR-1 or LGL-1 (Figure 7.5.a.v-viii,xvii-xx,b.ii&iv) (Note these knockdowns were performed using RNAi diluted with control RNAi).

Interestingly, the loss of PAR-1 and LGL-1 resulted in a reduction of the correlation between the centrosome's position relative to PAR-3 clearance when compared to the *nop-1* mutant alone, as seen by the more horizontal lines of regression (lower gradient value) in the graphs (Figure 7.4.b, Figure 7.5.b.ii&iv). As such, upon depletion of *par-1* or *lgl-1*, the clearance of PAR-3 appeared to bias from the posterior pole despite changes in the centrosome's position. Note that the differences between the slope of *nop-1* without RNAi KD and the slopes of the partial *par-1* and *lgl-1* knockdowns (ctrl/*par-1* and ctrl/*lgl-1* RNAi) were not significant P=0.1072 & 0.0609, respectively, but may improve with greater numbers (P values indicate the probability that the lines of regression are different (ANCOVA) – $P<0.05$ would be considered significantly different). This suggests that PAR-1 and LGL-1 may be the active components that clear PAR-3 from the cortex local to the centrosome in the absence of cortical flows and that there is likely an additional mechanism to clear PAR-3 preferentially from the presumptive posterior pole in the absence of cortical flows and pPARs. We performed the same analysis in *nop-1* embryos co-depleted of *par-2* with *par-1* and *lgl-1* to assess whether PAR-2 could act to clear PAR-3 in their absence but observed no difference between the double and single knockdowns.

It would be useful to eliminate the function of all three posterior proteins simultaneously to truly confirm that none of PAR-2, PAR-1 or LGL-1 remove PAR-3 in the absence of flows and the other two posterior proteins. PAR-1 relies of PAR-2 to localise to the cortex and act to remove PAR-3 (Cuenca, 2003; Hao, Boyd and Seydoux, 2006; Motegi *et al.*, 2011), and so we assumed that the *nop-1*; *lgl-1*/*par-2* condition should represent the absence of all three posterior proteins. We cannot rule out, however, that cytoplasmic PAR-1 near the centrosome

could contribute to the PAR-3 cortical removal we have measured. Future work would involve crossing the *nop-1* mutant with a temperature sensitive mutant of *par-1* which could then be depleted of *par-2* and *lgl-1* to assess the impact of the loss of function of all posterior proteins, in the absence of flows, on PAR-3 clearance.

Overall, these data indicate that aPARs can be antagonised from localising to the cortex despite compromising both previously known pathways required to achieve symmetry breaking (The actomyosin and MT-dependent pathways). Our data suggests that PAR-1 and LGL-1 are not responsible, in the absence of PAR-2 and actomyosin-driven flows, for the removal of PAR-3 from the cortex near to the centrosome but that, in their absence, PAR-3 will clear preferentially from the posterior cortex. How PAR-3 would clear in the absence of the pPARs and why preferentially from the pole remains unclear.

Figure 7.5

a.

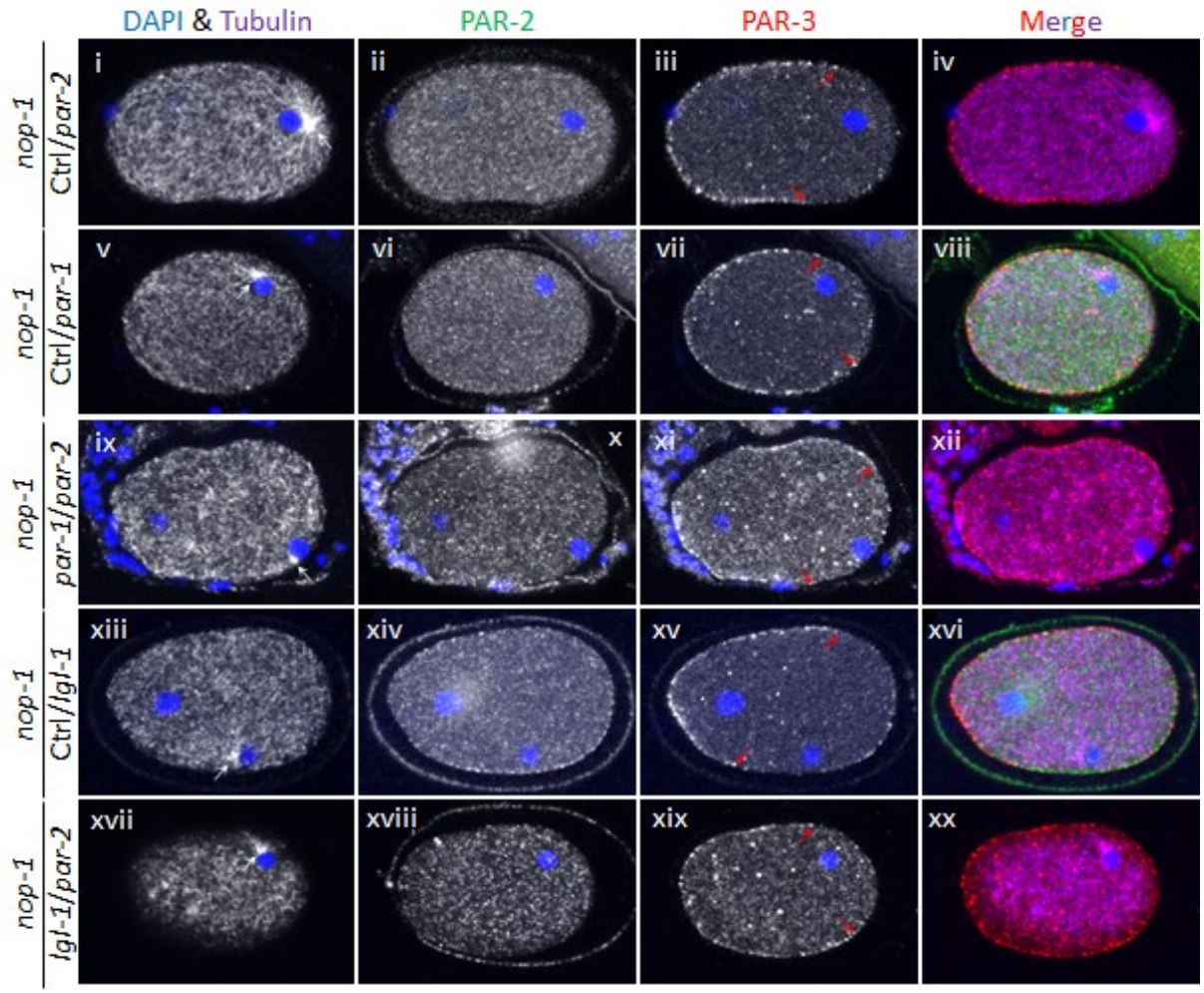

b. i.

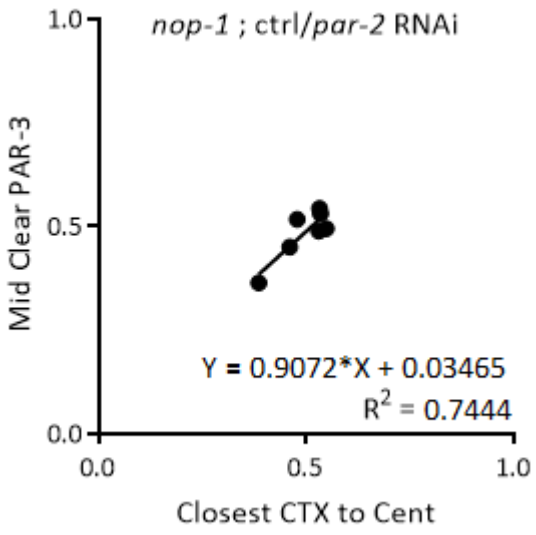

ii.

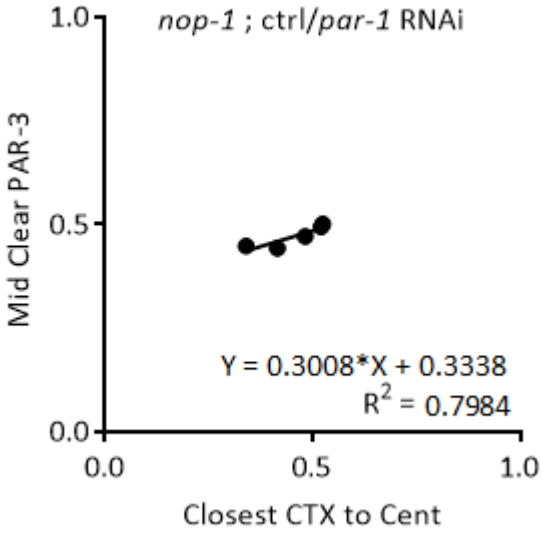

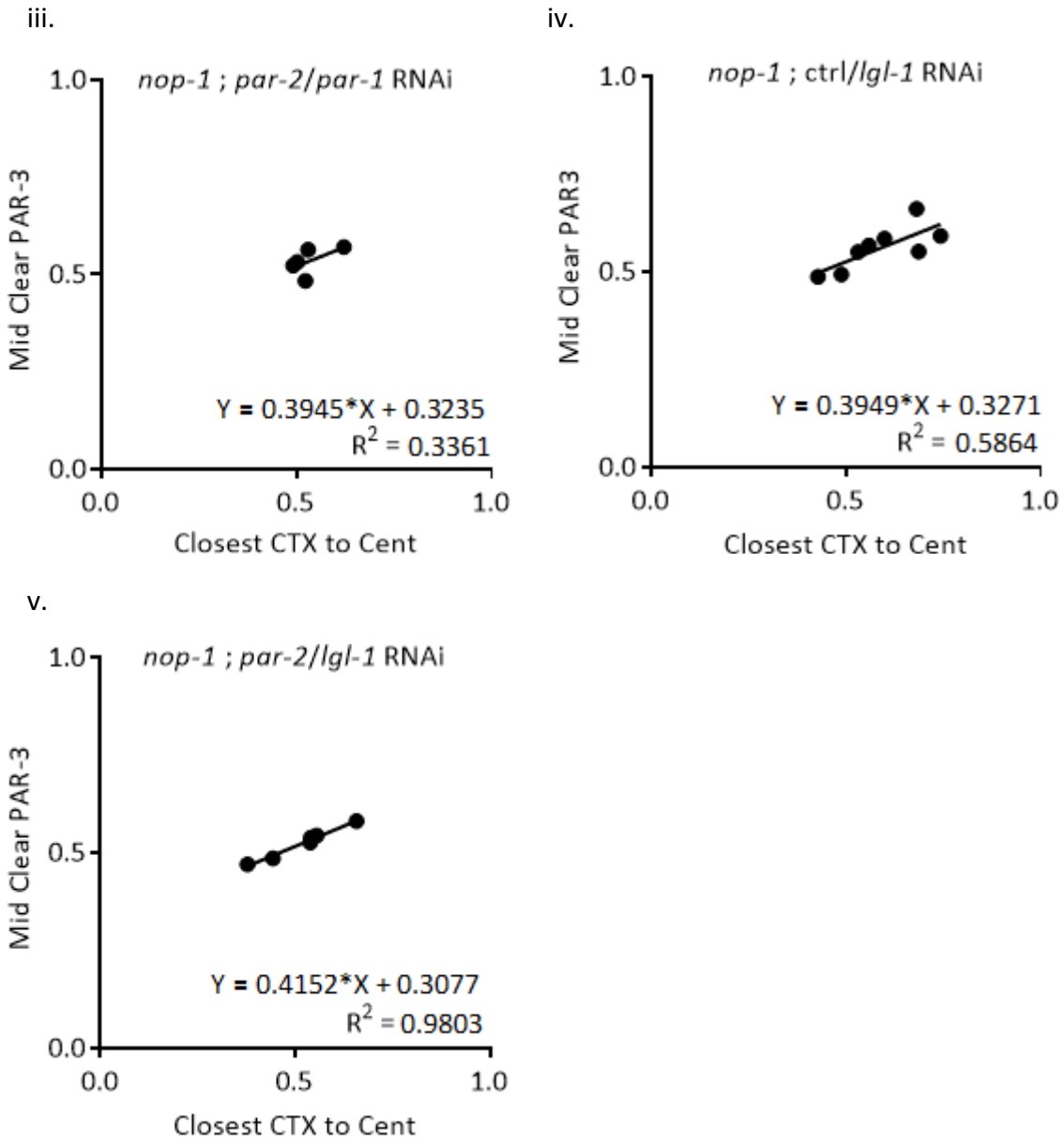

Figure 7.5 **The correlation between the position of the centrosome in the zygote and the clearance of PAR-3 in the *nop-1* mutant under combined depletion of *pPARs*.**

(a) Representative midsection images of fixed immunofluorescently stained *nop-1* mutant early PN touch embryos depleted of the posterior PARs via RNAi feeding, imaged via confocal microscopy. Note – Single knockdowns of *par-2*, *par-1* and *lgl-1* were diluted to 50% with control RNAi vector bacteria to act as real controls for the combined knockdowns. PAR-2 staining has not been included in the merged colour image of embryos with *par-2* RNAi knockdown. (White arrow points to centrosome, Red arrows point to boundaries of PAR-3 domain). Linear adjustment of brightness and contrast used for representation in figure. **(b)** Positions of the cortex closest to the centrosome plotted against the position of the centre of the PAR-3 cleared region of *nop-1* mutant; *pPAR* RNAi combination embryos during pronuclear touch. Lines of regression fitted by GraphPad Prism. Number of experiments: 1. Number of *nop-1;control/par-2* embryos: 7. Number of *nop-1;control/par-1* embryos: 5. Number of *nop-1;par-2/par-1* embryos: 5. Number of *nop-1;control/lgl-1* embryos: 8. Number of *nop-1;par-2/lgl-1* embryos: 5. Note: Double knockdowns through RNAi feeding are less efficient than

single knockdowns as the RNAi of each targeted gene is subsequently halved by mixing the bacteria containing the dsRNA. As such, residual gene expression for both genes may compromise the goal of loss of function. The appropriate controls for each gene were performed by mixing each targeted gene with control RNAi and processed/analysed in the same way as the experimental conditions. Of note, partial depletion of *par-2* (Figure 7.5.b.i) produced a graph of centrosome position vs PAR-3 clearance more closely matching the *nop-1* mutant without knockdown (Figure 7.3.c.ii) compared to sole *par-2* RNAi (Figure 7.4.b).

7.3 Discussion.

7.3.1 Delayed pPAR clearance in the absence of KLP-19.

In this chapter, we have confirmed that KLP-19 is required to ensure efficient and timely polarity establishment in *C. elegans* zygotes. KLP-19 most likely does this through its novel role in ensuring the centrosome is positioned correctly at the posterior cortex prior to symmetry breaking. *klp-19* KD embryos with aberrant centrosome position presented with delayed posterior PAR cortical recruitment compared to the control. Indeed, *klp-19* RNAi embryos with normal centrosome positioning presented PAR-2 domain size similar to control embryos, albeit slightly smaller but non-significant. It would be nice to increase the numbers from this experiment to confirm or rule out any real differences between pPAR domain sizes with and without aberrant SPCC positioning. It's possible that KLP-19 could act to directly transport PAR-2 to the cortex through its role as a plus end-directed microtubule motor protein. Indeed Motegi et al. (2011) presented evidence that PAR-2 appears to colocalise with microtubules/the centrosome in GFP::PAR-2-tagged and immunostained *C. elegans* zygotes (Motegi *et al.*, 2011). Chen et al. (2016) also demonstrated that KLP-19 and PAR-2 interact via co-immunoprecipitation (Chen *et al.*, 2016). KLP-19 transport of PAR-2 to the membrane along MTs would explain why PAR-2 is detected local to the position of the MT-rich centrosome and to the meiotic spindle of AIR-1 depleted embryos (Klinkert *et al.*, 2019; Reich *et al.*, 2019). Although this mechanism could be true, it cannot be the only way PAR-2 is recruited to the cortex as PAR-2 still loads to the cortex in *klp-19* RNAi embryos.

Saturno et al. (2017) studied the impact of centrosome-cortex distance on polarity establishment and demonstrated that 96.9% of WT *C. elegans* zygotes undergo normal symmetry breaking (Defined by cortical smoothening) in live analysis. This percentage drops to 83% in a mutant strain of the puromycin-sensitive aminopeptidase, *pam-1*, which is required to prevent aberrant early centrosome movement away from the posterior cortex (Lyczak *et al.*, 2006; Fortin *et al.*, 2010; Saturno *et al.*, 2017). Like *klp-19* RNAi embryos, *pam-*

1 mutant embryos show diminished pPAR localisation at the cortex. As discussed previously (Section 1.7.2), PAM-1 has been suggested to prime proteins for ubiquitin-dependent degradation through N-terminal peptide removal (Lyczak *et al.*, 2006). It is possible that KLP-19 and PAM-1 act in a common pathway in which an intermediate regulator of KLP-19 activity could be a target of PAM-1 induced degradation. Interestingly, however, the pPAR defects observed in *pam-1* mutants, visualising PAR-1::GFP, are worse than in our KLP-19 KD embryos analysing endogenous PAR-2 staining. In many *pam-1* embryos there is complete lack of PAR-1 recruitment beyond the early single-cell zygote stages and present with a smaller PAR-1 domain at nuclear envelope breakdown prior to metaphase (31% cortex occupied compared to the control (42%)) (Saturno *et al.*, 2017). PAR-2 defects in *klp-19* RNAi embryos resolve much sooner. The difference in phenotype severity could be due to higher penetrance of the mutant *pam-1* compared to *klp-19* RNAi or a consequence of the different strains used in our studies as the GFP tag used by Saturno et al. (2017) may hinder PAR-1 localisation. It is also possible that PAR-1 cortical localisation is more sensitive to perturbations in centrosome positioning-dependent symmetry breaking than PAR-2. Thus, Saturno et al. (2017) observe PAR-1 missing at the cortex of more embryos than we do of PAR-2. Alternatively, stronger pPAR loading defects in *pam-1* LoF embryos compared to *klp-19* LoF embryos could suggest PAM-1 has multiple targets that are required for centrosome positioning, thus making PAM-1 more essential for posterior polarity than KLP-19.

7.3.2 aPARs cortical clearance in the absence of cytoplasmic flows and PAR-2

The variable centrosome position in *nop-1* mutant embryos, or *nop-1*;*klp-19* double LoF, led to the interesting observation that ectopic PAR-3 clearance occurs at the cortex closest to the aberrant localisation of centrosome/MTs. In control embryos, the position of the centrosome is relatively stable at the posterior pole, with slight variation between embryos. The position of the clearance of PAR-3, however, remains unchanged and is centred at the posterior pole (Figure 7.3.c & Figure 7.6.i&ii). This is likely due to actomyosin generated cortical flows and the shape of the embryo. As cortical flows move outwards from the centrosome, they will converge at the far anterior and generate a posterior internal cytoplasmic flow. Once the flow reaches the posterior pole, it will diverge to become anterior directed cortical flows again (Figure 7.6.ii). Thus, PAR-3 clearance is corrected to clear from the posterior pole as we have observed (Figure 7.3.c.i). An example of this process in action can be seen in the recent

publication of Kapoor and Kotak (2019). In video 37 from their article (Appendix: Figure 9.1), the sperm pronucleus can be seen contacting the lateral posterior cortex where PAR-2 initially loads. Within approximately 40 seconds the positions of the pronucleus and the PAR-2 domain are corrected to the posterior pole (Kapoor and Kotak, 2019).

In the *nop-1* mutant, which lacks flows, PAR-3 clearance is more dependent on the position of the centrosomes. In this scenario, posterior PARs, recruited to the cortex in a microtubule dependent manner, could be responsible for clearing the aPARs local to the centrosome. In this project, however, we observed a small number of early zygotes in which PAR-2 had not yet localised to the cortex but still presented with a cortical clearance of aPAR near the centrosome.

Figure 7.6

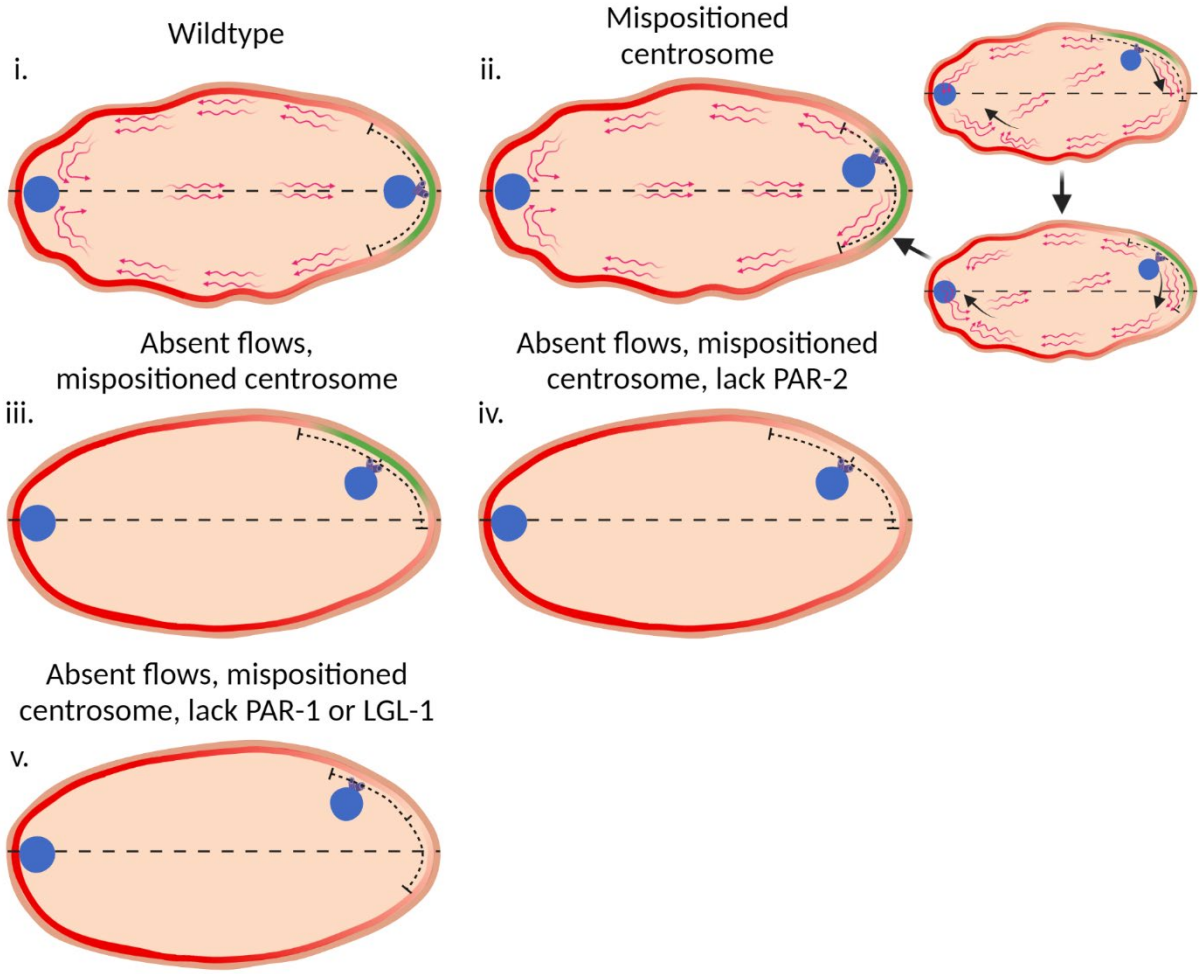

Figure 7.6 **PAR-3 clearance from the cortex in the absence of flows and posterior PARs.**

i: In the wild-type embryo, the centrosome is positioned between the pronucleus and the cortex at the posterior pole. Both flow dependent and pPAR dependent removal of PAR-3 clear PAR-3 from the posterior pole. **ii:** If the SPCC position is not at the posterior pole at the onset of symmetry breaking. The cortical flows, that move outwards from the centrosome,

initially result in clearance of aPARs (and subsequent pPAR recruitment) to the cortical site near the centrosome. Due to the embryos ovoid shape, it is likely that the flows converge at the anterior pole resulting in the gradual shift of the centrosome and pPARs to the posterior pole and corrects the aPAR/pPAR boundaries along the anterior-posterior axis. **iii:** In the absence of flows, MT-dependent removal of PAR-3 takes over. As pPARs are recruited to the cortex local to the centrosome, the polarity axis shift dependent on the centrosome's position and PAR-3 is cleared from the cortex wherever the centrosome is. **iv:** In the absence of flows and PAR-2, the cleared region of PAR-3 still follows the centrosome's position around the cortex. **v:** In the absence of flows and PAR-1 or LGL-1, the cleared region of PAR-3 still somewhat follows the centrosome's position around the cortex but centres more towards the posterior pole.

One could argue that undetectable PAR-2 or residual flows are responsible for the decrease in PAR-3 near the centrosome of *nop-1* embryos. To eliminate these possibilities, we performed PAR-2 RNAi in the *nop-1* mutant and saw that PAR-3 was still cleared from the cortex, local to the centrosome's position (Figure 7.4 & Figure 7.6.iv). PAR-2's role in polarity establishment is not typically described as an active component in the antagonism of the aPARs, but as a platform for the kinase PAR-1 which works alongside LGL-1 to remove PAR-3 and PAR-6/PKC-3 from the cortex, respectively (Beatty, Morton and Kemphues, 2010, 2013; Hoege *et al.*, 2010; Motegi *et al.*, 2011). The depletion of PAR-1 or LGL-1 in combination with PAR-2 still saw the clearance of PAR-3 from the cortex. Interestingly, however, the clearance of PAR-3 in the absence of PAR-1 or LGL-1 was skewed to come from the posterior pole despite the variations from the centrosome's position. This suggests that an additional pathway that preferentially clears PAR-3 from the pole becomes dominant in the absence of PAR-1/LGL-1. The correlation between centrosome and PAR-3 clearance had not been completely separated, however, as the PAR-3 clearance was still shifted towards the centrosome's position, possibly a result of residual PAR-1 or LGL-1 due to partial knockdowns (Figure 7.5 & Figure 7.6.v). It would be interesting to co-deplete PAR-1 and LGL-1 to assess whether the position of PAR-3 clearance becomes more decoupled from the centrosome's position. Both PAR-1 and LGL-1 have been shown to depend on PAR-2 to localise to the cortex (Boyd *et al.*, 1996; Hoege *et al.*, 2010; Motegi *et al.*, 2011) suggesting that cytoplasmic PAR-1/LGL-1 may be recruited/activated near to the centrosome and capable of removing aPARs in the absence of flows and PAR-2. Thus, PAR-3 clearance correlates highly with the centrosome's position in the absence of flows.

An alternative hypothesis to decoupling centrosome position and PAR-3 clearance is that the knockdown of PAR-1 and LGL-1 partially rescues cytoplasmic flows in the *nop-1* mutant, thus

favouring posterior pole removal more like WT embryos. Previous studies have shown that the knockdown of *par-2*, of the pPARs, in the *nop-1* mutant abrogates residual cortical flows rather than rescuing flows, so it is unlikely that PAR-1 or LGL-1 KD would rescue flows (Tse *et al.*, 2012; Gross *et al.*, 2019).

Together, these data suggest that aPARs can be cleared in the absence of actomyosin-dependent flows and PAR-2, likely through centrosomal recruitment/activation of PAR-1 and LGL-1. In addition, our results have revealed a steady state, whereby the aPAR tend to clear from the posterior pole in absence of flows, MTs or pPARs. One possibility is that aPAR are de-stabilised from membranes with high curvature. As previously discussed (Section 1.6.4), recent work has shown that the shape of the embryo can contribute to the clearance of aPARs. Klinkert et al. (2019) showed that pPAR domains form at the regions of highest membrane curvature when embryos are deformed and AIR-1 is depleted (Klinkert *et al.*, 2019). It is possible that an additional aPAR antagonistic factor is recruited to the curved membrane and acts with the centrosome to clear aPARs from the posterior pole, or that membrane curvature is unfavourable for aPAR membrane stability. Indeed, a common phenotype in the absence of KLP-19 was the disappearance of PAR-3 at the anterior pole without PAR-2 loading, indicating pPAR independent removal of aPARs.

As MTs grow extensively from the centrosome, and have previously been described to trigger polarity establishment (Motegi *et al.*, 2011), we wondered whether MTs could be directly involved in the removal of aPARs from the cortex. One MT-dependent possibility could be through the recycling endosome pathway. Nakayama et al. (2009) demonstrated that endocytosis is enriched in the anterior during polarity maintenance and pulls PAR-6 from the cortex in a dynamin dependent manner (Andrews and Ahringer, 2007; Nakayama *et al.*, 2009). They proposed that the removal of aPARs at the cortex may help to maintain polarity, but, as the PAR-3 clearance situates near the centrosome in our embryos, it is possible that endocytosis in the posterior may contribute to polarity establishment by removing the aPARs from the cortex. In support of this, Zhang, Squirell and White (2008) showed that depletion of the endosome enriched GTPase RAB-11 resulted in an extended aPAR domain, shrunken pPAR domain and localisation of PAR-3 within the posterior domain (i.e. colocalization of aPARs & pPARs) suggesting that endosomes may indeed be involved in removing aPARs from the cortex as a means to regulate polarity in the *C. elegans* zygote (Zhang, Squirrell and White, 2008). In

section 3.3 I discussed the presence of thick MT bundles concurrent with the absence of PAR-3 at the cortex of *let-754* embryos (Figure 3.7.a.v&vii). This would support a model in which MTs somehow act to remove aPARs from the cortex.

Overall, this chapter has demonstrated that KLP-19 is indeed involved in polarity establishment as loss of this kinesin results in a portion of embryos with compromised posterior domain formation. KLP-19 most likely does this through its ability to restrict the centrosome to the posterior cortex, but we cannot rule out a more direct mechanism (e.g., delivering PAR-2 to the cortex). As an interesting by-product of KLP-19 polarity characterisation, we observed that PAR-3 clears during polarity establishment even in embryos compromised in the actomyosin and microtubule-dependent pathways in response to the position of the centrosome and the microtubules it nucleates. This implies a third mechanism by which anterior PARs are cleared from the cortex in a centrosome/MT-dependent manner, possibly via the delivery of aPAR antagonists, LGL-1/PAR-1, or endocytosis of the aPARs. Destabilisation of aPAR localisation at high curvature membrane may then contribute to aPAR removal as the depletion of PAR-1 or LGL-1 appears to bias aPAR clearance back to the posterior pole in the absence of flows.

Chapter 8 Discussion

The role of microtubules in the establishment of polarity in *C. elegans* zygotes is a controversial topic. To date, two pathways that generate an anterior-posterior axis of asymmetry have been described in the worm. 1) A widely accepted actomyosin-dependent mechanism, reliant on a signal that diffuses from the centrosomes and induces actomyosin-dependent cytoplasmic flows and 2) A microtubule-dependent pathway whereby MTs grown from the centrosome act to promote membrane localisation of the posterior PAR proteins through protection against antagonism of the anterior PARs. This project focused on the study of the lesser understood MT-dependent pathway.

Wallenfang & Seydoux (2000) presented evidence of MT-dependent symmetry breaking as embryos under meiotic arrest, in which the sperm centrosome asters fail to form, undergo polarisation governed by the meiotic spindle. The result is reversed polarity as the typically posterior PAR-2 domain then establishes in the typical anterior (Wallenfang and Seydoux, 2000). Tsai & Ahringer (2007) and Motegi et al. (2011) later showed that MT depletion/ inability to interact with PAR-2 resulted in the delayed onset of symmetry breaking (i.e., pPARs took longer to localise to the cortex). Polarity establishment then failed when MT absence was combined with the loss of actomyosin flows (Tsai and Ahringer, 2007; Motegi *et al.*, 2011). Bienkowska and Cowan (2012), however, argued that microtubules are merely required to maintain close proximity of the SPCC (Sperm pronucleus-centrosome complex) to the cortex which ensures the actomyosin pathway is robust (Bienkowska and Cowan, 2012). Recent work further complicates the issue as elimination of the likely centrosome signal, AIR-1 (Aurora kinase A), abrogates actomyosin flows yet still establishes PAR-2 cortical domains upon depolymerisation of microtubules (Klinkert *et al.*, 2019), indicative of additional pathways to break symmetry in the zygote.

We find that the answer to the conundrum above likely lies somewhere in the middle. In this project we have expanded on previous efforts to understand the importance of SPCC positioning in the embryo and how its localisation is regulated. Studies have demonstrated that multiple forces act upon the centrosome to position the SPCC, including those by motor proteins and bulk cytoplasmic flows. Similarly, microtubule associated proteins have been described to act as linkers of the centrosome to other cell components such as the actomyosin

cortex (Gönczy *et al.*, 1999; Grill *et al.*, 2001; Nguyen-Ngoc, Afshar and Gönczy, 2007; Fortin *et al.*, 2010; Galli *et al.*, 2011; McCloskey and Kemphues, 2012; Portegijs *et al.*, 2016; Saturno *et al.*, 2017; Schmidt *et al.*, 2017; Kimura *et al.*, 2017; Panzica *et al.*, 2017; Kimura and Kimura, 2020). The full catalogue of proteins involved in SPCC positioning, however, have not been identified and we are still far from understanding how the processes involved are coordinated to finely tune SPCC positioning.

Here, we identified and discussed how the *C. elegans* chromokinesin KLP-19 (Human – Kif4a) contributes to the regulation of the SPCC's position in the early zygote. We believe that KLP-19 acts to ensure that the SPCC is maintained at the posterior cortex by stabilising/fixing centrosomal MTs and counteracting MT pulling forces mediated by the cortical motor dynein and its adaptors - LIN-5 (NuMA), GPR-1/2 (LGN) and Gα.

In this project we investigated the following questions:

- Could we identify novel regulators of polarity, particularly microtubule-dependent polarisation, in the absence of actomyosin induced cytoplasmic flows?
- How could the identified chromokinesin KLP-19 be required for efficient zygote polarity establishment?
- How does KLP-19 act to regulate SPCC positioning?

I will discuss all chapters of my work to give an overview of our findings, their interpretation into our model and significance. However, more specific, and detailed discussion can be found at the end of each results chapter.

8.1 Screening for regulators of microtubule-dependent polarity establishment.

The initial goal of this project was to identify candidate genes that regulate the microtubule-dependent polarity establishment pathway whereby microtubules inhibit PKC-3 phosphorylation of posterior PARs, which would otherwise inhibit pPAR recruitment to the cortex (Section 1.6.4)(Motegi *et al.*, 2011). Theoretically, in a *nop-1* mutant strain of *C. elegans* that lacks actomyosin-dependent polarity establishment (Fievet *et al.*, 2012; Tse *et al.*, 2012), the MT-dependent pathway would become the sole mechanism whereby zygotes can polarise. Thus, genes required for the MT-dependent pathway of polarisation become essential for embryonic survival in the *nop-1* mutant compared to wild-type embryos.

Of 15 genes screened, we identified 7 that enhanced lethality in the *nop-1* mutant upon RNAi depletion (*rack-1, cnt-2, let-754, gpb-1, klp-19, arf-1.2, plk-1*), all of which produced polarity defects and 4 of which are known to regulate microtubule dynamics and organisation (*rack-1, gpb-1, klp-19, plk-1*).

This screen proved that the *nop-1* mutant can be used as a tool to identify regulators of actomyosin-independent polarity establishment. In particular, the screen can capture microtubule regulators that have otherwise gone undetected in the wild-type strain. This opens the door to better understanding the poorly understood contributions of microtubules to polarity establishment. In future, it would be interesting to screen more genes for polarity regulators and further investigate their roles to elaborate how microtubules regulate asymmetry.

8.2 The chromokinesin, KLP-19, ensures robust symmetry breaking in the early zygote through regulation of the SPCC's position and an additional microtubule-dependent mechanism.

Of the genes that scored as enhancers of lethality in the *nop-1* mutant, we decided to follow up on the chromokinesin, KLP-19, previously known to mediate chromosomal alignment and segregation in metaphase and anaphase, respectively (Powers *et al.*, 2004; Wignall and Villeneuve, 2009; Pelisch *et al.*, 2017). Initial phenotypic characterisation via KLP-19 LoF presented no signs to suggest that actomyosin dynamics had been perturbed (e.g., loss of cortical ruffling or pseudocleavage) in immunofluorescently labelled embryos. We did, however, observe a portion of embryos in which the SPCC became aberrantly positioned, and PAR-2 had not localised to the cortex during early polarity establishment as would be expected if MTs could not efficiently protect PAR-2 from PKC-3 phosphorylation. Thus, we suspected that KLP-19 regulates polarisation via the MT-dependent pathway.

As some *klp-19* RNAi embryos had wild-type positioned SPCCs and PAR-2 recruitment, as would be expected in control embryos, we divided the measurements of PAR-2 cortical domain sizes between embryos with WT vs aberrant SPCC positioning. We found that all embryos that lacked PAR-2 also had aberrantly positioned SPCCs, indicating that KLP-19 predominantly regulates polarity establishment via its role in SPCC positioning. This was in agreement with previous studies in which other SPCC position regulators also compromised

polarity establishment such as the aminopeptidase, PAM-1, and the deubiquitylating enzymes, MATH-33, USP-46 & USP-47 (Fortin *et al.*, 2010; McCloskey and Kemphues, 2012; Saturno *et al.*, 2017).

Loss of PAM-1 has been shown to enhance centrosome positioning defects that arise in MATH-33 LoF embryos, suggesting multiple mechanisms working in parallel to ensure that the SPCC becomes, and remains, positioned at the posterior cortex during symmetry breaking. Embryos depleted of either MATH-33 or KLP-19 appear to have comparable centrosome position phenotypes to each other, i.e. increased initial centrosome distance to the cortex, unlike PAM-1 depleted embryos which initially see the centrosome targeted to the cortex but dissociate prematurely (Lyczak *et al.*, 2006; Fortin *et al.*, 2010; McCloskey and Kemphues, 2012; Saturno *et al.*, 2017). The similar SPCC positioning defects observed upon *klp-19* and *math-33* LoF suggests that KLP-19, or a KLP-19 positive regulator (enhancer of its function), could be targeted for degradation by ubiquitination and rescued from this fate via MATH-33. *pam-1* and *math-33* embryos show more severe polarity defects as the pPAR domain remains smaller in size than WT embryos for longer when compared to *klp-19* RNAi embryos which gain a WT proportion of the cortex occupied by PAR-2 prior to pronuclear migration (McCloskey and Kemphues, 2012; Saturno *et al.*, 2017).

Depletion of either MATH-33 or PAM-1 results in reduced duration of close centrosome-cortex proximity which correlates highly with compromised polarity establishment. We did not measure the time it takes for the centrosome to move away from the cortex in *klp-19* RNAi embryos which could account for the difference polarity phenotypes between *klp-19* and *math-33* embryos, despite similar initial centrosome position defects. It would be interesting, in the future, to confirm any impact of ubiquitylation on KLP-19's role in centrosome positioning. Pelisch et al. (2017) identified that KLP-19 is SUMOylated (**S**mall **U**biquitin-like **Mo**difier) (Protein sequence position - Lysine 873) to regulate its recruitment to a multi-protein ring complex between the chromosomes during meiosis (Pelisch *et al.*, 2017). Evidence from the past decade has shown that many SUMO sites can also be conjugated with ubiquitin (Liebelt and Vertegaal, 2016), leaving open the possibility that ubiquitylation could regulate KLP-19's activity.

The position of the SPCC cannot be the only factor that regulates recruitment of posterior PARs to the cortex, however, as we still saw a reduction in pPAR domain size in *klp-19* RNAi

embryos with WT positioned SPCCs compared to control embryos, albeit to a lesser extent than the effect that aberrant SPCC positioning had. This suggested that, although the position of the centrosome plays a large role in polarity establishment, there are additional mechanisms to promote posterior PAR cortical localisation in a KLP-19 dependent manner. A possibility is that KLP-19, as a plus-ended MT motor protein, acts to directly carry PAR-2 to the cortex, similarly to the transport of the HIV-1 Gag protein to the plasma membrane of COS-1 cells by the human KLP-19 homologue Kif4A (Tang *et al.*, 1999; Martinez *et al.*, 2008). In support of this theory, a previous *in vivo* proteomic screen found that KLP-19 interacted with PAR-2 via co-affinity purification (Chen *et al.*, 2016).

From our work with KLP-19, we made an interesting observation, with regards to zygote polarisation, in a number of early embryos that lacked cortical pPARs, actomyosin flows (*nop-1*), and had mispositioned SPCCs. Despite delayed pPAR cortical localisation, we saw that PAR-3, of the aPARs, still became cleared from the cortex relative to the centrosome's position. Without flows or cortical pPARs, neither of the previously described polarity pathways could be at work to displace PAR-3, thus how PAR-3 would be removed from the cortex is unclear. We observed that the correlation of PAR-3's clearance with the position of the centrosome somewhat depends on PAR-1 and LGL-1. The knockdown of PAR-1/LGL-1 shifts the clearance of PAR-3 to originate from the posterior pole as in WT, despite changes in the centrosome's position. This suggests that a population of PAR-1/LGL-1, derived from the centrosome, is delivered to the cortex by diffusion in the cytoplasm or via centrosomal MTs and removes PAR-3 from the cortex local to the centrosome. Interestingly, depletion of another MT regulator identified in our screen may provide further insights as we saw that PAR-3 was similarly cleared in PAR-2-free regions in LET-754 depleted embryos. Interestingly, microtubules appeared to form thick bundles in these regions (Figure 3.7.v-viii) indicating that microtubules may have a more direct role in the removal of cortical PAR-3 than previously thought.

Together, our observations demonstrate that it is likely naïve to think that there are only two pathways involved in polarity establishment and that we have found a novel one, whereby MTs, or another signal, emanating from centrosomes promote aPAR clearance in absence of flows or posterior PARs.

8.3 KLP-19 localises to the cortex of embryos where it limits microtubule dynamics.

As our results indicate that KLP-19's role in polarity establishment is predominantly through the positioning of the SPCC and emanating MTs, we have tried to characterise how KLP-19 could be mediating SPCC positioning.

We sought to determine where KLP-19 localises in the early zygote using a GFP tagged reporter strain. Interestingly, we saw KLP-19 in punctate patterns typically at the cortex of early zygotes undergoing polarity establishment, and punctate and thread-like patterns in late zygotes post-anaphase onset. Previously, KLP-19 had been observed localised to chromosomes, the spindle midzone, the nucleoplasm and in "linear elements" at the cortex of embryos during meiosis I (Monen *et al.*, 2005; Pelisch *et al.*, 2017). These linear elements, however, did not resemble the MT-like patterns of localisation we saw post-meiosis.

Seeing that KLP-19 localises to the cortex of zygotes, we wondered how KLP-19 is acting to limit the position of the SPCC to the posterior membrane. In Section 4.3.1 we postulated three different mechanisms. 1) KLP-19 could localise to the cortex and compete with the cortical dynein complex to interact with centrosomal MTs. Through this KLP-19 would reduce the availability of MT tips that are exposed to dynein-dependent cortical forces. If this was the case, however, we would expect the loss of KLP-19 to result in enhanced dynein facilitated pulling on the centrosomes and faster centrosome separation, the opposite of what we observed. As such, we discounted this hypothesis to investigate further. 2) KLP-19 homologues have been shown to stabilise MTs to prevent polymerisation and depolymerisation, dependent on substrate availability. This typically results in the reduction of MT growth *in vivo* (Bringmann *et al.*, 2004; Castoldi and Vernos, 2006; Bieling, Telley and Surrey, 2010; Hu *et al.*, 2011; Stumpff *et al.*, 2012; Wandke *et al.*, 2012). The absence of KLP-19 would lead to excessive growth of MTs which would then force the SPCC away from the membrane. 3) KLP-19 at the cortex could bind to single centrosomal MTs or bundle and cross-link antiparallel centrosomal-cortical MTs to confer resistance to pulling forces (Bieling, Telley and Surrey, 2010; Gaska *et al.*, 2020; Alfieri, Gaska and Forth, 2021). This mechanism could act as a way to fix the SPCC to the posterior membrane. Here I will discuss why we favour a model in which KLP-19 acts to tether the SPCC to the cortex rather than acting to regulate cortical MT dynamics prior to centrosome separation.

We investigated how KLP-19 localises to the cortex during polarity establishment and found that it relies on SPD-1, the homologues of which (e.g. PRC1) recruit KLP-19 homologues (e.g. Kif4A) to antiparallel MTs in the spindle midzone (Kurasawa *et al.*, 2004; Zhu and Jiang, 2005; Bieling, Telley and Surrey, 2010; Kuan and Betterton, 2016; Nguyen, Field and Mitchison, 2018; Hannabuss *et al.*, 2019). Interestingly, studies in fission yeast have demonstrated that the SPD-1 homologue, ASE1, is required for correct positioning of the nucleus in the centre of the cell, similar to KLP-19's requirement for proper positioning of the SPCC in the *C. elegans* zygote. During interphase in yeast, the minus ends of microtubules, that grow from MTOCs anchored to the nuclear membrane, overlap with cytoplasmic microtubules, and are bundled and stabilised by ASE1. Wild-type cells exhibit an oscillatory nuclear movement followed by positioning of the nucleus to the middle of the cell as MTs reach the membrane and generate pushing force to centre the nucleus. In the absence of functional ASE1, these oscillations were lost, and the nucleus was often mispositioned away from the cell centre. These studies suggested a role for ASE1 in positioning the nucleus via crosslinking nuclear tethered MTs with cytoplasmic MTs, thus facilitating the transfer of force from the membrane to the nucleus and holding it in place (Tran *et al.*, 2001; Loïodice *et al.*, 2005; Piel and Tran, 2009). As the SPCC is initially at the cortex of *C. elegans* zygotes rather than the centre, it is unlikely that centrosomal MTs are acting to push away from the membrane during polarity establishment. Instead, we propose that the *C. elegans* zygote utilises centrosome-cortical antiparallel MTs to tether the SPCC to the cortex, similar to how the nucleus is held in place at the yeast cell centre. This model supports our theory that KLP-19 (and SPD-1) may act to fix centrosomal microtubules, attached to the sperm pronucleus, to cortical cytoplasmic microtubules, thus restricting the SPCC's position in the *C. elegans* zygote.

Alternatively, it is possible that single microtubules reach the cortex where their plus ends are stabilised/fixed without the need for, or in addition to, antiparallel MT cross-linkage. We found that the ankyrin domain containing VAB-19 (KANK1), shown to recruit another KIF4 family member (KIF21A) to the cortex of neurons (Kakinuma and Kiyama, 2009; van der Vaart *et al.*, 2013; Weng *et al.*, 2018), is also required for cortical localisation of KLP-19 and generates embryos with aberrant SPCC positioning upon depletion. It is possible that KLP-19 both docks to single microtubules and mediates direct contact with other components of the cortex, and acts to bundle antiparallel centrosomal-cortical microtubules as in the anaphase central spindle to position the SPCC.

Preliminary observations of GFP::SPD-1 dynamics revealed that threads of SPD-1 at the cortex appear to shrink to a central point rather than being carried to one end of the threads. This is indicative of SPD-1 on antiparallel microtubules being slid apart; thus, the MT overlap that SPD-1 is recruited to shrinks, similar to what happens in the spindle midzone during anaphase (Bieling, Telley and Surrey, 2010; Wijeratne and Subramanian, 2018; Hannabuss *et al.*, 2019; Vukušić *et al.*, 2021). On single microtubules we would expect to see SPD-1 transported to the MT plus end (Hu *et al.*, 2011; Subramanian *et al.*, 2013; Nguyen, Field and Mitchison, 2018). Within threads of KLP-19::GFP, we saw KLP-19 move in a bidirectional manner (Figure 5.1.c). As a plus-end directed motor, this again overlapping antiparallel MTs.

To further support our theory that KLP-19 and SPD-1 localise to centrosomal-cortical antiparallel MTs at the cortex, it would be useful to eliminate centrosomal MTs and determine whether there is a reduction in cortical KLP-19 or SPD-1. If there was no change, this would suggest that both proteins are recruited only to antiparallel cortical-cortical MTs which would make it difficult to explain how these MTs regulate the position of the SPCC. As we saw similar cortical localisation patterns between SPD-1 and KLP-19, and KLP-19 is recruited to antiparallel MTs of the spindle midzone, it is likely that that we are seeing the same MT-bundling interaction at the cortex.

It is interesting to point out that human Kif4a and PRC1 do not interact prior to anaphase due to cyclin-dependent kinase 1 (CDK1) inhibition. As mentioned earlier (Section 1.3.1), this ensures that Kif4a's role is to remain associated with the chromosomes during chromosomal congression until the mitotic checkpoint is satisfied and cyclin B levels decline which inactivates CDK1 (Mollinari *et al.*, 2002; Zhu and Jiang, 2005; Voets *et al.*, 2015; Dong *et al.*, 2018; Takata *et al.*, 2018). This could explain why we see cortical KLP-19 and SPD-1 localisation primarily during polarity establishment and late anaphase at which points CDK1 would be inactive. The drop in CDK1 levels would allow KLP-19-SPD-1 interaction and raises the possibility of cell cycle dependent regulation of SPCC positioning. Rising CDK1 activity at later stages of polarity establishment could instruct KLP-19 to clear from cortical microtubules to ensure efficient SPCC migration. In support of this, the depletion of the phosphatase PP2A adaptor SUR-6, which contributes to inactivation of CDK1 via dephosphorylation (Castilho *et al.*, 2009; Mochida *et al.*, 2009), led to similar SPCC orientation phenotypes to the loss of KLP-

19 (Boudreau *et al.*, 2019), possibly a result of inappropriately active CDK1 during polarity establishment.

As mentioned, kinesins also regulate the dynamic instability of MTs (Sections 1.2.2 & 1.3). For example, the kinesin-13 family member, MCAK, localises to the plus end of MTs where it acts as an ATPase to destabilise and depolymerise the filament (Hunter *et al.*, 2003; Connolly *et al.*, 2015). The absence of *C. elegans* MCAK, KLP-7, was shown to hinder centrosome separation in the AB cell of the embryo after the first zygotic division as the astral MTs overgrow and push against the cell membrane, forcing the centrosomes towards each other (Bondaz *et al.*, 2019). If KLP-19 similarly suppresses MT growth in the *C. elegans* zygote, this could explain why we observed increased average distances of the SPCC to the cortex in the absence of KLP-19 as centrosomal MTs would grow excessively and push the SPCC away from the membrane. The KLP-19 homologues, Xklp1 and Kif4A, have been shown to stabilise microtubules, reducing both polymerisation and depolymerisation rates. In cells, the availability of tubulin monomers tends to lead to enhanced MT growth in the absence of Xklp1 and Kif4a (Bringmann *et al.*, 2004; Castoldi and Vernos, 2006; Bieling, Telley and Surrey, 2010; Hu *et al.*, 2011; Stumpff *et al.*, 2012; Wandke *et al.*, 2012). This could explain why we saw increased EBP-2 duration in the absence of KLP-19 as MTs would not be stabilised and MT growth can last longer than in control embryos.

KLP-19 and SPD-1 homologues have been shown to localise to both single and antiparallel MTs, influencing MT growth in different ways (Kapitein *et al.*, 2008; Bieling, Telley and Surrey, 2010; Subramanian *et al.*, 2010; Hannabuss *et al.*, 2019; Mani *et al.*, 2021). Saxton & McIntosh (1987) demonstrated that antiparallel microtubules in the spindle midzone have lower dynamic instability than single microtubules as fluorescent tubulin is incorporated at a slower rate (Saxton and McIntosh, 1987; Bieling, Telley and Surrey, 2010). Recent work by Mani et al. (2021) developed on the understanding of single vs antiparallel MT dynamic instability by demonstrating that CLASP1 and Kif4a act competitively to promote and suppress microtubule growth, respectively, through interaction with PRC1. They showed that CLASP1 outcompetes Kif4a on single microtubules whereas Kif4a activity wins out on antiparallel microtubules. The result is a module of the three proteins that act to promote the growth of single microtubules and suppress antiparallel MT growth (Mani *et al.*, 2021).

Work by Wandke et al. (2012), who performed Kif4A RNAi depletion in HeLa cells, saw increased durations of EB1-GFP tracks as we did with *klp-19* RNAi depletion in EBP-2::GFP embryos. This suggests that KLP-19 may have similar roles to its better studied homologues in the regulation of MT dynamics. Unlike Kif4a RNAi, however, we did not see a change in the displacement or velocity of cortical EBP-2 tracks nor did we see a change in density. These parameters increased in the absence of Kif4a and represented an increase in microtubule number and growth. This work in HeLa cells was performed during mitosis whereas the EBP-2 data of this project focused on polarity establishment and could explain the difference in effects observed between Kif4a and KLP-19 loss (Wandke *et al.*, 2012). Increased MT growth in embryos has previously resulted in thick bundles of MTs at the cortex as shown upon the depletion of EFA-6 and KLP-7 which halt MT growth at the cortex of WT embryos (O'Rourke, Christensen and Bowerman, 2010; Bondaz *et al.*, 2019). Again, we did not see this happen in the absence of KLP-19. This would suggest that KLP-19 does not have an impact on MT dynamic instability (i.e., The rate of conversion between MT assembly and catastrophe) at the cortex that could lead to excess MT growth. It is possible that KLP-19 does not act to regulate MT growth rate during polarity establishment as in mitosis, but instead acts to stabilise MTs to the cortex after growth, either by antiparallel MT cross-linkage or single MT anchorage rather than changes to MT growth. This would be difficult to see using the EBP-2::GFP reporter as it only tracks growing MT tips. Using α/β-tubulin as a reporter may provide greater insight into how microtubules reside/grow at the cortex.

It is interesting to point out that KLP-19 also acts at the cortex of embryos during mitosis. In KLP-19 depleted embryos, we observed increased velocities of spindle pole retraction to each pole during anaphase upon laser ablation of the spindle midzone. We reasoned that KLP-19 acts at the cortex to suppress MT pulling forces at this stage too. This is supportive of our theory that KLP-19 stabilises microtubules at the cortex but does not exclude other possible explanations. We reasoned that centrosome dynamics in anaphase zygotes are likely suppressed by KLP-19 as it acts to stabilise microtubules at the cortex.

8.4 Proposed model.

Microtubules are typically described as rigs which generate pulling/pushing forces and as tracks along which cargo can be carried, ultimately facilitating different types of movement within a cell. There are examples, as we have presented in this work, demonstrating that

microtubules can act to restrict intracellular movement through stabilisation/fixation. For example, the neuron-specific protein, syntaphilin, has been shown to dock mitochondria to microtubules within axons and limit mitochondrial movement. Through this, mitochondria can be focused within the neuron as needed to meet local energy demands. Defective syntaphilin results in more motile and less densely arranged mitochondria, and compromised neuron synaptic signalling (Kang *et al.*, 2008; Chen and Sheng, 2013).

Overall, the findings in this project have led us to propose a model in which KLP-19 acts to crosslink microtubules of the centrosome with microtubules grown at the cortex of the *C. elegans* zygote in order to resist other forces within the cell that could cause the SPCC to drift away from the cortex (Figure 8.1). As microtubules begin to grow radially from the centrosome, they will run into cortical microtubules, some of which in an antiparallel manner. SPD-1 localises with high affinity to antiparallel MTs and recruits KLP-19 which stabilises/crosslinks the MT-MT contacts as it does in the spindle midzone during anaphase. A second potential mechanism relies on single MTs reaching the cortex and being stabilised by KLP-19 and another partner, e.g. VAB-19 – note, however, that the data in this project on VAB-19 is limited to one experiment. Through both antiparallel and single MT interactions, cortical KLP-19 would effectively capture the centrosome and restrict its location to the posterior pole, between the sperm-derived pronucleus and the cortex. SPCC fixation to the cortex resists initial cortical pulling forces facilitated by the cortical dynein complex which binds to microtubules and respond to cortical cytoplasmic flows (De Simone, Nédélec and Gönczy, 2016). By maintaining close proximity between the centrosome and the cortex, KLP-19 ensures that the symmetry breaking signal is robust, required for the efficient clearing of aPARs and loading of pPARs to the cortex. Holding the centrosomes close to the posterior cortex and behind the sperm pronucleus also promotes effective centrosome separation as the duplicated centrosomes are pulled by cortical dynein tethered microtubules such that they are forced around the pronucleus on opposing sides to each other. Through this mechanism, the centrosomes can progress to form the bipolar spindle of metaphase/anaphase in the first cell division.

Figure 8.1

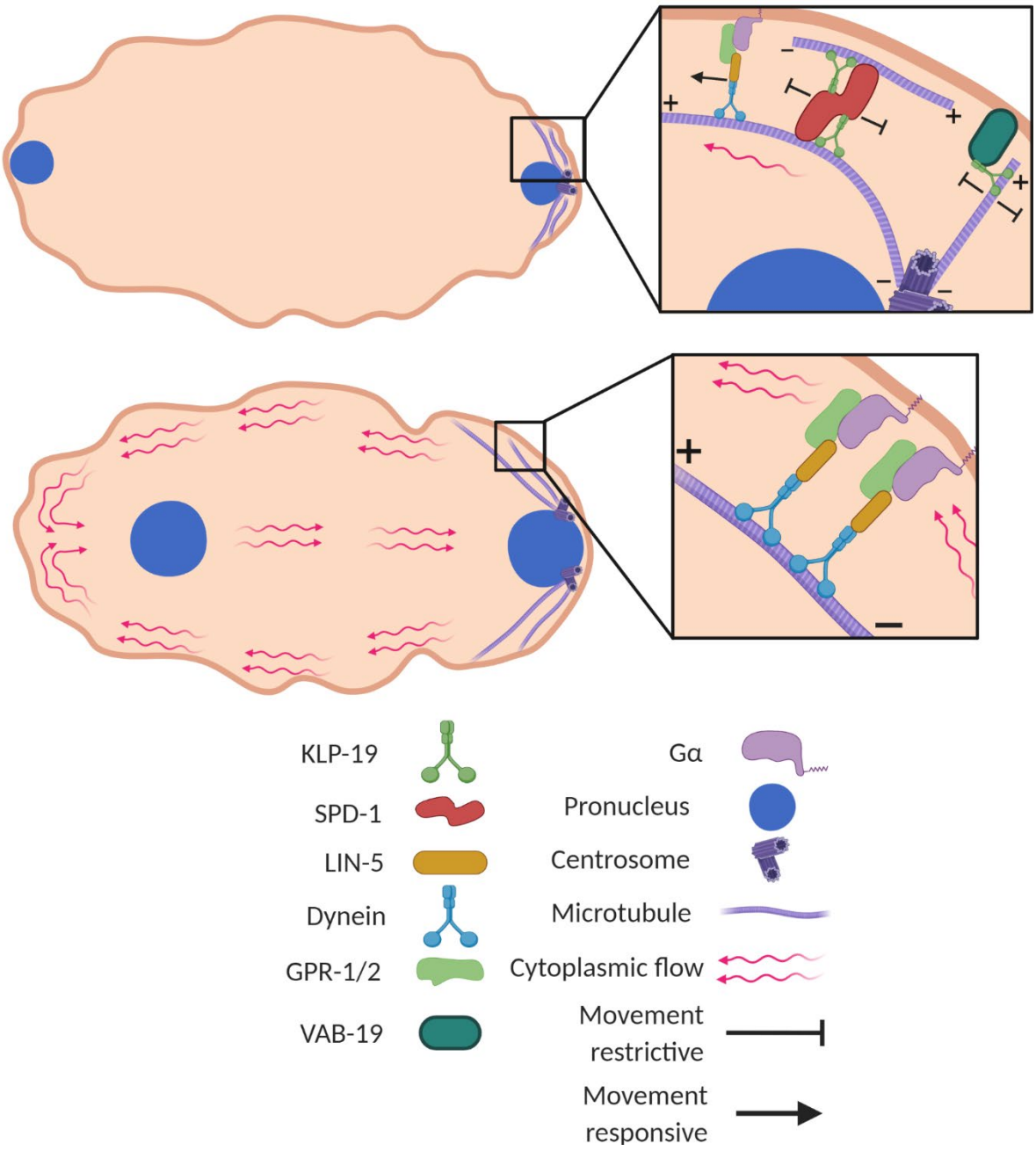

Figure 8.1 **Model of KLP-19 mediated centrosome restriction.**

Top: Centrosomal microtubules grow towards the cortex where they stabilised. In one potential mechanism, centrosomal microtubules are tethered directly to the membrane by VAB-19. In the other, the microtubule bundling protein, SPD-1, crosslinks antiparallel centrosomal and cortical microtubules and recruits KLP-19. Together, SPD-1 and KLP-19 effectively fix the SPCC in place at the posterior pole prior to centrosome separation. The cortical dynein complex (dynein, LIN-5, GPR-1/2, Gα) is responsive to movement within the cytoplasm and also binds to centrosomal microtubules via dynein. KLP-19, however, prevents early SPCC movement that the dynein complex would cause. **Bottom**: As actomyosin generated flows become stronger, the dynein complex is pulled towards the anterior. This results in the centrosomes being pulled around the pronucleus on opposing sides by their cortical dynein tethered MTs. At this timepoint, KLP-19 has either dropped from the MT-MT interaction or is no longer strong enough to prevent centrosomal movement.

8.5 Concluding remarks

From the results of project, we have contributed to the consolidation of known principles in the fields of; motor proteins, the microtubule cytoskeleton, and polarity establishment in the *C. elegans* zygote. For example, our data reaffirms the importance of the centrosome's position in the guidance of anterior-posterior polarity axis formation whilst supporting additional microtubule-dependent polarity establishment mechanisms. We have also successfully demonstrated the use of a *nop-1* mutant as a novel tool to identify regulators of polarity establishment and introduced the concept of microtubule-microtubule interaction as a mechanism to restrict the position of SPCC via kinesin-mediated antiparallel MT stabilisation. MT-MT antiparallel organisation is a well-known device of the spindle midzone to recruit the chromosomal passenger complex and aid in chromosomal segregation. The role of antiparallel microtubules is rarely discussed outside of the spindle midzone in existing literature. I previously discussed the important of the centrosome's position within migrating cells and the incomplete knowledge of the mechanisms behind this positioning (Sections 1.7.1 & 1.7.2). It is possible that antiparallel MTs have a role to play in many other cell types, not limited to positioning organelles such as the centrosome and organising the spindle midzone to facilitate chromosome dynamics.

References.

Ackema, K. B. *et al.* (2013) 'The ArfGEF GBF-1 Is Required for ER Structure, Secretion and Endocytic Transport in C. elegans', *PLoS ONE*, 8(6), p. e67076. doi: 10.1371/journal.pone.0067076.

Adames, N. R. and Cooper, J. A. (2000) 'Microtubule interactions with the cell cortex causing nuclear movements in Saccharomyces cerevisiae', *Journal of Cell Biology*, 149(4), pp. 863–874. doi: 10.1083/jcb.149.4.863.

Afshar, K. *et al.* (2004) 'RIC-8 Is Required for GPR-1/2-Dependent Gα Function during Asymmetric Division of C. elegans Embryos', *Cell*, 119(2), pp. 219–230. doi: https://doi.org/10.1016/j.cell.2004.09.026.

Afshar, K. *et al.* (2010) 'Regulation of cortical contractility and spindle positioning by the protein phosphatase 6 PPH-6 in one-cell stage C. elegans embryos', *Development*, 137(2), pp. 237–247. doi: 10.1242/dev.042754.

Agircan, F. G., Schiebel, E. and Mardin, B. R. (2014) 'Separate to operate: Control of centrosome positioning and separation', *Philosophical Transactions of the Royal Society B: Biological Sciences*, 369(1650), p. 20130461. doi: 10.1098/rstb.2013.0461.

Ai, E., Poole, D. S. and Skop, A. R. (2009) 'RACK-1 directs dynactin-dependent RAB-11 endosomal recycling during mitosis in Caenorhabditis elegans', *Molecular Biology of the Cell*, 20(6), pp. 1629–1638. doi: 10.1091/mbc.E08-09-0917.

Ai, E., Poole, D. S. and Skop, A. R. (2011) 'Long astral microtubules and RACK-1 stabilize polarity domains during maintenance phase in caenorhabditis elegans embryos', *PLoS ONE*. Edited by M. Klymkowsky, 6(4), p. e19020. doi: 10.1371/journal.pone.0019020.

Akhmanova, A. *et al.* (2001) 'CLASPs Are CLIP-115 and -170 Associating Proteins Involved in the Regional Regulation of Microtubule Dynamics in Motile Fibroblasts', *Cell*, 104(6), pp. 923–935. doi: https://doi.org/10.1016/S0092-8674(01)00288-4.

Akhmanova, A. and Hoogenraad, C. C. (2015) 'Microtubule minus-end-targeting proteins', *Current Biology*, 25(4), pp. R162–R171. doi: 10.1016/j.cub.2014.12.027.

Alfieri, A. C., Gaska, I. R. and Forth, S. T. (2021) 'Two Modes of PRC1-Mediated Mechanical Resistance to Kinesin-Driven Microtubule Network Disruption', *Biophysical Journal*, 120(3), p. 257a. doi: 10.1016/j.bpj.2020.11.1659.

Almeida, A. C. and Maiato, H. (2018) 'Chromokinesins', *Current Biology*, 28(19), pp. R1131–R1135. doi: 10.1016/j.cub.2018.07.017.

Alves-Cruzeiro, J. M. da C., Nogales-Cadenas, R. and Pascual-Montano, A. D. (2014) 'CentrosomeDB: A new generation of the centrosomal proteins database for Human and Drosophila melanogaster', *Nucleic Acids Research*, 42(D1), pp. D430–D436. doi: 10.1093/nar/gkt1126.

Anders, A. and Sawin, K. E. (2011) 'Microtubule stabilization in vivo by nucleation-incompetent γ-tubulin complex', *Journal of Cell Science*, 124(8), pp. 1207 LP – 1213. doi: 10.1242/jcs.083741.

Andersen, J. S. *et al.* (2003) 'Proteomic characterization of the human centrosome by protein correlation profiling', *Nature*, 426(6966), pp. 570–574. doi: 10.1038/nature02166.

Andrews, R. and Ahringer, J. (2007) 'Asymmetry of Early Endosome Distribution in C. elegans Embryos', *PLoS ONE*, 2(6), p. e493. doi: 10.1371/journal.pone.0000493.

Arata, Y. *et al.* (2016) 'Cortical Polarity of the RING Protein PAR-2 Is Maintained by Exchange Rate Kinetics at the Cortical-Cytoplasmic Boundary', *Cell Reports*, 16(8), pp. 2156–2168. doi: 10.1016/j.celrep.2016.07.047.

Arthur, W. T. and Burridge, K. (2001) 'RhoA inactivation by p190RhoGAP regulates cell spreading and migration by promoting membrane protrusion and polarity', *Molecular Biology of the Cell*, 12(9), pp. 2711–2720. doi: 10.1091/mbc.12.9.2711.

Ashcroft, N. R. *et al.* (1999) 'RNA-mediated interference of a cdc25 homolog in Caenorhabditis elegans results in defects in the embryonic cortical membrane, meiosis, and mitosis', *Developmental Biology*, 206(1), pp. 15–32. doi: 10.1006/dbio.1998.9135.

Asthana, J. *et al.* (2020) 'PRC1 and EB1 binding dynamics reveal a solidifying central spindle during anaphase compaction in human cells', *bioRxiv*, p. 2020.07.09.195347. doi: 10.1101/2020.07.09.195347.

Au, F. K. C., Hau, B. K. T. and Qi, R. Z. (2020) 'Nek2-mediated GAS2L1 phosphorylation and centrosome-linker disassembly induce centrosome disjunction', *Journal of Cell Biology*, 219(5). doi: 10.1083/jcb.201909094.

Aw, W. Y. and Devenport, D. (2017) 'Planar cell polarity: global inputs establishing cellular asymmetry', *Current Opinion in Cell Biology*. Elsevier Ltd, pp. 110–116. doi: 10.1016/j.ceb.2016.08.002.

Bahe, S. *et al.* (2005) 'Rootletin forms centriole-associated filaments and functions in centrosome cohesion', *Journal of Cell Biology*, 171(1), pp. 27–33. doi: 10.1083/jcb.200504107.
Bailey, M. J. and Prehoda, K. E. (2015) 'Establishment of Par-Polarized Cortical Domains via Phosphoregulated Membrane Motifs', *Developmental Cell*, 35(2), pp. 199–210. doi: 10.1016/j.devcel.2015.09.016.

Baines, A. J. *et al.* (2009) 'The CKK domain (DUF1781) binds microtubules and defines the CAMSAP/ssp4 family of animal proteins', *Molecular Biology and Evolution*, 26(9), pp. 2005–2014. doi: 10.1093/molbev/msp115.

Barbier, P. *et al.* (2019) 'Role of tau as a microtubule-associated protein: Structural and functional aspects', *Frontiers in Aging Neuroscience*, p. 204. doi: 10.3389/fnagi.2019.00204.
Barbosa, D. J. *et al.* (2017) 'Dynactin binding to tyrosinated microtubules promotes

centrosome centration in C. elegans by enhancing dynein-mediated organelle transport', *PLoS Genetics*, 13(7), p. e1006941. doi: 10.1371/journal.pgen.1006941.

Barrera, J. A. *et al.* (2010) 'CDK5RAP2 regulates centriole engagement and cohesion in mice', *Developmental Cell*, 18(6), pp. 913–926. doi: 10.1016/j.devcel.2010.05.017.

Bartles, J. R. (2000) 'Parallel actin bundles and their multiple actin-bundling proteins', *Current Opinion in Cell Biology*, 12(1), pp. 72–78. doi: 10.1016/S0955-0674(99)00059-9.

Basant, A. *et al.* (2015) 'Aurora B Kinase Promotes Cytokinesis by Inducing Centralspindlin Oligomers that Associate with the Plasma Membrane', *Developmental Cell*, 33(2), pp. 204–215. doi: 10.1016/j.devcel.2015.03.015.

Basant, A. and Glotzer, M. (2018) 'Spatiotemporal Regulation of RhoA during Cytokinesis', *Current Biology*, 28(9), pp. R570–R580. doi: 10.1016/j.cub.2018.03.045.

Bastos, R. N. *et al.* (2013) 'Aurora B suppresses microtubule dynamics and limits central spindle size by locally activating KIF4A', *Journal of Cell Biology*, 202(4), pp. 605–621. doi: 10.1083/jcb.201301094.

Beatty, A., Morton, D. G. and Kemphues, K. (2013) 'PAR-2, LGL-1 and the CDC-42 GAP CHIN-1 act in distinct pathways to maintain polarity in the C. elegans embryo', *Development*, 140(9), pp. 2005–2014. doi: 10.1242/dev.088310.

Beatty, A., Morton, D. and Kemphues, K. (2010) 'The C. elegans homolog of Drosophila Lethal giant larvae functions redundantly with PAR-2 to maintain polarity in the early embryo', *Development*, 137(23), pp. 3995–4004. doi: 10.1242/dev.056028.

Beeg, J. *et al.* (2008) 'Transport of beads by several kinesin motors', *Biophysical Journal*. 2007/09/14, 94(2), pp. 532–541. doi: 10.1529/biophysj.106.097881.

Bell, G. P. *et al.* (2015) 'Aurora Kinases Phosphorylate Lgl to Induce Mitotic Spindle Orientation in Drosophila Epithelia', *Current Biology*, 25(1), pp. 61–68. doi: https://doi.org/10.1016/j.cub.2014.10.052.

Bellanger, J.-M. and Gönczy, P. (2003) 'TAC-1 and ZYG-9 Form a Complex that Promotes Microtubule Assembly in C. elegans Embryos', *Current Biology*, 13(17), pp. 1488–1498. doi: 10.1016/S0960-9822(03)00582-7.

Bellanger, J. M. *et al.* (2007) 'ZYG-9, TAC-1 and ZYG-8 together ensure correct microtubule function throughout the cell cycle of C. elegans embryos', *Journal of Cell Science*, 120(16), pp. 2963–2973. doi: 10.1242/jcs.004812.

Bellett, G. *et al.* (2009) 'Microtubule plus-end and minus-end capture at adherens junctions is involved in the assembly of apico-basal arrays in polarised epithelial cells', *Cell Motility and the Cytoskeleton*, 66(10), pp. 893–908. doi: 10.1002/cm.20393.

Benton, R. and St Johnston, D. (2003) 'Drosophila PAR-1 and 14-3-3 inhibit Bazooka/PAR-3 to

establish complementary cortical domains in polarized cells', *Cell*, 115(6), pp. 691–704. doi: 10.1016/S0092-8674(03)00938-3.

Berdnik, D. and Knoblich, J. A. (2002) 'Drosophila Aurora-A Is Required for Centrosome Maturation and Actin-Dependent Asymmetric Protein Localization during Mitosis', *Current Biology*, 12(8), pp. 640–647. doi: 10.1016/S0960-9822(02)00766-2.

Berger, C., Urban, J. and Technau, G. M. (2001) 'Stage-specific inductive signals in the Drosophila neuroectoderm control the temporal sequence of neuroblast specification', *Development*, 128(17), pp. 3243–3251. doi: 10.1242/dev.128.17.3243.

Bergstralh, D. T., Dawney, N. S. and St Johnston, D. (2017) 'Spindle orientation: a question of complex positioning', *Development*, 144(7), pp. 1137–1145. doi: 10.1242/dev.140764.

Bianchi, S. *et al.* (2016) 'Structural basis for misregulation of kinesin KIF21A autoinhibition by CFEOM1 disease mutations', *Scientific Reports*, 6(1), p. 30668. doi: 10.1038/srep30668.

Bieling, P. *et al.* (2007) 'Reconstitution of a microtubule plus-end tracking system in vitro', *Nature*, 450(7172), pp. 1100–1105. doi: 10.1038/nature06386.

Bieling, P., Telley, I. A. and Surrey, T. (2010) 'A minimal midzone protein module controls formation and length of antiparallel microtubule overlaps', *Cell*, 142(3), pp. 420–432. doi: 10.1016/j.cell.2010.06.033.

Bienkowska, D. and Cowan, C. R. (2012) 'Centrosomes can initiate a polarity axis from any position within one-cell C. Elegans embryos', *Current Biology*, 22(7), pp. 583–589. doi: 10.1016/j.cub.2012.01.064.

Bilder, D. and Perrimon, N. (2000) 'Localization of apical epithelial determinants by the basolateral PDZ protein Scribble.', *Nature*, 403(6770), pp. 676–680. doi: 10.1038/35001108.

Bisbal, M. *et al.* (2009) 'KIF4 mediates anterograde translocation and positioning of ribosomal constituents to axons', *Journal of Biological Chemistry*, 284(14), pp. 9489–9497. doi: 10.1074/jbc.M808586200.

Bishop, J. D., Han, Z. and Schumacher, J. M. (2005) 'The Caenorhabditis elegans Aurora B Kinase AIR-2 Phosphorylates and Is Required for the Localization of a BimC Kinesin to Meiotic and Mitotic Spindles', *Molecular Biology of the Cell*. Edited by S. Strome, 16(2), pp. 742–756. doi: 10.1091/mbc.E04-08-0682.

Blangy, A. *et al.* (1995) 'Phosphorylation by p34cdc2 regulates spindle association of human Eg5, a kinesin-related motor essential for bipolar spindle formation in vivo', *Cell*, 83(7), pp. 1159–1169. doi: https://doi.org/10.1016/0092-8674(95)90142-6.

Bobinnec, Y., Fukuda, M. and Nishida, E. (2000) 'Identification and characterization of Caenorhabditis elegans gamma-tubulin in dividing cells and differentiated tissues', *Journal of Cell Science*, 113(21), pp. 3747 LP – 3759. Available at: http://jcs.biologists.org/content/113/21/3747.abstract.

Bogdan, S. *et al.* (2004) 'Sra-1 interacts with Kette and Wasp and is required for neuronal and bristle development in Drosophila', *Development*, 131(16). doi: 10.1242/dev.01274.

Boitard, M. *et al.* (2015) 'Wnt signaling regulates multipolar-to-bipolar transition of migrating neurons in the cerebral cortex', *Cell Reports*, 10(8), pp. 1349–1361. doi: 10.1016/j.celrep.2015.01.061.

Bolhy, S. *et al.* (2011) 'A Nup133-dependent NPC-anchored network tethers centrosomes to the nuclear envelope in prophase', *Journal of Cell Biology*, 192(5), pp. 855–871. doi: 10.1083/jcb.201007118.

Bondaz, A. *et al.* (2019) 'Cell polarity–dependent centrosome separation in the C. elegans embryo', *The Journal of Cell Biology*, p. jcb.201902109. doi: 10.1083/jcb.201902109.

Bornens, M. (2018) 'Cell polarity: Having and making sense of direction - On the evolutionary significance of the primary cilium/centrosome organ in Metazoa', *Open Biology*. Royal Society Publishing. doi: 10.1098/rsob.180052.

Bosveld, F., Ainslie, A. and Bellaïche, Y. (2017) 'Sequential activities of Dynein, Mud and Asp in centrosome- spindle coupling maintain centrosome number upon mitosis', *Journal of Cell Science*, 130(20), pp. 3557–3567. doi: 10.1242/jcs.201350.

Le Bot, N. *et al.* (2003) 'TAC-1, a regulator of microtubule length in the C. elegans embryo', *Current Biology*, 13(17), pp. 1499–1505. doi: 10.1016/S0960-9822(03)00577-3.

Bouchet, B. P. *et al.* (2016) 'Mesenchymal Cell Invasion Requires Cooperative Regulation of Persistent Microtubule Growth by SLAIN2 and CLASP1', *Developmental Cell*. 2016/12/08, 39(6), pp. 708–723. doi: 10.1016/j.devcel.2016.11.009.

Boudreau, V. *et al.* (2019) 'PP2A-B55/SUR-6 collaborates with the nuclear lamina for centrosome separation during mitotic entry', *Molecular Biology of the Cell*. Edited by M. Théry, 30(7), pp. 876–886. doi: 10.1091/mbc.E18-10-0631.

Bouvrais, H. *et al.* (2018) 'Microtubule Feedback and LET-99-Dependent Control of Pulling Forces Ensure Robust Spindle Position', *Biophysical Journal*, 115(11), pp. 2189–2205. doi: 10.1016/j.bpj.2018.10.010.

Bouvrais, H. *et al.* (2021) 'The coordination of spindle-positioning forces during the asymmetric division of the Caenorhabditis elegans zygote', *EMBO reports*, 22(5). doi: 10.15252/embr.202050770.

Bowman, S. K. *et al.* (2006) 'The Drosophila NuMA Homolog Mud Regulates Spindle Orientation in Asymmetric Cell Division', *Developmental Cell*, 10(6), pp. 731–742. doi: 10.1016/j.devcel.2006.05.005.

Boxem, M. and van den Heuvel, S. (2019) 'Cell Polarity: Getting the PARty Started', *Current Biology*, 29(13), pp. R637–R639. doi: 10.1016/j.cub.2019.05.032.

Boyd, L. *et al.* (1996) 'PAR-2 is asymmetrically distributed and promotes association of P granules and PAR-1 with the cortex in C. elegans embryos', *Development*, 122(10), pp. 3075–3084. doi: 10.1242/dev.122.10.3075.

Bradke, F. and Dotti, C. G. (1999) 'The Role of Local Actin Instability in Axon Formation', *Science*, 283(5409), pp. 1931 LP – 1934. doi: 10.1126/science.283.5409.1931.

Bradke, F. and Dotti, C. G. (2000) 'Differentiated neurons retain the capacity to generate axons from dendrites', *Current Biology*, 10(22), pp. 1467–1470. doi: https://doi.org/10.1016/S0960-9822(00)00807-1.

Brangwynne, C. P. *et al.* (2009) 'Germline P granules are liquid droplets that localize by controlled dissolution/condensation', *Science*, 324(5935), pp. 1729–1732. doi: 10.1126/science.1172046.

Brenner, S. (1974) 'The genetics of Caenorhabditis elegans.', *Genetics*, 77(1), pp. 71–94.

Bringmann, H. *et al.* (2004) 'A Kinesin-like Motor Inhibits Microtubule Dynamic Instability', *Science*, 303(5663), pp. 1519–1522. doi: 10.1126/science.1094838.

Bringmann, H. and Hyman, A. A. (2005) 'A cytokinesis furrow is positioned by two consecutive signals', *Nature*, 436(7051), pp. 731–734. doi: 10.1038/nature03823.

Brouhard, G. J. and Hunt, A. J. (2005) 'Microtubule movements on the arms of mitotic chromosomes: Polar ejection forces quantified in vitro', *Proceedings of the National Academy of Sciences of the United States of America*, 102(39), pp. 13903–13908. doi: 10.1073/pnas.0506017102.

Budirahardja, Y. and Gönczy, P. (2008) 'PLK-1 asymmetry contributes to asynchronous cell division of C. elegans embryos', *Development*, 135(7), pp. 1303–1313. doi: 10.1242/dev.019075.

Burakov, A. *et al.* (2003) 'Centrosome positioning in interphase cells ', *Journal of Cell Biology*, 162(6), pp. 963–969. doi: 10.1083/jcb.200305082.

Burakov, A. V. and Nadezhdina, E. S. (2020) 'Centering and Shifting of Centrosomes in Cells', *Cells*. doi: 10.3390/cells9061351.

Burbank, K. S. and Mitchison, T. J. (2006) 'Microtubule dynamic instability', *Current Biology*, 16(14), pp. R516–R517. doi: 10.1016/j.cub.2006.06.044.

Burridge, K. and Wennerberg, K. (2004) 'Rho and Rac Take Center Stage', *Cell*, 116(2), pp. 167–179. doi: 10.1016/S0092-8674(04)00003-0.

Burton, P. R. and Paige, J. L. (1981) 'Polarity of axoplasmic microtubules in the olfactory nerve of the frog (axoplasm/ultrastructure/detergent extraction/tubulin assembly/protofilament ribbons)', *Proceedings of the National Academy of Sciences of the United States of America*, 78(5 I), pp. 3269–3273. doi: 10.1073/pnas.78.5.3269.

Cai, Q. and Sheng, Z. H. (2009) 'Mitochondrial transport and docking in axons', *Experimental Neurology*, 218(2), pp. 257–267. doi: 10.1016/j.expneurol.2009.03.024.

Cain, N. E. *et al.* (2018) 'Conserved SUN-KASH Interfaces Mediate LINC Complex-Dependent Nuclear Movement and Positioning', *Current Biology*, 28(19), pp. 3086-3097.e4. doi: 10.1016/j.cub.2018.08.001.

Cao, J. *et al.* (2010) 'Cortical Actin Dynamics Facilitate Early-Stage Centrosome Separation', *Current Biology*, 20(8), pp. 770–776. doi: 10.1016/j.cub.2010.02.060.

Cao, L. G. and Wang, Y. L. (1996) 'Signals from the spindle midzone are required for the stimulation of cytokinesis in cultured epithelial cells.', *Molecular biology of the cell*, 7(2), pp. 225–32. doi: 10.1091/mbc.7.2.225.

Carmena, M. *et al.* (2012) 'The chromosomal passenger complex (CPC): From easy rider to the godfather of mitosis', *Nature Reviews Molecular Cell Biology*, 13(12), pp. 789–803. doi: 10.1038/nrm3474.

Carvalho, C. A. *et al.* (2015) 'Aurora a triggers Lgl cortical release during symmetric division to control planar spindle orientation', *Current Biology*, 25(1), pp. 53–60. doi: 10.1016/j.cub.2014.10.053.

Castilho, P. V. *et al.* (2009) 'The M phase kinase greatwall (Gwl) promotes inactivation of PP2A/B55δ, a phosphatase directed against CDK phosphosites', *Molecular Biology of the Cell*, 20(22), pp. 4777–4789. doi: 10.1091/mbc.E09-07-0643.

Castoldi, M. and Vernos, I. (2006) 'Chromokinesin Xklp1 Contributes to the Regulation of Microtubule Density and Organization during Spindle Assembly', *Molecular Biology of the Cell*. Edited by E. Holzbaur, 17(3), pp. 1451–1460. doi: 10.1091/mbc.E05-04-0271.

Cau, J. and Hall, A. (2005) 'Cdc42 controls the polarity of the actin and microtubule cytoskeletons through two distinct signal transduction pathways', *Journal of Cell Science*, 118(12), pp. 2579–2587. doi: 10.1242/jcs.02385.

Caussinus, E. and Gonzalez, C. (2005) 'Induction of tumor growth by altered stem-cell asymmetric division in Drosophila melanogaster', *Nature Genetics*, 37(10), pp. 1125–1129. doi: 10.1038/ng1632.

Chada, S. R. and Hollenbeck, P. J. (2003) 'Mitochondrial movement and positioning in axons: The role of growth factor signaling', *Journal of Experimental Biology*, 206(12), pp. 1985–1992. doi: 10.1242/jeb.00263.

Chafel, M. M., Shen, W. and Matsudaira, P. (1995) 'Sequential expression and differential localization of I-, L-, and T-Fimbrin during differentiation of the mouse intestine and yolk sac', *Developmental Dynamics*, 203(2), pp. 141–151. doi: 10.1002/aja.1002030203.

Chaigne, A. *et al.* (2016) 'F-actin mechanics control spindle centring in the mouse zygote',

Nature Communications, 7(1), p. 10253. doi: 10.1038/ncomms10253.

Chalfie, M. (2009) 'GFP: Lighting up life', *Proceedings of the National Academy of Sciences of the United States of America*, 106(25), pp. 10073–10080. doi: 10.1073/pnas.0904061106.

Chan, F. Y. *et al.* (2019) 'The ARP2/3 complex prevents excessive formin activity during cytokinesis', *Molecular Biology of the Cell*, 30(1), pp. 96–107. doi: 10.1091/mbc.E18-07-0471.
Chang, W., Worman, H. J. and Gundersen, G. G. (2015) 'Accessorizing and anchoring the LINC complex for multifunctionality', *Journal of Cell Biology*, 208(1), pp. 11–22. doi: 10.1083/jcb.201409047.

Cheeks, R. J. *et al.* (2004) 'C. elegans PAR proteins function by mobilizing and stabilizing asymmetrically localized protein complexes', *Current Biology*, 14(10), pp. 851–862. doi: 10.1016/j.cub.2004.05.022.

Chen, J.-X. *et al.* (2016) 'In Vivo Interaction Proteomics in Caenorhabditis elegans Embryos Provides New Insights into P Granule Dynamics', *Molecular & Cellular Proteomics*, 15(5), pp. 1642–1657. doi: 10.1074/mcp.M115.053975.

Chen, S. *et al.* (2013) 'Regulation of Microtubule Stability and Organization by Mammalian Par3 in Specifying Neuronal Polarity', *Developmental Cell*, 24(1), pp. 26–40. doi: 10.1016/j.devcel.2012.11.014.

Chen, Y. and Sheng, Z. H. (2013) 'Kinesin-1-syntaphilin coupling mediates activity-dependent regulation of axonal mitochondrial transport', *Journal of Cell Biology*, 202(2), pp. 351–364. doi: 10.1083/jcb.201302040.

Cheng, P. L. *et al.* (2011) 'Self-amplifying autocrine actions of BDNF in axon development', *Proceedings of the National Academy of Sciences of the United States of America*, 108(45), pp. 18430–18435. doi: 10.1073/pnas.1115907108.

Ciferri, C. *et al.* (2008) 'Implications for Kinetochore-Microtubule Attachment from the Structure of an Engineered Ndc80 Complex', *Cell*, 133(3), pp. 427–439. doi: 10.1016/j.cell.2008.03.020.

Cockell, M. M., Baumer, K. and Gönczy, P. (2004) 'lis-1 is required for dynein-dependent cell division processes in C. elegans embryos.', *Journal of cell science*, 117(Pt 19), pp. 4571–82. doi: 10.1242/jcs.01344.

Colombo, K. *et al.* (2003) 'Translation of polarity cues into asymmetric spindle positioning in Caenorhabditis elegans embryos', *Science*, 300(5627), pp. 1957–1961. doi: 10.1126/science.1084146.

Conde, C. *et al.* (2010) 'Evidence for the involvement of Lfc and Tctex-1 in axon formation', *Journal of Neuroscience*, 30(19), pp. 6793–6800. doi: 10.1523/JNEUROSCI.5420-09.2010.

Connolly, A. A. *et al.* (2015) 'KLP-7 acts through the Ndc80 complex to limit pole number in C. elegans oocyte meiotic spindle assembly', *Journal of Cell Biology*, 210(6), pp. 917–932. doi:

10.1083/jcb.201412010.

Coravos, J. S., Mason, F. M. and Martin, A. C. (2017) 'Actomyosin Pulsing in Tissue Integrity Maintenance during Morphogenesis', *Trends in cell biology*. 2016/12/16, 27(4), pp. 276–283. doi: 10.1016/j.tcb.2016.11.008.

Costanzo, M. *et al.* (2010) 'The genetic landscape of a cell', *Science*, 327(5964), pp. 425–431. doi: 10.1126/science.1180823.

Cowan, C. R. and Hyman, A. A. (2004) 'Centrosomes direct cell polarity independently of microtubule assembly in C. elegans embryos', *Nature*, 431(7004), pp. 92–96. doi: 10.1038/nature02825.

Craig, E. M. (2018) 'Model for coordination of microtubule and actin dynamics in growth cone turning', *Frontiers in Cellular Neuroscience*, p. 394. doi: 10.3389/fncel.2018.00394.

Cuenca, A. A. (2003) 'Polarization of the C. elegans zygote proceeds via distinct establishment and maintenance phases', *Development*, 130(7), pp. 1255–1265. doi: 10.1242/dev.00284.

Cuijpers, S. A. G. *et al.* (2020) 'Chromokinesin KIF4A teams up with stathmin 1 to regulate abscission in a SUMO-dependent manner', *Journal of cell science*, 133(14). doi: 10.1242/jcs.248591.

Dang, I. *et al.* (2013) 'Inhibitory signalling to the Arp2/3 complex steers cell migration', *Nature*, 503(7475), pp. 281–284. doi: 10.1038/nature12611.

Daniels, B. R. *et al.* (2010) 'MEX-5 enrichment in the C. elegans early embryo mediated by differential diffusion', *Development*, 137(15), pp. 2579–2585. doi: 10.1242/dev.051326.

Delgehyr, N., Sillibourne, J. and Bornens, M. (2005) 'Microtubule nucleation and anchoring at the centrosome are independent processes linked by ninein function', *Journal of Cell Science*, 118(8), pp. 1565–1575. doi: 10.1242/jcs.02302.

DeLuca, J. G. *et al.* (2006) 'Kinetochore Microtubule Dynamics and Attachment Stability Are Regulated by Hec1', *Cell*, 127(5), pp. 969–982. doi: 10.1016/j.cell.2006.09.047.

Denker, E., Bočina, I. and Jiang, D. (2013) 'Tubulogenesis in a simple cell cord requires the formation of bi-apical cells through two discrete Par domains', *Development (Cambridge)*, 140(14), pp. 2985–2996. doi: 10.1242/dev.092387.

Desai, A. and Mitchison, T. J. (1997) 'Microtubule polymerization dynamics', *Annual Review of Cell and Developmental Biology*, 13(1), pp. 83–117. doi: 10.1146/annurev.cellbio.13.1.83.

Dewey, E. B., Taylor, D. T. and Johnston, C. A. (2015) 'Cell fate decision making through oriented cell division', *Journal of Developmental Biology*, pp. 129–157. doi: 10.3390/jdb3040129.

Dickinson, D. J. *et al.* (2017) 'A Single-Cell Biochemistry Approach Reveals PAR Complex

Dynamics during Cell Polarization', *Developmental Cell*, 42(4), pp. 416-434.e11. doi: 10.1016/j.devcel.2017.07.024.

Ding, M. *et al.* (2003) 'C. elegans ankyrin repeat protein VAB-19 is a component of epidermal attachment structures and is essential for epidermal morphogenesis', *Development*, 130(23), pp. 5791–5801. doi: 10.1242/dev.00791.

Ding, W. Y. *et al.* (2017) 'Plastin increases cortical connectivity to facilitate robust polarization and timely cytokinesis', *Journal of Cell Biology*, 216(5), pp. 1371–1386. doi: 10.1083/jcb.201603070.

Ditchfield, C. *et al.* (2003) 'Aurora B couples chromosome alignment with anaphase by targeting BubR1, Mad2, and Cenp-E to kinetochores', *Journal of Cell Biology*, 161(2), pp. 267–280. doi: 10.1083/jcb.200208091.

Dogan, M. Y. *et al.* (2015) 'Kinesin's Front Head Is Gated by the Backward Orientation of Its Neck Linker', *Cell Reports*, 10(12), pp. 1967–1973. doi: https://doi.org/10.1016/j.celrep.2015.02.061.

Dokshin, G. A. *et al.* (2018) 'Robust genome editing with short single-stranded and long, partially single-stranded DNA donors in caenorhabditis elegans', *Genetics*, 210(3), pp. 781–787. doi: 10.1534/genetics.118.301532.

Dominguez, R. and Holmes, K. C. (2011) 'Actin structure and function', *Annual Review of Biophysics*, 40(1), pp. 169–186. doi: 10.1146/annurev-biophys-042910-155359.

Dong, Z. *et al.* (2018) 'Cdk phosphorylation licenses Kif4A chromosome localization required for early mitotic progression', *Journal of Molecular Cell Biology*, 10(4), pp. 358–370. doi: 10.1093/jmcb/mjy033.

Douglas, M. E. *et al.* (2010) 'Aurora B and 14-3-3 Coordinately Regulate Clustering of Centralspindlin during Cytokinesis', *Current Biology*, 20(10), pp. 927–933. doi: 10.1016/j.cub.2010.03.055.

Drewes, G. *et al.* (1997) 'MARK, a novel family of protein kinases that phosphorylate microtubule- associated proteins and trigger microtubule disruption', *Cell*, 89(2), pp. 297–308. doi: 10.1016/S0092-8674(00)80208-1.

Drewes, G., Ebneth, A. and Mandelkow, E. M. (1998) 'MAPs, MARKs and microtubule dynamics', *Trends in Biochemical Sciences*, 23(8), pp. 307–311. doi: 10.1016/S0968-0004(98)01245-6.

Du, Q. *et al.* (2002) 'LGN blocks the ability of NuMA to bind and stabilize microtubules: A mechanism for mitotic spindle assembly regulation', *Current Biology*, 12(22), pp. 1928–1933. doi: 10.1016/S0960-9822(02)01298-8.

Dujardin, D. L. *et al.* (2003) 'A role for cytoplasmic dynein and LIS1 in directed cell movement', *Journal of Cell Biology*, 163(6), pp. 1205–1211. doi: 10.1083/jcb.200310097.

Dumont, J. and Desai, A. (2012) 'Acentrosomal spindle assembly and chromosome segregation during oocyte meiosis', *Trends in Cell Biology*, 22(5), pp. 241–249. doi: 10.1016/j.tcb.2012.02.007.

Dumont, J., Oegema, K. and Desai, A. (2010) 'A kinetochore-independent mechanism drives anaphase chromosome separation during acentrosomal meiosis', *Nature Cell Biology*, 12(9), pp. 894–901. doi: 10.1038/ncb2093.

Edwards, D. C. *et al.* (1999) 'Activation of LIM-kinase by Pak1 couples Rac/Cdc42 GTPase signalling to actin cytoskeletal dynamics', *Nature Cell Biology*, 1(5), pp. 253–259. doi: 10.1038/12963.

Elbaum-Garfinkle, S. *et al.* (2015) 'The disordered P granule protein LAF-1 drives phase separation into droplets with tunable viscosity and dynamics', *Proceedings of the National Academy of Sciences of the United States of America*, 112(23), pp. 7189–7194. doi: 10.1073/pnas.1504822112.

Enomoto, T. (1996) 'Microtubule disruption induces the formation of actin stress fibers and focal adhesions in cultured cells: Possible involvement of the rho signal cascade', *Cell Structure and Function*, 21(5), pp. 317–326. doi: 10.1247/csf.21.317.

Estrem, C., Fees, C. P. and Moore, J. K. (2017) 'Dynein is regulated by the stability of its microtubule track', *Journal of Cell Biology*. 2017/06/01, 216(7), pp. 2047–2058. doi: 10.1083/jcb.201611105.

Etienne-Manneville, S. *et al.* (2005) 'Cdc42 and Par6-PKCη regulate the spatially localized association of Dlg1 and APC to control cell polarization', *Journal of Cell Biology*, 170(6), pp. 895–901. doi: 10.1083/jcb.200412172.

Etienne-Manneville, S. and Hall, A. (2001) 'Integrin-mediated activation of Cdc42 controls cell polarity in migrating astrocytes through PKCζ', *Cell*, 106(4), pp. 489–498. doi: 10.1016/S0092-8674(01)00471-8.

Etienne-Manneville, S. and Hall, A. (2002) 'Rho GTPases in cell biology', *Nature*, 420(6916), pp. 629–635. doi: 10.1038/nature01148.

Etienne-Manneville, S. and Hall, A. (2003) 'Cdc42 regulates GSK-3β and adenomatous polyposis coli to control cell polarity', *Nature*, 421(6924), pp. 753–756. doi: 10.1038/nature01423.

Evangelista, M. *et al.* (2002) 'Formins direct Arp2/3-independent actin filament assembly to polarize cell growth in yeast.', *Nature cell biology*, 4(3), pp. 260–269. doi: 10.1038/ncb718.
Ezratty, E. J., Partridge, M. A. and Gundersen, G. G. (2005) 'Microtubule-induced focal adhesion disassembly is mediated by dynamin and focal adhesion kinase', *Nature Cell Biology*, 7(6), pp. 581–590. doi: 10.1038/ncb1262.

Farrell, C. M. *et al.* (2002) 'The role of ATP hydrolysis for kinesin processivity', *Journal of*

Biological Chemistry, 277(19), pp. 17079–17087. doi: 10.1074/jbc.M108793200.

Feldman, J. L. and Priess, J. R. (2012) 'A role for the centrosome and PAR-3 in the hand-off of MTOC function during epithelial polarization.', *Current biology : CB*, 22(7), pp. 575–82. doi: 10.1016/j.cub.2012.02.044.

Ferrary, E. *et al.* (1999) 'In vivo, villin is required for Ca2+-dependent F-actin disruption in intestinal brush borders', *Journal of Cell Biology*, 146(4), pp. 819–829. doi: 10.1083/jcb.146.4.819.

Fielmich, L. E. *et al.* (2018) 'Optogenetic dissection of mitotic spindle positioning in vivo', *eLife*, 7. doi: 10.7554/eLife.38198.

Fievet, B. T. *et al.* (2012) 'Systematic genetic interaction screens uncover cell polarity regulators and functional redundancy', *Nature Cell Biology*, 15(1), pp. 103–112. doi: 10.1038/ncb2639.

Flynn, K. C. *et al.* (2012) 'ADF/Cofilin-Mediated Actin Retrograde Flow Directs Neurite Formation in the Developing Brain', *Neuron*, 76(6), pp. 1091–1107. doi: 10.1016/j.neuron.2012.09.038.

Fogeron, M. L. *et al.* (2013) 'LGALS3BP regulates centriole biogenesis and centrosome hypertrophy in cancer cells', *Nature Communications*, 4(1), p. 1531. doi: 10.1038/ncomms2517.

Fortin, S. M. *et al.* (2010) 'The PAM-1 aminopeptidase regulates centrosome positioning to ensure anterior-posterior axis specification in one-cell C. elegans embryos', *Developmental biology*, 344(2), pp. 992–1000. doi: 10.1016/j.ydbio.2010.06.016.

Fraser, A. G. *et al.* (2000) 'Functional genomic analysis of C. elegans chromosome I by systematic RNA interference', *Nature*, 408(6810), pp. 325–330. doi: 10.1038/35042517.

Fry, A. M., Meraldi, P. and Nigg, E. A. (1998) 'A centrosomal function for the human Nek2 protein kinase, a member of the NIMA family of cell cycle regulators', *EMBO Journal*, 17(2), pp. 470–481. doi: 10.1093/emboj/17.2.470.

Funahashi, Y. *et al.* (2013) 'ERK2-mediated phosphorylation of par3 regulates neuronal polarization', *Journal of Neuroscience*, 33(33), pp. 13270–13285. doi: 10.1523/JNEUROSCI.4210-12.2013.

Gallaud, E., Pham, T. and Cabernard, C. (2017) 'Drosophila melanogaster neuroblasts: A model for asymmetric stem cell divisions', in Tassan, J.-P. and Kubiak, J. Z. (eds) *Results and Problems in Cell Differentiation*. Cham: Springer International Publishing, pp. 183–210. doi: 10.1007/978-3-319-53150-2_8.

Galli, M. *et al.* (2011) 'APKC phosphorylates NuMA-related LIN-5 to position the mitotic spindle during asymmetric division', *Nature Cell Biology*, 13(9), pp. 1132–1140. doi: 10.1038/ncb2315.
Gallo, G., Yee, H. F. and Letourneau, P. C. (2002) 'Actin turnover is required to prevent axon

retraction driven by endogenous actomyosin contractility', *Journal of Cell Biology*, 158(7), pp. 1219–1228. doi: 10.1083/jcb.200204140.

Gaska, I. *et al.* (2020) 'The Mitotic Crosslinking Protein PRC1 Acts Like a Mechanical Dashpot to Resist Microtubule Sliding', *Developmental Cell*, 54(3), pp. 367-378.e5. doi: 10.1016/j.devcel.2020.06.017.

Gateff, E. (1994) 'Tumor suppressor and overgrowth suppressor genes of drosophila melanogaster: Developmental aspects', *International Journal of Developmental Biology*, 38(4), pp. 565–590. doi: 10.1387/ijdb.7779680.

Gauthier, S. *et al.* (2008) 'Co-regulation of yeast purine and phosphate pathways in response to adenylic nucleotide variations', *Molecular Microbiology*, 68(6), pp. 1583–1594. doi: 10.1111/j.1365-2958.2008.06261.x.

Gennerich, A. *et al.* (2007) 'Force-Induced Bidirectional Stepping of Cytoplasmic Dynein', *Cell*, 131(5), pp. 952–965. doi: 10.1016/j.cell.2007.10.016.

Glater, E. E. *et al.* (2006) 'Axonal transport of mitochondria requires milton to recruit kinesin heavy chain and is light chain independent', *Journal of Cell Biology*, 173(4), pp. 545–557. doi: 10.1083/jcb.200601067.

Goehring, N. W., Hoege, C., *et al.* (2011) 'PAR proteins diffuse freely across the anterior-posterior boundary in polarized C. elegans embryos', *Journal of Cell Biology*, 193(3), pp. 583–594. doi: 10.1083/jcb.201011094.

Goehring, N. W., Trong, P. K., *et al.* (2011) 'Polarization of PAR Proteins by Advective Triggering of a Pattern-Forming System', *Science*, 334(6059), pp. 1137–1141. doi: 10.1126/science.1208619.

Goldspink, D. A. *et al.* (2017) 'Ninein is essential for apico-basal microtubule formation and CLIP-170 facilitates its redeployment to non-centrosomal microtubule organizing centres', *Open Biology*, 7(2), p. 160274. doi: 10.1098/rsob.160274.

Goldstein, B. and Hird, S. N. (1996) 'Specification of the anteroposterior axis in Caenorhabditis elegans', *Development*, 122(5), pp. 1467–1474.

Goldstein, B., Hird, S. N. and White, J. G. (1993) 'Cell polarity in early C. elegans development', *Development*, 119(SUPPL.), pp. 279–287. Available at: http://dev.biologists.org/content/119/Supplement/279.abstract.

Gönczy, P. *et al.* (1999) 'Cytoplasmic Dynein Is Required for Distinct Aspects of Mtoc Positioning, Including Centrosome Separation, in the One Cell Stage Caenorhabditis elegans Embryo', *Journal of Cell Biology*, 147(1), pp. 135–150. doi: 10.1083/jcb.147.1.135.

Goold, R. G., Owen, R. and Gordon-Weeks, P. R. (1999) 'Glycogen synthase kinase 3β phosphorylation of microtubule-associated protein 1B regulates the stability of microtubules in growth cones', *Journal of Cell Science*, 112(19), pp. 3373–3384. doi:

10.1242/jcs.112.19.3373.

Gorelik, R. and Gautreau, A. (2015) 'The Arp2/3 inhibitory protein arpin induces cell turning by pausing cell migration', *Cytoskeleton*, 72(7), pp. 362–371. doi: 10.1002/cm.21233.

Gotta, M. *et al.* (2003) 'Asymmetrically distributed C. elegans Homologs of AGS3/PINS control spindle position in the early embryo', *Current Biology*, 13(12), pp. 1029–1037. doi: 10.1016/S0960-9822(03)00371-3.

Gotta, M., Abraham, M. C. and Ahringer, J. (2001) 'CDC-42 controls early cell polarity and spindle orientation in C. elegans', *Current Biology*, 11(7), pp. 482–488. doi: 10.1016/S0960-9822(01)00142-7.

Gotta, M. and Ahringer, J. (2001) 'Distinct roles for Gα and Gβγ in regulating spindle position and orientation in Caenorhabditis elegans embryos', *Nature Cell Biology*, 3(3), pp. 297–300. doi: 10.1038/35060092.

Graser, S., Stierhof, Y. D. and Nigg, E. A. (2007) 'Cep68 and Cep215 (Cdk5rap2) are required for centrosome cohesion', *Journal of Cell Science*, 120(24), pp. 4321–4331. doi: 10.1242/jcs.020248.

Griffin, E. E., Odde, D. J. and Seydoux, G. (2011) 'Regulation of the MEX-5 gradient by a spatially segregated kinase/phosphatase cycle', *Cell*, 146(6), pp. 955–968. doi: 10.1016/j.cell.2011.08.012.

Grill, S. W. *et al.* (2001) 'Polarity controls forces governing asymmetric spindle positioning in the caenorhabditis elegans embryo', *Nature*, 409(6820), pp. 630–633. doi: 10.1038/35054572.

Grishchuk, E. L. *et al.* (2008) 'The Dam1 ring binds microtubules strongly enough to be a processive as well as energy-efficient coupler for chromosome motion', *Proceedings of the National Academy of Sciences of the United States of America*, 105(40), pp. 15423–15428. doi: 10.1073/pnas.0807859105.

Grishok, A. (2005) 'RNAi mechanisms in Caenorhabditis elegans', *FEBS Letters*, 579(26), pp. 5932–5939. doi: https://doi.org/10.1016/j.febslet.2005.08.001.

Gross, P. *et al.* (2019) 'Guiding self-organized pattern formation in cell polarity establishment', *Nature Physics*, 15(3), pp. 293–300. doi: 10.1038/s41567-018-0358-7.

Gross, P., Kumar, K. V. and Grill, S. W. (2017) 'How Active Mechanics and Regulatory Biochemistry Combine to Form Patterns in Development', *Annual Review of Biophysics*, 46(1), pp. 337–356. doi: 10.1146/annurev-biophys-070816-033602.

Gruneberg, U. *et al.* (2006) 'KIF14 and citron kinase act together to promote efficient cytokinesis.', *The Journal of cell biology*, 172(3), pp. 363–72. doi: 10.1083/jcb.200511061.

Gu, G. J. *et al.* (2013) 'Elevated MARK2-dependent phosphorylation of tau in Alzheimer's disease', *Journal of Alzheimer's Disease*, 33(3), pp. 699–713. doi: 10.3233/JAD-2012-121357.

Gubieda, A. G. *et al.* (2020) ' Going with the flow: insights from Caenorhabditis elegans zygote polarization ', *Philosophical Transactions of the Royal Society B: Biological Sciences*, 375(1809), p. 20190555. doi: 10.1098/rstb.2019.0555.

Guil, Á. F. N. *et al.* (2017) 'IGF-1 receptor regulates dynamic changes in neuronal polarity during cerebral cortical migration', *Scientific Reports*, 7(1), p. 7703. doi: 10.1038/s41598-017-08140-5.

Gundersen, G. G. and Bulinski, J. C. (1988) 'Selective stabilization of microtubules oriented toward the direction of cell migration', *Proceedings of the National Academy of Sciences of the United States of America*, 85(16), pp. 5946–5950. doi: 10.1073/pnas.85.16.5946.

Gungabissoon, R. A. and Bamburg, J. R. (2003) 'Regulation of growth cone actin dynamics by ADF/cofilin', *Journal of Histochemistry and Cytochemistry*, 51(4), pp. 411–420. doi: 10.1177/002215540305100402.

Guo, S. and Kemphues, K. J. (1995) 'par-1, a gene required for establishing polarity in C. elegans embryos, encodes a putative Ser/Thr kinase that is asymmetrically distributed', *Cell*, 81(4), pp. 611–620. doi: 10.1016/0092-8674(95)90082-9.

Guo, S. and Kemphues, K. J. (1996) 'A non-muscle myosin required for embryonic polarity in Caenorhabditis elegans', *Nature*, 382(6590), pp. 455–458. doi: 10.1038/382455a0.

Gusnowski, E. M. and Srayko, M. (2011) 'Visualization of dynein-dependent microtubule gliding at the cell cortex: implications for spindle positioning', *The Journal of Cell Biology*, 194(3), pp. 377 LP – 386. Available at: http://jcb.rupress.org/content/194/3/377.abstract.

Van Haastert, P. J. M. and Devreotes, P. N. (2004) 'Chemotaxis: Signalling the way forward', *Nature Reviews Molecular Cell Biology*, 5(8), pp. 626–634. doi: 10.1038/nrm1435.

Hajjar, C., Sampuda, K. M. and Boyd, L. (2014) 'Dual roles for ubiquitination in the processing of sperm organelles after fertilization', *BMC Developmental Biology*, 14(1), p. 6. doi: 10.1186/1471-213X-14-6.

Hamill, D. R. *et al.* (2002) 'Centrosome Maturation and Mitotic Spindle Assembly in C. elegans Require SPD-5, a Protein with Multiple Coiled-Coil Domains', *Developmental Cell*, 3(5), pp. 673–684. doi: 10.1016/S1534-5807(02)00327-1.

Hannabuss, J. *et al.* (2019) 'Self-Organization of Minimal Anaphase Spindle Midzone Bundles', *Current Biology*, 29(13), pp. 2120-2130.e7. doi: 10.1016/j.cub.2019.05.049.

Hao, Y., Boyd, L. and Seydoux, G. (2006) 'Stabilization of cell polarity by the C. elegans RING protein PAR-2', *Developmental Cell*, 10(2), pp. 199–208. doi: 10.1016/j.devcel.2005.12.015.

Hartenstein, V. and Wodarz, A. (2013) 'Initial neurogenesis in Drosophila.', *Wiley interdisciplinary reviews. Developmental biology*. 2013/02/11, 2(5), pp. 701–721. doi: 10.1002/wdev.111.

Harterink, M. *et al.* (2018) 'Local microtubule organization promotes cargo transport in C. elegans dendrites', *Journal of Cell Science*, 131(20). doi: 10.1242/jcs.223107.

Hauf, S. *et al.* (2003) 'The small molecule Hesperadin reveals a role for Aurora B in correcting kinetochore-microtubule attachment and in maintaining the spindle assembly checkpoint', *Journal of Cell Biology*, 161(2), pp. 281–294. doi: 10.1083/jcb.200208092.

He, R. *et al.* (2013) 'LRRC45 Is a Centrosome Linker Component Required for Centrosome Cohesion', *Cell Reports*, 4(6), pp. 1100–1107. doi: 10.1016/j.celrep.2013.08.005.

Heath, C. M. and Wignall, S. M. (2019) 'Chromokinesin Kif4 promotes proper anaphase in mouse oocyte meiosis', *Molecular Biology of the Cell*. Edited by K. S. Bloom, 30(14), pp. 1691–1704. doi: 10.1091/mbc.E18-10-0666.

van Heesbeen, R. G. H. P. *et al.* (2017) 'Aurora A, MCAK, and Kif18b promote Eg5-independent spindle formation', *Chromosoma*, 126(4), pp. 473–486. doi: 10.1007/s00412-016-0607-4.

Heidemann, S. R., Landers, J. M. and Hamborg, M. A. (1981) 'Polarity orientation of axonal microtubules', *Journal of Cell Biology*, 91(3 I), pp. 661–665. doi: 10.1083/jcb.91.3.661.

Heintz, T. G. *et al.* (2014) 'Kinesin KIF4A transports integrin β1 in developing axons of cortical neurons', *Molecular and Cellular Neuroscience*, 63, pp. 60–71. doi: 10.1016/j.mcn.2014.09.003.

De Heredia, M. L. and Jansen, R. P. (2004) 'mRNA localization and the cytoskeleton', *Current Opinion in Cell Biology*, 16(1), pp. 80–85. doi: 10.1016/j.ceb.2003.11.002.

Higashi, T., Stephenson, R. E. and Miller, A. L. (2019) 'Comprehensive analysis of formin localization in Xenopus epithelial cells', *Molecular Biology of the Cell*, 30(1), pp. 82–95. doi: 10.1091/mbc.E18-02-0133.

Higgs, H. N., Blanchoin, L. and Pollard, T. D. (1999) 'Influence of the C terminus of Wiskott-Aldrich syndrome protein (WASp) and the Arp2/3 complex on actin polymerization', *Biochemistry*, 38(46), pp. 15212–15222. doi: 10.1021/bi991843+.

Higgs, H. N. and Pollard, T. D. (2000) 'Activation by Cdc42 and PIP2 of Wiskott-Aldrich Syndrome protein (WASp) stimulates actin nucleation by Arp2/3 complex', *Journal of Cell Biology*, 150(6), pp. 1311–1320. doi: 10.1083/jcb.150.6.1311.

Hill, D. P. and Strome, S. (1988) 'An analysis of the role of microfilaments in the establishment and maintenance of asymmetry in Caenorhabditis elegans zygotes', *Developmental Biology*, 125(1), pp. 75–84. doi: 10.1016/0012-1606(88)90060-7.

Hird, S. and White, J. (1993) 'Cortical and Cytoplasmic Flow in Early C. elegans Embryos', *Journal of Cell Biology*, 121(6), pp. 1343–1355. Available at: http://jcb.rupress.org/content/121/6/1343.long.

Hirokawa, N. *et al.* (1989) 'Submolecular domains of bovine brain kinesin identified by electron microscopy and monoclonal antibody decoration', *Cell*, 56(5), pp. 867–878. doi: https://doi.org/10.1016/0092-8674(89)90691-0.

Hoege, C. *et al.* (2010) 'LGL can partition the cortex of one-cell caenorhabditis elegans embryos into two domains', *Current Biology*, 20(14), pp. 1296–1303. doi: 10.1016/j.cub.2010.05.061.

Hoege, C. and Hyman, A. A. (2013) 'Principles of PAR polarity in Caenorhabditis elegans embryos.', *Nature reviews. Molecular cell biology*, 14(5), pp. 315–22. doi: 10.1038/nrm3558.

Howard, J., Hudspeth, A. J. and Vale, R. D. (1989) 'Movement of microtubules by single kinesin molecules', *Nature*, 342(6246), pp. 154–158. doi: 10.1038/342154a0.

Hu, C. K. *et al.* (2011) 'KIF4 regulates midzone length during cytokinesis', *Current Biology*, 21(10), pp. 815–824. doi: 10.1016/j.cub.2011.04.019.

Hu, D. J. K. *et al.* (2013) 'Dynein recruitment to nuclear pores activates apical nuclear migration and mitotic entry in brain progenitor cells', *Cell*, 154(6), p. 1300. doi: 10.1016/j.cell.2013.08.024.

Hueschen, C. L. *et al.* (2017) 'NuMA recruits dynein activity to microtubule minus-ends at mitosis', *eLife*. Edited by A. P. Carter, 6, p. e29328. doi: 10.7554/eLife.29328.

Huis In 'T Veld, P. J. *et al.* (2019) 'Molecular determinants of the Ska-Ndc80 interaction and their influence on microtubule tracking and force-coupling', *eLife*. Edited by A. D. McAinsh and V. Malhotra, 8, p. e49539. doi: 10.7554/eLife.49539.

Hummel, T. *et al.* (2000) 'Drosophila Futsch/22C10 is a MAP1B-like protein required for dendritic and axonal development', *Neuron*, 26(2), pp. 357–370. doi: 10.1016/S0896-6273(00)81169-1.

Hunter, A. W. *et al.* (2003) 'The kinesin-related protein MCAK is a microtubule depolymerase that forms an ATP-hydrolyzing complex at microtubule ends', *Molecular Cell*, 11(2), pp. 445–457. doi: 10.1016/S1097-2765(03)00049-2.

Hurov, J. B., Watkins, J. L. and Piwnica-Worms, H. (2004) 'Atypical PKC phosphorylates PAR-1 kinases to regulate localization and activity', *Current Biology*, 14(8), pp. 736–741. doi: 10.1016/j.cub.2004.04.007.

Illukkumbura, R., Bland, T. and Goehring, N. W. (2020) 'Patterning and polarization of cells by intracellular flows', *Current Opinion in Cell Biology*. Elsevier Ltd, pp. 123–134. doi: 10.1016/j.ceb.2019.10.005.

Isogai, T., Van Der Kammen, R. and Innocenti, M. (2015) 'SMIFH2 has effects on Formins and p53 that perturb the cell cytoskeleton', *Scientific Reports*, 5(1), p. 9802. doi: 10.1038/srep09802.

Izumi, Y. *et al.* (2006) 'Drosophila Pins-binding protein Mud regulates spindle-polarity coupling and centrosome organization', *Nature Cell Biology*, 8(6), pp. 586–593. doi: 10.1038/ncb1409.

Jagrić, M. *et al.* (2021) 'Optogenetic control of prc1 reveals its role in chromosome alignment on the spindle by overlap length-dependent forces', *eLife*, 10, pp. 1–79. doi: 10.7554/eLife.61170.

Januschke, J. and Gonzalez, C. (2010) 'The interphase microtubule aster is a determinant of asymmetric division orientation in Drosophila neuroblasts', *Journal of Cell Biology*, 188(5), pp. 693–706. doi: 10.1083/jcb.200905024.

Jenkins, N. (2006) 'CYK-4/GAP Provides a Localized Cue to Initiate Anteroposterior Polarity upon Fertilization', *Science*, 313(5791), pp. 1298–1301. doi: 10.1126/science.1130291.

Jewett, C. E. and Prekeris, R. (2018) 'Insane in the apical membrane: Trafficking events mediating apicobasal epithelial polarity during tube morphogenesis', *Traffic*, 19(9), pp. 666–678. doi: 10.1111/tra.12579.

Johnston, C. A. *et al.* (2009) 'Identification of an Aurora-A/PinsLINKER/ Dlg Spindle Orientation Pathway using Induced Cell Polarity in S2 Cells', *Cell*, 138(6), pp. 1150–1163. doi: 10.1016/j.cell.2009.07.041.

Jolly, A. L. *et al.* (2010) 'Kinesin-1 heavy chain mediates microtubule sliding to drive changes in cell shape', *Proceedings of the National Academy of Sciences of the United States of America*, 107(27), pp. 12151–12156. doi: 10.1073/pnas.1004736107.

Jordan, S. N. *et al.* (2016) 'Cortical PAR polarity proteins promote robust cytokinesis during asymmetric cell division', *Journal of Cell Biology*, 212(1), pp. 39–49. doi: 10.1083/jcb.201510063.

Jørgensen, L. H. *et al.* (2014) 'Duplication in the microtubule-actin cross-linking factor 1 gene causes a novel neuromuscular condition', *Scientific Reports*, 4(1), p. 5180. doi: 10.1038/srep05180.

Jossin, Y. and Cooper, J. A. (2011) 'Reelin, Rap1 and N-cadherin orient the migration of multipolar neurons in the developing neocortex', *Nature Neuroscience*, 14(6), pp. 697–703. doi: 10.1038/nn.2816.

Kabir, N. *et al.* (2001) 'Protein kinase C activation promotes microtubule advance in neuronal growth cones by increasing average microtubule growth lifetimes', *Journal of Cell Biology*, 152(5), pp. 1033–1043. doi: 10.1083/jcb.152.5.1033.

Kage-Nakadai, E. *et al.* (2019) 'The small GTPase ARF-1.2 is a regulator of unicellular tube formation in Caenorhabditis elegans', *Journal of Physiological Sciences*, 69(1), pp. 47–56. doi: 10.1007/s12576-018-0617-5.

Kaitna, S. *et al.* (2000) 'Incenp and an Aurora-like kinase form a complex essential for chromosome segregation and efficient completion of cytokinesis', *Current Biology*, 10(19), pp.

1172–1181. doi: 10.1016/S0960-9822(00)00721-1.

Kakinuma, N. and Kiyama, R. (2009) 'A major mutation of KIF21A associated with congenital fibrosis of the extraocular muscles type 1 (CFEOM1) enhances translocation of Kank1 to the membrane', *Biochemical and Biophysical Research Communications*, 386(4), pp. 639–644. doi: 10.1016/j.bbrc.2009.06.109.

Kamasaki, T. *et al.* (2013) 'Augmin-dependent microtubule nucleation at microtubule walls in the spindle', *Journal of Cell Biology*, 202(1), pp. 25–32. doi: 10.1083/jcb.201304031.

Kamath, R. S. *et al.* (2003) 'Systematic functional analysis of the Caenorhabditis elegans genome using RNAi', *Nature*, 421(6920), pp. 231–237. doi: 10.1038/nature01278.

Kamijo, K. *et al.* (2006) 'Dissecting the role of Rho-mediated signaling in contractile ring formation', *Molecular Biology of the Cell*, 17(1), pp. 43–55. doi: 10.1091/mbc.E05-06-0569.

Kang, J. S. *et al.* (2008) 'Docking of Axonal Mitochondria by Syntaphilin Controls Their Mobility and Affects Short-Term Facilitation', *Cell*, 132(1), pp. 137–148. doi: 10.1016/j.cell.2007.11.024.

Kapitein, L. C. *et al.* (2005) 'The bipolar mitotic kinesin Eg5 moves on both microtubules that it crosslinks', *Nature*, 435(7038), pp. 114–118. doi: 10.1038/nature03503.

Kapitein, L. C. *et al.* (2008) 'Microtubule-Driven Multimerization Recruits ase1p onto Overlapping Microtubules', *Current Biology*, 18(21), pp. 1713–1717. doi: 10.1016/j.cub.2008.09.046.

Kapoor, S. and Kotak, S. (2019) 'Centrosome Aurora A regulates RhoGEF ECT-2 localisation and ensures a single PAR-2 polarity axis in C. Elegans embryos', *Development (Cambridge)*, 146(22). doi: 10.1242/dev.174565.

Kelly, A. E. and Funabiki, H. (2009) 'Correcting aberrant kinetochore microtubule attachments: an Aurora B-centric view', *Current Opinion in Cell Biology*, 21(1), pp. 51–58. doi: 10.1016/j.ceb.2009.01.004.

Kemphues, K. J. *et al.* (1988) 'Identification of genes required for cytoplasmic localization in early C. elegans embryos', *Cell*, 52(3), pp. 311–320. doi: 10.1016/S0092-8674(88)80024-2.

Khaliullin, R. N. *et al.* (2018) 'A positive-feedback-based mechanism for constriction rate acceleration during cytokinesis in Caenorhabditis elegans', *eLife*. Edited by M. K. Balasubramanian and A. Akhmanova, 7, p. e36073. doi: 10.7554/eLife.36073.

Kim, A. J. and Griffin, E. E. (2021) 'PLK-1 Regulation of Asymmetric Cell Division in the Early C. elegans Embryo', *Frontiers in Cell and Developmental Biology*, p. 1853. doi: 10.3389/fcell.2020.632253.

Kim, K. *et al.* (2008) 'A novel function of CEP135 as a platform protein of C-NAP1 for its centriolar localization', *Experimental Cell Research*, 314(20), pp. 3692–3700. doi:

10.1016/j.yexcr.2008.09.016.

Kim, W. *et al.* (1998) 'Binding of Murine Leukemia Virus Gag Polyproteins to KIF4, a Microtubule-Based Motor Protein', *Journal of Virology*, 72(8), pp. 6898–6901. doi: 10.1128/jvi.72.8.6898-6901.1998.

Kim, W. *et al.* (2018) 'Ortholist 2: A new comparative genomic analysis of human and caenorhabditis elegans genes', *Genetics*, 210(2), pp. 445–461. doi: 10.1534/genetics.118.301307.

Kimura, K. *et al.* (2017) 'Endoplasmic-reticulum-mediated microtubule alignment governs cytoplasmic streaming', *Nature Cell Biology*, 19(4), pp. 399–406. doi: 10.1038/ncb3490.

Kimura, K. and Kimura, A. (2011) 'Intracellular organelles mediate cytoplasmic pulling force for centrosome centration in the Caenorhabditis elegans early embryo', *Proceedings of the National Academy of Sciences of the United States of America*, 108(1), pp. 137–142. doi: 10.1073/pnas.1013275108.

Kimura, K. and Kimura, A. (2020) 'Cytoplasmic streaming drifts the polarity cue and enables posteriorization of the *Caenorhabditis elegans* zygote at the side opposite of sperm entry', *Molecular Biology of the Cell*. Edited by K. Oegema, 31(16), pp. 1765–1773. doi: 10.1091/mbc.E20-01-0058.

Kirby, C., Kusch, M. and Kemphues, K. (1990) 'Mutations in the par genes of Caenorhabditis elegans affect cytoplasmic reorganization during the first cell cycle', *Developmental Biology*, 142(1), pp. 203–215. doi: 10.1016/0012-1606(90)90164-E.

Kirstein-Miles, J. *et al.* (2013) 'The nascent polypeptide-associated complex is a key regulator of proteostasis', *The EMBO Journal*, 32(10), pp. 1451–1468. doi: 10.1038/emboj.2013.87.

Kita, K. *et al.* (2006) 'Adenomatous polyposis coli on microtubule plus ends in cell extensions can promote microtubule net growth with or without EB1', *Molecular Biology of the Cell*, 17(5), pp. 2331–2345. doi: 10.1091/mbc.E05-06-0498.

Klinkert, K. *et al.* (2019) 'Aurora A depletion reveals centrosome-independent polarization mechanism in Caenorhabditis elegans', *eLife*, 8. doi: 10.7554/elife.44552.

Ten Klooster, J. P. *et al.* (2006) 'Targeting and activation of Rac1 are mediated by the exchange factor β-Pix', *Journal of Cell Biology*, 172(5), pp. 759–769. doi: 10.1083/jcb.200509096.

Ko, C. S., Tserunyan, V. and Martin, A. C. (2019) 'Microtubules promote intercellular contractile force transmission during tissue folding', *Journal of Cell Biology*, 218(8), pp. 2726–2742. doi: 10.1083/JCB.201902011.

Kojima, Y. *et al.* (2007) 'Suppression of tubulin polymerization by the LKB1-microtubule-associated protein/microtubule affinity-regulating kinase signaling', *Journal of Biological Chemistry*, 282(32), pp. 23532–23540. doi: 10.1074/jbc.M700590200.

Komarova, Y. *et al.* (2009) 'Mammalian end binding proteins control persistent microtubule growth', *Journal of Cell Biology*, 184(5), pp. 691–706. doi: 10.1083/jcb.200807179.

Kosuga, S. *et al.* (2005) 'GSK-3β directly phosphorylates and activates MARK2/PAR-1', *Journal of Biological Chemistry*, 280(52), pp. 42715–42722. doi: 10.1074/jbc.M507941200.

Kotak, S. (2019) 'Mechanisms of spindle positioning: Lessons from worms and mammalian cells', *Biomolecules*, 9(2), p. 80. doi: 10.3390/biom9020080.

Kotak, S., Busso, C. and Gönczy, P. (2012) 'Cortical dynein is critical for proper spindle positioning in human cells', *Journal of Cell Biology*, 199(1), pp. 97–110. doi: 10.1083/jcb.201203166.

Kotak, S., Busso, C. and Gönczy, P. (2014) 'NuMA interacts with phosphoinositides and links the mitotic spindle with the plasma membrane', *The EMBO Journal*, 33(16), pp. 1815–1830. doi: 10.15252/embj.201488147.

Kotak, S. and Gönczy, P. (2013) 'Mechanisms of spindle positioning: Cortical force generators in the limelight', *Current Opinion in Cell Biology*, 25(6), pp. 741–748. doi: 10.1016/j.ceb.2013.07.008.

Kotýnková, K. *et al.* (2016) 'Plasma Membrane Association but Not Midzone Recruitment of RhoGEF ECT2 Is Essential for Cytokinesis', *Cell Reports*, 17(10), pp. 2672–2686. doi: 10.1016/j.celrep.2016.11.029.

Kozielski, F. *et al.* (1997) 'The crystal structure of dimeric kinesin and implications for microtubule-dependent motility', *Cell*, 91(7), pp. 985–994. doi: 10.1016/S0092-8674(00)80489-4.

Kozlowski, C., Srayko, M. and Nedelec, F. (2007) 'Cortical Microtubule Contacts Position the Spindle in C. elegans Embryos', *Cell*, 129(3), pp. 499–510. doi: 10.1016/j.cell.2007.03.027.

Kraynov, V. S. *et al.* (2000) 'Localized Rac activation dynamics visualized in living cells', *Science*, 290(5490), pp. 333–337. doi: 10.1126/science.290.5490.333.

Krendel, M., Zenke, F. T. and Bokoch, G. M. (2002) 'Nucleotide exchange factor GEF-H1 mediates cross-talk between microtubules and the actin cytoskeleton', *Nature Cell Biology*, 4(4), pp. 294–301. doi: 10.1038/ncb773.

Kress, E. *et al.* (2013) 'The UBXN-2/p37/p47 adaptors of CDC-48/p97 regulate mitosis by limiting the centrosomal recruitment of Aurora A', *Journal of Cell Biology*, 201(4), pp. 559–575. doi: 10.1083/jcb.201209107.

Krueger, L. E. *et al.* (2010) 'LET-99 inhibits lateral posterior pulling forces during asymmetric spindle elongation in C. elegans embryos', *Journal of Cell Biology*, 189(3), pp. 481–495. doi: 10.1083/jcb.201001115.

Kuan, H. S. and Betterton, M. D. (2016) 'Motor Protein Accumulation on Antiparallel

Microtubule Overlaps', *Biophysical Journal*, 110(9), pp. 2034–2043. doi: 10.1016/j.bpj.2016.03.039.

Kuhn, T. B. *et al.* (2000) 'Regulating actin dynamics in neuronal growth cones by ADF/cofilin and Rho family GTPases', *Journal of Neurobiology*, 44(2), pp. 126–144. doi: 10.1002/1097-4695(200008)44:2<126::AID-NEU4>3.0.CO;2-Z.

Kulić, I. M. *et al.* (2008) 'The role of microtubule movement in bidirectional organelle transport', *Proceedings of the National Academy of Sciences of the United States of America*, 105(29), pp. 10011–10016. doi: 10.1073/pnas.0800031105.

Kumfer, K. T. *et al.* (2010) 'CGEF-1 and CHIN-1 regulate CDC-42 activity during asymmetric division in the Caenorhabditis elegans embryo', *Molecular Biology of the Cell*, 21(2), pp. 266–277. doi: 10.1091/mbc.E09-01-0060.

Kunda, P. *et al.* (2008) 'Moesin Controls Cortical Rigidity, Cell Rounding, and Spindle Morphogenesis during Mitosis', *Current Biology*, 18(2), pp. 91–101. doi: 10.1016/j.cub.2007.12.051.

Kupfer, A., Louvard, D. and Singer, S. J. (1982) 'Polarization of the Golgi apparatus and the microtubule-organizing center in cultured fibroblasts at the edge of an experimental wound', *Proceedings of the National Academy of Sciences of the United States of America*, 79(8 I), pp. 2603–2607. doi: 10.1073/pnas.79.8.2603.

Kurasawa, Y. *et al.* (2004) 'Essential roles of KIF4 and its binding partner PRC1 in organized central spindle midzone formation', *The EMBO Journal*, 23(16), pp. 3237–3248. doi: 10.1038/sj.emboj.7600347.

L, J. *et al.* (2011) 'Novel Asymmetrically Localizing Components of Human Centrosomes Identified by Complementary Proteomics Methods', *The EMBO journal*, 30(8). doi: 10.1038/EMBOJ.2011.63.

Laan, L. *et al.* (2012) 'Cortical dynein controls microtubule dynamics to generate pulling forces that position microtubule asters', *Cell*, 148(3), pp. 502–514. doi: 10.1016/j.cell.2012.01.007.

Labbé, J.-C. *et al.* (2003) 'PAR Proteins Regulate Microtubule Dynamics at the Cell Cortex in C. elegans', *Current Biology*, 13(9), pp. 707–714. doi: https://doi.org/10.1016/S0960-9822(03)00251-3.

Lang, C. F. and Munro, E. (2017) 'The PAR proteins: From molecular circuits to dynamic self-stabilizing cell polarity', *Development (Cambridge)*, 144(19), pp. 3405–3416. doi: 10.1242/dev.139063.

Lange, K. I. *et al.* (2013) 'Suppressor mutations identify amino acids in PAA-1/PR65 that facilitate regulatory RSA-1/B" subunit targeting of PP2A to centrosomes in C. Elegans', *Biology Open*, 2(1), pp. 88–94. doi: 10.1242/bio.20122956.

Lawrence, C. J. *et al.* (2004) 'A standardized kinesin nomenclature.', *The Journal of cell biology*,

167(1), pp. 19–22. doi: 10.1083/jcb.200408113.

Leary, A. *et al.* (2019) 'Successive Kinesin-5 Microtubule Crosslinking and Sliding Promote Fast, Irreversible Formation of a Stereotyped Bipolar Spindle', *Current Biology*, 29(22), pp. 3825-3837.e3. doi: https://doi.org/10.1016/j.cub.2019.09.030.

Lee, K. Y. *et al.* (2015) 'Direct interaction between centralspindlin and PRC1 reinforces mechanical resilience of the central spindle', *Nature Communications*, 6, p. 7290. doi: 10.1038/ncomms8290.

Lee, Y. M. *et al.* (2001) 'Human kinesin superfamily member 4 is dominantly localized in the nuclear matrix and is associated with chromosomes during mitosis.', *The Biochemical journal*, 360(Pt 3), pp. 549–56. doi: 10.1042/bj3600549.

Lee, Y. U. *et al.* (2016) 'CDC-25.2, a C. elegans ortholog of cdc25, is essential for the progression of intestinal divisions', *Cell Cycle*, 15(5), pp. 654–666. doi: 10.1080/15384101.2016.1146839.

Leibfried, A. *et al.* (2008) 'Drosophila Cip4 and WASp Define a Branch of the Cdc42-Par6-aPKC Pathway Regulating E-Cadherin Endocytosis', *Current Biology*, 18(21), pp. 1639–1648. doi: 10.1016/j.cub.2008.09.063.

Lepicard, S. *et al.* (2014) 'A presynaptic role of microtubule-associated protein 1/Futsch in Drosophila: Regulation of active zone number and neurotransmitter release', *Journal of Neuroscience*, 34(20), pp. 6759–6771. doi: 10.1523/JNEUROSCI.4282-13.2014.

Levy, J. R. and Holzbaur, E. L. F. (2008) 'Dynein drives nuclear rotation during forward progression of motile fibroblasts', *Journal of Cell Science*, 121(19), pp. 3187–3195. doi: 10.1242/jcs.033878.

Lewellyn, L. *et al.* (2011) 'The chromosomal passenger complex and centralspindlin independently contribute to contractile ring assembly', *Journal of Cell Biology*, 193(1), pp. 155–169. doi: 10.1083/jcb.201008138.

Lewkowicz, E. *et al.* (2008) 'The microtubule-binding protein CLIP-170 coordinates mDia1 and actin reorganization during CR3-mediated phagocytosis', *Journal of Cell Biology*, 183(7), pp. 1287–1298. doi: 10.1083/jcb.200807023.

Li, B. *et al.* (2010) 'Different domains of C. elegans PAR-3 are required at different times in development', *Developmental Biology*, 344(2), pp. 745–757. doi: 10.1016/j.ydbio.2010.05.506.

Li, S., Wang, H. and Groth, C. (2014) 'Drosophila neuroblasts as a new model for the study of stem cell self-renewal and tumour formation', *Bioscience Reports*, 34(4), pp. 401–414. doi: 10.1042/BSR20140008.

Li, X. H. *et al.* (2020) 'PRC1 is a critical regulator for anaphase spindle midzone assembly and cytokinesis in mouse oocyte meiosis', *FEBS Journal*, n/a(n/a). doi: 10.1111/febs.15634.

Liebelt, F. and Vertegaal, A. C. O. (2016) 'Ubiquitin-dependent and independent roles of SUMO in proteostasis', *American Journal of Physiology - Cell Physiology*. 2016/06/22, 311(2), pp. C284–C296. doi: 10.1152/ajpcell.00091.2016.

Lin, Y. C. *et al.* (2013) 'Human microcephaly protein CEP135 binds to hSAS-6 and CPAP, and is required for centriole assembly', *EMBO Journal*, 32(8), pp. 1141–1154. doi: 10.1038/emboj.2013.56.

Lipp, J. J. *et al.* (2007) 'Aurora B controls the association of condensin I but not condensin II with mitotic chromosomes', *Journal of Cell Science*, 120(7), pp. 1245–1255. doi: 10.1242/jcs.03425.

Liu, B. P., Chrzanowska-Wodnicka, M. and Burridge, K. (1998) 'Microtubule depolymerization induces stress fibers, focal adhesions, and DNA synthesis via the GTP-binding protein Rho', *Cell Adhesion and Communication*, 5(4), pp. 249–255. doi: 10.3109/15419069809040295.

Liu, D., Davydenko, O. and Lampson, M. A. (2012) 'Polo-like kinase-1 regulates kinetochore-microtubule dynamics and spindle checkpoint silencing', *Journal of Cell Biology*, 198(4), pp. 491–499. doi: 10.1083/jcb.201205090.

Liu, J. *et al.* (2009) 'PRC1 cooperates with CLASP1 to organize central spindle plasticity in mitosis', *Journal of Biological Chemistry*, 284(34), pp. 23059–23071. doi: 10.1074/jbc.M109.009670.

Liu, X. *et al.* (2018) 'Reducing protein regulator of cytokinesis 1 as a prospective therapy for hepatocellular carcinoma', *Cell Death & Disease*, 9(5), p. 534. doi: 10.1038/s41419-018-0555-4.

Liu, Y. and Maine, E. M. (2007) 'The Bro1-domain protein, EGO-2, promotes Notch signaling in Caenorhabditis elegans', *Genetics*, 176(4), pp. 2265–2277. doi: 10.1534/genetics.107.071225.

Loïodice, I. *et al.* (2005) 'Ase1p organizes antiparallel microtubule arrays during interphase and mitosis in fission yeast', *Molecular Biology of the Cell*. Edited by T. Stearns, 16(4), pp. 1756–1768. doi: 10.1091/mbc.E04-10-0899.

Lord, C. E. N. and Gunawardena, A. H. L. A. N. (2012) 'Programmed cell death in C. elegans, mammals and plants', *European Journal of Cell Biology*, 91(8), pp. 603–613. doi: https://doi.org/10.1016/j.ejcb.2012.02.002.

Lorson, M. A., Horvitz, H. R. and Van Den Heuvel, S. (2000) 'LIN-5 is a novel component of the spindle apparatus required for chromosome segregation and cleavage plane specification in Caenorhabditis elegans', *Journal of Cell Biology*, 148(1), pp. 73–86. doi: 10.1083/jcb.148.1.73.

Loyer, N. and Januschke, J. (2018) 'The last-born daughter cell contributes to division orientation of Drosophila larval neuroblasts', *Nature Communications*, 9(1), p. 3745. doi: 10.1038/s41467-018-06276-0.

Lu, W. *et al.* (2013) 'Initial neurite outgrowth in drosophila neurons is driven by kinesin-

powered microtubule sliding', *Current Biology*, 23(11), pp. 1018–1023. doi: 10.1016/j.cub.2013.04.050.

Lu, W. *et al.* (2016) 'Microtubule-microtubule sliding by kinesin-1 is essential for normal cytoplasmic streaming in Drosophila oocytes', *Proceedings of the National Academy of Sciences of the United States of America*, 113(34), pp. E4995–E5004. doi: 10.1073/pnas.1522424113.

Lüdecke, A. *et al.* (2018) 'Diffusive tail anchorage determines velocity and force produced by kinesin-14 between crosslinked microtubules', *Nature Communications*, 9(1), p. 2214. doi: 10.1038/s41467-018-04656-0.

Luxton, G. W. G. and Gundersen, G. G. (2011) 'Orientation and function of the nuclear–centrosomal axis during cell migration', *Current Opinion in Cell Biology*, 23(5), pp. 579–588. doi: https://doi.org/10.1016/j.ceb.2011.08.001.

Ly, D. *et al.* (2017) 'Asymmetrically deployed actomyosin-based contractility generates a boundary between developing leg segments in Drosophila', *Developmental Biology*. 2017/07/06, 429(1), pp. 165–176. doi: 10.1016/j.ydbio.2017.06.031.

Lyczak, R. *et al.* (2006) 'The puromycin-sensitive aminopeptidase PAM-1 is required for meiotic exit and anteroposterior polarity in the one-cell Caenorhabditis elegans embryo', *Development*. doi: 10.1242/dev.02615.

Machesky, L. M. *et al.* (1999) 'Scar, a WASp-related protein, activates nucleation of actin filaments by the Arp2/3 complex', *Proceedings of the National Academy of Sciences of the United States of America*, 96(7), pp. 3739–3744. doi: 10.1073/pnas.96.7.3739.

Maddox, A. S. and Burridge, K. (2003) 'RhoA is required for cortical retraction and rigidity during mitotic cell rounding ', *Journal of Cell Biology*, 160(2), pp. 255–265. doi: 10.1083/jcb.200207130.

Malone, C. J. *et al.* (2003) 'The C. elegans Hook Protein, ZYG-12, Mediates the Essential Attachment between the Centrosome and Nucleus', *Cell*, 115(7), pp. 825–836. doi: 10.1016/S0092-8674(03)00985-1.

Mandelkow, E. M., Mandelkow, E. and Milligan, R. A. (1991) 'Microtubule dynamics and microtubule caps: a time-resolved cryo-electron microscopy study.', *Journal of Cell Biology*, 114(5), pp. 977–991. doi: 10.1083/jcb.114.5.977.

Mangal, S. *et al.* (2018) 'TPXL-1 activates Aurora A to clear contractile ring components from the polar cortex during cytokinesis', *Journal of Cell Biology*, 217(3), pp. 837–848. doi: 10.1083/jcb.201706021.

Mani, N. *et al.* (2021) 'Differential regulation of single microtubules and bundles by a three-protein module', *Nature Chemical Biology*. doi: 10.1038/s41589-021-00800-y.

Maninová, M., Iwanicki, M. P. and Vomastek, T. (2014) 'Emerging role for nuclear rotation and

orientation in cell migration', *Cell Adhesion and Migration*, 8(1), pp. 42–48. doi: 10.4161/cam.27761.

Manser, E. *et al.* (1998) 'PAK kinases are directly coupled to the PIX family of nucleotide exchange factors', *Molecular Cell*, 1(2), pp. 183–192. doi: 10.1016/S1097-2765(00)80019-2.

Martin-Belmonte, F., Bernascone, I. and Galvez-Santisteban, M. (2016) 'Cell Polarity', in *Encyclopedia of Cell Biology*. Elsevier Inc., pp. 741–750. doi: 10.1016/B978-0-12-394447-4.20072-2.

Martinez, N. W. *et al.* (2008) 'Kinesin KIF4 Regulates Intracellular Trafficking and Stability of the Human Immunodeficiency Virus Type 1 Gag Polyprotein', *Journal of Virology*, 82(20), pp. 9937 LP – 9950. Available at: http://jvi.asm.org/content/82/20/9937.abstract.

Marudhupandiyan, S. *et al.* (2017) 'RACK-1, a multifaceted regulator is required for C. elegans innate immunity against S. flexneri M9OT infection', *Developmental and Comparative Immunology*, 74, pp. 227–236. doi: 10.1016/j.dci.2017.05.008.

Masatoshi, N. *et al.* (2017) 'Controlling contractile instabilities in the actomyosin cortex', *eLife*. Edited by M. Piel, 6, p. e19595. doi: 10.7554/eLife.19595.

De Matos Simões, S., Mainieri, A. and Zallen, J. A. (2014) 'Rho GTPase and Shroom direct planar polarized actomyosin contractility during convergent extension', *Journal of Cell Biology*, 204(4), pp. 575–589. doi: 10.1083/jcb.201307070.

Matthews, L. R. *et al.* (1998) 'ZYG-9, a Caenorhabditis elegans protein required for microtubule organization and function, is a component of meiotic and mitotic spindle poles', *Journal of Cell Biology*, 141(5), pp. 1159–1168. doi: 10.1083/jcb.141.5.1159.

Mayer, M. *et al.* (2010) 'Anisotropies in cortical tension reveal the physical basis of polarizing cortical flows', *Nature*, 467(7315), pp. 617–621. doi: 10.1038/nature09376.

Mayor, T. *et al.* (2000) 'The centrosomal protein C-Nap1 is required for cell cycle-regulated centrosome cohesion', *Journal of Cell Biology*, 151(4), pp. 837–846. doi: 10.1083/jcb.151.4.837.

Mazumdar, M. and Misteli, T. (2005) 'Chromokinesins: Multitalented players in mitosis', *Trends in Cell Biology*, 15(7), pp. 349–355. doi: 10.1016/j.tcb.2005.05.006.

Mazumdar, M., Sundareshan, S. and Misteli, T. (2004) 'Human chromokinesin KIF4A functions in chromosome condensation and segregation', *Journal of Cell Biology*, 166(5), pp. 613–620. doi: 10.1083/jcb.200401142.

Mazumdar, M., Sung, M. H. and Misteli, T. (2011) 'Chromatin maintenance by a molecular motor protein', *Nucleus*, 2(6), pp. 591–600. doi: 10.4161/nucl.2.6.18044.

McCloskey, R. J. and Kemphues, K. J. (2012) 'Deubiquitylation Machinery Is Required for Embryonic Polarity in Caenorhabditis elegans', *PLoS Genetics*. Edited by S. E. Mango, 8(11), p.

e1003092. doi: 10.1371/journal.pgen.1003092.

McNally, K. L. *et al.* (2010) 'Kinesin-dependent transport results in polarized migration of the nucleus in oocytes and inward movement of yolk granules in meiotic embryos', *Developmental Biology*, 339(1), pp. 126–140. doi: 10.1016/j.ydbio.2009.12.021.

McNally, K. L. P. *et al.* (2012) 'Kinesin-1 Prevents Capture of the Oocyte Meiotic Spindle by the Sperm Aster', *Developmental Cell*, 22(4), pp. 788–798. doi: 10.1016/j.devcel.2012.01.010.

Medley, J. C. *et al.* (2017) 'Casein kinase II is required for proper cell division and acts as a negative regulator of centrosome duplication in Caenorhabditis elegans embryos', *Biology Open*, 6(1), pp. 17–28. doi: 10.1242/bio.022418.

Merdes, A. *et al.* (2000) 'Formation of spindle poles by dynein/dynactin-dependent transport of NuMA', *Journal of Cell Biology*, 149(4), pp. 851–861. doi: 10.1083/jcb.149.4.851.

Meunier, S. and Vernos, I. (2012) 'Microtubule assembly during mitosis - from distinct origins to distinct functions?', *Journal of Cell Science*. The Company of Biologists Ltd, pp. 2805–2814. doi: 10.1242/jcs.092429.

Michaux, J. B. *et al.* (2018) 'Excitable RhoA dynamics drive pulsed contractions in the early C. Elegans embryo', *Journal of Cell Biology*, 217(12), pp. 4230–4252. doi: 10.1083/JCB.201806161.

Midorikawa, R., Takei, Y. and Hirokawa, N. (2006) 'KIF4 Motor Regulates Activity-Dependent Neuronal Survival by Suppressing PARP-1 Enzymatic Activity', *Cell*, 125(2), pp. 371–383. doi: 10.1016/j.cell.2006.02.039.

Miki, H. *et al.* (1998) 'Induction of filopodium formation by a WASP-related actin-depolymerizing protein N-WASP', *Nature*, 391(6662), pp. 93–96. doi: 10.1038/34208.

Miki, H. *et al.* (2001) 'All kinesin superfamily protein, KIF, genes in mouse and human.', *Proceedings of the National Academy of Sciences of the United States of America*, 98(13), pp. 7004–11. doi: 10.1073/pnas.111145398.

Miki, H., Okada, Y. and Hirokawa, N. (2005) 'Analysis of the kinesin superfamily: Insights into structure and function', *Trends in Cell Biology*, 15(9), pp. 467–476. doi: 10.1016/j.tcb.2005.07.006.

Mimori-Kiyosue, Y. *et al.* (2005) 'CLASP1 and CLASP2 bind to EB1 and regulate microtubule plus-end dynamics at the cell cortex', *Journal of Cell Biology*, 168(1), pp. 141–153. doi: 10.1083/jcb.200405094.

Mimori-Kiyosue, Y., Shiina, N. and Tsukita, S. (2000) 'The dynamic behavior of the APC-binding protein EB1 on the distal ends of microtubules', *Current Biology*, 10(14), pp. 865–868. doi: 10.1016/S0960-9822(00)00600-X.

Minn, I. L. *et al.* (2009) 'SUN-1 and ZYG-12, mediators of centrosome-nucleus attachment, are

a functional SUN/KASH pair in Caenorhabditis elegans', *Molecular Biology of the Cell*, 20(21), pp. 4586–4595. doi: 10.1091/mbc.E08-10-1034.

Minoshima, Y. *et al.* (2003) 'Phosphorylation by Aurora B Converts MgcRacGAP to a RhoGAP during Cytokinesis', *Developmental Cell*, 4(4), pp. 549–560. doi: https://doi.org/10.1016/S1534-5807(03)00089-3.

Mishima, M., Kaitna, S. and Glotzer, M. (2002) 'Central Spindle Assembly and Cytokinesis Require a Kinesin-like Protein/RhoGAP Complex with Microtubule Bundling Activity', *Developmental Cell*, 2(1), pp. 41–54. doi: https://doi.org/10.1016/S1534-5807(01)00110-1.

Mitchison, T. and Kirschner, M. (1984) 'Dynamic instability of microtubule growth', *Nature*, 312(5991), pp. 237–242. doi: 10.1038/312237a0.

Mittasch, M. *et al.* (2018) 'Non-invasive perturbations of intracellular flow reveal physical principles of cell organization', *Nature Cell Biology*, 20(3), pp. 344–351. doi: 10.1038/s41556-017-0032-9.

Mittasch, M. *et al.* (2020) 'Regulated changes in material properties underlie centrosome disassembly during mitotic exit', *Journal of Cell Biology*, 219(4). doi: 10.1083/JCB.201912036.

Mochida, S. *et al.* (2009) 'Regulated activity of PP2A-B55 is crucial for controlling entry into and exit from mitosis in Xenopus egg extracts', *EMBO Journal*, 28(18), pp. 2777–2785. doi: 10.1038/emboj.2009.238.

Mogensen, M. M. *et al.* (1997) 'Centrosomal deployment of γ-tubulin and pericentrin: Evidence for a microtubule-nucleating domain and a minus-end docking domain in certain mouse epithelial cells', *Cell Motility and the Cytoskeleton*, 36(3), pp. 276–290. doi: 10.1002/(SICI)1097-0169(1997)36:3<276::AID-CM8>3.0.CO;2-5.

Mogensen, M. M. *et al.* (2000) 'Microtubule minus-end anchorage at centrosomal and non-centrosomal sites: the role of ninein', *Journal of Cell Science*, 113(17), pp. 3013 LP – 3023. Available at: http://jcs.biologists.org/content/113/17/3013.abstract.

Mollinari, C. *et al.* (2002) 'PRC1 is a microtubule binding and bundling protein essential to maintain the mitotic spindle midzone', *Journal of Cell Biology*, 157(7), pp. 1175–1186. doi: 10.1083/jcb.200111052.

Mollinari, C. *et al.* (2005) 'Ablation of PRC1 by small interfering RNA demonstrates that cytokinetic abscission requires a central spindle bundle in mammalian cells, whereas completion of furrowing does not', *Molecular Biology of the Cell*, 16(3), pp. 1043–1055. doi: 10.1091/mbc.E04-04-0346.

Molodtsov, M. I. *et al.* (2005) 'Force production by depolymerizing microtubules: A theoretical study', *Proceedings of the National Academy of Sciences of the United States of America*, 102(12), pp. 4353–4358. doi: 10.1073/pnas.0501142102.

Monen, J. *et al.* (2005) 'Differential role of CENP-A in the segregation of holocentric C. elegans

chromosomes during meiosis and mitosis', *Nature Cell Biology*, 7(12), pp. 1248–1255. doi: 10.1038/ncb1331.

Moores, C. A. *et al.* (2002) 'A mechanism for microtubule depolymerization by KinI kinesins', *Molecular Cell*, 9(4), pp. 903–909. doi: 10.1016/S1097-2765(02)00503-8.

Morais-de-Sá, E., Mirouse, V. and St Johnston, D. (2010) 'aPKC Phosphorylation of Bazooka Defines the Apical/Lateral Border in Drosophila Epithelial Cells', *Cell*, 141(3), pp. 509–523. doi: 10.1016/j.cell.2010.02.040.

Morris, E. J. *et al.* (2014) 'Kif4 Interacts with EB1 and Stabilizes Microtubules Downstream of Rho-mDia in Migrating Fibroblasts', *PLOS ONE*, 9(3), p. e91568. Available at: https://doi.org/10.1371/journal.pone.0091568.

Morris, R. L. and Hollenbeck, P. J. (1993) 'The regulation of bidirectional mitochondrial transport is coordinated with axonal outgrowth', *Journal of Cell Science*, 104(3), pp. 917–927. Available at: http://jcs.biologists.org/content/104/3/917.abstract.

Moss, D. K. *et al.* (2007) 'Ninein is released from the centrosome and moves bi-directionally along microtubules', *Journal of Cell Science*, 120(17), pp. 3064–3074. doi: 10.1242/jcs.010322.

Motegi, F. *et al.* (2011) 'Microtubules induce self-organization of polarized PAR domains in Caenorhabditis elegans zygotes.', *Nature cell biology*, 13(11), pp. 1361–7. doi: 10.1038/ncb2354.

Motegi, F. and Seydoux, G. (2013) 'The PAR network: redundancy and robustness in a symmetry-breaking system.', *Philosophical transactions of the Royal Society of London. Series B, Biological sciences*, 368(1629), p. 20130010. doi: 10.1098/rstb.2013.0010.

Motegi, F. and Sugimoto, A. (2006) 'Sequential functioning of the ECT-2 RhoGEF, RHO-1 and CDC-42 establishes cell polarity in Caenorhabditis elegans embryos', *Nature Cell Biology*, 8(9), pp. 978–985. doi: 10.1038/ncb1459.

Mullen, T. J. and Wignall, S. M. (2017) 'Interplay between microtubule bundling and sorting factors ensures acentriolar spindle stability during C. elegans oocyte meiosis', *PLOS Genetics*. Edited by M. P. Colaiácovo, 13(9), p. e1006986. doi: 10.1371/journal.pgen.1006986.

Munjal, A. *et al.* (2015) 'A self-organized biomechanical network drives shape changes during tissue morphogenesis', *Nature*, 524(7565), pp. 351–355. doi: 10.1038/nature14603.

Munro, E., Nance, J. and Priess, J. R. (2004) 'Cortical flows powered by asymmetrical contraction transport PAR proteins to establish and maintain anterior-posterior polarity in the early C. elegans embryo', *Developmental Cell*, 7(3), pp. 413–424. doi: 10.1016/j.devcel.2004.08.001.

Muroyama, A. and Lechler, T. (2017) 'Microtubule organization, dynamics and functions in differentiated cells', *Development (Cambridge)*, 144(17), pp. 3012–3021. doi: 10.1242/dev.153171.

Muroyama, A., Seldin, L. and Lechler, T. (2016) 'Divergent regulation of functionally distinct γ-tubulin complexes during differentiation', *Journal of Cell Biology*, 213(6), pp. 679–692. doi: 10.1083/jcb.201601099.

Muscat, C. C. *et al.* (2015) 'Kinetochore-independent chromosome segregation driven by lateral microtubule bundles', *eLife*, 4(MAY), pp. 1–53. doi: 10.7554/eLife.06462.

Nahaboo, W. *et al.* (2015) 'Chromatids segregate without centrosomes during Caenorhabditis elegans mitosis in a Ran- and CLASP-dependent manner', *Molecular Biology of the Cell*, 26(11), pp. 2020–2029. doi: 10.1091/mbc.E14-12-1577.

Nakamuta, S. *et al.* (2011) 'Local application of neurotrophins specifies axons through inositol 1,4,5-trisphosphate, calcium, and Ca2+/calmodulin-dependent protein kinases', *Science Signaling*, 4(199), p. ra76 LP-ra76. doi: 10.1126/scisignal.2002011.

Nakaya, M. A. *et al.* (2000) 'Meiotic maturation induces animal-vegetal asymmetric distribution of aPKC and ASIP/PAR-3 in Xenopus oocytes', *Development*, 127(23), pp. 5021–5031. doi: 10.1242/dev.127.23.5021.

Nakayama, Y. *et al.* (2009) 'Dynamin Participates in the Maintenance of Anterior Polarity in the Caenorhabditis elegans Embryo', *Developmental Cell*, 16(6), pp. 889–900. doi: 10.1016/j.devcel.2009.04.009.

Nance, J., Munro, E. M. and Priess, J. R. (2003) 'C. elegans PAR-3 and PAR-6 are required for apicobasal asymmetries associated with cell adhesion and gastrulation', *Development*, 130(22), pp. 5339–5350. doi: 10.1242/dev.00735.

Nashchekin, D., Fernandes, A. R. and St Johnston, D. (2016) 'Patronin/Shot Cortical Foci Assemble the Noncentrosomal Microtubule Array that Specifies the Drosophila Anterior-Posterior Axis', *Developmental Cell*, 38(1), pp. 61–72. doi: 10.1016/J.DEVCEL.2016.06.010.

Naumanen, P., Lappalainen, P. and Hotulainen, P. (2008) 'Mechanisms of actin stress fibre assembly', *Journal of Microscopy*, 231(3), pp. 446–454. doi: 10.1111/j.1365-2818.2008.02057.x.

Nayal, A. *et al.* (2006) 'Paxillin phosphorylation at Ser273 localizes a GIT1-PIX-PAK complex and regulates adhesion and protrusion dynamics', *Journal of Cell Biology*, 173(4), pp. 587–599. doi: 10.1083/jcb.200509075.

Nguyen-Ngoc, T., Afshar, K. and Gönczy, P. (2007) 'Coupling of cortical dynein and G alpha proteins mediates spindle positioning in Caenorhabditis elegans.', *Nature cell biology*, 9(11), pp. 1294–302. doi: 10.1038/ncb1649.

Nguyen, P. A. *et al.* (2014) 'Spatial organization of cytokinesis signaling reconstituted in a cell-free system', *Science*, 346(6206), pp. 244–247. doi: 10.1126/science.1256773.

Nguyen, P. A., Field, C. M. and Mitchison, T. J. (2018) 'Prc1E and Kif4A control microtubule

organization within and between large Xenopus egg asters', *Molecular Biology of the Cell*, 29(3), pp. 304–316. doi: 10.1091/mbc.E17-09-0540.

Nicklas, R. B. (1983) 'Measurements of the force produced by the mitotic spindle in anaphase', *Journal of Cell Biology*, 97(2), pp. 542–548. doi: 10.1083/jcb.97.2.542.

Nishi, Y. *et al.* (2008) 'Polo kinases regulate C. elegans embryonic polarity via binding to DYRK2-primed MEX-5 and MEX-6', *Development*, 135(4), pp. 687–697. doi: 10.1242/dev.013425.

Nishimura, T. *et al.* (2004) 'Role of the PAR-3-KIF3 complex in the establishment of neuronal polarity', *Nature Cell Biology*, 6(4), pp. 328–334. doi: 10.1038/ncb1118.

Nishimura, Y. *et al.* (2012) 'Automated screening of microtubule growth dynamics identifies MARK2 as a regulator of leading edge microtubules downstream of RAC1 in migrating cells', *PLoS ONE*, 7(7), p. e41413. doi: 10.1371/journal.pone.0041413.

Nishimura, Y. and Yonemura, S. (2006) 'Centralspindlin regulates ECT2 and RhoA accumulation at the equatorial cortex during cytokinesis', *Journal of Cell Science*, 119(1), pp. 104–114. doi: 10.1242/jcs.02737.

Nogales, E. *et al.* (1998) 'Tubulin and FtsZ form a distinct family of GTPases', *Nature Structural Biology*, 5(6), pp. 451–458. doi: 10.1038/nsb0698-451.

Nogales, E. *et al.* (1999) 'High-resolution model of the microtubule', *Cell*, 96(1), pp. 79–88. doi: 10.1016/S0092-8674(00)80961-7.

Nogales, E. and Wang, H.-W. (2006) 'Structural intermediates in microtubule assembly and disassembly: how and why?', *Current Opinion in Cell Biology*, 18(2), pp. 179–184. doi: https://doi.org/10.1016/j.ceb.2006.02.009.

Nogales, E., Wolf, S. G. and Downing, K. H. (1998) 'Erratum: Structure of the αβ tubulin dimer by electron crystallography', *Nature*, 393(6681), p. 191. doi: 10.1038/30288.

Nunes, V. *et al.* (2020) 'Centrosome-nuclear axis repositioning drives the assembly of a bipolar spindle scaffold to ensure mitotic fidelity', *Molecular Biology of the Cell*, 31(16), pp. 1675–1690. doi: 10.1091/mbc.E20-01-0047.

O'Connell, K. F., Leys, C. M. and White, J. G. (1998) 'A genetic screen for temperature-sensitive cell-division mutants of Caenorhabditis elegans', *Genetics*, 149(3), pp. 1303–1321. doi: 10.1093/genetics/149.3.1303.

O'Connell, K. F., Maxwell, K. N. and White, J. O. (2000) 'The spd-2 gene is required for polarization of the anteroposterior axis and formation of the sperm asters in the Caenorhabditis elegans zygote', *Developmental Biology*, 222(1), pp. 55–70. doi: 10.1006/dbio.2000.9714.

O'Rourke, S. M., Christensen, S. N. and Bowerman, B. (2010) 'Caenorhabditis elegans EFA-6 limits microtubule growth at the cell cortex', *Nature Cell Biology*, 12(12), pp. 1235–1241. doi:

10.1038/ncb2128.

Oakley, B. R., Paolillo, V. and Zheng, Y. (2015) 'Γ-Tubulin Complexes in Microtubule Nucleation and Beyond', *Molecular Biology of the Cell*, 26(17), pp. 2957–2962. doi: 10.1091/mbc.E14-11-1514.

Ogawa, T. *et al.* (2004) 'A Common Mechanism for Microtubule Destabilizers—M Type Kinesins Stabilize Curling of the Protofilament Using the Class-Specific Neck and Loops', *Cell*, 116(4), pp. 591–602. doi: https://doi.org/10.1016/S0092-8674(04)00129-1.

Okumura, M. *et al.* (2018) 'Dynein–dynactin–NuMA clusters generate cortical spindle-pulling forces as a multiarm ensemble', *eLife*, 7. doi: 10.7554/eLife.36559.

Pacquelet, A. *et al.* (2015) 'PAR-4 and anillin regulate myosin to coordinate spindle and furrow position during asymmetric division', *Journal of Cell Biology*, 210(7), pp. 1085–1099. doi: 10.1083/jcb.201503006.

Padmanabhan, A., Ong, H. T. and Zaidel-Bar, R. (2017) 'Non-junctional E-Cadherin Clusters Regulate the Actomyosin Cortex in the C. elegans Zygote', *Current Biology*, 27(1), pp. 103–112. doi: 10.1016/j.cub.2016.10.032.

Pamula, M. C. *et al.* (2019) 'High-resolution imaging reveals how the spindle midzone impacts chromosome movement', *Journal of Cell Biology*, 218(8), pp. 2529–2544. doi: 10.1083/jcb.201904169.

Panbianco, C. *et al.* (2008) 'A Casein Kinase 1 and PAR Proteins Regulate Asymmetry of a PIP2 Synthesis Enzyme for Asymmetric Spindle Positioning', *Developmental Cell*, 15(2), pp. 198–208. doi: 10.1016/j.devcel.2008.06.002.

Panzica, M. T. *et al.* (2017) 'F-actin prevents interaction between sperm DNA and the oocyte meiotic spindle in C. elegans', *Journal of Cell Biology*, 216(8), pp. 2273–2282. doi: 10.1083/jcb.201702020.

Park, D. H. and Rose, L. S. (2008) 'Dynamic localization of LIN-5 and GPR-1/2 to cortical force generation domains during spindle positioning', *Developmental Biology*, 315(1), pp. 42–54. doi: 10.1016/j.ydbio.2007.11.037.

Pavlova, G. A. *et al.* (2019) 'The role of Patronin in Drosophila mitosis', *BMC Molecular and Cell Biology*, 20(Suppl 1), p. 7. doi: 10.1186/s12860-019-0189-0.

Pazour, G. J., Wilkerson, C. G. and Witman, G. B. (1998) 'A dynein light chain is essential for the retrograde particle movement of intraflagellar transport (IFT)', *Journal of Cell Biology*, 141(4), pp. 979–992. doi: 10.1083/jcb.141.4.979.

Pegtel, D. M. *et al.* (2007) 'The Par-Tiam1 Complex Controls Persistent Migration by Stabilizing Microtubule-Dependent Front-Rear Polarity', *Current Biology*, 17(19), pp. 1623–1634. doi: 10.1016/j.cub.2007.08.035.

Pelisch, F. *et al.* (2017) 'A SUMO-Dependent Protein Network Regulates Chromosome Congression during Oocyte Meiosis', *Molecular Cell*, 65(1), pp. 66–77. doi: 10.1016/j.molcel.2016.11.001.

Peretti, D. *et al.* (2000) 'Evidence for the involvement of KIF4 in the anterograde transport of L1- containing vesicles', *Journal of Cell Biology*, 149(1), pp. 141–152. doi: 10.1083/jcb.149.1.141.

Petry, S. *et al.* (2013) 'Branching microtubule nucleation in xenopus egg extracts mediated by augmin and TPX2', *Cell*, 152(4), pp. 768–777. doi: 10.1016/j.cell.2012.12.044.

Piel, M. and Tran, P. T. (2009) 'Cell Shape and Cell Division in Fission Yeast', *Current Biology*, 19(17), pp. R823–R827. doi: 10.1016/j.cub.2009.08.012.

Pilling, A. D. *et al.* (2006) 'Kinesin-1 and Dynein Are the Primary Motors for Fast Transport of Mitochondria in Drosophila Motor Axons', *Molecular Biology of the Cell*, 17(4), pp. 2057–2068. doi: 10.1091/mbc.e05-06-0526.

Pimenta-Marques, A. and Bettencourt-Dias, M. (2020) 'Pericentriolar material', *Current Biology*, 30(12), pp. R687–R689. doi: 10.1016/j.cub.2020.04.064.

Portegijs, V. *et al.* (2016) 'Multisite Phosphorylation of NuMA-Related LIN-5 Controls Mitotic Spindle Positioning in C. elegans', *PLoS Genetics*, 12(10), p. e1006291. doi: 10.1371/journal.pgen.1006291.

Powers, J. *et al.* (2004) 'Loss of KLP-19 polar ejection force causes misorientation and missegregation of holocentric chromosomes', *Journal of Cell Biology*, 166(7), pp. 991–1001. doi: 10.1083/jcb.200403036.

Prigozhina, N. L. and Waterman-Storer, C. M. (2004) 'Protein Kinase D-Mediated Anterograde Membrane Trafficking Is Required for Fibroblast Motility', *Current Biology*, 14(2), pp. 88–98. doi: https://doi.org/10.1016/j.cub.2004.01.003.

Pring, M. *et al.* (2003) 'Mechanism of formin-induced nucleation of actin filaments', *Biochemistry*, 42(2), pp. 486–496. doi: 10.1021/bi026520j.

Prosser, S. L. and Pelletier, L. (2017) 'Mitotic spindle assembly in animal cells: A fine balancing act', *Nature Reviews Molecular Cell Biology*. Nature Publishing Group, pp. 187–201. doi: 10.1038/nrm.2016.162.

Putnam, A. *et al.* (2019) 'A gel phase promotes condensation of liquid P granules in Caenorhabditis elegans embryos', *Nature Structural and Molecular Biology*, 26(3), pp. 220–226. doi: 10.1038/s41594-019-0193-2.

Raaijmakers, J. A. *et al.* (2012) 'Nuclear envelope-associated dynein drives prophase centrosome separation and enables Eg5-independent bipolar spindle formation', *EMBO Journal*, 31(21), pp. 4179–4190. doi: 10.1038/emboj.2012.272.

Raman, R., Pinto, C. S. and Sonawane, M. (2018) 'Polarized Organization of the Cytoskeleton: Regulation by Cell Polarity Proteins', *Journal of Molecular Biology*, 430(19), pp. 3565–3584. doi: https://doi.org/10.1016/j.jmb.2018.06.028.

Ramanathan, S. P. *et al.* (2015) 'Cdk1-dependent mitotic enrichment of cortical myosin II promotes cell rounding against confinement', *Nature Cell Biology*, 17(2), pp. 148–159. doi: 10.1038/ncb3098.

Ramanujam, R. *et al.* (2018) 'Establishment of the PAR-1 cortical gradient by the aPKC-PRBH circuit', *Nature Chemical Biology*, 14(10), pp. 917–927. doi: 10.1038/s41589-018-0117-1.

Rappleye, C. A. *et al.* (2002) 'The anaphase-promoting complex and separin are required for embryonic anterior-posterior axis formation', *Developmental Cell*, 2(2), pp. 195–206. doi: 10.1016/S1534-5807(02)00114-4.

Rashid, A. *et al.* (2020) 'Inhibition of polo-like kinase 1 suppresses microtubule dynamics in MCF-7 cells', *Molecular and Cellular Biochemistry*, 465(1), pp. 27–36. doi: 10.1007/s11010-019-03664-y.

Rebollo, E. *et al.* (2007) 'Functionally Unequal Centrosomes Drive Spindle Orientation in Asymmetrically Dividing Drosophila Neural Stem Cells', *Developmental Cell*, 12(3), pp. 467–474. doi: 10.1016/j.devcel.2007.01.021.

Redemann, S. *et al.* (2010) 'Membrane invaginations reveal cortical sites that pull on mitotic spindles in one-cell C. elegans embryos', *PLoS ONE*, 5(8), p. e12301. doi: 10.1371/journal.pone.0012301.

Reich, J. D. *et al.* (2019) 'Regulated Activation of the PAR Polarity Network Ensures a Timely and Specific Response to Spatial Cues', *Current Biology*, 29(12), pp. 1911-1923.e5. doi: 10.1016/j.cub.2019.04.058.

Reichmann, J. *et al.* (2018) 'Dual-spindle formation in zygotes keeps parental genomes apart in early mammalian embryos', *Science*, 361(6398), pp. 189–193. doi: 10.1126/science.aar7462.

Ren, X. D., Kiosses, W. B. and Schwartz, M. A. (1999) 'Regulation of the small GTP-binding protein Rho by cell adhesion and the cytoskeleton', *EMBO Journal*, 18(3), pp. 578–585. doi: 10.1093/emboj/18.3.578.

Ren, Y. *et al.* (1998) 'Cloning and characterization of GEF-H1, a microtubule-associated guanine nucleotide exchange factor for Rac and Rho GTPases', *Journal of Biological Chemistry*, 273(52), pp. 34954–34960. doi: 10.1074/jbc.273.52.34954.

Reya, T. *et al.* (2001) 'Stem cells, cancer, and cancer stem cells', *Nature*, 414(6859), pp. 105–111. doi: 10.1038/35102167.

Reymann, A. C. *et al.* (2016) 'Cortical flow aligns actin filaments to form a furrow', *eLife*. Edited by P. Lappalainen, 5(OCTOBER2016), p. e17807. doi: 10.7554/eLife.17807.

Ridley, A. J. *et al.* (2003) 'Cell Migration: Integrating Signals from Front to Back', *Science*, 302(5651), pp. 1704–1709. doi: 10.1126/science.1092053.

Rivers, D. M. *et al.* (2008) 'PAR proteins direct asymmetry of the cell cycle regulators Polo-like kinase and Cdc25', *Journal of Cell Biology*, 180(5), pp. 877–885. doi: 10.1083/jcb.200710018.

Rizvi, S. A. *et al.* (2009) 'Identification and Characterization of a Small Molecule Inhibitor of Formin-Mediated Actin Assembly', *Chemistry and Biology*, 16(11), pp. 1158–1168. doi: 10.1016/j.chembiol.2009.10.006.

Robin, F. B. *et al.* (2014) 'Single-molecule analysis of cell surface dynamics in Caenorhabditis elegans embryos', *Nature Methods*, 11(6), pp. 677–682. doi: 10.1038/nmeth.2928.

Roca-Cusachs, P., Sunyer, R. and Trepat, X. (2013) 'Mechanical guidance of cell migration: Lessons from chemotaxis', *Current Opinion in Cell Biology*, 25(5), pp. 543–549. doi: 10.1016/j.ceb.2013.04.010.

Rodriguez-Garcia, R. *et al.* (2018) 'The polarity-induced force imbalance in Caenorhabditis elegans embryos is caused by asymmetric binding rates of dynein to the cortex', *Molecular Biology of the Cell*, 29(26), pp. 3093–3104. doi: 10.1091/mbc.E17-11-0653.

Rodriguez, J. *et al.* (2017) 'aPKC Cycles between Functionally Distinct PAR Protein Assemblies to Drive Cell Polarity', *Developmental Cell*, 42(4), pp. 400-415.e9. doi: 10.1016/j.devcel.2017.07.007.

Rohatgi, R., Ho, H. Y. H. and Kirschner, M. W. (2000) 'Mechanism of N-WASP activation by CDC42 and phosphatidylinositol 4,5-bisphosphate', *Journal of Cell Biology*, 150(6), pp. 1299–1309. doi: 10.1083/jcb.150.6.1299.

Rooney, C. *et al.* (2010) 'The Rac activator STEF (Tiam2) regulates cell migration by microtubule-mediated focal adhesion disassembly', *EMBO Reports*, 11(4), pp. 292–298. doi: 10.1038/embor.2010.10.

Roos, J. *et al.* (2000) 'Drosophila Futsch regulates synaptic microtubule organization and is necessary for synaptic growth', *Neuron*, 26(2), pp. 371–382. doi: 10.1016/S0896-6273(00)81170-8.

Rose, L. and Gönczy, P. (2014) 'Polarity establishment, asymmetric division and segregation of fate determinants in early C. elegans embryos', *WormBook : the online review of C. elegans biology*, pp. 1–43. doi: 10.1895/wormbook.1.30.2.

Rose, L. S. *et al.* (1995) 'Pseudocleavage Is Dispensable for Polarity and Development in C. elegans Embryos', *Developmental Biology*, 168(2), pp. 479–489. doi: 10.1006/dbio.1995.1096.

Rosenblatt, J. *et al.* (2004) 'Myosin II-dependent cortical movement is required for centrosome separation and positioning during mitotic spindle assembly', *Cell*, 117(3), pp. 361–372. doi: 10.1016/S0092-8674(04)00341-1.

Rotty, J. D. and Bear, J. E. (2014) 'Competition and collaboration between different actin assembly pathways allows for homeostatic control of the actin cytoskeleton', *BioArchitecture*. 2015/10/02, 5(1–2), pp. 27–34. doi: 10.1080/19490992.2015.1090670.
Ruane, P. T. *et al.* (2016) 'Tumour Suppressor Adenomatous Polyposis Coli (APC) localisation is regulated by both Kinesin-1 and Kinesin-2', *Scientific Reports*, 6(1), p. 27456. doi: 10.1038/srep27456.

Ruiz-Canada, C. *et al.* (2004) 'New synaptic bouton formation is disrupted by misregulation of microtubule stability in aPKC mutants', *Neuron*, 42(4), pp. 567–580. doi: 10.1016/s0896-6273(04)00255-7.

Rusan, N. M. and Peifer, M. (2007) 'A role for a novel centrosome cycle in asymmetric cell division', *Journal of Cell Biology*, 177(1), pp. 13–20. doi: 10.1083/jcb.200612140.

Sadler, P. L. and Shakes, D. C. (2000) 'Anucleate Caenorhabditis elegans sperm can crawl, fertilize oocytes and direct anterior-posterior polarization of the I-cell embryo', *Development*, 127(2), pp. 355–366. Available at: http://dev.biologists.org/content/127/2/355.abstract.

Sailer, A. *et al.* (2015) 'Dynamic Opposition of Clustered Proteins Stabilizes Cortical Polarity in the C. elegans Zygote', *Developmental Cell*, 35(1), pp. 131–142. doi: 10.1016/j.devcel.2015.09.006.

Sana, S. *et al.* (2018) 'Plk1 regulates spindle orientation by phosphorylating NuMA in human cells', *Life Science Alliance*, 1(6), p. e201800223. doi: 10.26508/lsa.201800223.

Sastre-Perona, A., Hoang-Phou, S. and Schober, M. (2019) 'Self-renewal and differentiation in squamous cell carcinomas', *Aging*. 2019/10/18, 11(20), pp. 8736–8738. doi: 10.18632/aging.102381.

Saturno, D. M. *et al.* (2017) 'Sustained centrosome-cortical contact ensures robust polarization of the one-cell C. elegans embryo', *Developmental Biology*, 422(2), pp. 135–145. doi: 10.1016/j.ydbio.2016.12.025.

Saunders, A. M. *et al.* (2007) 'Kinesin-5 acts as a brake in anaphase spindle elongation', *Current Biology*. Elsevier, pp. R453-4. doi: 10.1016/j.cub.2007.05.001.

Saxton, W. M. and McIntosh, J. R. (1987) 'Interzone microtubule behavior in late anaphase and telophase spindles', *Journal of Cell Biology*, 105(2), pp. 875–886. doi: 10.1083/jcb.105.2.875.

Schaefer, M. *et al.* (2000) 'A protein complex containing inscuteable and the Gα-binding protein pins orients asymmetric cell divisions in Drosophila', *Current Biology*, 10(7), pp. 353–362. doi: 10.1016/S0960-9822(00)00401-2.

Schaefer, M. *et al.* (2001) 'Heterotrimeric G proteins direct two modes of asymmetric cell division in the Drosophila nervous system', *Cell*, 107(2), pp. 183–194. doi: 10.1016/S0092-8674(01)00521-9.

Scheffler, K. *et al.* (2021) 'Two mechanisms drive pronuclear migration in mouse zygotes', *Nature Communications*, 12(1), p. 841. doi: 10.1038/s41467-021-21020-x.

Schenk, C. *et al.* (2010) 'Cortical domain correction repositions the polarity boundary to match the cytokinesis furrow in C. elegans embryos', *Development*, 137(10), pp. 1743–1753. doi: 10.1242/dev.040436.

Schmidt, D. J. *et al.* (2005) 'Functional analysis of cytoplasmic dynein heavy chain in Caenorhabditis elegans with fast-acting temperature-sensitive mutations', *Molecular Biology of the Cell*, 16(3), pp. 1200–1212. doi: 10.1091/mbc.E04-06-0523.

Schmidt, R. *et al.* (2017) 'Two populations of cytoplasmic dynein contribute to spindle positioning in C. elegans embryos', *Journal of Cell Biology*, 216(9), pp. 2777–2793. doi: 10.1083/jcb.201607038.

Schmoranzer, J. *et al.* (2009) 'Par3 and Dynein Associate to Regulate Local Microtubule Dynamics and Centrosome Orientation during Migration', *Current Biology*, 19(13), pp. 1065–1074. doi: 10.1016/j.cub.2009.05.065.

Schmoranzer, J. and Simon, S. M. (2003) 'Role of microtubules in fusion of post-Golgi vesicles to the plasma membrane', *Molecular Biology of the Cell*, 14(4), pp. 1558–1569. doi: 10.1091/mbc.E02-08-0500.

Schnapp, B. J. and Reese, T. S. (1989) 'Dynein is the motor for retrograde axonal transport of organelles', *Proceedings of the National Academy of Sciences of the United States of America*, 86(5), pp. 1548–1552. doi: 10.1073/pnas.86.5.1548.

Schober, M., Schaefer, M. and Knoblich, J. A. (1999) 'Bazooka recruits inscuteable to orient asymmetric cell divisions in Drosophila neuroblasts', *Nature*, 402(6761), pp. 548–551. doi: 10.1038/990135.

Schonegg, S. (2006) 'CDC-42 and RHO-1 coordinate acto-myosin contractility and PAR protein localization during polarity establishment in C. elegans embryos', *Development*, 133(18), pp. 3507–3516. doi: 10.1242/dev.02527.

Schonegg, S. *et al.* (2007) 'The Rho GTPase-activating proteins RGA-3 and RGA-4 are required to set the initial size of PAR domains in Caenorhabditis elegans one-cell embryos', *Proceedings of the National Academy of Sciences of the United States of America*, 104(38), pp. 14976–14981. doi: 10.1073/pnas.0706941104.

Schubert, C. M. *et al.* (2000) 'MEX-5 and MEX-6 function to establish soma/germline asymmetry in early C. elegans embryos', *Molecular Cell*, 5(4), pp. 671–682. doi: 10.1016/S1097-2765(00)80246-4.

Schwalbe, M. *et al.* (2013) 'Phosphorylation of human tau protein by microtubule affinity-regulating kinase 2', *Biochemistry*, 52(50), pp. 9068–9079. doi: 10.1021/bi401266n.

Schwamborn, J. C. and Püschel, A. W. (2004) 'The sequential activity of the GTPases Rap1B and Cdc42 determines neuronal polarity', *Nature Neuroscience*, 7(9), pp. 923–929. doi: 10.1038/nn1295.

Sekine, Y. *et al.* (1994) 'A novel microtubule-based motor protein (KIF4) for organelle transports, whose expression is regulated developmentally', *Journal of Cell Biology*, 127(1), pp. 187–201. doi: 10.1083/jcb.127.1.187.

Seldin, L., Muroyama, A. and Lechler, T. (2016) 'NuMA-microtubule interactions are critical for spindle orientation and the morphogenesis of diverse epidermal structures', *eLife*. Edited by Y. M. Yamashita, 5, p. e12504. doi: 10.7554/elife.12504.

Sept, D. and McCammon, J. A. (2001) 'Thermodynamics and kinetics of actin filament nucleation', *Biophysical Journal*, 81(2), pp. 667–674. doi: 10.1016/S0006-3495(01)75731-1.

Seydoux, G. (2018) 'The P Granules of C. elegans: A Genetic Model for the Study of RNA–Protein Condensates', *Journal of Molecular Biology*, 430(23), pp. 4702–4710. doi: 10.1016/j.jmb.2018.08.007.

Shaye, D. D. and Greenwald, I. (2011) 'OrthoList: A Compendium of C. elegans Genes with Human Orthologs', *PLoS ONE*. Edited by K. M. Iijima, 6(5), p. e20085. doi: 10.1371/journal.pone.0020085.

Shelly, M. *et al.* (2010) 'Local and long-range reciprocal regulation of cAMP and cGMP in axon/dendrite formation', *Science*, 327(5965), pp. 547–552. doi: 10.1126/science.1179735.

Shelton, C. A. *et al.* (1999) 'The Nonmuscle Myosin Regulatory Light Chain Gene mlc-4 Is Required for Cytokinesis, Anterior-Posterior Polarity, and Body Morphology during Caenorhabditis elegans Embryogenesis', *Journal of Cell Biology*, 146(2), pp. 439–451. doi: 10.1083/jcb.146.2.439.

Shi, Q. *et al.* (2019) 'Tubulin polymerization promoting protein, ringmaker, and MAP1B homolog futsch coordinate microtubule organization and synaptic growth', *Frontiers in Cellular Neuroscience*, p. 192. doi: 10.3389/fncel.2019.00192.

Shi, S. H. *et al.* (2004) 'APC and GSK-3β are involved in mPar3 targeting to the nascent axon and establishment of neuronal polarity', *Current Biology*, 14(22), pp. 2025–2032. doi: 10.1016/j.cub.2004.11.009.

Shi, S. H., Jan, L. Y. and Jan, Y. N. (2003) 'Hippocampal neuronal polarity specified by spatially localized mPar3/mPar6 and PI 3-kinase activity', *Cell*. Cell Press, pp. 63–75. doi: 10.1016/S0092-8674(02)01249-7.

Siegrist, S. E. and Doe, C. Q. (2005) 'Microtubule-induced pins/Gαi cortical polarity in Drosophila neuroblasts', *Cell*, 123(7), pp. 1323–1335. doi: 10.1016/j.cell.2005.09.043.

Siegrist, S. E. and Doe, C. Q. (2007) 'Microtubule-induced cortical cell polarity', *Genes and Development*, 21(5), pp. 483–496. doi: 10.1101/gad.1511207.

Silkworth, W. T. and Cimini, D. (2012) 'Transient defects of mitotic spindle geometry and chromosome segregation errors', *Cell Division*, 7(1), p. 19. doi: 10.1186/1747-1028-7-19.

Siller, K. H., Cabernard, C. and Doe, C. Q. (2006) 'The NuMA-related Mud protein binds Pins and regulates spindle orientation in Drosophila neuroblasts', *Nature Cell Biology*, 8(6), pp. 594–600. doi: 10.1038/ncb1412.

De Simone, A. (2016) *Mechanisms of centrosome separation in C. elegans*. EPFL PP - Lausanne. doi: 10.5075/epfl-thesis-6916.

De Simone, A. *et al.* (2018) 'Uncovering the balance of forces driving microtubule aster migration in C. Elegans zygotes', *Nature Communications*, 9(1), p. 938. doi: 10.1038/s41467-018-03118-x.

De Simone, A. and Gönczy, P. (2017) 'Computer simulations reveal mechanisms that organize nuclear dynein forces to separate centrosomes', *Molecular Biology of the Cell*, 28(23), pp. 3165–3170. doi: 10.1091/mbc.E16-12-0823.

De Simone, A., Nédélec, F. and Gönczy, P. (2016) 'Dynein Transmits Polarized Actomyosin Cortical Flows to Promote Centrosome Separation', *Cell Reports*, 14(9), pp. 2250–2262. doi: 10.1016/j.celrep.2016.01.077.

Singhvi, A. *et al.* (2011) 'The arf GAP CNT-2 regulates the apoptotic fate in C. elegans asymmetric neuroblast divisions', *Current Biology*, 21(11), pp. 948–954. doi: 10.1016/j.cub.2011.04.025.

Small, J. V. *et al.* (2002) 'The lamellipodium: Where motility begins', *Trends in Cell Biology*, 12(3), pp. 112–120. doi: 10.1016/S0962-8924(01)02237-1.

Small, L. E. and Dawes, A. T. (2017) 'PAR proteins regulate maintenance-phase myosin dynamics during Caenorhabditis elegans zygote polarization', *Molecular Biology of the Cell*, 28(16), pp. 2220–2231. doi: 10.1091/mbc.E16-04-0263.

Smith, J. *et al.* (2016) 'Spatial patterning of P granules by RNA-induced phase separation of the intrinsically-disordered protein MEG-3', *eLife*. Edited by J. Ahringer, 5(DECEMBER2016), p. e21337. doi: 10.7554/eLife.21337.

Sontag, J. M. *et al.* (2012) 'The protein phosphatase PP2A/Bα binds to the microtubule-associated proteins Tau and MAP2 at a motif also recognized by the kinase Fyn: Implications for tauopathies', *Journal of Biological Chemistry*, 287(18), pp. 14984–14993. doi: 10.1074/jbc.M111.338681.

Splinter, D. *et al.* (2010) 'Bicaudal D2, dynein, and kinesin-1 associate with nuclear pore complexes and regulate centrosome and nuclear positioning during mitotic entry', *PLoS Biology*, 8(4), p. e1000350. doi: 10.1371/journal.pbio.1000350.

Srayko, M. *et al.* (2005) 'Identification and characterization of factors required for microtubule

growth and nucleation in the early C. elegans embryo', *Developmental Cell*, 9(2), pp. 223–236. doi: 10.1016/j.devcel.2005.07.003.

Srinivasan, D. G. *et al.* (2003) 'A complex of LIN-5 and GPR proteins regulates G protein signaling and spindle function in C. elegans', *Genes and Development*, 17(10), pp. 1225–1239. doi: 10.1101/gad.1081203.

Stepanova, T. *et al.* (2003) 'Visualization of microtubule growth in cultured neurons via the use of EB3-GFP (end-binding protein 3-green fluorescent protein)', *J Neurosci*, 23.

Stone, M. C., Roegiers, F. and Rolls, M. M. (2008) 'Microtubules have opposite orientation in axons and dendrites of Drosophila neurons', *Molecular Biology of the Cell*, 19(10), pp. 4122–4129. doi: 10.1091/mbc.E07-10-1079.

Strome, S. (1986) 'Fluorescence visualization of the distribution of microfilaments in gonads and early embryos of the nematode caenorhabditis elegans', *Journal of Cell Biology*, 103(6), pp. 2241–2252. doi: 10.1083/jcb.103.6.2241.

Strome, S. *et al.* (2001) 'Spindle dynamics and the role of γ-tubulin in early Caenorhabditis elegans embryos', *Molecular Biology of the Cell*, 12(6), pp. 1751–1764. doi: 10.1091/mbc.12.6.1751.

Strome, S. and Updike, D. (2015) 'Specifying and protecting germ cell fate', *Nature Reviews Molecular Cell Biology*, 16(7), pp. 406–416. doi: 10.1038/nrm4009.

Strothman, C. *et al.* (2019) 'Microtubule minus-end stability is dictated by the tubulin off-rate', *Journal of Cell Biology*, 218(9), pp. 2841–2853. doi: 10.1083/JCB.201905019.

Stumpff, J. *et al.* (2012) 'Kif18A and Chromokinesins Confine Centromere Movements via Microtubule Growth Suppression and Spatial Control of Kinetochore Tension', *Developmental Cell*, 22(5), pp. 1017–1029. doi: 10.1016/j.devcel.2012.02.013.

Subramanian, R. *et al.* (2010) 'Insights into antiparallel microtubule crosslinking by PRC1, a conserved nonmotor microtubule binding protein', *Cell*, 142(3), pp. 433–443. doi: 10.1016/j.cell.2010.07.012.

Subramanian, R. *et al.* (2013) 'Marking and measuring single microtubules by PRC1 and kinesin-4', *Cell*, 154(2), p. 377. doi: 10.1016/j.cell.2013.06.021.

Sugioka, K. *et al.* (2018) 'Tumor suppressor APC is an attenuator of spindle-pulling forces during C. elegans asymmetric cell division', *Proceedings of the National Academy of Sciences of the United States of America*, 115(5), pp. E954–E963. doi: 10.1073/pnas.1712052115.

Sulston, J. E. *et al.* (1983) 'The embryonic cell lineage of the nematode Caenorhabditis elegans', *Developmental Biology*, 100(1), pp. 64–119. doi: 10.1016/0012-1606(83)90201-4.

Sumi, T. *et al.* (1999) 'Cofilin phosphorylation and actin cytoskeletal dynamics regulated by Rho- and Cdc42-activated LIM-kinase 2', *Journal of Cell Biology*, 147(7), pp. 1519–1532. doi:

10.1083/jcb.147.7.1519.

Suraneni, P. *et al.* (2012) 'The Arp2/3 complex is required for lamellipodia extension and directional fibroblast cell migration', *Journal of Cell Biology*. 2012/04/09, 197(2), pp. 239–251. doi: 10.1083/jcb.201112113.

Suzuki, A. *et al.* (2001) 'Atypical protein kinase C is involved in the evolutionarily conserved par protein complex and plays a critical role in establishing epithelia- specific junctional structures.', *J. Cell Biol.*, 152(6), pp. 1183–1196. doi: 10.1083/jcb.152.6.1183.

Suzuki, A. *et al.* (2016) 'How the kinetochore couples microtubule force and centromere stretch to move chromosomes', *Nature Cell Biology*, 18(4), pp. 382–392. doi: 10.1038/ncb3323.

Swaney, K. F. and Li, R. (2016) 'Function and regulation of the Arp2/3 complex during cell migration in diverse environments', *Current opinion in cell biology*. 2016/05/08, 42, pp. 63–72. doi: 10.1016/j.ceb.2016.04.005.

Tabuse, Y. *et al.* (1998) 'Atypical protein kinase C cooperates with PAR-3 to establish embryonic polarity in Caenorhabditis elegans.', *Development (Cambridge, England)*, 125(18), pp. 3607–3614. Available at: http://dev.biologists.org/content/125/18/3607.long (Accessed: 19 May 2017).

Takano, T. *et al.* (2017) 'Discovery of long-range inhibitory signaling to ensure single axon formation', *Nature Communications*, 8(1), p. 33. doi: 10.1038/s41467-017-00044-2.

Takano, T., Funahashi, Y. and Kaibuchi, K. (2019) 'Neuronal polarity: Positive and negative feedback signals', *Frontiers in Cell and Developmental Biology*, p. 69. doi: 10.3389/fcell.2019.00069.

Takata, H. *et al.* (2018) 'Cdk1-dependent phosphorylation of KIF4A at S1186 triggers lateral chromosome compaction during early mitosis', *PLoS ONE*, 13(12), p. e0209614. doi: 10.1371/journal.pone.0209614.

Takemura, R. *et al.* (1992) 'Increased microtubule stability and alpha tubulin acetylation in cells transfected with microtubule-associated proteins MAP1B, MAP2 or tau', *Journal of Cell Science*, 103(4), pp. 953–964. doi: 10.1242/jcs.103.4.953.

Tame, M. A. *et al.* (2014) 'Astral microtubules control redistribution of dynein at the cell cortex to facilitate spindle positioning', *Cell Cycle*, 13(7), pp. 1162–1170. doi: 10.4161/cc.28031.

Tanenbaum, M. E. *et al.* (2009) 'Kif15 Cooperates with Eg5 to Promote Bipolar Spindle Assembly', *Current Biology*, 19(20), pp. 1703–1711. doi: 10.1016/j.cub.2009.08.027.

Tanenbaum, M. E. and Medema, R. H. (2010) 'Mechanisms of Centrosome Separation and Bipolar Spindle Assembly', *Developmental Cell*, 19(6), pp. 797–806. doi: 10.1016/j.devcel.2010.11.011.

Tang, Y. *et al.* (1999) 'Cellular Motor Protein KIF-4 Associates with Retroviral Gag', *Journal of Virology*, 73(12), pp. 10508–10513. doi: 10.1128/jvi.73.12.10508-10513.1999.

Telley, I. A., Bieling, P. and Surrey, T. (2009) 'Obstacles on the microtubule reduce the processivity of kinesin-1 in a minimal in vitro system and in cell extract', *Biophysical Journal*, 96(8), pp. 3341–3353. doi: 10.1016/j.bpj.2009.01.015.

Tenlen, J. R. *et al.* (2008) 'MEX-5 asymmetry in one-cell C. elegans embryos requires PAR-4- and PAR-1-dependent phosphorylation', *Development*, 135(22), pp. 3665–3675. doi: 10.1242/dev.027060.

Tepass, U., Theres, C. and Knust, E. (1990) 'crumbs encodes an EGF-like protein expressed on apical membranes of Drosophila epithelial cells and required for organization of epithelia', *Cell*, 61(5), pp. 787–799. doi: 10.1016/0092-8674(90)90189-L.

Teuliere, J. *et al.* (2014) 'Asymmetric neuroblast divisions producing apoptotic cells require the cytohesin GRP-1 in caenorhabditis elegans', *Genetics*, 198(1), pp. 229–247. doi: 10.1534/genetics.114.167189.

Thaiparambil, J. T., Eggers, C. M. and Marcus, A. I. (2012) 'AMPK Regulates Mitotic Spindle Orientation through Phosphorylation of Myosin Regulatory Light Chain', *Molecular and Cellular Biology*, 32(16), pp. 3203–3217. doi: 10.1128/mcb.00418-12.

Thyagarajan, K., Afshar, K. and Gonczy, P. (2011) 'Polarity mediates asymmetric trafficking of the G heterotrimeric G-protein subunit GPB-1 in C. elegans embryos', *Development*, 138(13), pp. 2773–2782. doi: 10.1242/dev.063354.

Timm, T. *et al.* (2008) 'Glycogen Synthase Kinase (GSK) 3β directly phosphorylates serine 212 in the regulatory loop and inhibits microtubule affinity-regulating kinase (MARK) 2', *Journal of Biological Chemistry*, 283(27), pp. 18873–18882. doi: 10.1074/jbc.M706596200.

Tinevez, J.-Y. *et al.* (2017) 'TrackMate: An open and extensible platform for single-particle tracking', *Methods*, 115, pp. 80–90. doi: https://doi.org/10.1016/j.ymeth.2016.09.016.

Tissenbaum, H. A. (2015) 'Using C. elegans for aging research', *Invertebrate Reproduction and Development*, 59(sup1), pp. 59–63. doi: 10.1080/07924259.2014.940470.

Tivodar, S. *et al.* (2015) 'Rac-GTPases Regulate Microtubule Stability and Axon Growth of Cortical GABAergic Interneurons', *Cerebral Cortex*, 25(9), pp. 2370–2382. doi: 10.1093/cercor/bhu037.

Tojkander, S., Gateva, G. and Lappalainen, P. (2012) 'Actin stress fibers - Assembly, dynamics and biological roles', *Journal of Cell Science*, 125(8), pp. 1855–1864. doi: 10.1242/jcs.098087.

Tokai, N. *et al.* (1996) 'Kid, a novel kinesin-like DNA binding protein, is localized to chromosomes and the mitotic spindle.', *The EMBO journal*, 15(3), pp. 457–67. doi: 10.1002/j.1460-2075.1996.tb00378.x.

Tokunaga, M., Imamoto, N. and Sakata-Sogawa, K. (2008) 'Highly inclined thin illumination enables clear single-molecule imaging in cells', *Nature Methods*, 5(2), pp. 159–161. doi: 10.1038/nmeth1171.

Tomancak, P. *et al.* (2000) 'A Drosophila melanogaster homologue of Caenorhabditis elegans par-1 acts at an early step in embryonic-axis formation', *Nature Cell Biology*, 2(7), pp. 458–460. doi: 10.1038/35017101.

Tooley, J. G., Miller, S. A. and Stukenberg, P. T. (2011) 'The Ndc80 complex uses a tripartite attachment point to couple microtubule depolymerization to chromosome movement', *Molecular Biology of the Cell*. 2011/02/16, 22(8), pp. 1217–1226. doi: 10.1091/mbc.E10-07-0626.

Touré, A. *et al.* (2008) 'Phosphoregulation of MgcRacGAP in mitosis involves Aurora B and Cdk1 protein kinases and the PP2A phosphatase', *FEBS Letters*, 582(8), pp. 1182–1188. doi: https://doi.org/10.1016/j.febslet.2007.12.036.

Tran, P. T. *et al.* (2001) 'A mechanism for nuclear positioning in fission yeast based on microtubule pushing', *Journal of Cell Biology*, 153(2), pp. 397–411. doi: 10.1083/jcb.153.2.397.

Traweger, A. *et al.* (2008) 'Protein phosphatase 1 regulates the phosphorylation state of the polarity scaffold Par-3', *Proceedings of the National Academy of Sciences of the United States of America*, 105(30), pp. 10402–10407. doi: 10.1073/pnas.0804102105.

Tsai, M.-C. and Ahringer, J. (2007) 'Microtubules are involved in anterior-posterior axis formation in C. elegans embryos.', *The Journal of cell biology*, 179(3), pp. 397–402. doi: 10.1083/jcb.200708101.

Tsankova, A. *et al.* (2017) 'Cell Polarity Regulates Biased Myosin Activity and Dynamics during Asymmetric Cell Division via Drosophila Rho Kinase and Protein Kinase N', *Developmental Cell*, 42(2), pp. 143-155.e5. doi: 10.1016/j.devcel.2017.06.012.

Tse, Y. C. *et al.* (2012) 'RhoA activation during polarization and cytokinesis of the early Caenorhabditis elegans embryo is differentially dependent on NOP-1 and CYK-4', *Molecular Biology of the Cell*, 23(20), pp. 4020–4031. doi: 10.1091/mbc.E12-04-0268.

Tsou, M. F. B. *et al.* (2002) 'LET-99 determines spindle position and is asymmetrically enriched in response to PAR polarity cues in C. elegans embryos', *Development*, 129(19), pp. 4469–4481. doi: 10.1242/dev.129.19.4469.

Tsou, M. F. B., Hayashi, A. and Rose, L. S. (2003) 'Let-99 opposes Gα/GPR signaling to generate asymmetry for spindle positioning in response to PAR and MES-1/SRC-1 signaling', *Development*, 130(23), pp. 5717–5730. doi: 10.1242/dev.00790.

Turgay, Y. *et al.* (2014) 'SUN proteins facilitate the removal of membranes from chromatin during nuclear envelope breakdown', *Journal of Cell Biology*, 204(7), pp. 1099–1109. doi: 10.1083/jcb.201310116.

Updike, D. L. *et al.* (2014) 'Germ-granule components prevent somatic development in the C. elegans germline', *Current biology : CB*. 2014/04/17, 24(9), pp. 970–975. doi: 10.1016/j.cub.2014.03.015.

van der Vaart, B. *et al.* (2013) 'CFEOM1-associated kinesin KIF21A is a cortical microtubule growth inhibitor', *Developmental Cell*, 27(2), pp. 145–160. doi: 10.1016/j.devcel.2013.09.010.

Vanneste, D. *et al.* (2009) 'The Role of Hklp2 in the Stabilization and Maintenance of Spindle Bipolarity', *Current Biology*, 19(20), pp. 1712–1717. doi: 10.1016/j.cub.2009.09.019.

Vanneste, D., Ferreira, V. and Vernos, I. (2011) 'Chromokinesins: localization-dependent functions and regulation during cell division', *Biochemical Society Transactions*, 39(5), pp. 1154 LP – 1160. Available at: http://www.biochemsoctrans.org/content/39/5/1154.abstract.

Vasquez, C. G., Tworoger, M. and Martin, A. C. (2014) 'Dynamic myosin phosphorylation regulates contractile pulses and tissue integrity during epithelial morphogenesis', *Journal of Cell Biology*, 206(3), pp. 435–450. doi: 10.1083/jcb.201402004.

Veeman, M. T. and McDonald, J. A. (2016) 'Dynamics of cell polarity in tissue morphogenesis: a comparative view from Drosophila and Ciona', *F1000Research*, 5, p. F1000 Faculty Rev-1084. doi: 10.12688/f1000research.8011.1.

Velez-Aguilera, G. *et al.* (2020) 'PLK-1 promotes the merger of the parental genome into a single nucleus by triggering lamina disassembly', *eLife*. Edited by J. Pines, A. Akhmanova, and B. Burke, 9, p. e59510. doi: 10.7554/eLife.59510.

Vernos, I. *et al.* (1995) 'Xklp1 a chromosomal xenopus kinesin-like protein essential for spindle organization and chromosome positioning', *Cell*, 81(1), pp. 117–127. doi: 10.1016/0092-8674(95)90376-3.

Voets, E. *et al.* (2015) 'The lethal response to Cdk1 inhibition depends on sister chromatid alignment errors generated by KIF4 and isoform 1 of PRC1', *Scientific Reports*, 5, p. 14798. doi: 10.1038/srep14798.

Volkmann, N. *et al.* (2001) 'An atomic model of actin filaments cross-linked by fimbrin and its implications for bundle assembly and function', *Journal of Cell Biology*, 153(5), pp. 947–956. doi: 10.1083/jcb.153.5.947.

Volkov, V. A. *et al.* (2018) 'Multivalency of NDC80 in the outer kinetochore is essential to track shortening microtubules and generate forces', *eLife*. Edited by J. K. Tyler, 7, p. e36764. doi: 10.7554/eLife.36764.

De Vos, K. J. *et al.* (2003) 'Expression of phosphatidylinositol (4,5) bisphosphate-specific pleckstrin homology domains alters direction but not the level of axonal transport of mitochondria', *Molecular Biology of the Cell*, 14(9), pp. 3636–3649. doi: 10.1091/mbc.E02-10-0638.

Voutev, R. and Hubbard, E. J. A. (2008) 'A "FLP-out" system for controlled gene expression in

Caenorhabditis elegans', *Genetics*, 180(1), pp. 103–119. doi: 10.1534/genetics.108.090274.

Vukušić, K. *et al.* (2021) 'Microtubule-sliding modules based on kinesins EG5 and PRC1-dependent KIF4A drive human spindle elongation', *Developmental Cell*. doi: https://doi.org/10.1016/j.devcel.2021.04.005.

Wallenfang, M. R. and Seydoux, G. (2000) 'Polarization of the anterior-posterior axis of C. Elegans is a microtubule-directed process', *Nature*, 408(6808), pp. 89–92. doi: 10.1038/35040562.

Walther, R. F. and Pichaud, F. (2010) 'Crumbs/DaPKC-dependent apical exclusion of bazooka promotes photoreceptor polarity remodeling', *Current Biology*, 20(12), pp. 1065–1074. doi: 10.1016/j.cub.2010.04.049.

Wan, X. *et al.* (2009) 'Protein Architecture of the Human Kinetochore Microtubule Attachment Site', *Cell*, 137(4), pp. 672–684. doi: 10.1016/j.cell.2009.03.035.

Wandke, C. *et al.* (2012) 'Human chromokinesins promote chromosome congression and spindle microtubule dynamics during mitosis', *Journal of Cell Biology*, 198(5), pp. 847–863. doi: 10.1083/jcb.201110060.

Wang, H.-W. *et al.* (2007) 'Architecture of the Dam1 kinetochore ring complex and implications for microtubule-driven assembly and force-coupling mechanisms', *Nature Structural & Molecular Biology*, 14(8), pp. 721–726. doi: 10.1038/nsmb1274.

Wang, H. W. and Nogales, E. (2005) 'Nucleotide-dependent bending flexibility of tubulin regulates microtubule assembly', *Nature*, 435(7044), pp. 911–915. doi: 10.1038/nature03606.

Wang, S. *et al.* (2015) 'NOCA-1 functions with γ-tubulin and in parallel to Patronin to assemble non-centrosomal microtubule arrays in C. elegans', *eLife*, 4(September), p. e08649. doi: 10.7554/eLife.08649.

Wang, S. C. *et al.* (2017) 'Cortical forces and CDC-42 control clustering of PAR proteins for Caenorhabditis elegans embryonic polarization', *Nature Cell Biology*, 19(8), pp. 988–995. doi: 10.1038/ncb3577.

Wang, S. Z. and Adler, R. (1995) 'Chromokinesin: A DNA-binding, kinesin-like nuclear protein', *Journal of Cell Biology*, 128(5), pp. 761–768. doi: 10.1083/jcb.128.5.761.

Wang, W. *et al.* (2008) 'Centrosome separation driven by actin-microfilaments during mitosis is mediated by centrosome-associated tyrosine-phosphorylated cortactin', *Journal of Cell Science*, 121(8), pp. 1334–1343. doi: 10.1242/jcs.018176.

Watabe-Uchida, M. *et al.* (2006) 'The Rac Activator DOCK7 Regulates Neuronal Polarity through Local Phosphorylation of Stathmin/Op18', *Neuron*, 51(6), pp. 727–739. doi: 10.1016/j.neuron.2006.07.020.

Waterman-Storer, C. M. *et al.* (1999) 'Microtubule growth activates Rac1 to promote

lamellipodial protrusion in fibroblasts', *Nature Cell Biology*, 1(1), pp. 45–50. doi: 10.1038/9018.

Watts, J. L. *et al.* (1996) 'par-6, a gene involved in the establishment of asymmetry in early C. elegans embryos, mediates the asymmetric localization of PAR-3.', *Development (Cambridge, England)*, 122(10), pp. 3133–3140. Available at: http://dev.biologists.org/content/122/10/3133.long (Accessed: 19 May 2017).

Watts, J. L. and Ristow, M. (2017) 'Lipid and carbohydrate metabolism in Caenorhabditis elegans', *Genetics*, 207(2), pp. 413–446. doi: 10.1534/genetics.117.300106.

Welch, M. D., Iwamatsu, A. and Mitchison, T. J. (1997) 'Actin polymerization is induced by Arp2/3 protein complex at the surface of Listeria monocytogenes', *Nature*, 385(6613), pp. 265–269. doi: 10.1038/385265a0.

Welte, M. A. (2004) 'Bidirectional transport along microtubules', *Current Biology*, 14(13), pp. R525–R537. doi: 10.1016/j.cub.2004.06.045.

Wen, Y. *et al.* (2004) 'EB1 and APC bind to mDia to stabilize microtubules downstream of Rho and promote cell migration', *Nature Cell Biology*, 6(9), pp. 820–830. doi: 10.1038/ncb1160.

Weng, Z. *et al.* (2018) 'Structural analyses of key features in the KANK1 · KIF21A complex yield mechanistic insights into the cross-talk between microtubules and the cell cortex', *Journal of Biological Chemistry*, 293(1), pp. 215–225. doi: 10.1074/jbc.M117.816017.

Werner, M., Munro, E. and Glotzer, M. (2007) 'Astral Signals Spatially Bias Cortical Myosin Recruitment to Break Symmetry and Promote Cytokinesis', *Current Biology*, 17(15), pp. 1286–1297. doi: 10.1016/j.cub.2007.06.070.

Westermann, S. *et al.* (2006) 'The Dam1 kinetochore ring complex moves processively on depolymerizing microtubule ends', *Nature*, 440(7083), pp. 565–569. doi: 10.1038/nature04409.

Wiese, C. and Zheng, Y. (2000) 'A new function for the γ-tubulin ring complex as a microtubule minus-end cap', *Nature Cell Biology*, 2(6), pp. 358–364. doi: 10.1038/35014051.

Wignall, S. M. and Villeneuve, A. M. (2009) 'Lateral microtubule bundles promote chromosome alignment during acentrosomal oocyte meiosis', *Nature Cell Biology*, 11(7), pp. 839–844. doi: 10.1038/ncb1891.

Wijeratne, S. and Subramanian, R. (2018) 'Geometry of antiparallel microtubule bundles regulates relative sliding and stalling by PRC1 and kif4A', *eLife*, 7. doi: 10.7554/eLife.32595.

Williams, B. C. *et al.* (1997) 'The Drosophila kinesin-like protein KLP3A is required for proper behavior of male and female pronuclei at fertilization.', *Development (Cambridge, England)*, 124(12), pp. 2365–2376. Available at: http://dev.biologists.org/content/124/12/2365.abstract.

Wirtz-Peitz, F., Nishimura, T. and Knoblich, J. A. (2008) 'Linking Cell Cycle to Asymmetric Division: Aurora-A Phosphorylates the Par Complex to Regulate Numb Localization', *Cell*, 135(1), pp. 161–173. doi: 10.1016/j.cell.2008.07.049.

Witte, H., Neukirchen, D. and Bradke, F. (2008) 'Microtubule stabilization specifies initial neuronal polarization ', *Journal of Cell Biology*, 180(3), pp. 619–632. doi: 10.1083/jcb.200707042.

Wittmann, T., Bokoch, G. M. and Waterman-Storer, C. M. (2003) 'Regulation of leading edge microtubule and actin dynamics downstream of Rac1', *Journal of Cell Biology*, 161(5), pp. 845–851. doi: 10.1083/jcb.200303082.

Wittmann, T., Bokoch, G. M. and Waterman-Storer, C. M. (2004) 'Regulation of Microtubule Destabilizing Activity of Op18/Stathmin Downstream of Rac1', *Journal of Biological Chemistry*, 279(7), pp. 6196–6203. doi: 10.1074/jbc.M307261200.

Wodarz, A. *et al.* (1999) 'Bazooka provides an apical cue for inscuteable localization in Drosophila neuroblasts', *Nature*, 402(6761), pp. 544–547. doi: 10.1038/990128.

Wollman, R. *et al.* (2005) 'Efficient chromosome capture requires a bias in the "search-and-capture" process during mitotic-spindle assembly', *Current Biology*, 15(9), pp. 828–832. doi: 10.1016/j.cub.2005.03.019.

Woodard, G. E. *et al.* (2010) 'Ric-8A and Giα Recruit LGN, NuMA, and Dynein to the Cell Cortex To Help Orient the Mitotic Spindle', *Molecular and Cellular Biology*, 30(14), pp. 3519–3530. doi: 10.1128/mcb.00394-10.

Worthylake, R. A. *et al.* (2001) 'RhoA is required for monocyte tail retraction during transendothelial migration', *Journal of Cell Biology*, 154(1), pp. 147–160. doi: 10.1083/jcb.200103048.

Wu, G. *et al.* (2008) 'A novel role of the chromokinesin Kif4A in DNA damage response ES RIB ND ES SC', *Cell Cycle*, 7(July 2008), pp. 2013–2020. Available at: http://www.ncbi.nlm.nih.gov/pmc/articles/PMC3121316/.

Wu, G. and Chen, P. L. (2008) 'Structural requirements of chromokinesin Kif4A for its proper function in mitosis', *Biochemical and Biophysical Research Communications*, 372(3), pp. 454–458. doi: 10.1016/j.bbrc.2008.05.065.

Wu, J.-C. and Rose, L. S. (2007) 'PAR-3 and PAR-1 inhibit LET-99 localization to generate a cortical band important for spindle positioning in Caenorhabditis elegans embryos.', *Molecular biology of the cell*, 18(11), pp. 4470–82. doi: 10.1091/mbc.E07-02-0105.

Wu, J. C., Espiritu, E. B. and Rose, L. S. (2016) 'The 14-3-3 protein PAR-5 regulates the asymmetric localization of the LET-99 spindle positioning protein', *Developmental Biology*, 412(2), pp. 288–297. doi: 10.1016/j.ydbio.2016.02.020.

Wu, Y. *et al.* (2018) 'Rapid diffusion-state switching underlies stable cytoplasmic gradients in

the Caenorhabditis elegans zygote', *Proceedings of the National Academy of Sciences of the United States of America*, 115(36), pp. E8440–E8449. doi: 10.1073/pnas.1722162115.

Xiao, B. *et al.* (2007) 'Structural basis for AMP binding to mammalian AMP-activated protein kinase', *Nature*, 449(7161), pp. 496–500. doi: 10.1038/nature06161.

Xie, Y., Miao, H. and Blankenship, J. T. (2018) 'Membrane trafficking in morphogenesis and planar polarity', *Traffic*, 19(9), pp. 679–689. doi: 10.1111/tra.12580.

Xu, Z. *et al.* (2009) 'INCENP–aurora B interactions modulate kinase activity and chromosome passenger complex localization', *Journal of Cell Biology*, 187(5), pp. 637–653. doi: 10.1083/jcb.200906053.

Yan, J. *et al.* (2013) 'Kinesin-1 regulates dendrite microtubule polarity in Caenorhabditis elegans', *eLife*, 2013(2). doi: 10.7554/eLife.00133.

Yang, J. *et al.* (2002) 'Rootletin, a novel coiled-coil protein, is a structural component of the ciliary rootlet', *Journal of Cell Biology*, 159(3), pp. 431–440. doi: 10.1083/jcb.200207153.

Yang, J., Adamian, M. and Li, T. (2006) 'Rootletin interacts with C-Nap1 and may function as a physical linker between the pair of centrioles/basal bodies in cells', *Molecular Biology of the Cell*, 17(2), pp. 1033–1040. doi: 10.1091/mbc.E05-10-0943.

Yang, S. *et al.* (2017) 'Phenotype Analysis Method for Identification of Gene Functions Involved in Asymmetric Division of Caenorhabditis elegans', *Journal of Computational Biology*, 24(5), pp. 436–446. doi: 10.1089/cmb.2016.0210.

Yarar, D. *et al.* (1999) 'The Wiskott-Aldrich syndrome protein directs actin-based motility by stimulating actin nucleation with the Arp2/3 complex', *Current Biology*, 9(10), pp. 555–558. doi: 10.1016/S0960-9822(99)80243-7.

Yi, J. J. *et al.* (2010) 'TGF-β Signaling Specifies Axons during Brain Development', *Cell*, 142(1), pp. 144–157. doi: 10.1016/j.cell.2010.06.010.

Yildiz, A. *et al.* (2004) 'Kinesin Walks Hand-Over-Hand', *Science*, 303(5658), pp. 676–678. doi: 10.1126/science.1093753.

Yoon, S., Kawasaki, I. and Shim, Y.-H. (2012) 'Cell Cycle CDC-25.1 controls the rate of germline mitotic cell cycle by counteracting WEE-1.3 and by positively regulating CDK-1 in Caenorhabditis elegans', *Cell Cycle*, 11(7), pp. 1354–1354. doi: 10.4161/cc.19755.

Yu, F. *et al.* (2000) 'Analysis of partner of inscuteable, a novel player of Drosophila asymmetric divisions, reveals two distinct steps in inscuteable apical localization', *Cell*, 100(4), pp. 399–409. doi: 10.1016/S0092-8674(00)80676-5.

Yu, F. *et al.* (2003) 'Distinct roles of Gαi and Gβ13F subunits of the heterotrimeric G protein complex in the mediation of Drosophila neuroblast asymmetric divisions', *Journal of Cell Biology*, 162(4), pp. 623–633. doi: 10.1083/jcb.200303174.

Yüce, Ö., Piekny, A. and Glotzer, M. (2005) 'An ECT2-centralspindlin complex regulates the localization and function of RhoA', *Journal of Cell Biology*, 170(4), pp. 571–582. doi: 10.1083/jcb.200501097.

Yue, Y. *et al.* (2018) 'Altered chemomechanical coupling causes impaired motility of the kinesin-4 motors KIF27 and KIF7', *The Journal of Cell Biology*. Available at: http://jcb.rupress.org/content/early/2018/01/18/jcb.201708179.abstract.

Zhang, D. and Glotzer, M. (2015) 'The RhoGAP activity of CYK-4/MgcRacGAP functions non-canonically by promoting RhoA activation during cytokinesis', *eLife*. Edited by M. Balasubramanian, 4(AUGUST2015), p. e08898. doi: 10.7554/eLife.08898.

Zhang, H., Squirrell, J. M. and White, J. G. (2008) 'RAB-11 permissively regulates spindle alignment by modulating metaphase microtubule dynamics in Caenorhabditis elegans early embryos.', *Molecular biology of the cell*, 19(6), pp. 2553–2565. doi: 10.1091/mbc.E07-09-0862.

Zhao, P. *et al.* (2019) 'Aurora-A Breaks Symmetry in Contractile Actomyosin Networks Independently of Its Role in Centrosome Maturation', *Developmental Cell*, 48(5), pp. 631-645.e6. doi: 10.1016/j.devcel.2019.02.012.

Zhao, W. M. and Fang, G. (2005) 'MgcRacGAP controls the assembly of the contractile ring and the initiation of cytokinesis', *Proceedings of the National Academy of Sciences of the United States of America*, 102(37), pp. 13158–13163. doi: 10.1073/pnas.0504145102.

Zhou, K. *et al.* (2009) 'A ZYG-12-dynein interaction at the nuclear envelope defines cytoskeletal architecture in the C. elegans gonad', *Journal of Cell Biology*, 186(2), pp. 229–241. doi: 10.1083/jcb.200902101.

Zhu, C. and Jiang, W. (2005) 'Cell cycle-dependent translocation of PRC1 on the spindle by Kif4 is essential for midzone formation and cytokinesis', *Proceedings of the National Academy of Sciences*, 102(2), pp. 343–348. doi: 10.1073/pnas.0408438102.

Zhu, J. *et al.* (2016) 'An Atypical MAGUK GK Target Recognition Mode Revealed by the Interaction between DLG and KIF13B', *Structure*, 24(11), pp. 1876–1885. doi: https://doi.org/10.1016/j.str.2016.08.008.

Zhu, M. *et al.* (2017) 'Actomyosin polarisation through PLC-PKC triggers symmetry breaking of the mouse embryo', *Nature Communications*, 8(1), p. 921. doi: 10.1038/s41467-017-00977-8.

Zhu, R., Liu, C. and Gundersen, G. G. (2018) 'Nuclear positioning in migrating fibroblasts', *Seminars in Cell and Developmental Biology*, 82, pp. 41–50. doi: 10.1016/j.semcdb.2017.11.006.

Zonies, S. *et al.* (2010) 'Symmetry breaking and polarization of the C. elegans zygote by the polarity protein PAR-2', *Development*, 137(10), pp. 1669–1677. doi: 10.1242/dev.045823.

Zwaal, R. R. *et al.* (1996) ‘G proteins are required for spatial orientation of early cell cleavages in C. elegans embryos’, *Cell*, 86(4), pp. 619–629. doi: 10.1016/S0092-8674(00)80135-X.

Appendices.

Table 9.1 **Polarity phenotypes observed through knockdown of screen hits.**

Gene	PAR Phenotypes								
	Tilted PARs (Strong tilt*)	Bipolar PAR-2 domains	aPAR & pPARs co-habiting	Cleared anterior cap	Patchy PAR-3 domain	No PAR-2 during early touch	Still no PAR-2 by late touch	Small PAR-2 domain by Pn Mig	PAR-2 grown past 50% (PAR-2 Dominant)
Control (n= 67)	0/67 (0%)	3/67 (4.5%)	1/67 (1.5%)	5/67 (7.5%)	0/67 (0%)	0/10 (0%)	1/30 (3.3%)	0/27 (0%)	1/67 (1/5%)
nop-1(n=43)	5/43 (11.6%)*	1/43 (2.3%)	20/43 (46.5%)	0/43 (0%)	3/43 (7.0%)	3/10 (30%)	2/13 (15.4%)	0/20 (0%)	0/43 (0%)
rack-1 (n=6)	1/6 (16.7%)	0/6 (0%)	0/6 (0%)	0/6 (0%)	0/6 (0%)	0/2 (0%)	0/3 (0%)	0/1 (0%)	0/6 (0%)
nop-1; *rack-1* (n=9)	3/9 (33.3%)	1/9 (11.1%)	2/9 (22.2%)	0/9 (0%)	0/9 (0%)	0/2 (0%)	0/2 (0%)	0/5 (0%)	0/9 (0%)
cnt-2 (n=17)	0/17 (0%)	6/17 (35.3%)	1/17 (5.9%)	3/17 (17.6%)	0/17 (0%)	1/5 (20%)	0/5 (0%)	0/7 (0%)	3/17 (17.6%)
nop-1; cnt-2 (n=13)	2/3 (15%)*	0/13 (0%)	4/13 (30.8%)	0/13 (0%)	0/13 (0%)	1/2 (50%)	0/5 (0%)	1/6 (16.7%)	0/13 (0%)
let-754 (n=10)	0/10 (0%)	3/10 (30%)	1/10 (10%)	1/10 10%	5/10 (50%)	0/1 (0%)	0/4 (0%)	0/5 (0%)	0/10 (0%)
nop-1; let-754 (n=6)	4/6 (66.7%)*	1/6 (16.7%)	0/6 (0%)	0/6 (0%)	1/6 (16.7%)	NA	0/3 (0%)	0/3 (0%)	0/6 (0%)
klp-19 (n=53)	2/53 (3.8%)*	12/53 (22.6%)	0/53 (0%)	9/53 (17.0%)	0/53 (0%)	4/11 (36.4%)	0/13 (0%)	0/29 (0%)	2/53 (0%)
nop-1; klp-19 (n=22)	9/22 (40.9%)*	0/22 (0%)	7/22 (31.8%)	0/22 (0%)	3/22 (13.6%)	6/11 (54.5%)	0/6 (0%)	0/5 (0%)	0/22 (0%)
arf-1.2 (n=5)	1/5 (20%)	2/5 (40%)	0/5 (0%)	0/5 (0%)	0/5 (0%)	NA	0/2 (0%)	0/3 (0%)	0/5 (0%)
nop-1; arf-1.2 (n=6)	1/6 (16.7%)	0/6 (0%)	0/6 (0%)	0/6 (0%)	0/6 (0%)	NA	2/3 (66.7%)	0/3 (0%)	0/6 (0%)

Table 9.2 **Microtubule phenotypes observed through knockdown of screen hits.**

Gene	Microtubule Phenotypes						
	Cent orientated anterior early	Cent oriented posterior late	One cent facing post, one facing ant	Cents migrating around same side of PN (Late touch)	Cent not separated by Pn Mig	Cent detached from PN	Abnormal MT growth
Control (n= 44)	0/25 (0%)	1/19 (5.3%)	0/19 (0%)	3/18 (16.7%)	0/19 (0%)	0/44 (0%)	0/44 (0%)
nop-1 (n=43)	7/23 (30.4)	6/20 (30%)	0/20 (0%)	1/13 (7.7%)	9/20 (45%)	0/43 (0%)	0/43 (0%)
rack-1 (n=6)	0/5 (0%)	0/1 (0%)	0/1 (0%)	0/3 (0%)	0/1 (0%)	0/6 (0%)	(0/6 (0%)
nop-1; *rack-1* (n=9)	0/4 (0%)	0/5 (0%)	1/5 (20%)	0/2 (0%)	0/5 (0%)	0/9 (0%)	0/9 (0%)
cnt-2 (n=10)	0/6 (0%)	0/4 (0%)	0/4 (0%)	1/4 (25%)	0/4 (0%)	0/10 (0%)	0/10 (0%)
nop-1; cnt-2 (n=13)	0/7 (0%)	4/6 (66.7%)	0/6 (0%)	0/5 (0%)	2/6 (33.3%)	0/13 (0%)	0/13 (0%)
let-754 (n=10)	0/5 (0%)	0/5 (0%)	0/5 (0%)	0/4 (0%)	0/5 (0%)	1/10 (10%)	3/10 (30%)
nop-1; let-754 (n=6)	1/3 (33.3%)	0/3 (0%)	0/3 (0%)	0/3 (0%)	0/3 (0%)	2/6 (33.3%)	1/6 (16.7%)
klp-19 (n=42)	4/21 (19.0%)	0/21 (0%)	0/21 (0%)	1/10 (10%)	4/21 (19.0%)	0/42 (0%)	0/42 (0%)
nop-1; klp-19 (n=20)	3/15 (20%)	0/5 (0%)	0/5 (0%)	0/6 (0%)	2/5 (40%)	0/20 (0%)	0/20 (0%)
arf-1.2 (n=3)	0/2 (0%)	0/1 (0%)	0/1 (0%)	0/2 (0%)	0/3 (0%)	0/3 (0%)	0/3 (0%)
nop-1; arf-1.2 (n=6)	0/3 (0%)	2/3 (66.7%)	0/3 (0%)	2/3 (66.7%)	1/3 (33.3%)	0/6 (0%)	0/3 (0%)

Table 9.3 **Other phenotypes observed through knockdown of screen hits.**

Gene	Other Phenotypes				
	SPCC detached from cortex	SPCC lateral	Male PN anterior during estab	Cytokinetic defects	Vacuoles in cytoplasm
Control (n=67)	1/40 (2.5%)	1/40 (2.5%)	0/67 (0%)	NA	0/67 (0%)
nop-1(n=43)	9/23 (39.1%)	5/23 (21.7%)	0/43 (0%)	NA	0/43 (0%)
rack-1 (n=6)	2/5 (40%)	1/5 (20%)	0/6 (0%)	NA	0/6 (0%)
nop-1; *rack-1* (n=9)	1/4 (25%)	2/4 (50%)	0/9 (0%)	NA	0/9 (0%)
cnt-2 (n=17)	1/10 (10%)	2/10 (20%)	0/17 (0%)	NA	0/17 (0%)
nop-1; cnt-2 (n=13)	2/7 (28.6%)	1/7 (14.3%)	0/13 (0%)	NA	0/13 (0%)
let-754 (n=10)	0/5 (0%)	0/5 (0%)	0/10 (0%)	N=1	0/10 (0%)
nop-1; let-754 (n=6)	0/3 (0%)	2/3 (66.7%)	0/6 (0%)	N=1	0/6 (0%)
klp-19 (n=53)	7/24 (29.2%)	2/24 (8.3%)	1/53 (1.9%)	N=1	0/53 (0%)
nop-1; klp-19 (n=22)	6/17 (35.3%)	7/17 (41.2%)	0/22 (0%)	NA	0/22 (0%)
arf-1.2 (n=5)	0/2 (0%)	0/2 (0%)	0/5 (0%)	NA	3/5 (60%)
nop-1; arf-1.2 (n=6)	0/3 (0%)	0/3 (0%)	0/6 (0%)	NA	5/6 (83.3%)

Notes on Tables 9.1, 9.2 & 9.3. N = Number of embryos. Within each cell, the number of embryos with a phenotype out of the number of embryos that could potentially have that phenotype is displayed as well as a percentage of this. Cytokinetic defects were not imaged for analysis (i.e., we only took images when we saw an interesting defect) and so have not been reported as a proportion of embryos but simply that an embryo with cytokinetic defect was present in a given condition. Embryos with phenotypes at a notably greater frequency than their appropriate control have been highlighted in orange.

Figure 9.1

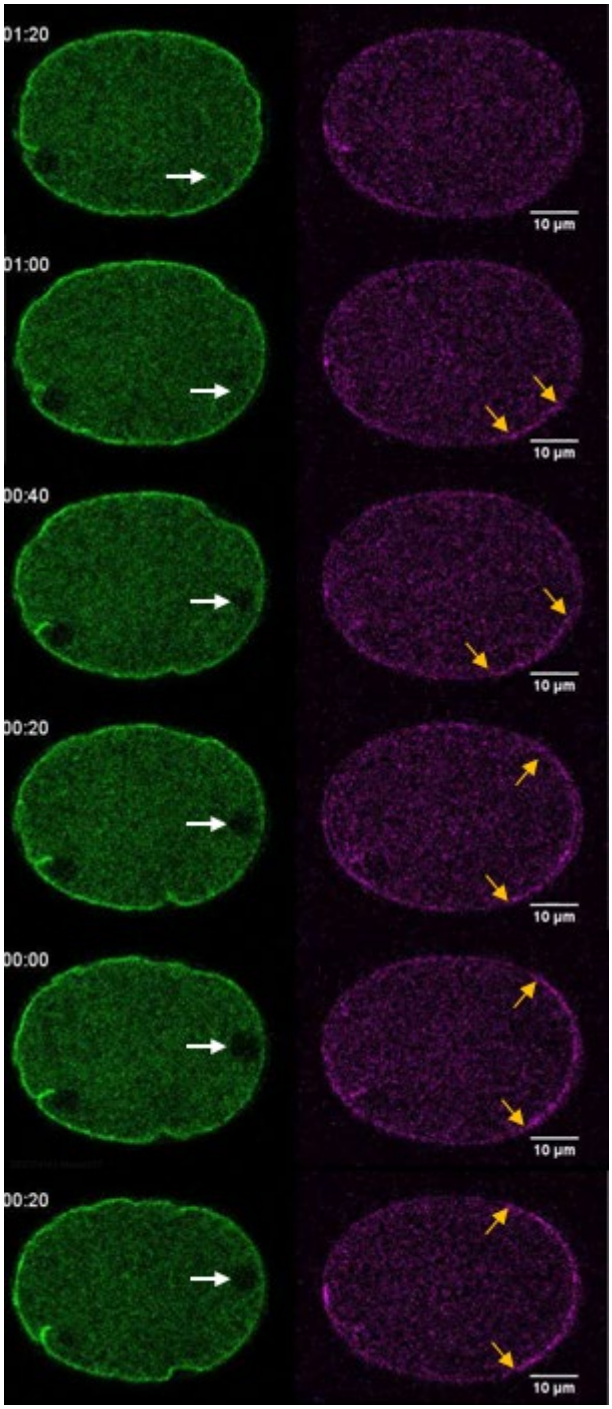

Figure 9.1 **pPAR cortical loading in embryo with lateral SPCC.**

Snapshots of confocal microscopy time-lapse of GFP::ECT-2; mCherry-PAR-2 in a control *C. elegans* zygote recorded by Kapoor Kotak (2019) (Video 37). In the video, the pronucleus initially localises to the lateral-posterior cortex where PAR-2 is then recruited to the nearby cortex. The pronucleus and PAR-2 domain eventually shift towards the posterior pole. White arrows point to the pronucleus. Orange arrows point to PAR-2 domain boundaries. Note: The authors set time 00:00 as polarity onset, however we note that cortical PAR-2 can be seen in the second snapshot 1 minute prior.